A STUDY ON NEW APPROACHES FOR DELINEATING GROUNDWATER PROTECTION ZONES IN FRACTURED-ROCK AQUIFERS

Júlio Carneiro

UNIVERSITY COLLEGE LONDON

2005

A thesis submitted as partial fulfilment of the requirements for the degree of Doctor of Philosophy

ProQuest LLC
789 East Eisenhower Parkway
P.O. Box 1346
Ann Arbor, MI 48106-1346

ABSTRACT

Delineation of groundwater protection zones in fractured-rock aquifers usually involves the equivalent porous media (EPM) assumption, although research studies have proved that, often, such an assumption is inadequate. This thesis is concerned with the study of flow and transport models that, while preserving the main hydrodynamic features of fractured rocks, are still practical enough to be applied to low-budget studies such as the delineation of groundwater protection zones.

Methodologies are developed for three different types of fractured-rock aquifers.

The first group comprises **composite aquifer systems**, a single linear structure in an otherwise homogeneous aquifer. The transport model adopted is based on advection and the procedure for delineation of protection zones involves the derivation of advective velocity and stream function equations. The stream function facilitates visualisation of the capture zones, while isochrones are delineated through particle tracking.

Dual and multiple-porosity aquifers, the second group, are dealt with analytically. The well-known flow and transport features of dual-porosity media are used to develop a method that takes into account the influence of matrix diffusion on the shape and size of protection zones. The methodology returns probability related protection zones that, when compared with single-porosity models, show that matrix diffusion has a dramatic effect on protection zones size. Additionally, a new multiple-porosity model is developed, that simulates the hydraulic behaviour of hierarchical fracture systems. Analytical solutions are presented for 2-D flow and 1-D transport.

The third group comprises **fracture network aquifers**. The work conducted involves the implementation of practical tools for simulating solute transport in fracture networks, which are then used to delineate probabilistic protection zones. A first approach applies the *Statistical Continuum Method*, a hybrid tool that combines the use of Discrete Fracture Networks and Continuum Models. A second method relies on a *Continuous Time Random Walk (CTRW)*. Analytical solutions for modelling solute transport in fracture networks according to a CTRW are found and combined with MODFLOW to simulate solute transport in catchment-scale domains.

Additionally, the following are discussed: methodologies for assessing protection zones in fractured-rocks delineated using EPM approaches; ways for implementing a 3-D CTRW; and the two issues of probability versus concentration and of forward versus reverse particle tracking, when simulating solute transport in fractured-rock aquifers.

Ao meu pai, Eduardo Carneiro, e à minha mãe, Maria Rosa Ferreira, a quem devo tudo.

À minha esposa, Helena Lima, pela sua dedicação durante estes anos, e ao meu filho, Pedro Carneiro.

ACKNOWLEDGMENTS

I would like to thank all those who made easier the completion of this thesis. In particular, thanks are due to:

Golder Associates, providers of the FRACMAN / MAFIC software package and whose technical staff spent a considerable amount of time providing support or even adapting some of their utilities at my request;

Ken Bradbury, from the Wisconsin Geological and Natural History Survey, who supplied the software SDF used extensively throughout the thesis;

Nicky Robinson, who in spite of working towards a PhD degree in this very same topic was always generous enough to discuss her results with me. In addition, Nicky provided many of the references I quote;

José Martins Carvalho, my supervisor at Universidade de Évora, for always being available whenever I requested his guidance and assistance;

Special thanks go to John Barker, my supervisor at UCL. There are plenty of reasons to thank him, but I think it suffices to say that to meet John and to work under his supervision are amongst the best and most influential events that ever happened to me.

The research presented in this thesis was partially funded by FCT, the portuguese Foundation for Science and Technology, and by the European Social Fund, under the Third Community Support Framework.

TABLE OF CONTENTS

LIST OF TABLES

LIST OF FIGURES

Appendices

NOTATION

(Symbols with an over-bar denote the Laplace transform of the variable. Symbols with a tilde denote the Fourier cosine transform of the variable. Subscripts m and f refer to matrix and fracture system properties respectively, except in Chapter 3, where subscript f is used for properties of a linear structure. Dimensions of the variables are shown in square brackets.)

Latin symbols

a	volume to area ratio in multiple-porosity model	[L]
$a_e = (X^+ - X^-)/2$	semi-major axis of travel-time ellipse	[L]
A	recharge area	[L^2]
b	half fracture aperture	[L]
$b_e = \frac{A}{\pi a_e}$	semi-minor axis of travel-time ellipse	[L]
B(u)	block shape parameter	[-]
$B_{eff}(u)$	effective BGF	[-]
$B'_{eff}(u)$	normalised effective BGF	[-]
c	minimum of Pareto distribution	
C	solute concentration	[M/L^3]
C_0	inlet constant solute concentration	[M/L^3]
$C_{i,j}$	constant of proportionality (section 5.4)	[-]
d	distance from a well to a linear structure	[L]
d_{KS}	maximum deviation in Kolmogorov-Smirnov test	[-]
D	dispersion (or diffusion) coefficient	[L^2/T]
D*	matrix diffusion coefficient	[L^2/T]
$E(X^n)$	n^{th} moment of a distribution	
F(x)	cumulative probability function	
g	gravity	[L/T^2]
h	hydraulic potential	[L]
H	aquifer thickness	[L]
i	square root of -1	
I_n	modified Bessel function of the 1^{st} kind, order n	
j	index usually referring to fracture set	
J	uniform hydraulic gradient	[-]
K	hydraulic conductivity	[L/T]
K_0	modified Bessel function of the 2^{nd} kind, order zero	
l	characteristic length	[L]
L	distance between points of measured h	[L]
$\mathcal{L}$	Laplace transform operator	
$M_x(z)$	moment generating function	
n_e	effective (kinematic) porosity	[-]
n_f	effective (kinematic) porosity of linear structure	[-]
p	Laplace transform variable	
p_{KS}	level of significance in Kolmogorov-Smirnov test	[-]
P	probability	[-]
P(n,t)	probability of taking *n* steps in time t	[-]
$P_n(x)$	probability of reaching x in n steps	[-]
P(x,t)	probability of being at x in time t	[-]
$P_0(x,t)$	standard CTRW probability distribution	[-]
P_e	Peclet number	[-]
q	specific discharge	[L/T]
$q_i(r,t)$	discharge from the i^{th} fractures into the (i-1)th fractures per unit area of aquifer	[L/T]
q_j	flow rate in fracture set j (section 6.4)	[L^3/T]
Q	pumping rate	[L^3/T]
Q_Θ	bulk flow rate in the hydraulic gradient direction	[L^3/T]
r	radial distance	[L]
R	recharge	[L]
R_i	radius of influence of a pumping well	[L]
s	drawdown	[L]
S	storage coefficient	[-]
S_{eff}	effective storage coefficient	[-]
$S_T = \sum_{i=2}^{n} S_i$	total storage coefficient in the multiple-porosity model	[-]
t	time	[T]
$t' = \frac{2\pi (TJ)^2}{n_e Q H} t$	dimensionless time	[-]
t_a	advection time	[T]
t_d	characteristic time for diffusion	[T]
T	transmissivity	[L^2/T]
$u = a\sqrt{p/D*}$	parameter of BGF in transport or	
$u = a\sqrt{pS_m/T_m}$	in flow model	[-]
U	volume in REV	[L^3]
v	advective velocity	[L/T]
v_x, v_y	x and y components of velocity	[L/T]
$v_{reg} = -gb^2 J/3\upsilon$	flow velocity due to regional hydraulic gradient	[L/T]
w_f	width of linear structure	[L]

$w = -\frac{Q(a+b)}{2\pi Hb}$, product of steady radial flow velocity at distance r by r [L^2/T]

$W(x) = \int_x^\infty (e^{-u}/u)du$, the Theis well function [-]

x spatial coordinate [L]

$x' = 2\pi TJx/Q$, dimensionless spatial coordinate [-]

$x_e = (X^+ + X^-)/2$, centre of travel-time ellipse [L]

X_L distance from well to stagnation point [L]

X^+, X^- *x-axis* limits of travel-time ellipse [L]

y spatial coordinate [L]

$y' = 2\pi TJ\, y/Q$, dimensionless spatial coordinate [-]

Y_L asymptotic limit of the capture zone [L]

Y_0 reference point along the *y-axis* [L]

$z_1 = ix - |y|$, complex variable [L]

$z_2 = d - ix + y$, complex variable [L]

Z real variable

$\overline{Z_j}$ unit vector in direction *j* [L]

Greek symbols

α dispersivity [L]

β shape parameter of gamma and Pareto distributions or

$\beta_i = 1 + (S_i/S_{i-1})\beta_{i+1} B(u_i)$, in multiple-porosity model (section 4.3)

$\chi = p[1 + \phi_m B(u)a/b]$ parameter of dual-porosity transport models [T^{-1}]

η main flow direction [-]

δ(z) Dirac delta function [-]

$\langle \delta x^n \rangle$ n^{th} spatial moment [L^n]

Δs drawdown difference [L]

ε Fourier cosine transform variable [L^{-1}]

ϕ porosity [-]

Φ potential

γ step rate in Poisson Process [T^{-1}]

γ_j^T step rate in direction j for Poisson Process with multiple directions of movement [T^{-1}]

Γ(x) the gamma function of argument x

Γ(x, y) the incomplete gamma function of arguments x and y

φ angle with *x-axis* [-]

λ scale parameter of exponential and gamma distributions

$\Lambda = \sqrt{pS/T + \varepsilon^2}$ parameter used for simplification of equations in section 3.2 [L^{-1}]

$\overline{\mu}$ mean of a random variable

μ (z) unit step function [-]

θ angle between fracture set orientation and *x-axis* [-]

Θ angle between hydraulic gradient orientation and *x-axis* [-]

ρ directional choice parameter [-]

σ^2 variance of a random variable

τ transition time [T]

υ kinematic viscosity [L^2/T]

$\omega = 2(\Theta - \chi)/\pi$, error in main flow direction [-]

$\xi = \sqrt{\frac{pS_f}{T_f}\left[1 + \frac{S_m}{S_f} B(u)\right]}$ parameter of dual-porosity flow models [L^{-1}]

ψ stream function [L^2/T]

Ω skewness

Acronyms

BEZ	Best estimate zone
BGF	Block geometry function
CI	Confidence index
CTRW	Continuous time random walk
DFN	Discrete fracture network
EPM	Equivalent porous medium
HFS	Hierarchical fracture system
REV	Representative elementary volume
RMS	Root mean square deviation
SCM	Statistical continuum method
USGS	United States Geological Survey
USEPA	United States Environmental Protection Agency
WHPA	Well head protection area
ZOC	Zone of confidence
ZOU	Zone of uncertainty

(FRACMAN, FLOWPATH, MAFIC, MODFLOW, MODPATH, NAPSAC, PMPATH, PMWIN and SDF refer to modelling software. References are provided where these codes are first mentioned. GPZFAULT, GPZDUALP, MULTIPOROSITY, PROBCONT, SCPATH and STATMOV refer to computer codes developed within the scope of this thesis. A description is made where these codes are first mentioned.)

Chapter 1

INTRODUCTION

The role of groundwater as a major resource for water supply has prompted the regulation authorities of many countries to impose pre-emptive measures aiming to protect the sources (wells or springs). This preventive approach acknowledges that groundwater, when contaminated, is extremely difficult and expensive to remediate. Often, one pre-emptive action required is the definition of **Groundwater Protection Zones**, also known as Wellhead Protection Areas (WHPA), which are areas surrounding the sources in which deterioration of groundwater quality and quantity is prevented by restraining or prohibiting hazardous activities.

By imposing limits to activities that may be undertaken in an area, delineation of groundwater protection zones is important not only to the protection of the source, but also to the economic development of the region. Robust and consistent methods for delineation of protection zones are required in order to ensure protection while imposing only the necessary restrictions to further activities. Despite being a task routinely conducted by hydrogeologists, protection zone delineation is still an active area of research, particularly in relation to fractured rock aquifers where reliable and sound methodologies have yet to be established.

1.1 STATEMENT OF THE PROBLEM

Groundwater protection policies usually require the definition of travel-time related protection zones around wells. Delineation of those zones was initially conducted using advection as the only transport mechanism and simplified hydrogeologic conditions, resulting in simple analytical solutions based on the concepts of *capture zone* and *isochrone* (Bear and Jacobs 1965). Such solutions are only applicable in simple situations involving a single well, and including assumptions such as homogeneity and continuity of the aquifer and uniformity of the flow field (fig. 1.1a).

The development of **computational methods** made it possible to treat the problem in more realistic and complex situations. Using, for example, *analytic elements* (Haitjema et al. 1994) and *particle tracking* (Pollock 1989) techniques, situations involving multiple wells, anisotropy and non-uniform flow conditions became tractable (fig. 1.1b). Most protection zones have been delineated using either these methods or analytical solutions.

In recent years the use of **stochastic solutions** (Bair et al. 1991) has enhanced protection zone delineation. Stochastic models acknowledge uncertainty in the hydraulic parameters of the aquifers and, by treating these parameters as non-deterministic, seek to delineate uncertainty-based protection zones (fig. 1.1c). Stochastic methods eventually led to analytical formulations that use the distribution of hydraulic parameters to assign uncertainty to the protection zones of single wells in a uniform flow field (Franzetti and Guadagnini 1996). Although promising, these stochastic methods demand a considerable amount of information to characterise parameter variation, and assume that the aquifer behaves as a **continuous porous media**.

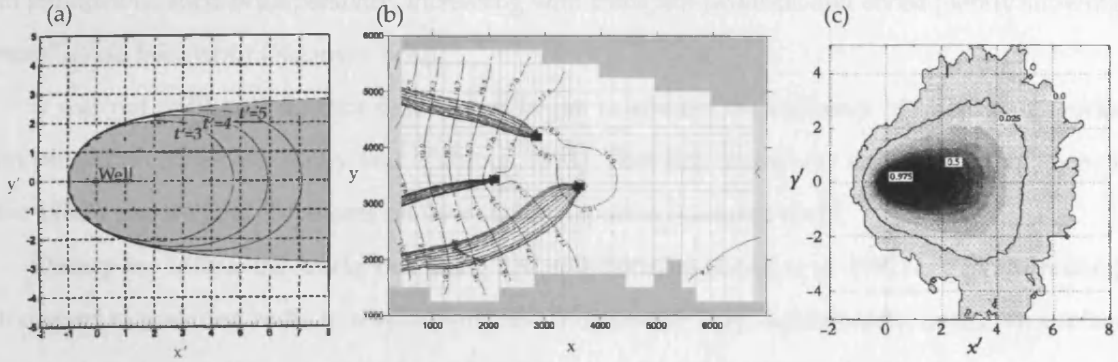

Figure 1.1 – Protection zones in continuous porous medium aquifers. a) capture zone (shaded area) and *t*-isochrones (solid lines) delineated with Bear and Jacobs (1965) analytical solution. b): capture zone delineated using particle tracking in an aquifer discretized in finite differences. c) after van Leeuwen (2000), shows a probabilistic protection zone for a *t*-isochrone; the contours show increasing probability of a particle reaching the well within time *t*.

It is this assumption of **continuity** of the porous media that is unlikely to be acceptable in fractured rocks. In addition, heterogeneity in fractured rocks may be so conspicuous that it cannot be handled through any of the techniques mentioned. These are well known difficulties and the delineation of protection zones in fractured rock aquifers has always been considered more troublesome than in *continuous porous media*. Often, difficulties have led to a more intensive use of hydrogeologic mapping and hydrogeochemical techniques as the main tools to delineate capture zones (USEPA 1991a). Although these methods are useful, they aim to protect the whole resource and are not concerned with the definition of the travel time isochrones that are usually required.

To comply with regulations it has been customary to ignore the specific features of solute transport in fractured rocks and resort to the same analytical or computational techniques used for continuous porous media aquifers. Fractured rock aquifers are then envisaged as **Equivalent Porous Media** (EPM) aquifers, with heterogeneity and discontinuity imposed by fractures being largely ignored.

Although assuming EPM behaviour is a widely used practice, the effect of ignoring the influence of fractures is usually not quantified, resulting in hardly defensible protection zones, especially considering that field tests have indicated that transport of solutes in fractured rocks can be extremely complex (Bear et al. 1993). It is not unusual for tracer tests in fractured rocks to fail, either because tracer recovery is unsatisfactory, or because the results are too intricate for description with standard interpretation methods. In fact, several studies have shown that transport in fractured rocks may not follow the physical models (*Fick's laws*) that explain solute transport in continuous media. Specifically, it is commonly accepted that a 'scale effect' may result in parameters, such as dispersivity, increasing with transport distance, and consequently showing non-Fickian behaviour (Neuman 1990).

It was not until 1993 that the first studies began to address the influence of fracture networks on protection zones (Bradbury and Muldoon 1993). That first study was a direct consequence of the 1980's research developments on flow and transport in fractured rocks.

During the 1980's, the works of J. Long and collaborators (Long et al. 1982) began addressing transport in fractured rocks in a systematic and quantitative way. Additionally, extensive studies conducted during the same decade in potential radioactive disposal sites have improved knowledge about the hydraulic behaviour of fractured rocks. All this research resulted in two main approaches to simulate flow and solute transport in fractured rocks. One approach assumes the explicit modelling of the fractures using **Discrete Fracture Network (DFN) models**, while others favour **stochastic continuum models**, whereby heterogeneity is introduced in a continuous medium through the use of various types of stochastic solutions for generating the velocity field (National Research Council 1996). In recent years, **hybrid models**, that jointly use continuous models and fracture network models have also gained prevalence (Smith et al. 1990) (fig. 1.2).

Stochastic continuum models involve assumptions such as Fickian behaviour and definition of a *Representative Elementary Volume* (REV). These assumptions often fail in fractured rocks. A currently active area of research is the assessment of the accuracy of these continuous models as approximations to fracture networks, and, particularly, if it is possible to define a REV to which effective hydraulic parameters can be assigned. Some authors argue that for a continuum to

accurately approximate the behaviour of a fracture network, the discretization of the domain must be so intensive that the computational effort approximates those of DFN models (Parney 1999).

DFN models have a crucial advantage over Continuum models, in that they do not need to assume that transport is Fickian, that a REV exists or that advection is the only transport mechanism: the variation of velocity in the ensemble of fractures produces dispersion without the need to consider any specific dispersive model.

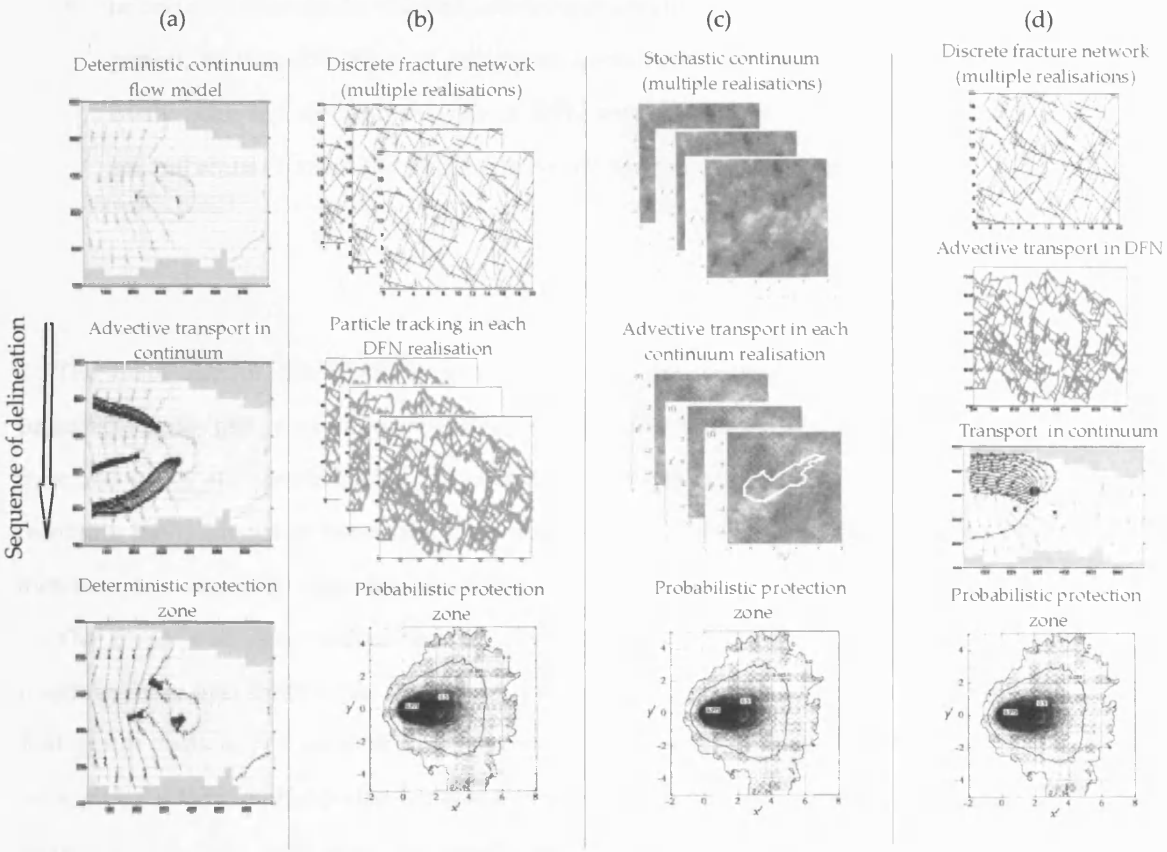

Figure 1.2 – Some approaches for modelling solute transport and delineate protection zones in fractured-rocks. a) deterministic equivalent porous media model; b) discrete fracture network model; c) stochastic continuum model; d) hybrid model.

However, the most striking features of DFN models are the quantity of information that is necessary and the large computational effort involved. Some of the information required, such as fracture apertures or connectivity, is so illusive that it may be considered almost impossible to obtain in routine studies. Additionally, DFN models have proved extremely difficult to constrain on field data (Nakao et al. 2000). Further, the financial resources for conducting studies in hydrogeology are much lower than the resources involved in studies for radioactive waste repositories where these modelling techniques have been extensively used. Consequently, the

method that most accurately simulates flow and transport in fractures is probably not compatible with the type of work that must be conducted in hydrogeology.

It is considered that for any techniques of modelling flow and transport in fractured rocks to be effectively applied to delineate groundwater protection zones, it should be acknowledged that:

- a limited amount of local field information exists. This information is often restricted to data collected in the well being protected;
- the techniques must be efficient, allowing multiple simulations to be carried out in a short period, so that the effect of parameter uncertainty can be fully appreciated (this is not easily achieved through the use of DFN models, where each modelling event involves several realisations of the fracture network and may require several days to complete).

1.2 OBJECTIVES

The main aim of this thesis is to contribute to the development of tools for delineating protection zones that, while encompassing an acceptable representation of the solute transport in fractured rocks, also acknowledge the existence of limited information. Such tools should further recognise the existence of considerable uncertainty about the flow and transport conditions and, therefore, a probabilistic approach should be used.

The thesis addresses delineation of groundwater protection zones in fractured rocks by dividing these into three types of fracture patterns with different hydrodynamic behaviour[1]. A first group deals with fractured rocks involving a **single linear feature**, such as a fault, fracture zone, dyke or vein, embedded in a medium that is envisaged as an Equivalent Porous Medium. A second group deals with **dual and multiple-porosity media**, that is, rocks characterised by a regular fracture pattern that divides the rock mass into blocks susceptible to being described by simple geometries such as slabs, spheres or cylinders. Finally, rocks that exhibit a complex fracture pattern with multiple fracture sets of finite extent, defining **fracture networks**, are also studied.

[1] Throughout this thesis the term 'fracture' will be used for "any discrete discontinuity, natural or induced, which provides a conduit for the movement of the fluid" (Barker 1991). Thus, and since no consideration is given to its origin, fractures include all cracks, fissures, joints, faults, schistosity and stratification of the rocks.

1.3 OUTLINE OF THE THESIS

This thesis is structured into eight chapters. **Chapter 2** is a review of the state of the art on delineation of protection zones. The main concepts are introduced and a discussion of the existing methodologies is made (**section 2.1**). To facilitate understanding of the issues addressed in subsequent chapters, a review of existing studies concerning delineation of protection zones in fractured rock aquifers is made (**section 2.2**).

Chapter 3 concerns groundwater protection zones in composite aquifer systems, i.e., aquifers involving single linear features. Wells in or close to linear structures are quite common in igneous and metamorphic rocks, where often faults and dykes show higher permeability than the surrounding rocks. The existing models for explaining the hydrodynamic behaviour of such structures are discussed (**section 3.1**). Delineation of protection zones in such media cannot be approached using the standard techniques that consider the media as uniform. This approach can be improved, since it is possible to describe analytically the behaviour of this kind of groundwater environment (**section 3.2**). It is possible to compute the stream function of the aquifer and, thus, the capture zone, which is very sensitive to the angle between the regional hydraulic gradient and the linear feature. The isochrones are found through particle tracking (**section 3.3**).

Chapter 4 addresses regular fracture patterns that can be treated as dual-porosity aquifers (**section 4.1**). Analytical solutions for transport from a well injecting a contaminant into a dual-porosity aquifer in which a uniform hydraulic gradient exists are used to compute the travel distance for a t-isochrone (**section 4.2**). Still regarding rocks with regular fracture patterns, models that consider several hierarchical levels of fractures are studied. These models permit to consider multiple porosities within the same rock, thus reflecting the fact that different scales of fractures can co-exist in the same rock (**sections 4.3 and 4.4**).

Chapters 5 and 6 deal with fracture patterns that are more complex and less amenable to analysis. While addressing the issue of Discrete Fracture Networks models and stochastic continuum models (**section 5.1**), the thesis is more concerned with the use of other methodologies. Two techniques are analysed in detail: the Statistical Continuum Method (SCM), addressed in **Chapter 5**, and the Continuous Time Random Walk (CTRW), addressed in **Chapter 6**. Both methods provide probabilistic solutions to the protection zones problem.

The SCM has been developed since the end of the 1980's and, in this thesis, is implemented in conjunction with a standard groundwater flow model, so that it can deal with complex flow patterns. The implementation involves conducting particle tracking in a continuum medium

using the statistics of movement previously collected in a DFN model. The locations of the particles are used to compute probabilistic protection zones (**section 5.2**).

The SCM is a reliable method that preserves the main features of solute transport, although it requires collecting of a lot of information. The CTRW also attempts to mimic movement of particles in a fracture network but without resorting to DFN models. Two analytical solutions are presented. In the first one, movements of particles follow an exponential law, exhibiting scale effect and non-Fickian behaviour for early times but converging to Fickian behaviour for late times. The second analytical solution uses a power-law for the distribution of movements, which never converges to Fickian behaviour, making it impossible to define a REV (**sections 6.1 and 6.2**).

The CTRW is implemented in a two-dimensional numerical environment using the flow solution provided by MODFLOW and then conducting particle tracking according to the distributions of time and path-length. In this way, it is possible to model transport in a fracture network, reproducing scale effects and non-Fickian behaviour, whilst avoiding the use of very intensive computational techniques (**sections 6.3 to 6.5**).

Chapter 7 discusses several issues that arose as pertinent during the study of transport in fracture networks. A first issue deals with the fact that the vast majority of protection zones in fractured rocks are delineated with standard techniques that assume an Equivalent Porous Media (EPM) approach. The accuracy of those protection zones can be assessed, at least in an approximate manner, using a combination of the parameters that compose the analytical solutions of the CTRW (**section 7.1**). A second issue acknowledges that protection zones in fracture networks can be highly dependent on the 3-D features of solute transport and both the SCM and CTRW should be implemented so that vertical movement can be incorporated. The ways in which this can be accomplished are discussed (**section 7.2**). Thirdly, since the solutions of groundwater protection zones in fracture networks are probabilistic, the usually accepted interchangeable relation between probability and concentration is analysed (**section 7.3**). Finally, the differences between forward and reverse particle tracking in fracture networks is considered: these are thought to give different probabilistic distributions of particles. The CTRW technique is used in simple examples to illustrate the case (**section 7.4**).

Finally, **chapter 8** presents the conclusions and suggestions for further research.

Several computer programs were developed within the framework of this PhD thesis. The executable files and the source codes of those programs are included in the CR-ROM supplied with this thesis. Appendix F contains a brief description of each program.

Chapter 2

GROUNDWATER PROTECTION ZONES: A REVIEW OF CURRENT KNOWLEDGE

Delineation of protection zones is closely linked to the task of defining the area contributing groundwater to a pumping well. Although protection zones[1] and contributing areas are not necessarily coincident, since the latter are defined on a scientific basis only, while the first also involves policy and management considerations, the two concepts will be used interchangeably throughout this thesis, as only technical aspects are of concern here.

Additional concepts to be used are **capture zone** (or zone of contribution), meaning the area where discharge of the well matches aquifer recharge, thus coinciding with the source catchment area, and **isochrones**, surfaces that define the ensemble of points from which particles (or solutes) take the same time t to reach the well. Isochrones coincide with the limit of the protection zone for time t.

This chapter presents a review of concepts and methods involved in delineation of protection zones, with a special emphasis (section 2.2) on previous studies concerning fractured-rock aquifers.

2.1 Overview of Groundwater Protection Zones

Delineation of groundwater protection zones is often regarded as a low-budget task and, thus, frequently faces a recurrent problem in hydrogeology: scarcity of field data. Often the information available is restricted to data collected at the well to be protected.

This shortage of information has led to a widespread use of simple techniques that require a minimum amount of data. These techniques are normally based on analytical solutions to the

[1] American literature often refers to **well head protection areas (WHPA)** with the same meaning as Groundwater Protection Zones, but such term will be avoided in this thesis.

groundwater flow problem. However, the complexity of the problem eventually led to the implementation of computational techniques (semi-analytical and numerical) that aim to represent the hydrogeologic setting in a more realistic manner. The latest models recognise the uncertainty in the hydraulic parameters of a natural environment, and include that uncertainty in the delineation of probabilistic protection zones.

2.1.1 Analytical and semi-analytical solutions for wells in a uniform flow field

The simplest analytical solution for the capture zone of a well is the equation of the Calculated Fixed Radius (USEPA 1987b) that equilibrates the volume of water pumped in time *t* with the volume of a cylinder surrounding the well that would provide such an amount of water (fig. 2.1):

$$r(t) = \sqrt{\frac{Qt}{\pi n_e H}} \tag{2.1}$$

where Q is a constant pumping rate, r is the radius of the cylinder, H is aquifer thickness and n_e is effective porosity.

Equation (2.1) is widely used when hydrogeologic information is restricted to a single well and there is no information about the regional hydraulic gradient. A minimum amount of hydrogeologic information is required and it delineates circular protection zones corresponding to the radius of the cylinder. Its simplicity is based on a set of restrictive assumptions, namely:

a) the aquifer is confined, homogeneous, isotropic and of constant saturated thickness;
b) the well has infinitesimal radius and is fully penetrating;
c) no regional hydraulic gradient exists, that is, the initial piezometric surface is horizontal;
d) steady-state flow conditions exist.

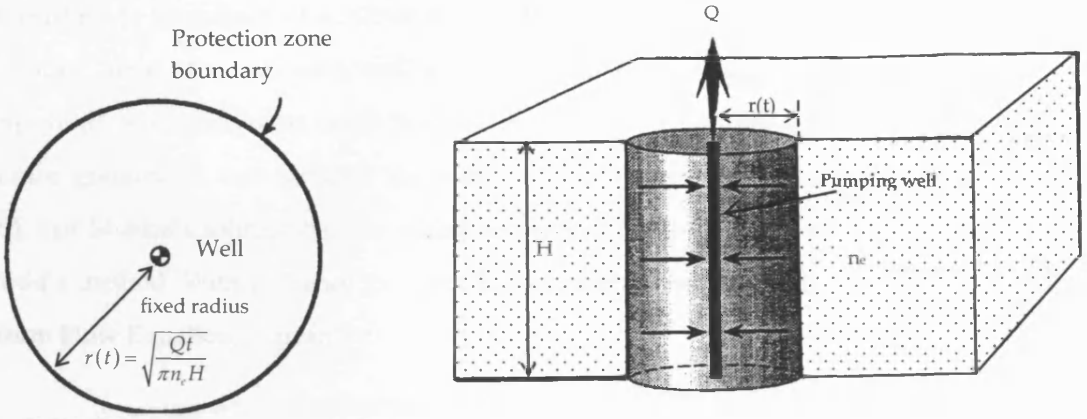

Figure 2.1 – Groundwater protection zone delineated using the Calculated Fixed Radius method.

As a result of these restrictions, the solution is only acceptable when the regional hydraulic gradient is negligible, otherwise the isochrones will deviate from a circular shape.

Forchheimer seems to have been the first to be interested in the **capture zone**, i.e. the area contributing inflow to a well pumping an aquifer where uniform flow conditions exist (Forchheimer 1935). He was mainly interested in the situation involving an unconfined aquifer and a fixed head boundary, such as a river (fig. 2.2), aiming to compute the amount of water coming from the river. He also analysed the situation in which the well is located at a large distance from the river, without visible influence to the shape of the area contributing inflow to the well, which is essentially the capture zone of the well under uniform flow conditions. Forchheimer (1935) gives equations for computing the stagnation point (X_L) and for the limit width (Y_L) of the capture zone (fig. 2.2), but he did not put forward an analytical solution for the capture zone boundary.

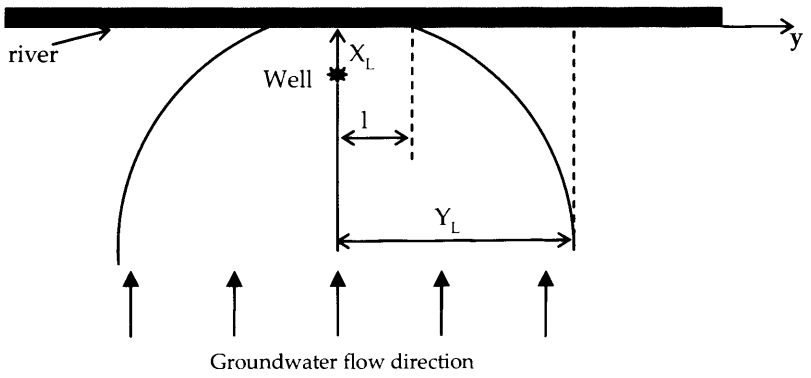

Figure 2.2 – Setup of the situation studied by Forchheimer. Capture zone of a well pumping an unconfined aquifer with influent flow from a nearby river. X_L is the distance from the well to the river (which coincides with the stagnation point), Y_L is the limit with of the capture zone, l is the with of the capture zone at the interface with the river. After Forchheimer (1935).

According to Kinzelbach et al. (1992) it was Muskat (1937) who first derived the solution for the capture zone of a pumping well in an uniform flow field. The solution involves the superposition of a steady-state radial flow solution (such as the Thiem equation) to the uniform hydraulic gradient. It was not until the publication of Todd's book, Groundwater Hydrology (1959), that Muskat's solution became widely recognised: the solution eventually became known as Todd's method. With reference to figure 2.3, Muskat's solution, hereafter designated as the **Uniform Flow Equation**, is given by:

$$\begin{cases} -\dfrac{y}{x} = \tan\left(\dfrac{2\pi TJ}{Q} y\right) \\ X_L = -\dfrac{Q}{2\pi TJ} \\ Y_L = \pm\dfrac{Q}{2TJ} \end{cases} \tag{2.2}$$

where, J is the regional hydraulic gradient and T is aquifer transmissivity. The second and third equations allow one to compute, respectively, the location of the stagnation point (X_L) and the limit width (Y_L as $x \to \infty$) of the capture zone (fig. 2.3). The first equation gives the envelope of the total capture zone.

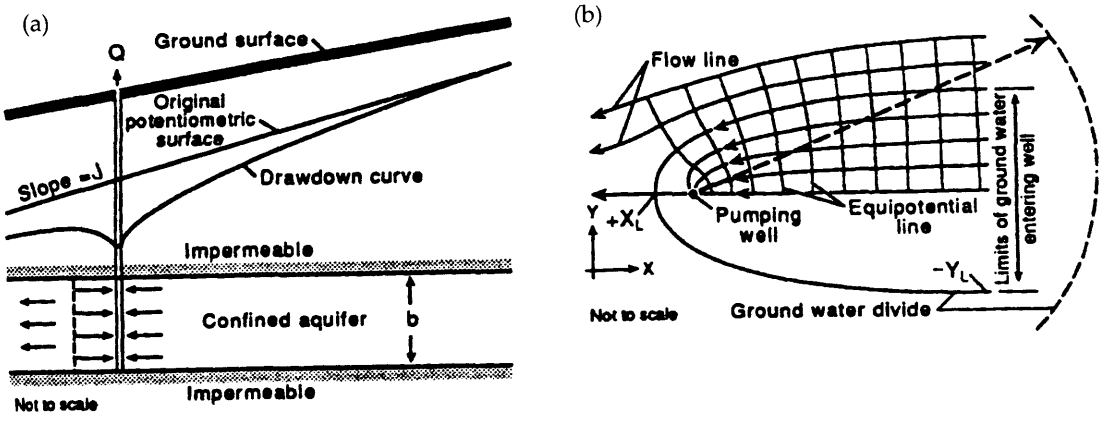

Figure 2.3 – Protection zone delineated using the Uniform Flow Equation. a) cross-section view; b) plan view. From USEPA (1994).

This analytical solution involves the same assumptions listed in page 23, for the Calculated Fixed Radius solution (equation 2.1), except that the regional uniform hydraulic gradient is non-zero.

The Uniform Flow Equation (2.2) does not involve the concept of isochrone, since it computes the area contributing inflow to a well for $t \to \infty$. Therefore, it is only useful when aiming to protect the source catchment area.

Bear and Jacobs (1965) dealt with this issue by deriving the solution for the time taken for a particle to get from any location to a pumping well (the isochrone) as:

$$t' = x' + \ln\frac{\sin\varphi}{\sin(y'+\varphi)} \tag{2.3}$$

where x', y', t' and φ are the following dimensionless parameters:

$$x' = \frac{2\pi TJ}{Q}x, \quad y' = \frac{2\pi TJ}{Q}y, \quad t' = \frac{2\pi (TJ)^2}{n_e QH}t, \quad \varphi = \tan^{-1}\left(\frac{y'}{x'}\right) \tag{2.4}$$

This solution converges to the Uniform Flow Equation (2.2) as $t \to \infty$ (fig. 2.4)

The assumptions made in the derivation of equation (2.3) are the same as for the Uniform Flow Equation (2.2). According to Grubb (1993) the aquifer is allowed to be unconfined, provided the product TJ is replaced by $\frac{K(h_1^2 - h_2^2)}{2L}$, where K is hydraulic conductivity, h is hydraulic head and L is the distance between the two locations where h_1 and h_2 are measured. In fact, the solution for the total capture zone (equation 2.2) also applies to unconfined aquifers, provided the same transformation is made.

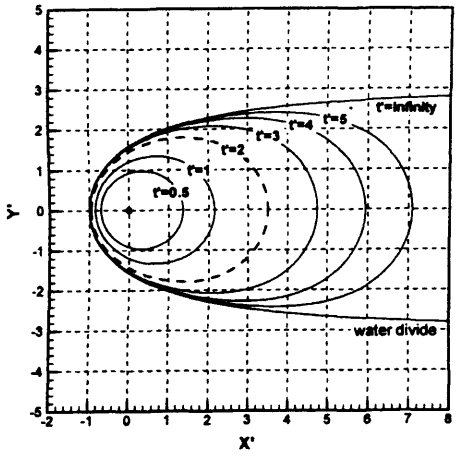

Figure 2.4 – Isochrones computed with the Bear and Jacobs (1965) analytical solution.

Equation (2.3) cannot be solved explicitly for x' and y', given a time t', but several numerical procedures have been suggested to delineate the capture zone and isochrones, usually starting from the stagnation point (McElwee 1991, USEPA 1994) or from the isochrone width for x = 0 (Barker and MacDonald 1990).

Almendinger (1994) tried to find a simpler method that approximates the solution of the isochrone in equation (2.3). He suggested the use of a Travel-time Ellipse (fig. 2.5), resulting from an empirical combination of equation (2.3) and the volume of aquifer that would provide the amount of water pumped during time t. The equation of the travel-time ellipse is:

$$\frac{(x - x_e)^2}{a_e^2} + \frac{y^2}{b_e^2} = 1 \qquad (2.5)$$

where $x_e = \frac{X^+ + X^-}{2}$ (ellipse centre), $a_e = \frac{X^+ - X^-}{2}$ (semi-major axis), $b_e = \frac{A}{\pi a_e}$ (semi-minor axis), and A is the area of the ellipse computed by algebraic manipulation of the volumetric flow equation (2.1). X^+ and X^- are the *x-axis* limits of the ellipse.

The procedure to define the travel-time ellipse is as follows:

1. the values of X^+ and X^- are computed from the Bear and Jacobs model (equation 2.3) for the travel time along the *x-axis*, the solution of which is $t' = x' - \ln(1+x')$, where the dimensionless parameters are given by equation (2.4);
2. the ellipse centre (x_c) and the semi-major axis (a_c) are evaluated from the X^+ and X^-;
3. finally, the semi-minor axis (b_c) is evaluated from $b_c = \frac{A}{\pi a_c}$, where A results from the manipulating equation (2.1) into $A = \frac{Qt}{n_e H}$.

The travel-time ellipse is a simple construction, easily implemented in a spreadsheet, and that shows good agreement with the exact analytical solution for short time isochrones. However, for large times the isochrones do not approach ellipses and the method fails (fig. 2.5). Nevertheless, it can be a useful procedure for a first assessment of the isochrone size.

The solutions so far presented, with exception to equation (2.1), imply that the hydraulic potential tends to infinity with distance and that the aquifer has infinite extent. Furthermore, no recharge was considered.

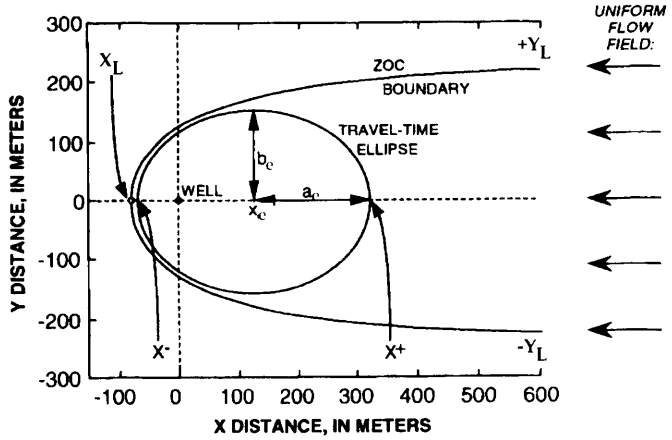

Figure 2.5 – Travel-time ellipse approximation to the Bear and Jacobs (1965) solution for isochrone delineation. After Almendinger (1994).

According to Kinzelbach et al. (1992), again it was Todd (1959) to first try to compute the capture zone taking into account the recharge rate. He suggested that equation (2.2) could still apply, but the capture zone should only be extended (starting from the stagnation point) until its area equals the recharge area (A) estimated according to:

$$A(t) = \frac{Q}{R} \tag{2.6}$$

where R is recharge. Therefore, the capture zone would extend throughout the area necessary for recharge to match discharge in time *t*. Equation (2.2) would still provide the shape of the capture

zone (see fig. 2.3b), with the up-gradient boundary located, with a somewhat arbitrary shape, at a distance that would ensure that the capture zone would enclose the estimated recharge area.

This simple procedure lacks consistency, because it combines the use of equation (2.2), which does not consider recharge, with a catchment area computed from equation (2.6) using the recharge rate during a specified finite time.

Still, in attempts to apply the solutions to finite aquifers some authors suggested crude approximations, such as using Y_L (equation (2.2) as the limit width of the capture zone at the impermeable boundary and then extend the capture zone according to equation (2.2) or according to a flow-net delineation (fig. 2.6) (USEPA 1991a, 1993a).

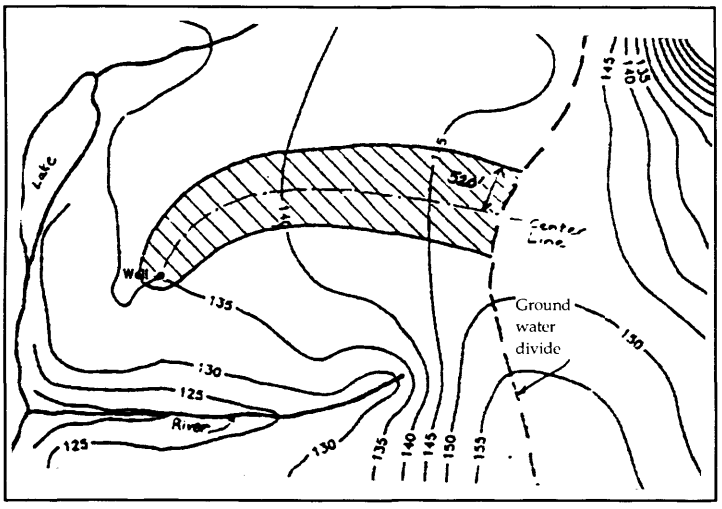

Figure 2.6 – Combination of the analytical solution for capture zone delineation (equation 2.2) and hydrogeologic mapping. From USEPA (1993a).

Other authors have preferred to derive solutions including an impermeable boundary and recharge, which is necessary in order to reach steady-state, (Barker and MacDonald 1990, Kinzelbach et al. 1992, Lerner 1992). These authors provide semi-analytical solutions usually involving the computation of the flow field, the isochrone being found either by numerical integration of the relevant equations or by **particle tracking**. Barker and MacDonald (1990), however, provide analytical solutions for the stagnation point (X_L) location and for the intersection of the isochrone with the positive *x-axis* (fig. 2.7).

Further analytic or semi-analytic solutions exist that try to overcome limitations of the original solutions of Muskat and Bear/Jacobs. Those include recharge and vertical flow (Barker and MacDonald 1990, Kinzelbach et al. 1992), partially penetrating wells in confined (Faybishenko et al. 1995) and unconfined environments (Bair and Lahm 1996), multiple wells located along a line

(Javandel and Tsang 1986), anisotropic aquifers (Zlotnik 1997), multiple wells located arbitrarily (Yeo and Lee 2003) and even for non-vertical wells (Zhan 1999, Steward and Jin 2003).

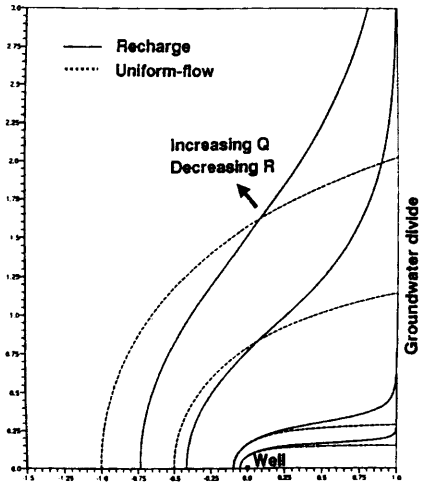

Location of stagnation point:

$$X_s = L\left(1-\sqrt{1+\frac{Q}{\pi RL^2}}\right)$$

Travel time along the positive x-axis:

$$t = -\frac{n_e H}{2R\left(1+\pi RL^2/Q\right)}\left[\ln\left(1+2\frac{\pi RLx}{Q}-\frac{\pi Rx^2}{Q}\right)+2\frac{\pi RL^2}{Q}\ln\left(1-\frac{x}{L}\right)\right]$$

Figure 2.7 – Comparison of capture zones for uniform flow model (equation 2.2) and model of Barker and MacDonald (1991). The latter, to which the equations refer, includes recharge (R) and an impermeable boundary at distance L from the well. From Barker and MacDonald (1991).

Although these solutions have not become widely used, mainly because they do not result in closed-form equations and frequently involve numerical integration of partial differential equations, they provide valuable insight into the factors that influence the size and shape of capture zones.

All the methods described so far require steady-state flow conditions. The use of transient-state conditions to delineate capture zones has not been addressed systematically. Bear and Jacobs (1965) state that those conditions would result in smaller capture zones due to water being released from storage. Some applications of Theis non-equilibrium equation have been made to calculate the radius of the primary zone of protection (USEPA 1987b, 1994), but the approach used lacks consistency. Certainly, the effect of transient-state flow conditions on the protection zone size will be important whenever there is significant seasonal recharge or cycles of pumping.

All analytical and semi-analytical solutions ignore dispersive effects, although it is known that those can play a major role in contaminant transport. Considering dispersion in a uniform flow field would result in capture zones with a wide boundary (instead of a sharp limit) with width proportional to the dispersion coefficient (Grubb 1993). The middle line of the boundary would coincide with the advective capture zone. That is, an isochrone delineated with advection represents the mean solution if Fickian dispersion is considered.

2.1.2 Multiple wells and non-uniform flow

Although the solutions described above are widely used, the assumptions involved are not appropriate for complex situations involving multiple wells, complex boundary conditions or heterogeneity of the aquifers. Different tools had to be developed taking advantage of the progress in computational techniques that took place over the last decades.

Two approaches became common. The first is based on ***numerical methods*** of groundwater flow modelling. Either using finite differences or finite elements the velocity field can be found. A ***particle tracking*** (Bear and Verruijt 1987) procedure is then implemented to delineate the capture zone. The procedure consists in tracing the streamlines by tracking the path of particles with time. Since a steady-state flow solution is used, streamlines coincide with the particles' paths. The capture zone results from the interpolation of the particles' location at a given time *t* (fig. 2.8).

Particles can be tracked backwards in time (**reverse particle tracking**), with particles being released at the well, or forward in time (**forward particle tracking**), in which case particles are released at each cell and the capture zone envelope is delineated with the starting locations of the particles that reach the well within time *t*. In continuous porous media, both procedures should return similar results[1].

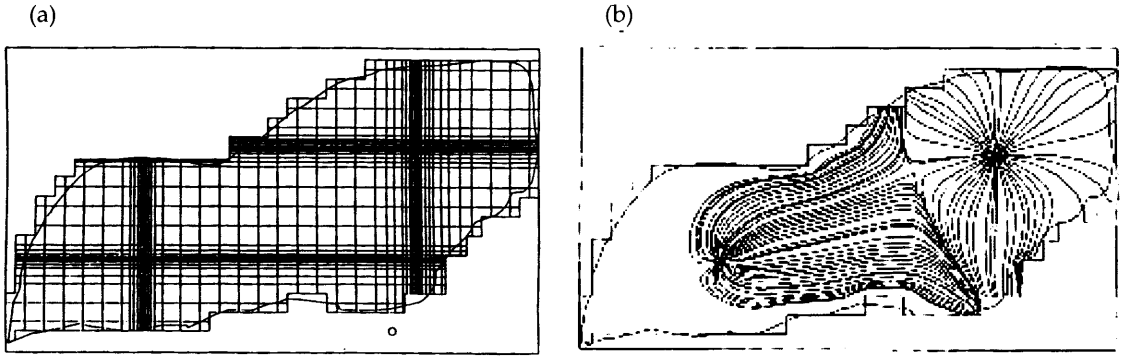

Figure 2.8 – Example of particle tracking delineation of groundwater protection zones. a) finite difference discretisation of aquifer; b) particle tracking delineation of the capture zone. After Keating and Packman (1996).

The particle tracking procedure has the same strengths and weaknesses as the numerical groundwater models. It addresses situations as complex as desired, thus reproducing better the field conditions. However, it suffers from the numerical errors resulting from using ***velocities*** that are computed using hydraulic heads that are known only at nodes of a grid. This problem is

[1] In fact forward particle tracking retrieves a more precise definition of the capture zone because the pathlines are defined for every cell, thus resulting in a more clear definition of the protection zone then in backward tracking in which only the pathlines that reach the well are delineated (van Leeuwen 2000).

particularly acute when steep gradients (such as in the vicinity of wells) are involved and in the vicinity of the stagnation point of a well (Schafer-Perini 1991, Kinzelbach et al. 1992, Zheng 1994).

Nevertheless, the strengths of this method surpass its weaknesses, so much that this method eventually became the 'standard' for dealing with realistic hydrogeologic scenarios. Several numerical codes have been developed that include particle tracking; the most successful are FLOWPATH (Franz and Guiguer 1992), for two-dimensional, steady-state conditions, and MODPATH (Pollock 1989) for three-dimensional, steady or transient-state conditions.

Numerous uses of this method have been reported, involving multiple wells, 2-D and 3-D flow modelling, transient-flow conditions and even involving the unsaturated zone (Franke et al. 1998).

Recently Rock and Kupfersberger (2002) have used a numerical model to compute capture zones using transient-state flow conditions. The authors concluded that the differences between the capture zones computed using steady-state and transient-state flow conditions can be noteworthy and should not be ignored (fig. 2.9), with the steady-state solution overestimating the upgradient extent of the protection zone. The conclusions are site specific, but their results indicate that the influence of transient-state conditions should not be overlooked, and may be particularly relevant if transient conditions (such as recharge or cycles of pumping) dominate the flow regime (Zawadzki et al. 2002, Rasmussen and Rouleau 2003).

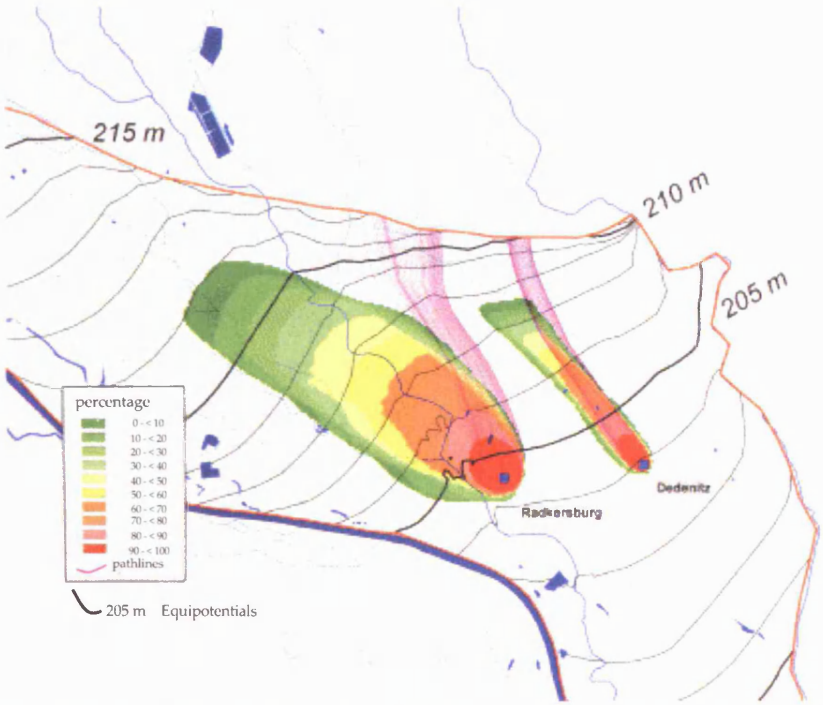

Figure 2.9 – Influence of transient-state conditions on the shape of capture zones. Comparison between capture zones delineated using the transient-state flow solution (percentage of particles per release location that reach the pumping well) and using the steady-state flow solution (pathlines). Particle tracking was used in both cases. After Rock and Kupfersberger (2002).

The major difficulty mentioned by Rock and Kupfersberger (2002) was the very intensive computational requirements, with more than one million particles being tracked. The procedure used involves an explicit particle tracking scheme, which requires releasing particles in each cell at every time step, since the flow pattern changes with time. Particles starting at one location at some time step may eventually reach the well, while other particles released at the same location at a different time step may take another path and never reach the well. Therefore, to every location it is possible to assign a probability of a particle reaching the well, even though transport is purely advective.

A second computational technique to delineate protection zones that became widely used involves the ***Analytic Elements Method***. Developed at the end of the 1970's, this method avoids the discretization of groundwater flow domain. Instead, only the boundaries of surface water bodies and aquifer features are discretized and entered into the model. Each of these boundaries is represented by a closed form analytic solution, the superposition of which provides the solution for the groundwater flow problem. Using the velocity field provided by the flow solution the capture zone and isochrones are computed through algorithms that identify the stagnation points and uses them as the basis to delineate the streamlines and groundwater divides (Bakker and Strack 1996).

Several codes use this method to delineate capture zones, but those of most common use are WHPA (USEPA 1993b) and WHAEM (Haitjema et al. 1994, Haitjema et al. 1995), both developed by the United States Environment Protection Agency (USEPA).

Compared to the particle tracking procedures, the Analytic Element Method provides more accurate capture zones, being free from the numerical interpolations required in the later method. Additionally, it delineates the actual streamlines and groundwater divides, instead of relying on the approximations provided by tracking particles (fig. 2.10). However, the Analytic Element Method is less capable of dealing with complex hydrogeologic situations, such as three-dimensional flow, highly heterogeneous media, unsaturated zone or very complex boundary conditions. Although being widely used, it still has some limitations that are not found in numerical models

2.1.3 Uncertainty-based protection zones

The methods enunciated so far are based on the adoption of precise values for the hydraulic parameters. Thus, the parameters and the resulting protection zones are ***deterministic***.

However, the information available in any hydrogeological study is always subject to ***uncertainty***. This is particularly the case for hydraulic conductivity, which often varies by orders of magnitude.

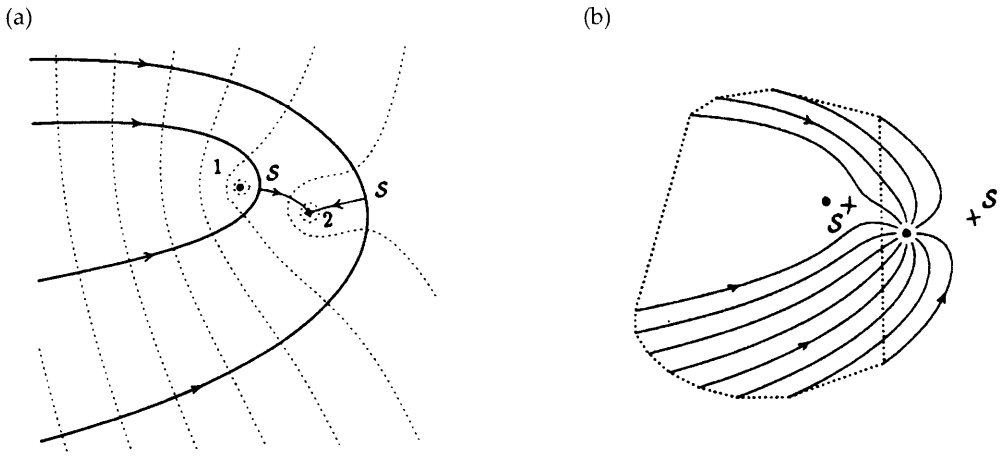

Figure 2.10 – Capture zone of two wells, delineated with: a) Analytic Elements; b) Particle tracking. S represents the stagnation points, which are correctly identified in *a)* but only approximately in *b)*. After Bakker and Strack (1996).

This uncertainty in hydraulic parameters reflects itself on uncertainty in the protection zones.

The UK Environment Agency deals with uncertainty in a qualitative way. The ***Qualitative Uncertainty Analysis*** consists in adopting capture zones that reflect the multiple acceptable calibration solutions of a numerical model (Keating and Packman 1996).

Several flow solutions are found using a plausible range of the uncertain parameters (for instance K, H, n_e, R, etc.). Particle tracking procedures delineate the capture zone for each flow solution. Therefore, for each isochrone there are several possible different capture zones. These are then used to build a *Zone of Confidence* (ZOC, the region common to all capture zones), a *Zone of Uncertainty* (ZOU, the area lying within the boundaries of all capture zones), and a *Best Estimate Zone* (BEZ, or BEC – best estimate catchment, the capture zone delineated with the parameters providing the best calibration of the flow model) (fig. 2.11).

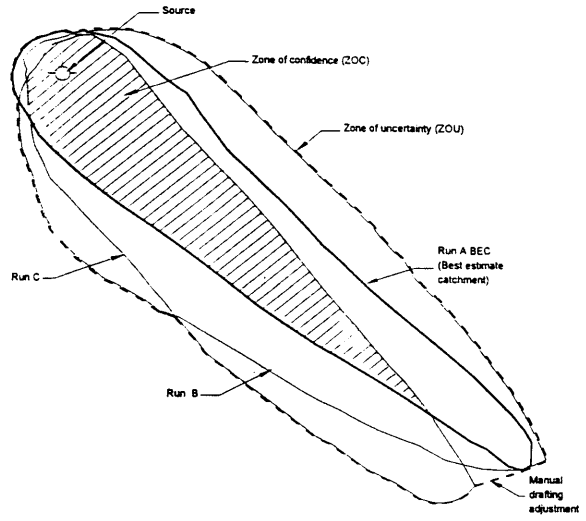

Figure 2.11 – Example of application of the Qualitative Uncertainty Analysis.

A *Confidence Index (CI)* is assigned to the Zone of Confidence:

$$\mathrm{CI}(\%) = \frac{\text{Area of ZOC}}{\text{Area of ZOU}} \times 100 \tag{2.7}$$

This index provides a measure of the confidence that can be placed on the results of the capture zone delineation process. If low index values are obtained probably further data collection should be conducted in order to reduce uncertainty in the relevant parameters.

Qualitative Uncertainty Analysis (Evers and Lerner 1995) is a very pragmatic way of dealing with uncertainty in the shape of protection zones. It is based, still, on deterministic modelling and expert judgement, resulting in Deterministic Protection Zones.

Other authors approach uncertainty by recognising that the best way to describe the variability of any hydraulic parameter is by introducing the concept of *probability density function*, which describes uncertainty by assuming that the hydraulic parameters are distributed according to continuous probability distributions. This approach, known as ***stochastic***, results in the delineation of ***probabilistic protection zones***.

The simplest solutions (Franzetti and Guadagnini 1996, van Leeuwen et al. 1998, Guadagnini and Franzetti 1999) try to delineate probabilistic protection zones assuming a known distribution for transmissivity and, using the mean and variance of the distribution, find the solution for the isochrones of a pumping well in a uniform flow field (fig. 2.12). The solutions are purely analytical. For instance van Leeuwen (2000) provides the following equation for determining the probabilistic capture zone in an aquifer with homogeneous but random distribution of transmissivity:

$$P(x',t') = \frac{1}{2} \pm \frac{1}{2}\mathrm{erf}\left(\frac{\ln T - \bar{\mu}}{\sigma\sqrt{2}}\right) \tag{2.8}$$

where P(x',t') is the probability that a particle released at x' will be captured by the well within time t'. T is the transmissivity associated with the isochrone which goes through location x' at time t'. It is assumed that transmissivity is distributed log-normally, with geometric mean $\overline{\mu}$ and variance σ^2.

This type of stochastic analytical solution is not, however, the most common approach for dealing with uncertainty in protection zones. Usually, stochastic studies involve a Monte Carlo procedure, with multiple realisations of the aquifer domain, for which the hydraulic parameters

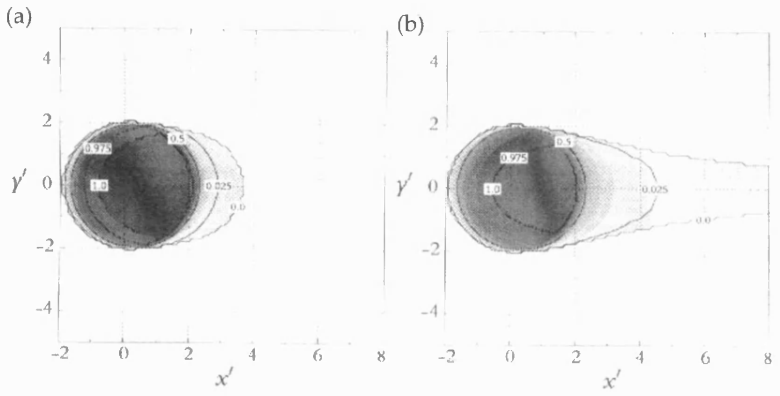

Figure 2.12 – Probabilistic protection zone. Probability contours of a particle released at (x', y') being captured by the well within time t', according to equation (2.8). a) $\sigma^2 = 0.5$; b) $\sigma^2 = 1.0$. After van Leeuwen (2000).

are randomly sampled from some given probability distribution.

In the earliest applications of stochastic modelling the uncertain hydraulic parameters were treated as spatially homogeneous throughout the aquifer (Bair et al. 1991, Bhatt 1993). Multiple realisations of the flow solution (computed using either numerical or analytic models) in conjunction with semi-analytical particle tracking procedures provided a set of capture zones to which a probability of occurrence could be assigned.

Still within the framework of spatially homogenous parameters, later studies include conditioning of the realisations on field data, such as transmissivity at known locations (Kinzelbach and Vassolo 1996, Vassolo et al. 1998).

Stochastic methods eventually came to include spatial heterogeneity of the uncertain parameters (generally transmissivity) throughout the aquifer domain (fig. 2.13). Early studies by Varljen and Schafer (1991) were subsequently refined (Franzetti and Guadagnini 1996, van Leeuwen et al. 1998, Guadagnini and Franzetti 1999, van Leeuwen 2000) to include conditioning on transmissivity.

The use of stochastic methods is nowadays a very active area of research. Further enhancements of the technique are trying to integrate a Bayesian methodology to incorporate not only uncertainty in the hydraulic parameters (for instance, uncertainty in the transmissivity values), but also on the stochastic model parameters (mean, variance and correlation structure) that characterise the distribution of, say, transmissivity (Feyen et al. 2001, Feyen et al. 2002, Feyen et al. 2003). These studies try to use the values of transmissivity and hydraulic head to condition the most probable realisations and thus to select the most likely probability density functions.

The Monte Carlo method is widely used but, since it is based on multiple realisations, the computational requirements can be quite heavy. Furthermore, conditioning the models requires an amount of field data that usually is not available. For instance, the application of Bayesian techniques by Feyen et al. (2001, 2002, 2003) used sets of 4, 25 and 41 measurements of transmissivity, the effects of conditioning becoming apparent only for 25 and 41 measurements.

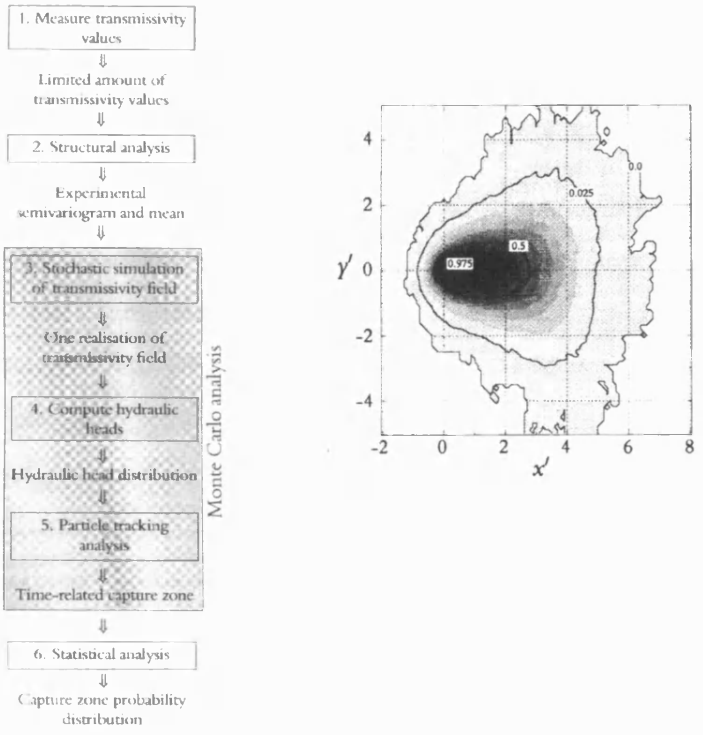

Figure 2.13 – Methodology and example of delineation of probabilistic capture zones using stochastic modelling, with multiple realisations of the transmissivity field (Monte Carlo method). After van Leeuwen (2000).

Some authors are conducting research in order to model stochastically without using Monte Carlo procedures. This has been accomplished by using the first and second moments of the distributions (more commonly log-normal distributions of T) to build covariance matrices, that allow solving the groundwater flow problem in a probabilistic manner. Particle tracking then

delineates the probabilistic protection zones (Kunstmann and Kinzelbach 2000, Lu and Zhang 2003, Zhang and Lu 2004). The results of this methodology, when compared to the Monte Carlo method, have been excellent and the technique seems promising. However, the techniques used are only valid for small to moderate variance of the hydraulic parameters, otherwise the Monte Carlo approach is still necessary to obtain probabilistic delineation of groundwater protection zones.

2.2 PROTECTION ZONES IN FRACTURED-ROCKS AQUIFERS: PREVIOUS WORK

Research concerning delineation of groundwater protection zones in fractured-rock aquifers has been very limited. Two reasons can help explain that fact:

- fractured-rock aquifers, although being an essential resource in many countries, tend to produce lower yields than continuous porous aquifers. Often, wells in hard-rock aquifers are seen as small sources not worthy of a large investment to delineate protection zones. Some fractured rocks (mainly sedimentary) can, of course, provide very significant yields and become major sources for public supply;
- difficulties in dealing with the complex hydraulic behaviour of fractured rocks have led to few publishable case studies.

Nevertheless, the significance of fractured-rock aquifers to water supply in many countries cannot be overemphasized, with the consequence that methodologies must be developed to protect those sources from pollution.

Analytical and semi-analytical solutions for delineation of protection zones (section 2.1) in general assume isotropy, homogeneity and continuity of the medium. Fractured-rock aquifers generally do not meet these assumptions. Approaches involving numerical and stochastic modelling can deal with anisotropy and heterogeneity, but no technique has yet satisfactorily overcome the problem of discontinuity of the medium.

These problems have long been identified and led to three different approaches for delineating protection zones in fractured-rock aquifers, namely:

- assuming equivalence to a porous medium aquifer (EPM approach);
- application of mapping and physical-chemical methods;
- solute transport modelling in fracture networks.

2.2.1 Equivalent Porous Medium (EPM) approach

The EPM approach assumes that fractured-rock aquifers behave hydraulically as a continuous porous medium aquifer and, accordingly, the methods described in section 2.1 apply directly. Such assumption greatly simplifies the task of delineating protection zones, making this approach undoubtedly the most applied.

Analytical, semi-analytical, numerical and stochastic techniques described in section 2.1 have been widely used in fractured-rock aquifers. Analytical and semi-analytical solutions have been used primarily for small sources (USEPA 1991a) but have also been recommended for low vulnerability sources or for sources located in low heterogeneity fractured-rock aquifers (Pochon 2002).

For small sources in hard-rock aquifers, Robins (1999) recommends estimating the capture zone area using equation (2.6) and then adjusting its shape according to the hydrogeological features of the area (namely main fracture orientation) (fig. 2.14).

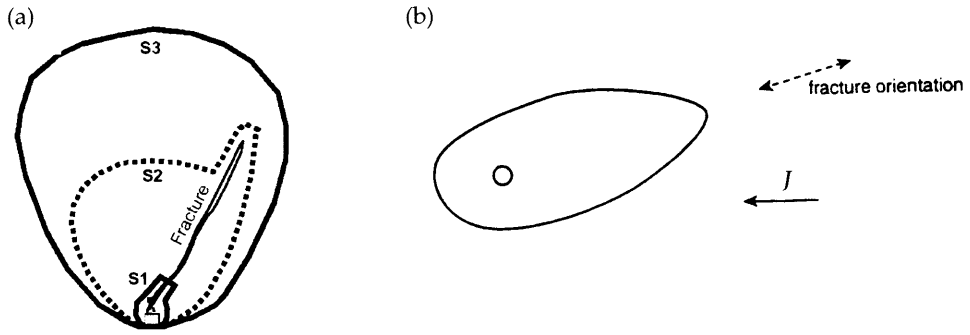

Figure 2.14 – Application of analytical solutions to fractured-rock environments with adjustments according to: a) main fracture (adapted from Pochon (2002)); **b) overall fracture orientation** (after Robins (1999).

Numerical modelling techniques are also widely applied, MODFLOW (McDonald and Harbaugh 1988) and MODPATH (Pollock 1989) being extensively used in fractured-rock aquifers (fig. 2.15). Many examples are provided by the United States Geological Survey (USGS) open-file reports (Risser and Barton 1995, Franke et al. 1998, Barton et al. 1999), but this methodology has been followed far and wide (Dassargues et al. 1996, Podgorney and Ritzi 1997, Rayne et al. 2001). The United Kingdom Environment Agency (Keating and Packman 1996, Environment Agency 2001) and the Geological Survey of Ireland (Daly 1995) also recommend the use of continuous porous media numerical codes, such as FLOWPATH (Guiguer and Franz 1991) and latterly MODFLOW, to delineate protection zones in fractured-rock aquifers.

Stochastic continuum modelling has been used in attempts to replicate the heterogeneity of fractured-rock aquifers (Niemi 1994, Hendricks-Franssen 2000, Gylling and Eriksson 2001). However, direct application of stochastic continuum modelling aiming to delineate protection zones in fractured-rock aquifers does not seem to have been attempted. Stochastic methods are a somewhat recent technique, still being developed for (the less complex) continuous porous media aquifers, and it does not come as a surprise that few applications to fractured rocks exist.

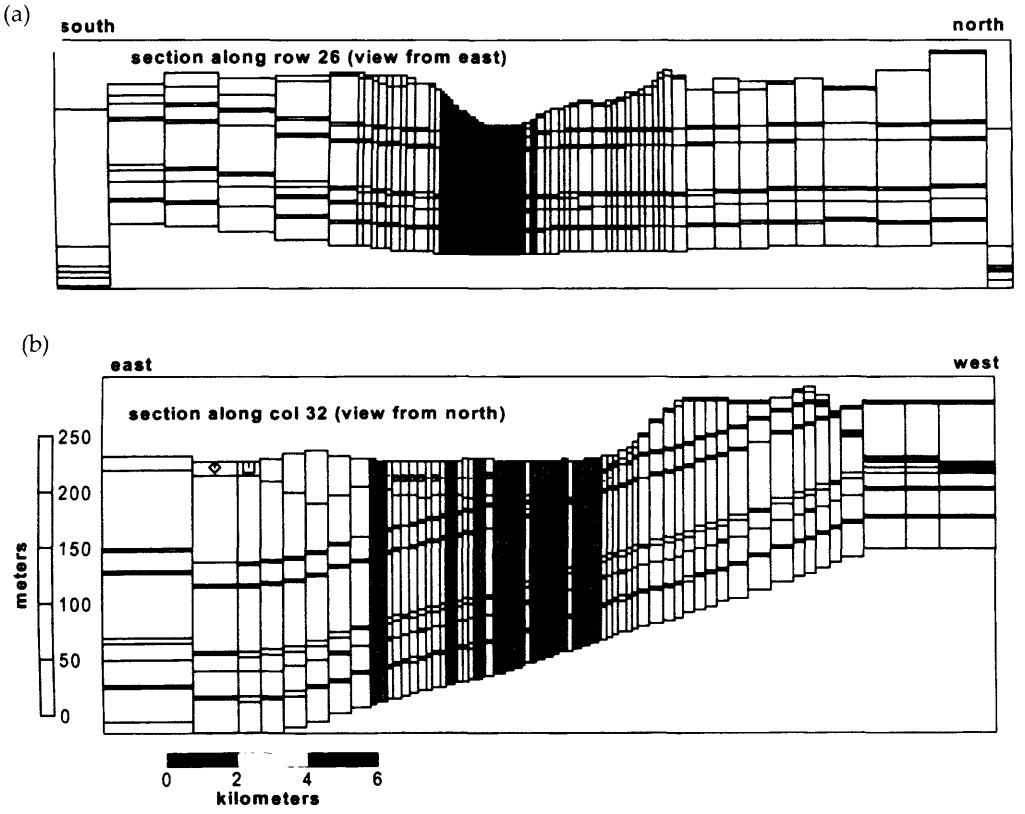

Figure 2.15 – Finite-differences discretisation of a fractured-rock aquifer. Major fractures are represented by individual cell layers. From Rayne et al. (2001).

Reliability of the EPM approach depends on the definition of a ***Representative Elementary Volume (REV)*** and on the size of it. The concept of REV consists in assigning to a point in space hydraulic parameters (for instance K and n_e) representing a certain volume of aquifer surrounding that point (fig. 2.16). Those parameters can then be used to define the 'mean' properties of the volume in question (de Marsily 1986).

Whenever it is feasible to define a REV it is possible to use any of the methods described in section 2.1, since the mean hydraulic behaviour of an aquifer block is a function of the hydraulic parameters defined for the REV, provided the aquifer block is bigger than the REV.

However, usually EPM methods are applied without any assessment on the existence of a REV or on its size (which has to be small with respect to aquifer block and the scale of study). USEPA

(1991a) gives some insight into criteria that would support treating fractured-rock aquifers as an equivalent porous medium, but no study is presented that justifies the adoption of those criteria.

In effect, it is now widely accepted that fractured rocks may exhibit REV sizes which are extremely large (de Marsily 1986) or that a REV may not exist at all (National Research Council 1996), in which case the EPM approach is not valid.

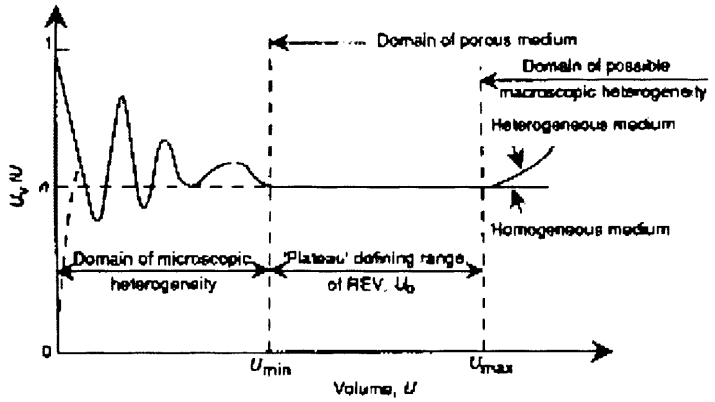

Figure 2.16 – Definition of the Representative Elementary Volume (REV) and EPM conditions. From Bear et al. (1993)

2.2.2 Mapping and physical-chemical methodologies

Heterogeneity of some fractured-rock aquifers is so conspicuous or some discontinuities are so prominent that it becomes immediately obvious that an EPM approach does not apply. This is the case for:

- wells located in or close to a fault or fracture zone, in which the hydraulic properties of the linear feature are so different from the country rock that it would not make sense to treat this composite system as a continuous aquifer. This is often the case for wells located in crystalline rock aquifers;
- wells located in sparse fracture networks, where heterogeneity is so important that a REV seems hard to define (at the scale of the predicted protection zone). This is also the case, for instance, of fractured-rock aquifers in which fracture sets show different scale lengths;
- wells exploiting deep groundwater systems, where extent and boundaries of fractured-rock aquifers are hard to define and residence times are high. This is often the case for mineral and hydrothermal water resources.

Difficulties in dealing with these situations in a quantitative manner has led some authors to abandon attempts to delineate capture zones and instead adopting mapping and physical-chemical techniques to directly identify the areas to protect.

Vulnerability mapping, particularly, has been widely applied to delineate protection zones, not only in fractured-rock aquifers but also in any aquifer type. The reasoning behind its use is that groundwater recharge mechanisms and the natural attenuation capacity of subsoil should play a dominant role when evaluating the need to protect the resource. Thus, instead of applying general restrictions over potentially hazardous activities, it is considered more cost effective to vary the type and level of restriction according to the attenuation capacity of the aquifer (Foster et al. 2002).

Discussion of the various techniques for vulnerability mapping is not within the scope of this thesis. Nevertheless, it is worth mentioning that several vulnerability classification systems have been applied for protection zone definition. DRASTIC (USEPA 1987a) and GOD (Foster et al. 2002) are well-known classifications systems that have been used for this purposes, involving not only the aquifer properties, but also the attenuation capacity of unsaturated and saturated soil.

Some vulnerability indices were developed specifically for fractured-rock aquifers. It is the case of EPIK (Doerfliger and Zwahlen 1998), specifically developed for karstic aquifers, and of DISCO.

DISCO (Pochon 2002) is a vulnerability index specifically devised by the Swiss Federal Office of Environment, Forests and Landscapes (OFEFP) for delineation of protection zones in highly heterogeneous non-karstic fractured-rock aquifers. This method is applied only when physical and chemical data shows considerable variation, regarded as an indication of aquifer vulnerability. Whenever the aquifer is envisaged as having low vulnerability, OFEFP recommends the adoption of a local protection zone, based on a fixed distance method. When the aquifer is vulnerable, but regarded as having low heterogeneity, OFEFP recommends the use of an EPM approach, with adjustments to account for the major fractures in the area (see fig. 2.14).

DISCO is based on evaluation of three parameters:

- discontinuities – mapping of discontinuities and assessment (mainly using tracer tests) of their connection to the pumping well;
- cover soil – mapping of soil type and classification according to its attenuation characteristics;
- topography – evaluation of ground slope, to assess the possibility of contaminant movement at the surface for large distances.

DISCO classifies the investigated areas into four classes, from 'Particularly Strong' to 'Weak' vulnerability. There is direct correspondence between those classes and the level of protection to implement, since the Swiss regulations require the delineation of four protection zones (table 2.1). Therefore, by defining the vulnerability index, the protection zones are also delineated (fig. 2.17).

Table 2.1 – Correspondence between vulnerability and protection zones according to the DISCO method

Protection indices (F)	*Vulnerability*	*Protection Zone*
F (0, 1)	Particularly strong	S1
F (2, 3, 4)	Strong	S2
F (5, 6, 7)	Medium	S3
F (8, 9, 10)	Weak	Catchment area

Vulnerability mapping is relatively easy to conduct and does not require detailed knowledge about the hydraulic behaviour of the aquifer. However, this advantage uncovers a conceptual weakness, since vulnerability mapping is not concerned with aquifer flow and transport properties, it does not delineate the areas that contribute inflow to the well. Therefore, vulnerability techniques may turn out to be unreliable and will probably tend to overestimate the areas in need of protection. Probably, rather than being applied directly to delineate protection zones, they should act as tools to complement delineation made by rigorous methods.

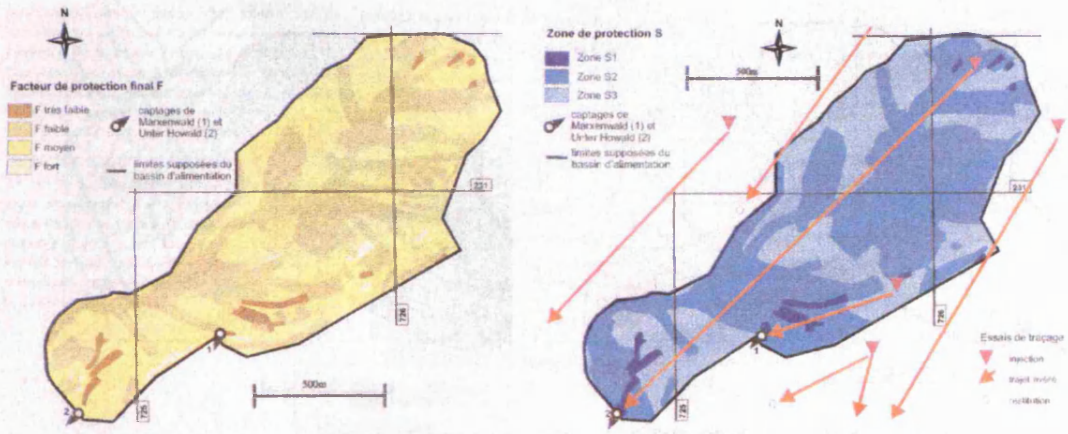

Figure 2.17 – Example of application of DISCO vulnerability mapping for delineation of groundwater protection zones in fractured-rock aquifers. From Pochon (2002).

Other mapping methods that have been applied to protection zone delineation do not involve the use of vulnerability indices. Those are based on ***flow system mapping*** and ***fracture mapping***. If information on boundaries of the aquifer system, hydraulic gradient and main fracture characteristics is gathered, protection zones can be delineated using empirical methods, such as the ones suggested by USEPA (1991b), Pochon (2002) and Robins (1999).

Some research conducted at USGS (Risser and Barton 1995, Barton et al. 1999) is particularly focused on characterising the hydraulic behaviour of fracture systems, using field observations and geophysics, to allow a more sensible delineation of the protection zones. Both Risser and Barton (1995) and Barton et al. (1999) had difficulties in characterising the hydraulic behaviour of fracture systems and chose to apply an EPM approach when delineating the protection zones.

USEPA (1991b) also applied fracture mapping, based on fieldwork and aerial photographs, for defining the total capture zone of a well, while the 10-year protection zone was delineated assuming EPM conditions and using a semi-analytical code (WHPA). The information about fracture traces is used in an empirical manner, by enlarging or restraining the catchment area according to fracture density (fig. 2.18).

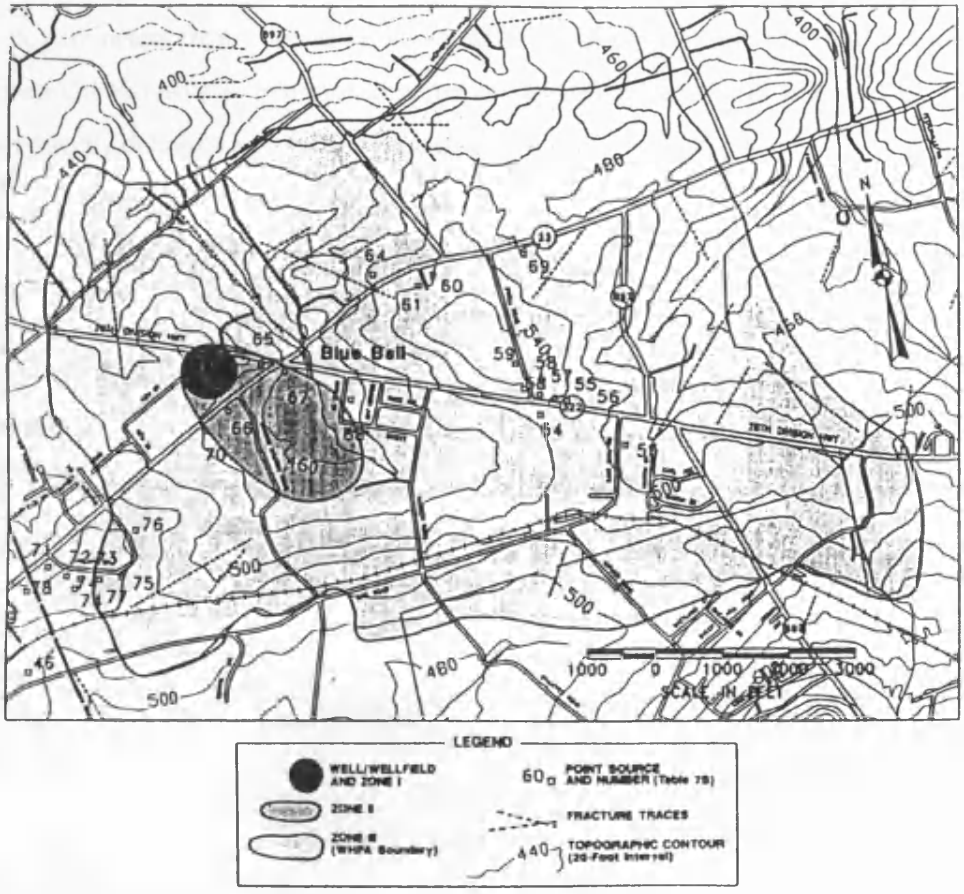

Figure 2.18 – Delineation of protection zones taking into account fracture trace mapping. Zone I was delineated with a fixed distance criteria, Zone II was delineated using WHPA semi-analytical code and Zone III was delineated empirically using the flow system boundaries and the fracture trace mapping. From USEPA (1991b).

These techniques of flow system and fracture mapping applied to protection zone delineation are based on ambiguous criteria, and implicitly rely on assumptions of continuity, homogeneity

and isotropy of the aquifer. It could be said that such methods are crude, empirical, approximations to the far more sophisticated groundwater modelling techniques.

Physical-chemical methods that estimate groundwater residence times have also been used to delineate protection zones in fractured-rock aquifers (USEPA 1991a, 1994, Pochon 2002).

Physical-chemical methods are useful because the relative age determinations (for instance using ^{18}O or tritium) provide a measure of residence time, which, if very high, can dismiss the need to delineate local protection zones. On the contrary, when the isotopic and chemical signatures vary considerably, local protection zones must be emplaced (USEPA 1991a).

In a way, this approach relates to vulnerability mapping, since the physical-chemical stability and the residence time are measures of the vulnerability of the water source.

The advantages of this approach are that the EPM assumption and detailed knowledge of hydraulic parameters are not necessary. However, this method requires much skill and experience in geochemical and isotopic interpretation and can be very expensive. In addition, this approach does not directly delineate a protection zone (fig. 2.19).

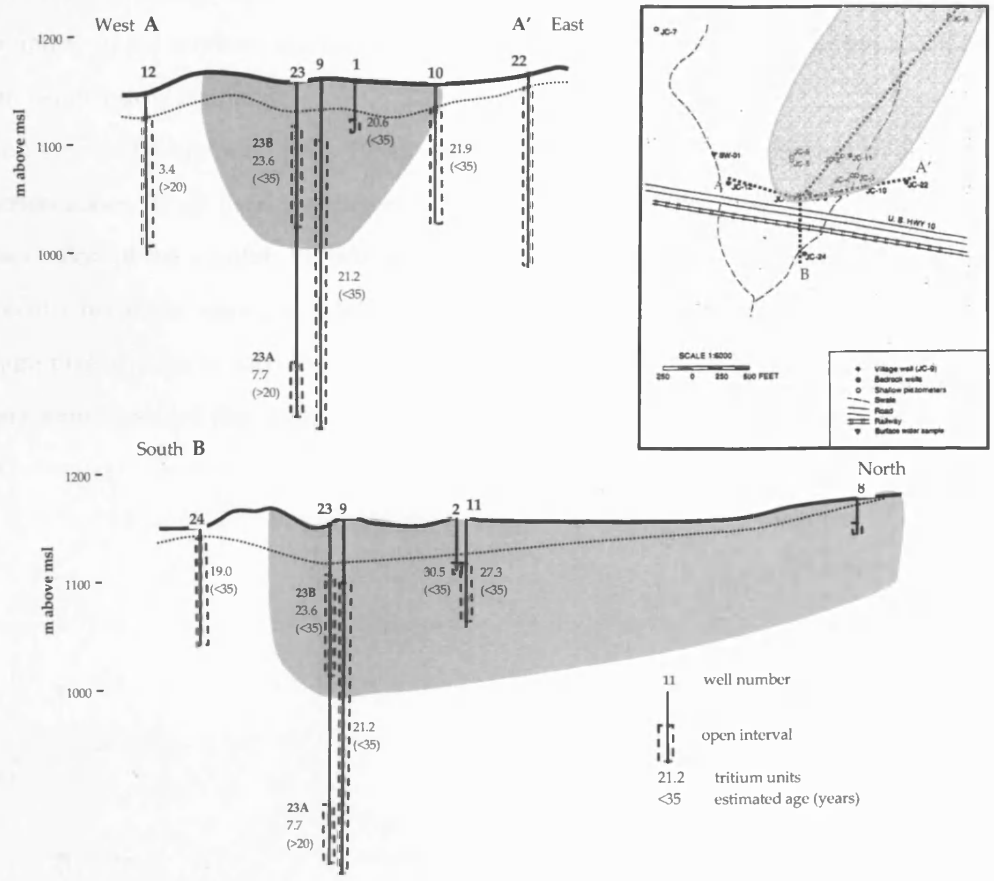

Figure 2.19 – Use of hydrogeochemistry to delineate the capture zone of a well. Tritium units allow water younger than 35 years old to be distinguishable from older water, helping to identify the capture zone. After USEPA (1991a)

Notably, this methodology is subjective and may be ambiguous. In fact, for high residence times the United States Environmental Protection Agency (1991a) suggests that local protection zones may not be necessary, while the Swiss OFEFP (Pochon 2002) considers that in those cases only the local protection zone (a fixed distance) is necessary.

2.2.3 Solute transport modelling in fracture networks

The approaches described in the previous sections (2.2.1 and 2.2.2) are widely used due to necessity rather than by choice. In fact, tools accomplishing reliable simulation of flow and solute transport in fractured-rock aquifers only recently became available.

The influential research of J. Long and collaborators in the 1980's (Long et al. 1982, Long and Witherspoon 1985, Long and Billaux 1987) regarding groundwater modelling in fracture networks led to the proliferation of Discrete Fracture Network (DFN) models. These tools aim to represent each fracture that may occur in a fractured-rock aquifer according to statistical distributions that describe the fracture network. Thus, in these models no assumptions about isotropy, homogeneity or continuity of the medium are necessary. In addition, with regard to solute transport, not even Fickian behaviour is assumed.

Bradbury and Muldoon (1993, 1994) were the first to apply DFN models to delineation of protection zones. They used fracture statistics to generate a two-dimensional fracture network representation of the aquifer. Particle tracking completed delineation of the capture zone. Since the fracture networks were generated with a Monte Carlo method, statistical methods were used to assign probabilities to each location of being part of the capture zone. Therefore, ***Probabilistic Capture Zones*** resulted (fig. 2.20).

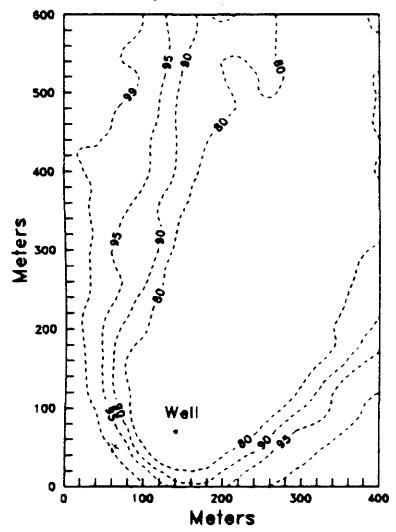

Figure 2.20 – Probabilistic capture zone delineated with a DFN model. Particle tracking was conducted in multiple realisations of the fracture network. Contours represent the percentage of particles captured by the pumping well. From Bradbury and Muldoon (1994).

Bradbury and Muldoon compared the capture zones delineated according to that procedure with the capture zones delineated applying an EPM approach. MODFLOW/MODPATH was used, with the hydraulic parameters assigned to each cell being determined from the DFN model. They concluded that the EPM approach underestimates the capture zones, not providing adequate resource protection (fig. 2.21).

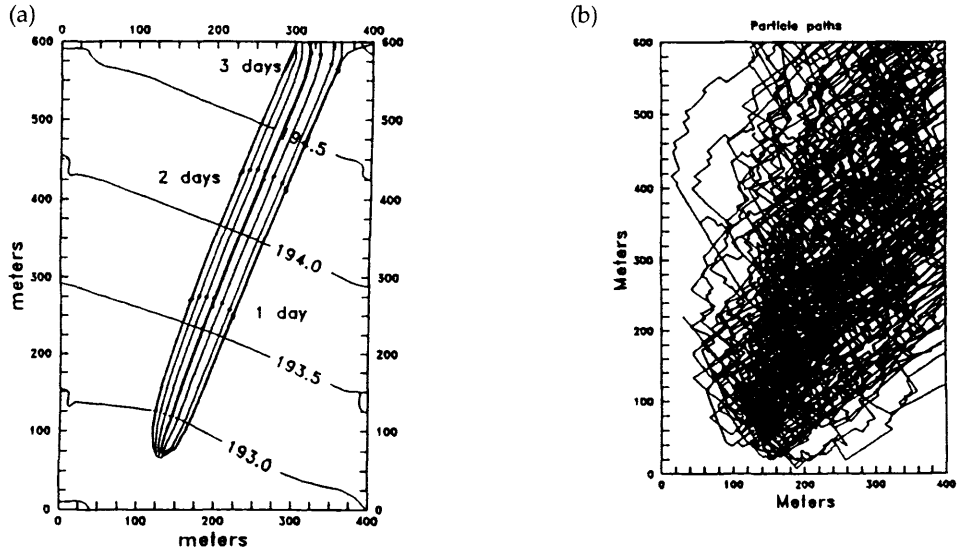

Figure 2.21 – Comparison between capture zones delineated with: a) an EPM approach (MODFLOW / MODPATH); b) a DFN model (one realisation). From Bradbury and Muldoon (1994).

Despite remarkable progress during the 1990's, with development of three-dimensional DFN models (Dershowitz et al. 1995), pipe models (Cacas et al. 1990a, Cacas et al. 1990b, Dershowitz and Fidelibus 1998), hybrid techniques coupling DFN models and stochastic continuum models (Smith et al. 1990, Clemo and Smith 1997, Parney 1999, Svensson 1999), no applications of these tools appears to have been made to protection zones until Robinson and Barker (1999).

Robinson and Barker reviewed the developments in flow and transport modelling in fractured-rock aquifers, with particular concern on ***upscaling methods***. Although DFN models have proved reliable, they require considerable computer resources when modelling large areas since every fracture is modelled discretely. Therefore, they are difficult to apply at the catchment scale at which, often, the protection zones extend. This problem of upscaling has been a subject of interest for many researchers, but Robinson and Barker (1999) suggest an hybrid approach that couples the use of the consistent DFN models with stochastic continuum models, that are more able to model aquifers at the catchment scale.

The method proposed consists in (fig. 2.22):

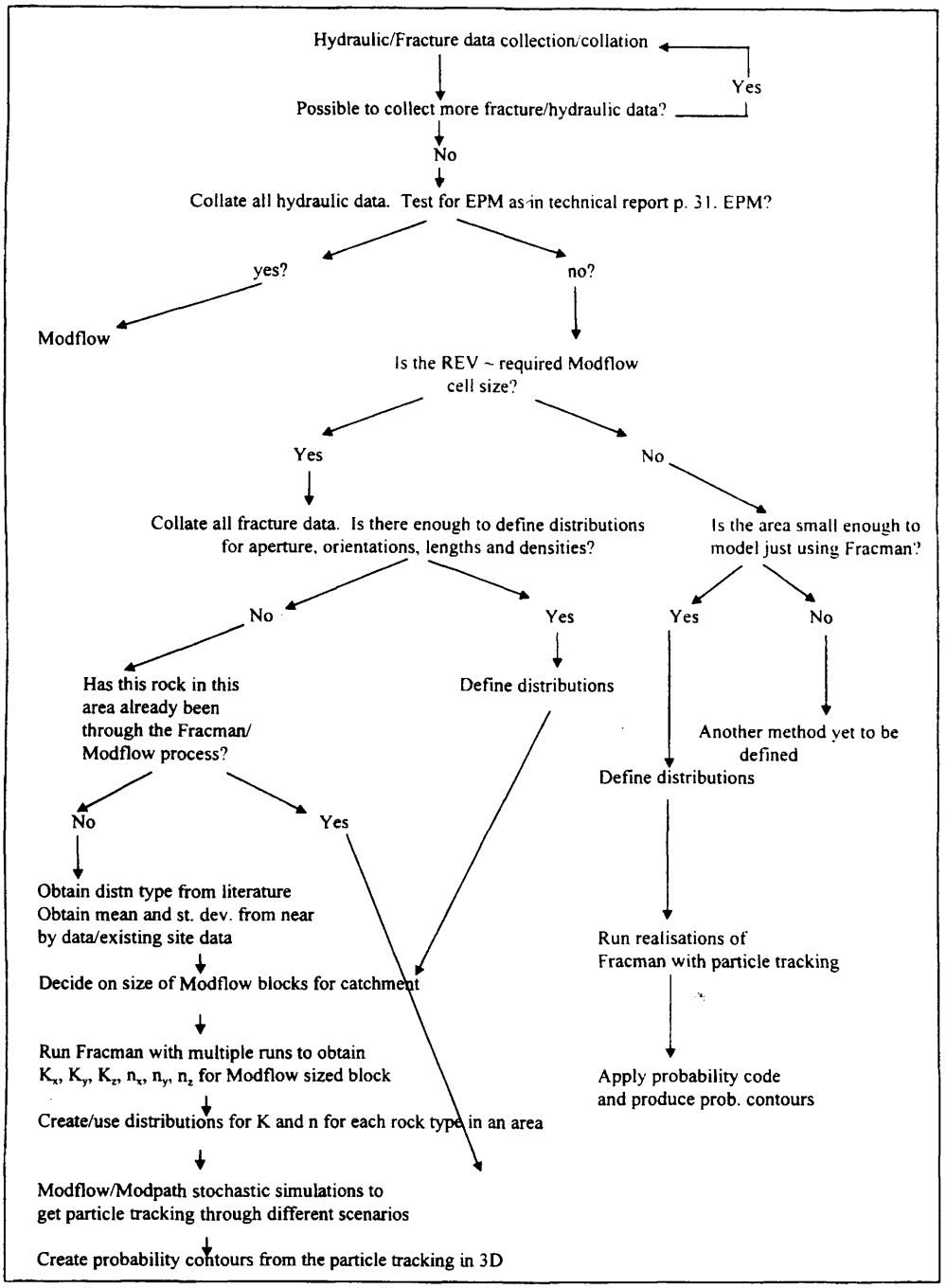

Figure 2.22 – Flow chart illustrating methodology suggested by Robinson and Barker (1999).

a) a small size domain (e.g. 100×100×100 m) is modelled using a three-dimensional DFN code. Multiple realisations of this domain would give distributions of directional hydraulic conductivity and kinematic porosity;

b) stochastic continuum modelling of the catchment scale domain, with each cell having dimensions at least of the same size of small size domain modelled previously, and hydraulic parameters sampled from the continuous distributions;

c) particle tracking conducted in the stochastic continuum domain to establish the capture zone. Since Monte Carlo simulation is used, statistical treatment of particles' locations results in probabilistic protection zones.

A pilot application of this methodology was conducted by Robinson (2003) but the methodology still needs to be tested and verified in a systematic manner. Nevertheless, this approach seems feasible, since it combines the reliability of DFN models with the powerful stochastic continuum models.

Rayne et al. (2001) used a two-dimensional DFN code to assess the influence that vertical flow in the fractured unsaturated zone would have on the size of a capture zone delineated with MODFLOW. They show that, in their case study, the capture zone should be widened by tens of metres to account for the effect of fractures in the unsaturated zone (fig. 2.23).

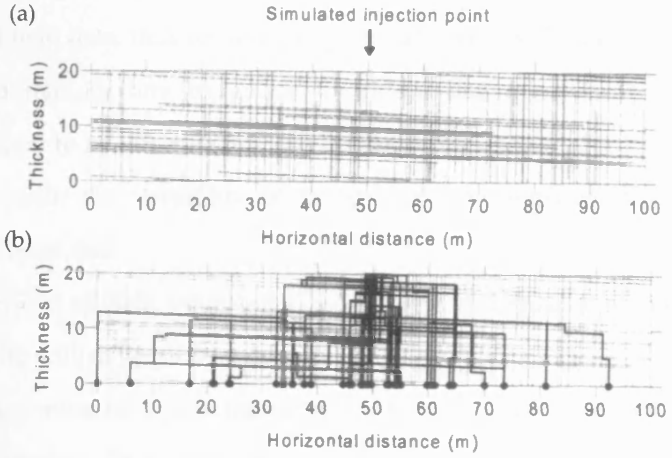

Figure 2.23 – Solute transport modelling in the unsaturated zone using a DFN model. a) simulated fractures b) particle-tracking results. Notice the dispersion induced by advective movement along sub-horizontal fractures. The protection zone delineated in the saturated medium must be enlarged to encompass the effect of transport in the unsaturated zone. From Rayne et al. (2001).

More recently Chevalier et al. (2001) used a three-dimensional DFN code to delineate protection zones in a fractured environment, concluding that fracture aperture and orientation are key elements in determining size and shape of capture zones.

2.2.4 Discussion

Although the use of DFN models is by far the most reliable method to model groundwater flow and solute transport in fractured-rock aquifers, they present some limitations that are considerable constraints on their use to delineate groundwater protection zones:

- computational requirements are very high and the models are applicable only to small areas. The use of computer clusters is probably a solution, but low budget studies such as delineation of protection zones will, generally, not be able to use such costly facilities;
- for the moment, DFN models are still very complex and difficult to use. In addition, simulations are a lengthy process that can take several hours or even days. This is also an impairment to their widespread use in routine hydrogeology studies, since it does not allow the scenario testing that is often of great importance in hydrogeology;
- some parameters required in DFN models can be quite illusive. This is the case, for instance, of the statistics of the fracture network, particularly the evaluation of the percentage of fractures that are effectively conducting water. Also, parameters such as fracture aperture can be so illusive that only educated guessing can be done;
- it has proved extremely difficult to constrain the hydraulic behaviour of DFN models with the results of field data, thus resulting in poor validation of the models.

It is considered that for any technique for delineating groundwater protection zones in fractured-rock aquifers to be effective it should combine the rigour of solute transport modelling in fractured rocks with the versatility of the continuum approach. It is necessary that the techniques acknowledge that:

- a limited amount of field information exists. This information is often restricted to data collected in the well to be protected;
- the techniques must be highly interactive, returning quick feedback on the sensitivity to parameter variation. This can hardly be achieved through the use of DFN models, where each simulation involves several realisations of the fracture network;
- the peculiarities of solute transport in fractured rocks cannot be ignored. That is, features such as 'scale effect', 'non-Fickian behaviour' and the possibility of non-existence of a REV are relevant and should not be overlooked;
- the method should perform equally well for local-scale and catchment-scale delineation of protection zones.

Mapping and physical-chemical techniques must be part of the process of developing a conceptual model of the aquifer, but should not be envisaged as methods for delineating the protection zones, since they do not provide the theoretical and physical background to support robust delineation of protection zones.

As for the vulnerability mapping approaches discussed above, they should be seen as tools to use *'a posteriori'*, when taking into account that the implementation of a protection zones should also consider a risk assessment for the activities already existing in the area.

The EPM approach is very useful, particularly when combined with stochastic modelling, as long as the main features of solute transport in fractured rocks show that a REV with reasonable size can be assumed and that Fickian behaviour is an adequate assumption. That is, it is necessary to validate the hypothesis that a fractured medium can be approximated by an equivalent porous medium.

An EPM assumption is likely to be acceptable when considering a continuous porous medium (or a network of small scale fractures) surrounding long isolated fractures (such as a fault or a dyke). In addition, situations involving fracture networks that define blocks that can be described by simple geometries (slabs, spheres or cylinders) can be dealt with using the dual-porosity concept, which involves the existence of a REV. These cases will be addressed in chapters three and four of this thesis.

Where the EPM assumption proves unacceptable, alternative ways of delineating protection zones in fractured-rock aquifers must be sought. Either using DFN models or hybrid techniques involving both DFN and stochastic continuum, the characteristic features of solute transport in fractured rock are the relevant factors that will determine the shape and size of the groundwater protection zones.

Chapter 3

PROTECTION ZONES INVOLVING FAULTS, DYKES AND OTHER LINEAR STRUCTURES

Linear structures, such as faults, fracture zones, dykes or veins, are often the target of groundwater exploration strategies. This is particularly the case when trying to site wells in hard-rock aquifers, either crystalline or metamorphic environments where permeability of sound rock tends to be low, but where tectonics may have played a role developing major fractures or installing long dykes or veins.

Linear structures can function as low-permeability barriers that obstruct groundwater flow or as high–permeability pathways that enhance flow. In either case, they can exercise a major influence on the hydraulic response of aquifers.

Since faults are fractures along which significant movement occurred, the rock adjacent to the fault is often pulverized into a clayey, soft material, the *'fault gouge'*. This material reduces the permeability and causes the fault to behave as a low-permeability barrier. Depending on the nature of the country rock, instead of a *'fault gouge'* a *'fault zone breccia'* can occur, due to broken and sheared rock. This *'breccia'* may be highly permeable becoming a preferable groundwater pathway. Finally, under some circumstances, a fault can work as a zone of preferred flow along its length, while functioning transversely as a barrier, inhibiting significant cross-flow. Such can occur, for instance, when the fault itself is very permeable, but it creates contact between very distinct rock types, so that the country-rock on one side of the fault is much more permeable than the country-rock on the other side

As for dykes and veins, it is known that they can be highly fractured due to cooling of magma or hydrothermal fluids intruded along a tensional fracture. These contraction joints can be responsible for a considerable increase in the permeability with respect to the country-rock. As such, dykes and veins can be highly permeable and may represent promising sources of water, particularly where the country-rock is non-productive (Boonstra and Boehmer 1986).

Depending on the contrast between permeability of the linear structure and permeability of the country-rock, it is possible to identify three distinct hydraulic roles for linear structures:

- tight linear structures (hydraulic conductivity $K \approx 0$), which for practical purposes are impermeable boundaries of the aquifer;
- constant head linear structures ($K \rightarrow \infty$), which can be interpreted as connecting the aquifer to a large constant head body of water and, thus, are constant head boundaries of the aquifer;
- non-constant head leaky linear structures ($0 < K < \infty$) through which flow can occur and which may have a strong influence on the hydraulic behaviour of the aquifer.

For delineation of protection zones, tight and constant-head linear structures must be regarded as hydraulic boundaries of the aquifers and should be treated as any other type of structure that imposes a boundary. Analytical solutions for those situations were discussed in the previous chapter.

Leaky faults cannot be dealt in the same way, since they influence groundwater flow, but do not constitute a boundary to the aquifer.

The storage capacity of long linear structures tends to be very low and, therefore, pumping a well in such structures may quickly deplete them. Although the country-rock alone can be unsuitable for water supply, it often transmits enough water to the linear structure to guarantee a sustained yield from a well sited in the linear structure. Therefore, the linear structure and the country-rock form a **composite aquifer system**.

Since in fractured rocks porosity and permeability are closely linked, solute transport properties are also strongly influenced by linear structures. In fact, extensive studies conducted in radioactive waste repositories, such as the Stripa and the Äspö Hard Rock Laboratory sites in Sweden, have shown that long faults and fracture zones must be modelled as discrete features, even if the remaining of the aquifer is treated as a continuum (National Research Council 1996, Andersson et al. 2002, Doe 2002).

The influence of linear structures on the hydraulic and transport behaviour is naturally reflected on the shape of groundwater protection zones. This has been widely recognised, although no quantitative method for delineating capture zones as been developed. Faults, dykes and veins are not ignored when delineating protection zones, but they are usually treated in an empirical manner (USEPA 1991a, Robins 1999, Pochon 2002).

This chapter attempts to develop analytical and semi-analytical methods for delineating protection zones for wells located in composite aquifer systems. It is assumed that for very long

structures, intersecting many fractures in the country-rock, the country-rock can be treated as an equivalent porous medium. Even if the country-rock is composed of a fracture network, the EPM approach is still valid provided the length of such fractures is negligible when compared to the single linear structure.

For the remainder of this chapter, *'linear structure'* refers to a ***non-constant head leaky*** linear structure ($0<K<\infty$) through which flow takes place and that is not amenable to be interpreted as a constant-head or an impermeable boundary, and *'aquifer'* implies a ***composite aquifer*** system involving both a linear structure and the country-rock.

Only strongly dipping linear structures will be addressed. Low dipping features, such as horizontal fractures intersected by a well, can be treated as a confined aquifer, for which the Theis solution is applicable, or as a leaky aquifer, if it receives inflow from the surrounding rock. In such cases, the Uniform Flow Equation (2.2) and Bear and Jacobs (1965) solutions for protection zone delineation are suitable and, therefore, they will be disregarded in the remainder of this chapter.

3.1 EXISTING FLOW AND TRANSPORT MODELS

Although the influence of faults and fracture zones on the hydrodynamic behaviour of aquifers is widely acknowledged, few quantitative studies are available concerning that influence. Extensive studies were conducted in radioactive waste repositories where faults and fracture zones play a vital role, such as at the Stripa (Sweden), Äspö Hard rock Laboratory (Sweden), Yucca Mountain (United States), Sellafield (United Kingdom) and Grimsel (Switzerland) test sites. However, those studies were concerned primarily with the possibility of a contaminant reaching a major conductive feature, rather than with the influence of the linear structure on the drawdown field imposed by a pumping well.

Hicks et al. (2000) deal specifically with the influence of a fault zone heterogeneity and the consequences of fault movement in the flow and contaminant transport in hydrogeological systems. Those authors apply numerical modelling to synthetic aquifer systems, including complex fault structures, with each fault itself showing anisotropy and heterogeneity along its length. The same study addresses the relevance of the stress state to the hydraulic behaviour of the faulted system. However, no considerations are made about the relevance of faults under a pumping regime.

Despite the scientific relevance of the works conducted in the high-level radioactive waste sites and the research of Hicks et al. (2000), these studies rely on highly complex modelling and therefore are not suitable for the purposes outlined for this chapter.

Of greater interest are analytical and semi-analytical solutions that allow us to construct velocity fields, raising the possibility of finding solutions for delineating protection zones in composite aquifer systems. In this respect, petroleum engineering has shown greater interest in faulted aquifer systems than has hydrogeology.

Gringarten and Witherspoon (1972) derived the solution for drawdown imposed by a well pumping a single vertical fracture. The fracture is treated as a plane of finite extent with uniform flux; the country-rock is assumed to release water to the fracture at a uniform rate per unit area. Gringarten and Witherspoon found the solution only for points located in the fracture, or at 45° and 90° to it. It is not possible to compute the velocity field at every point (fig. 3.1). Furthermore, numerical integration of the relevant equations is necessary, which introduces complexity into the procedure.

Some refinements were made to this model in order to retrieve the fracture and aquifer hydraulic parameters using only drawdown at the well, either neglecting well storage effects (Gringarten and Ramey 1974) or including those same effects (Ramey and Gringarten 1976). Although giving insight on the hydraulic behaviour of single finite fractures, these solutions cannot be used to delineate groundwater protection zones.

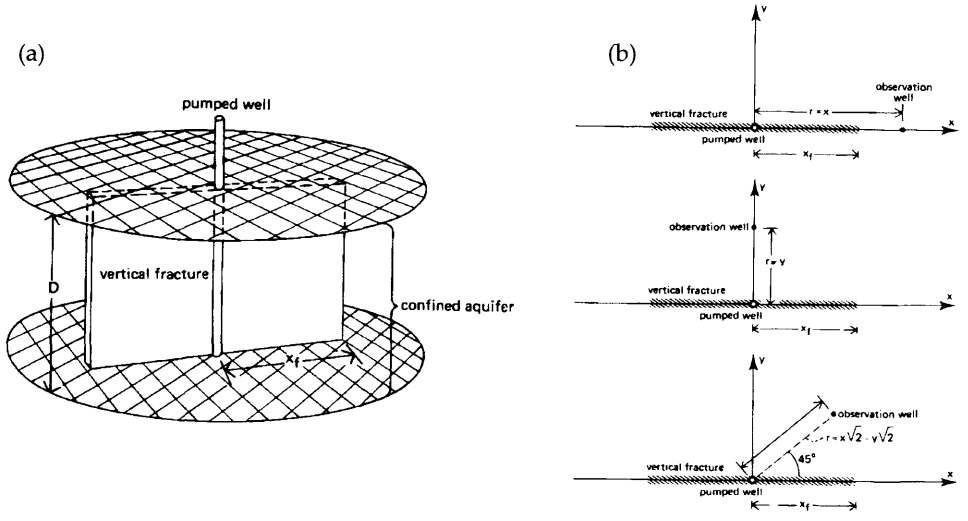

Figure 3.1 – Layout studied by Gringarten and Witherspoon (1972). a) finite fracture with uniform flux; b) observation well locations for which analytical solutions for drawdown were found. From Kruseman and Ridder (1994).

Other authors addressed the problem from a perspective more related to hydrogeology and derived the solution for drawdown imposed by a well located in an infinite vertical dyke receiving inflow from the less permeable country-rock. Flow in the dyke was assumed parallel to the dyke walls, implying that the dyke has uniform and small width (fig. 3.2). Solutions were found for drawdown in the well (Boonstra and Boehmer 1986) and in the country-rock (Boehmer and Boonstra 1987).

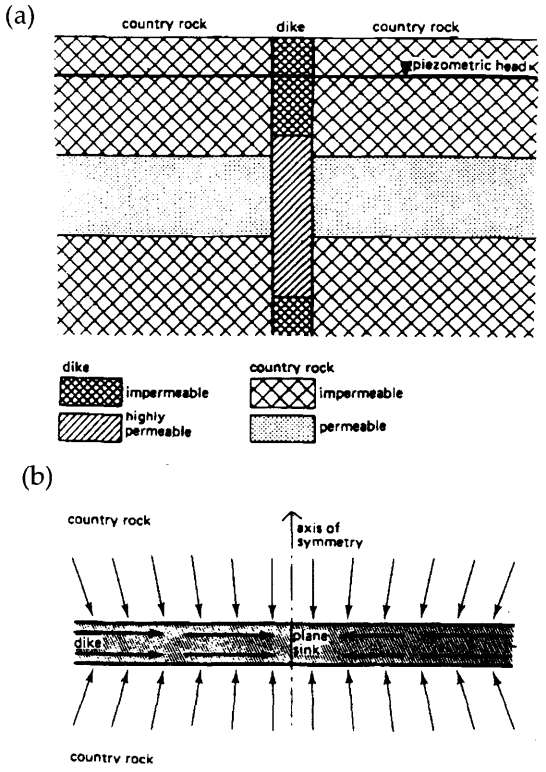

Figure 3.2 – Layout of the composite dyke-aquifer system studied by Boonstra and Boehmer (1986). a) cross-sectional view; b) plan view.

However, these solutions are applicable only to early and medium pumping times, which means that steady-state behaviour is not included, rendering those solutions unsuitable for delineation of capture zones based on advective transport.

Haneberg (1995) studied the effects of vertical faults on steady-state groundwater flow using analytical solutions for horizontal flow. The solutions clearly show the relevance of including the effect of long faults when interpreting regional flow systems. However, only one-dimensional analysis was done and it is not possible to include the effect of radial flow due to pumping.

The issue of transient hydraulic behaviour imposed by a well pumping an aquifer in which a vertical leaky fault separates two regions with the same hydraulic parameters was addressed first by Yaxley (1987), who considered that the fault had isotropic behaviour, and later by Shan et al. (1995).

Both works considered that the fault has no storage, has infinite horizontal extent and that flow in it is assumed proportional to the instantaneous pressure difference across the fault (fig. 3.3). Shan et al. (1995) assumes that the fault connects vertically two aquifers separated by an aquitard and is a source of recharge to the pumped aquifer (fig. 3.3b).

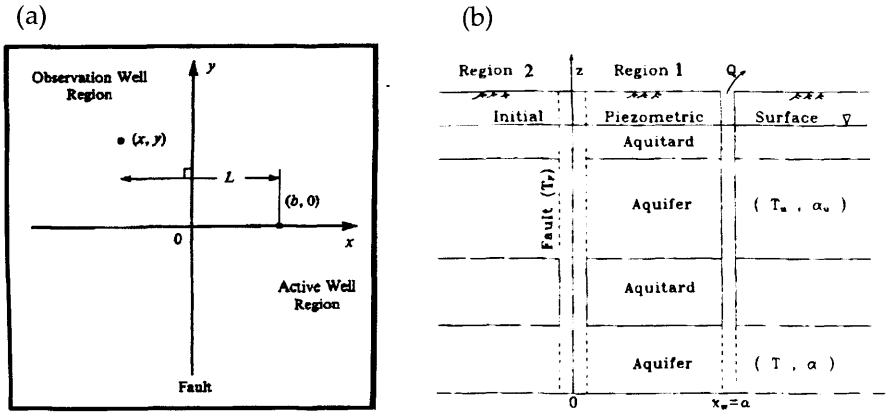

Figure 3.3 – Composite aquifer system, with a fault separating an aquifer into two regions. a) layout studied by Yaxley (1987); b) layout studied by Shan et al. (1995).

The analytical solutions obtained by Yaxley (1987) and Shan et al. (1995) are valid for any region of the aquifer and the authors present sample type-curves. In addition, Yaxley (1987) studied the asymptotic behaviour of the relevant functions, concluding that they differ from the asymptotic behaviour of the Theis solution by a constant amount.

As for transport models in composite aquifer systems, no specific models are known, not even considering advection as the only transport mechanism. Analytical solutions for one-dimensional transport in a single fracture have been derived (Bear et al. 1993) and, at the limit, dual-porosity transport solutions can be used to interpret tracer tests in which a fault may play a prominent role (Maloszewski et al. 1999). Nevertheless, no solutions are known involving radial flow that can be of assistance in delineation of protection zones involving transport along a fault, fracture zone, dyke or vein.

3.2 DELINEATING CAPTURE ZONES IN COMPOSITE AQUIFER SYSTEMS

The existing analytical flow solutions involving a well pumping a composite aquifer system are unsuitable for protection zone delineation, either directly, or through indirect techniques, such as using the velocity field. The Gringarten and Witherspoon (1972) solution cannot be used because it is not valid for every location, while the Boonstra and Boehmer (1986) solution is not

valid for steady-state conditions. Yaxley's (1987) solution is the most encouraging one, but it does not cover the possibility that the well might be located in the linear structure.

In order to overcome these difficulties a general analytical solution is developed here.

3.2.1 Analytical model

3.2.1.1 Geometry and model assumptions

Figure 3.4 depicts the geometry of the model. It includes a vertical linear infinite structure with transmissivity T_f, storage coefficient S_f and effective porosity n_f, embedded in a country-rock of hydraulic conductivity K, effective porosity n_e and thickness H. A Cartesian coordinate system was adopted, with the x-axis coinciding with the linear structure. The well is located on the positive y-axis at a distance $d\ [0,\infty]$ from the origin and pumps at constant flow rate Q. Prior to pumping, a regional uniform hydraulic gradient J is oriented at an angle θ with the x-axis[1].

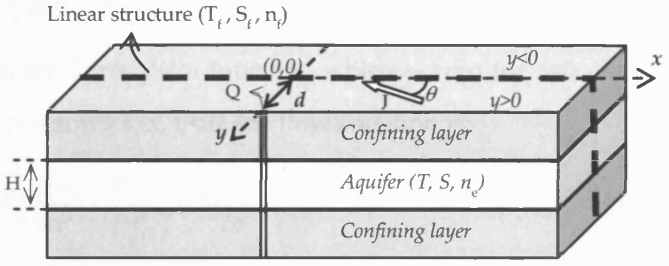

Figure 3.4 – Model geometry. T_f, S_f, and n_f applies to the plane y=0.

The geometry of the model is very similar to the one adopted by Yaxley (1987), except that the well can be located on the linear structure (d=0), the linear structure is assigned a storage capacity and the initial piezometric level may not be horizontal. The solution method is also similar to the one used by Yaxley (1987).

The following assumptions apply:

- the linear structure is planar, vertical, and of uniform width, homogeneous and isotropic;
- the linear structure has infinite length and fully penetrates the aquifer, so that flow in it and in the country-rock will be two-dimensional;
- the country-rock is homogenous and isotropic on both sides of the linear structure;
- the composite aquifer is fully confined, of uniform thickness and of infinite length;

[1] Notice that no width is assigned to the linear structure, so that its transmissivity and storage coefficient already refer to the products of the infinitesimal width of linear structure by hydraulic conductivity and by specific storage, respectively.

- the well fully penetrates the aquifer, there are no well-losses or well-storage and the pumping rate is constant;
- before pumping initiates, drawdown in the whole system is zero.

3.2.1.2 Governing equations

The pumping well can be located outside the linear structure ($d \geq 0$), and therefore it is necessary to consider drawdown on the area being directly pumped by the well, $s_1(x, \mathbf{y>0}, t)$, and drawdown in the area that is partly isolated by the linear structure, $s_2(x, \mathbf{y<0}, t)$ (fig. 3.4). In addition, drawdown in the linear structure, $s_f(x, t)$, must also be studied. For the moment, the uniform (regional) hydraulic gradient is not applied.

Drawdown in the side of the country-rock where the well is located, $s_1(x, \mathbf{y>0})$, is expressed by the transient flow equation:

$$T\left(\frac{\partial^2 s_1}{\partial x^2}+\frac{\partial^2 s_1}{\partial y^2}\right)+Q\delta(x)\delta(y-d)=S\frac{\partial s_1}{\partial t} \qquad y>0 \qquad (3.1)$$

where $\delta(z)$ represents the Dirac delta function, which is zero for $z \neq 0$. On the other side of the linear structure, for drawdown $s_2(x, \mathbf{y<0})$, the flow equation is:

$$T\left(\frac{\partial^2 s_2}{\partial x^2}+\frac{\partial^2 s_2}{\partial y^2}\right)=S\frac{\partial s_2}{\partial t} \qquad y<0 \qquad (3.2)$$

Drawdown in the linear structure, $s_f(x)$, is given by:

$$HT_f\frac{\partial^2 s_f}{\partial x^2}-T\left(\frac{\partial s_2}{\partial y}-\frac{\partial s_1}{\partial y}\right)_{x=0}=S_f\frac{\partial s_f}{\partial t} \qquad y=0 \qquad (3.3)$$

As a result of symmetry of the model, there will be no flow across the line $x = 0$:

$$\left.\frac{\partial s_1}{\partial x}\right|_{x=0}=\left.\frac{\partial s_2}{\partial x}\right|_{x=0}=0 \qquad (3.4)$$

At infinite distance from the well, for any finite time, drawdown is zero:

$$\begin{cases} s_1(x,+\infty,t)=s_2(x,-\infty,t)=0 & \textit{(in the y direction)} \\ s_1(\pm\infty,y,t)=s_2(\pm\infty,y,t)=s_f(\pm\infty,t)=0 & \textit{(in the x direction)} \end{cases} \qquad (3.5)$$

Drawdown in the country-rock and in the linear structure will be the same at their interface:

$$s_1(x,0,t)=s_2(x,0,t)=s_f(x,t) \qquad (3.6)$$

The initial condition is that drawdown is zero throughout the whole system:

$$s_1(x,y,0)=s_2(x,y,0)=s_f(x,0)=0 \qquad (3.7)$$

Finally, in order to represent the possibility of the well being located in the linear structure, it is necessary to include a further boundary condition. If the well is located outside the linear

structure, i.e. $d>0$, then $\left.\frac{\partial s_f}{\partial x}\right|_{x=0} = 0$. If the well is located in the linear structure at the coordinate axis origin, $d = 0$ and $\left.\frac{\partial s_f}{\partial x}\right|_{x=0} = \frac{Q}{2HT_f}$. This behaviour can be represented by a single equation:

$$\left.\frac{ds_f}{dx}\right|_{x=0} = \frac{Q}{2HT_f}\mu(-d) \tag{3.8}$$

where $\mu(z)$ is the unit step function, which equals zero for z<0 and one for z≥0.

3.2.1.3 Transient-state solution for drawdown

The solution of the problem can best be found by using Laplace transforms with respect to time, using p as the Laplace transform variable and with the transformed variable being represented with an over-bar, such as in $\overline{s}_1$.

Using the initial condition (equation 3.7), the Laplace transform of drawdown in the country-rock (equations 3.1 and 3.2) and in the linear structure (equation 3.3) are given, respectively, by :

$$T\left(\frac{\partial^2 \overline{s}_1}{\partial x^2} + \frac{\partial^2 \overline{s}_1}{\partial y^2}\right) + \frac{Q}{p}\delta(x)\delta(y-d) = pS\overline{s}_1 \qquad y > 0 \tag{3.9}$$

$$T\left(\frac{\partial^2 \overline{s}_2}{\partial x^2} + \frac{\partial^2 \overline{s}_2}{\partial y^2}\right) = pS\overline{s}_2 \qquad y < 0 \tag{3.10}$$

$$HT_f \frac{\partial^2 \overline{s}_f}{\partial x^2} - T\left(\frac{\partial \overline{s}_2}{\partial y} - \frac{\partial \overline{s}_1}{\partial y}\right)_{x=0} = pS_f\overline{s}_f \qquad y=0 \tag{3.11}$$

The method for finding the solution to these partial differential equations involves the use of Fourier cosine transforms[1] with respect to x, using ε as the Fourier cosine transform variable and with the transformed variable being represented with a tilde, such as in $\tilde{s}_1$. The transform of drawdown in the aquifer area where the well is located, using the boundary condition represented by equation (3.4), becomes[2]:

$$T\left(-\varepsilon^2\tilde{\overline{s}}_1 + \frac{d^2\tilde{\overline{s}}_1}{dy^2}\right) + \frac{Q}{p}\sqrt{\frac{2}{\pi}}\delta(d-y) = pS\tilde{\overline{s}}_1 \qquad y > 0 \tag{3.12}$$

or:

---

[1] Different scientific and technical fields use slightly different formulae for the Fourier cosine transform. Throughout this thesis the following definitions apply (Wolfram 1999):

a) the Fourier Cosine transform of a function f(x) is given by $\tilde{f}(\varepsilon) = \sqrt{2/\pi}\int_0^\infty f(x)\cos(\varepsilon x)dx$

b) the Inverse Fourier cosine transform of a function $\tilde{f}(\varepsilon)$ is given by $f(x) = \sqrt{2/\pi}\int_0^\infty \tilde{f}(\varepsilon)\cos(\varepsilon x)d\varepsilon$

[2] The following operational property of the Fourier cosine transform was used $\frac{\partial^2 f(x)}{\partial x^2} = -\varepsilon^2\tilde{f}(\varepsilon) - \sqrt{\frac{2}{\pi}}\left.\frac{\partial f(x)}{\partial x}\right|_{x=0}$.

$$\frac{d^2\tilde{\tilde{s}}_1}{dy^2}+\frac{Q}{pT}\sqrt{\frac{2}{\pi}}\delta(d-y)=\Lambda^2\tilde{\tilde{s}}_1 \qquad y<0 \qquad (3.13)$$

where $\Lambda^2=\frac{pS}{T}+\varepsilon^2$. The solution of that ordinary differential equation is:

$$\tilde{\tilde{s}}_1(y)=e^{-y\Lambda}C_1+e^{y\Lambda}C_2+\frac{e^{(-y+d)\Lambda}Q\mu(y-d)}{\sqrt{2\pi}Tp\Lambda}-\frac{e^{(y-d)\Lambda}Q\mu(y-d)}{\sqrt{2\pi}Tp\Lambda} \qquad y>0 \qquad (3.14)$$

C_1 and C_2 being constants of integration. The boundary condition, equation (3.5), that when y goes to infinity $\tilde{\tilde{s}}_1$ goes to zero[1], gives $C_2 = 0$ (assuming $\Lambda \geq 0$), hence:

$$\tilde{\tilde{s}}_1(y)=e^{-y\Lambda}C_1+Q\frac{e^{(-d+y)\Lambda}+e^{(-y+d)\Lambda}\mu(y-d)-e^{(y-d)\Lambda}\mu(y-d)}{\sqrt{2\pi}Tp\Lambda} \qquad y>0 \qquad (3.15)$$

Using the same procedure for drawdown on the other side of the linear structure ($y<0$), equation (3.10), the solution of the ordinary differential equation resulting from the Fourier cosine transform of (3.10), combined with boundary condition (3.4) is:

$$\tilde{\tilde{s}}_2(y)=e^{-y\Lambda}C_3+e^{y\Lambda}C_4 \qquad y<0 \qquad (3.16)$$

Boundary condition (3.5) implies $C_3 = 0$, so:

$$\tilde{\tilde{s}}_2(y)=e^{y\Lambda}C_4 \qquad y<0 \qquad (3.17)$$

Using boundary condition (3.6) on equations (3.15) and (3.17) gives:

$$C_1=\tilde{\tilde{s}}_f-Q\frac{e^{-d\Lambda}+e^{d\Lambda}\mu(-d)-e^{-d\Lambda}\mu(-d)}{\sqrt{2\pi}Tp\Lambda} \qquad (3.18)$$

$$C_4=\tilde{\tilde{s}}_f \qquad (3.19)$$

Replacing this results into equations (3.15) and (3.17):

$$\tilde{\tilde{s}}_1(y)=e^{-y\Lambda}\left(\tilde{\tilde{s}}_f-Q\frac{e^{-d\Lambda}+e^{d\Lambda}\mu(-d\Lambda)-e^{-d\Lambda}\mu(-d)}{\sqrt{2\pi}Tp\Lambda}\right)+Q\frac{e^{(-d+y)\Lambda}+e^{(-y+d)\Lambda}\mu(y-d)-e^{(y-d)\Lambda}\mu(y-d)}{\sqrt{2\pi}Tp\Lambda} \qquad y>0 \qquad (3.20)$$

$$\tilde{\tilde{s}}_2(y)=e^{y\Lambda}\tilde{\tilde{s}}_f \qquad y<0 \qquad (3.21)$$

of which the first derivative with respect to y at the interface linear structure – country-rock $(y=0)$ are, respectively:

$$\left.\frac{d\tilde{\tilde{s}}_1}{dy}\right|_{y=0}=-\Lambda\tilde{\tilde{s}}_f-Q\sqrt{\frac{2}{\pi}}\frac{e^{-d\Lambda}\left[-1+\mu(-d)\right]}{Tp} \qquad (3.22)$$

$$\left.\frac{d\tilde{\tilde{s}}_2}{dy}\right|_{y=0}=\Lambda\tilde{\tilde{s}}_f \qquad (3.23)$$

[1] Notice that the condition that when x goes to infinity $\tilde{s}_1$ goes to zero (equation 3.5) is implicit in the use of the operational property related to the Fourier cosine transform of the second derivative of a function (see footnote 2 on previous page).

The Fourier cosine transform of drawdown in the linear structure (equation 3.11), with respect to x, using the same operational property already mentioned to retrieve equation (3.12), is:

$$HT_f\left(-\varepsilon^2\tilde{\bar{s}}_f-\sqrt{\frac{2}{\pi}}\frac{d\bar{s}_f}{dx}\bigg|_{x=0}\right)-T\left(\frac{d\tilde{\bar{s}}_2}{dy}-\frac{d\tilde{\bar{s}}_1}{dy}\right)_{y=0}=pS_f\tilde{\bar{s}}_f \qquad \text{y=0} \qquad (3.24)$$

Using boundary condition (3.8), equations (3.22) and (3.23), it is possible to get, after some manipulation, the equation for drawdown in the linear structure:

$$\tilde{\bar{s}}_f=-\frac{Qe^{-d\Lambda}\left[-2+e^{d\Lambda}\mu(-d)+2\mu(-d)\right]}{\sqrt{2\pi}p\left(pS_f+2T\Lambda+\varepsilon^2T_fH\right)} \qquad \text{y=0} \qquad (3.25)$$

Replacing equation (3.25) into equation (3.21) allows obtaining drawdown in the $y<0$ side of the linear structure:

$$\tilde{\bar{s}}_2(y)=-\frac{Qe^{(-d+y)\Lambda}\left[-2+e^{d\Lambda}\mu(-d)+2\mu(-d)\right]}{\sqrt{2\pi}p\left(pS_f+2T\Lambda+\varepsilon^2T_fH\right)} \qquad \text{y < 0} \qquad (3.26)$$

On the other side of the linear structure ($y>0$) the solution is obtained by replacing equation (3.25) into equation (3.20). Using the definition of the unit step function and after algebraic manipulation the transient-state solution for drawdown in the country-rock, (y>0) is:

$$\tilde{\bar{s}}_1(y)=\frac{Q}{\sqrt{2\pi}Tp}\left[\frac{e^{-\Lambda|-d+y|}}{\Lambda}-\frac{e^{-(d+y)\Lambda}\left(pS_f+H\varepsilon^2T_f+3T\Lambda\mu(-d)\right)}{\Lambda\left(2T+H\Lambda T_f+pS_f\right)}\right] \qquad \text{y > 0} \qquad (3.27)$$

3.2.2 Well located in the linear structure (d = 0)

Of particular interest is the delineation of capture zones when the pumping well is located in a linear structure more permeable than the country-rock. In this case, the equation for transient-state drawdown in the linear structure (3.25) reduces to:

$$\tilde{\bar{s}}_f=-\frac{Q}{\sqrt{2\pi}p\left(pS_f+2T\Lambda+\varepsilon^2T_fH\right)} \qquad (3.28)$$

while the equations that describe drawdown in either side of the linear structure (3.26 and 3.27) reduce to the same equation, with drawdown being represented by the same variable $s(x, y)$:

$$\tilde{\bar{s}}(y)=-\frac{Qe^{-|y|\Lambda}}{\sqrt{2\pi}p\left(pS_f+2T\Lambda+\varepsilon^2T_fH\right)} \qquad (3.29)$$

Using $T = KH$, where K and H are, respectively, hydraulic conductivity and thickness of the country-rock, the inverse Fourier cosine transform of equation (3.29) is:

$$\bar{s}(x,y)=\frac{-Q}{\pi p}\int_0^{\infty}\frac{e^{-|y|\Lambda}\cos(x\varepsilon)}{pS_f+2KH\Lambda+\varepsilon^2T_fH}d\varepsilon \qquad (3.30)$$

Drawdown in the linear structure given by equation (3.28) can also be obtained from equation (3.29) provided y is set to zero (boundary condition (3.6)). From this point onwards we shall refer only to the drawdown solution in the country-rock, bearing in mind that any solutions presented hereafter are applicable to the linear structure as long as $y = 0$.

3.2.2.1 Steady-state solution

The physical model used as the basis for deriving the transient-state solutions of drawdown, given by equations (3.28) and (3.29), is not compatible with reaching an equilibrium state, in which drawdown at every location stabilises for some given time (say $t \to \infty$). In fact, the transient-state solution indicates that drawdown increases continuously regardless the time of observation. Therefore, no equilibrium hydraulic heads will exist. However, it is reasonable to assume that steady-state flow conditions can be invoked.

In fact, the hydraulic head difference (and therefore the drawdown difference) between any two locations (x_0, y_0) and (x_1,y_1) will tend to a constant value as time tends to infinity. Thus, at any given moment in time, the drawdown difference Δs between any observation location and a reference location (x_0, y_0) can be computed from equation (3.30), as:

$$\Delta\bar{s}(x,y) = \frac{-Q}{\pi p}\int_0^\infty \frac{e^{-|y|\Lambda}\cos(x\varepsilon) - e^{-|y_0|\Lambda}\cos(x_0\varepsilon)}{pS_f + 2KH\Lambda + \varepsilon^2 T_f H}d\varepsilon \tag{3.31}$$

The steady-state flow solution can be found from equation (3.31) by letting time go to infinity, $t \to \infty$ or correspondingly, by letting the Laplace transform variable go to zero, $p \to 0$. The relation $\Lambda^2 = \frac{pS}{T} + \varepsilon^2$ becomes $\Lambda = \varepsilon$. Using the final-value theorem for the Laplace transform (Chen and Stone 1993, Mathias and Zimmerman 2003), which states that $\lim_{t\to\infty} F(t) = \lim_{p\to 0} p\bar{F}(p)$ as long as $\lim_{t\to\infty} F(t)$ exists, which is the case of Δs that converges for a constant value (but not for s, which has no limit), it is possible to retrieve **the steady-state flow solution**:

$$\Delta s(x,y) = \frac{-Q}{\pi H}\int_0^\infty \frac{e^{-|y|\varepsilon}\cos(x\varepsilon) - e^{-|y_0|\varepsilon}\cos(x_0\varepsilon)}{2K\varepsilon + \varepsilon^2 T_f}d\varepsilon \tag{3.32}$$

This can be further simplified by using a reference point along the Y axis, (0,Y_0). Equation (3.32) can be rewritten, in terms of Fourier cosine transform:

$$\Delta\tilde{s}(y) = \frac{-Q}{\pi H}\left(\frac{e^{-|y|\varepsilon} - e^{-Y_0\varepsilon}}{2K\varepsilon + \varepsilon^2 T_f}\right) \tag{3.33}$$

It is to this steady-state solution that we shall refer throughout this section.

If, by analogy with what is usually assumed for the steady-state solution in a homogeneous aquifer, it is admitted that drawdown is negligible at some finite distance from the pumping well, steady-state drawdown can then be computed according to the equation above, as long as the reference point $(0,Y_0)$ is assumed as having zero drawdown difference. In such situation, Y_0 has the same physical meaning as the steady-state **radius of influence** of a well pumping a homogeneous aquifer and $\Delta\tilde{s}(y)$ can be replaced in equation (3.33) by $\tilde{s}(y)$.

3.2.2.2 Advective velocities

The aim of finding solutions for drawdown is ultimately to enable computation of advective velocities, which are necessary for the delineation of isochrones and capture zones based on transport by advection.

The components of advective velocity are:

$$v_x = -\frac{K}{n_e}\frac{\partial s}{\partial x},\ v_y = -\frac{K}{n_e}\frac{\partial s}{\partial y} \tag{3.34}$$

Again, attention is drawn to the fact that although transient-state drawdown increases continuously, without converging for a specific value, the same does not occur with advective velocities along the x and y directions that, being the result of drawdown differences, will converge to a constant value as $t \to \infty$. The final-value theorem can once again be used on the first derivatives of the transient-state drawdown equation (3.30), with respect to x and with respect to y, to retrieve the **steady-state hydraulic gradients**:

$$\frac{\partial s}{\partial x} = \frac{Q}{\pi H}\int_0^\infty \frac{e^{-\varepsilon|y|}\sin(x\varepsilon)}{2K+\varepsilon T_f}d\varepsilon \tag{3.35}$$

$$\frac{\partial s}{\partial y} = \mathrm{sgn}(y)\frac{Q}{\pi H}\int_0^\infty \frac{e^{-\varepsilon|y|}\cos(x\varepsilon)}{2K+\varepsilon T_f}d\varepsilon \tag{3.36}$$

Notice that these same equations can be found by derivation of the steady-state flow equation (3.32), bearing in mind that the reference point (X_0,Y_0) is constant.

The trigonometric functions are expandable into exponential functions, according to:

$$\cos(x\varepsilon) = \frac{e^{-ix\varepsilon}+e^{ix\varepsilon}}{2},\ \text{and}\ \sin(x\varepsilon) = i\frac{e^{-ix\varepsilon}-e^{ix\varepsilon}}{2} \tag{3.37}$$

Using these transformations into equations (3.35) and (3.36) makes it possible to evaluate the integrals and computing the directional advective velocities. If the complex number $z_1 = ix-|y|$ is used for simplification, then:

$$v_x = \frac{K}{2n_e}\frac{iQ}{H\pi T_f}\left\{e^{-\frac{2K}{T_f}z_1}W\left(\frac{-2K}{T_f}z_1\right) - e^{\frac{2K}{T_f}(2ix-z_1)}W\left[\frac{2K}{T_f}(2ix-z_1)\right]\right\} \quad (3.38)$$

$$v_y = -\mathrm{sgn}(y)\frac{K}{2n_e}\frac{Q}{H\pi T_f}\left\{e^{-\frac{2K}{T_f}z_1}W\left(\frac{-2K}{T_f}z_1\right) + e^{\frac{2K}{T_f}(2ix-z_1)}W\left[\frac{2K}{T_f}(2ix-z_1)\right]\right\} \quad (3.39)$$

where W(x) is the Theis Well function, or the exponential integral function, given by $W(x) = \int_x^\infty \frac{e^{-u}}{u}du$. These results were obtained using the software *Mathematica*.

3.2.2.3 Introducing a regional uniform hydraulic gradient

If the regional hydraulic gradient is considered, there is already a constant advective velocity before pumping begins, with components described by:

$$v_x = -\frac{KJ}{n_e}\cos(\theta),\ v_y = -\frac{KJ}{n_e}\sin(\theta) \quad (3.40)$$

where J is the uniform hydraulic gradient and θ is the angle between hydraulic gradient orientation and the linear structure (the *x-axis*) (fig. 3.4).

Due to the linearity of the velocity equations, the components of velocity due to the hydraulic gradient (equation 3.40) can be added to the velocity components imposed by the pumping well and described by equations (3.38) and (3.39), resulting in:

$$v_x = -\frac{K}{n_e}\left\{J\cos(\theta) - \frac{iQ}{2H\pi T_f}\left[e^{-\frac{2K}{T_f}z_1}W\left(\frac{-2K}{T_f}z_1\right) - e^{\frac{2K}{T_f}(2ix-z_1)}W\left[\frac{2K}{T_f}(2ix-z_1)\right]\right]\right\} \quad (3.41)$$

$$v_y = -\frac{K}{n_e}\left\{J\sin(\theta) + \mathrm{sgn}(y)\frac{Q}{2H\pi T_f}\left[e^{-\frac{2K}{T_f}z_1}W\left(\frac{-2K}{T_f}z_1\right) + e^{\frac{2K}{T_f}(2ix-z_1)}W\left[\frac{2K}{T_f}(2ix-z_1)\right]\right]\right\} \quad (3.42)$$

Because drawdown in the linear structure equals drawdown in the country-rock for $y = 0$ (boundary condition represented by equation (3.6)), then advective velocity in the linear structure (v_f) equals equations (3.41), provided y is set to zero, K is replaced by K_f and n_e by n_f, the linear structure hydraulic parameters.

3.2.2.4 Analytical solution for the stream function

The stream function describes the line whose tangent is parallel to the velocity vector at each location. That is, the stream function defines the flowlines, and because steady-state conditions exist, those coincide with particles path. If the stream function is defined analytically, then it is possible to visualise the path of particles released at any location in the aquifer.

The stream function (ψ) is defined as (de Marsily 1986):

$$d\psi = v_x dy - v_y dx \tag{3.43}$$

Along the flowlines the stream function (ψ) is constant.

The solution for the exact differential equation (3.43) is of the form (Weisstein 1999):

$$\psi = \int v_x dy + \int \left[-v_y - \frac{\partial\left(\int v_x dy\right)}{\partial x} \right] dx \tag{3.44}$$

Using the velocity components provided by equations (3.47) and (3.48), the stream function can be found as:

$$\psi = \frac{-Q}{4\pi H n_e}\left\{ 2\tan^{-1}\left(\frac{x}{|y|}\right) - \left[ie^{-\frac{2K}{T_f}z_1} W\left(\frac{-2K}{T_f}z_1\right) - ie^{\frac{2K}{T_f}(2ix - z_1)} W\left[\frac{2K}{T_f}(2ix - z_1)\right]\right] \mathrm{sgn}(y) \right\} + \frac{K}{n_e} J[x\sin(\theta) - y\cos(\theta)] \tag{3.45}$$

This result was obtained using the software *Mathematica* to evaluate the integrals.

3.2.3 Well located outside the linear structure (d>0)

The case of well located at a distance d>0 from the linear structure can also be computed from the general equations (3.25) to (3.27). In this case, the hydraulic behaviour on the two sides of the linear structure is different and, thus, three equations are necessary to describe transient-state drawdown in the aquifer.

$$\tilde{\tilde{s}}_f = \sqrt{\frac{2}{\pi}} \frac{Qe^{-d\Lambda}}{p\left(pS_f + 2T\Lambda + \varepsilon^2 T_f H\right)} \qquad \text{y=0} \tag{3.46}$$

$$\tilde{\tilde{s}}_1(y) = \frac{Q}{\sqrt{2\pi T}p}\left[\frac{e^{-\Lambda|-d+y|}}{\Lambda} - \frac{e^{-(d+y)\Lambda}\left(pS_f + H\varepsilon^2 T_f\right)}{\Lambda\left(2T + H\Lambda T_f + pS_f\right)} \right] \qquad \text{y>0} \tag{3.47}$$

$$\tilde{\tilde{s}}_2(y) = \sqrt{\frac{2}{\pi}} \frac{Qe^{(-d+y)\Lambda}}{p\left(pS_f + 2T\Lambda + \varepsilon^2 T_f H\right)} \qquad \text{y<0} \tag{3.48}$$

Following a procedure similar to the one used for the case $d = 0$, it is possible to find the steady-state flow solutions, directional advective velocities and the stream functions for this case.

The steady-state flow solutions are given by:

$$\Delta\tilde{s}_1(y) = \frac{Q}{\sqrt{2\pi T}}\left[\frac{e^{-\varepsilon|-d+y|}}{\varepsilon} - \frac{e^{-(d+y)\varepsilon} H\varepsilon^2 T_f - 2e^{-(d+Y_0)\varepsilon}}{\varepsilon\left(2T + H\varepsilon T_f\right)} \right] \qquad \text{y > 0} \tag{3.49}$$

$$\Delta\tilde{s}_2(y) = \frac{Q}{H}\sqrt{\frac{2}{\pi}}\left(\frac{e^{-\varepsilon(-d+y)} - e^{-\varepsilon(-d+Y_0)}}{2K\varepsilon + \varepsilon^2 T_f} \right) \qquad \text{y<0} \tag{3.50}$$

Notice that in this case, and for simplicity of the analytical solutions, the reference point $(0,Y_0)$ is located on the y<0 side of the linear structure. The considerations regarding the existence of a location where drawdown is zero are also applicable in this case, allowing to compute steady-state drawdown from the equations above, in the same manner as described in section 3.2.2.1.

Advective velocities are given, for **y>0**, by the following equations:

$$v_x = -\frac{K}{n_e}\left\{J\cos(\theta) - \frac{Q}{\pi HT_f}\left[-\frac{4HT_f dxy}{T\left[d^4 + 2d^2(x-y)(x+y) + (x^2+y^2)^2\right]} + ie^{\frac{2K}{T_f}z_2}W\left(\frac{2K}{T_f}z_2\right) - ie^{\frac{2K}{T_f}(z_2-2ix)}W\left(\frac{2K}{T_f}(z_2+2ix)\right)\right]\right\} \quad (3.51)$$

$$v_y = -\frac{K}{n_e}\left\{J\sin(\theta) + \frac{Q}{\pi HT_f}\left[\frac{HT_f(d+y)}{Tx^2 + T(d+y)^2} - \frac{HT_f|d-y|}{Tx^2 + T|d+y|^2} - ie^{\frac{2K}{T_f}z_2}W\left(\frac{2T}{HT_f}z_2\right) - ie^{\frac{2K}{T_f}(z_2-2ix)}W\left(\frac{2K}{T_f}(z_2+2ix)\right)\right]\right\} \quad (3.52)$$

where z_2 is a complex number given by $z_2 = d - ix + y$.

On the other side of the linear structure, for **y<0**, the velocities are:

$$v_x = -\frac{K}{n_e}\left\{J\cos(\theta) + \frac{iQ}{H\pi T_f}\left[e^{\frac{2K}{T_f}(d-ix-y)}W\left(\frac{2K}{T_f}(d-ix-y)\right) - e^{\frac{2K}{T_f}(d+ix-y)}W\left(\frac{2K}{T_f}(d+ix-y)\right)\right]\right\} \quad (3.53)$$

$$v_x = -\frac{K}{n_e}\left\{J\sin(\theta) + \frac{Q}{H\pi T_f}\left[e^{\frac{2K}{T_f}(d-ix-y)}W\left(\frac{2K}{T_f}(d-ix-y)\right) + e^{\frac{2K}{T_f}(d+ix-y)}W\left(\frac{2K}{T_f}(d+ix-y)\right)\right]\right\} \quad (3.54)$$

As for the stream functions, they were also computed by a similar procedure as in the case $d=0$. The stream function is represented by the following equation for the **y>0** side of the linear structure:

$$\psi = \frac{-Q}{2\pi Hn_e}\left\{\frac{2\left[(d-y+|d-y|)\tan^{-1}\left(\frac{x}{d-y}\right)\right]}{d-y} + 2\tan^{-1}\left(\frac{x}{-d+y}\right) + ie^{\frac{2K}{T_f}z_2}W\left(\frac{2K}{T_f}z_2\right) - ie^{\frac{2K}{T_f}(z_2+2ix)}W\left[\frac{2K}{T_f}(z_2+2ix)\right]\right\} + \frac{K}{n_e}J\left[x\sin(\theta) - y\cos(\theta)\right] \quad (3.55)$$

while on the other side (**y<0**) of the linear structure:

$$\psi = \frac{-Q}{2\pi Hn_e}\left\{2\tan^{-1}\left(\frac{x}{-d+y}\right) - ie^{\frac{2K}{T_f}(d-ix+y)}W\left[\frac{2K}{T_f}(d-ix+y)\right] + ie^{\frac{2K}{T_f}(d+ix+y)}W\left[\frac{2K}{T_f}(d+ix+y)\right]\right\} + \frac{K}{n_e}J\left[x\sin(\theta) - y\cos(\theta)\right] \quad (3.56)$$

These results were obtained using the software *Mathematica* to perform the integrals.

3.3 IMPLEMENTATION OF A SEMI-ANALYTICAL PROCEDURE FOR DELINEATING PROTECTION ZONES

Equations (3.45), (3.55) and (3.56), describing the stream function in composite aquifers systems, are quite complex, making difficult their inversion to obtain the x and y pairs that define a constant stream function, or in the case of interest to us, the pathline that defines the envelope of the capture zone. In addition, integration of the inverse of advective velocities (equations (3.41) and (3.42) and equations (3.51) to (3.54)) to find the equations describing the isochrones, was also not possible.

Therefore, it was necessary to find alternative ways of using the analytical formulae derived in the previous section to delineate the total capture zone and the isochrones.

Because the stream function is constant along a streamline, contour maps of the stream function in an x, y aquifer domain will define all possible particle paths, allowing visualisation of the capture zone.

As for isochrones, the procedure implemented involves particle tracking that relies on computation of advective velocity at any location, using equations (3.41) and (3.42) in the case of well located in the linear structure, or equations (3.51) through (3.54) when the well is located in the country-rock.

3.3.1 Well located in the linear structure (d = 0)

Delineating the pathlines and, consequently, the source capture zone involves evaluating the stream function in an x, y domain. Those values are then contoured in order to establish the pathlines.

Since evaluation of the stream function is purely analytical it was decided to use the *Mathematica* (Wolfram 1999) software to build a *Mathematica Notebook*. The notebook not only evaluates the stream function (equation (3.45)), but also computes the equipotentials (equation (3.33)) imposed by the pumping well and produces the contours that materialise pathlines and capture zone.

The influence of the linear structure on the flow field is a function of the ratio KH/T_f and can be assessed by defining the drawdown imposed by a well pumping an aquifer with an initially horizontal piezometric surface. Evaluation of equation (3.33), which can be made to represent drawdown in the linear structure and in the country-rock, was used for this purpose.

Figure 3.5 was built using the *Mathematica notebook*, for several different values of ratio KH/T_f. The other parameters involved were kept constant throughout all the simulations: the values are given in figure 3.5. The inverse Fourier cosine transform was computed numerically, using the tools available in *Mathematica*.

For the situation $KH/T_f = 1$ the drawdown curves tend to circles, resembling the steady-state behaviour of homogeneous confined aquifers (fig. 3.5a). As the ratio KH/T_f decreases (fig. 3.5b to 3.5d), the drawdown contours deviate increasingly from circles and become elongated along the discontinuity. As expected, the imposed hydraulic gradient is more tenuous in the direction of the linear structure.

In the examples shown in figure 3.5, the elongation of the drawdown curves only becomes

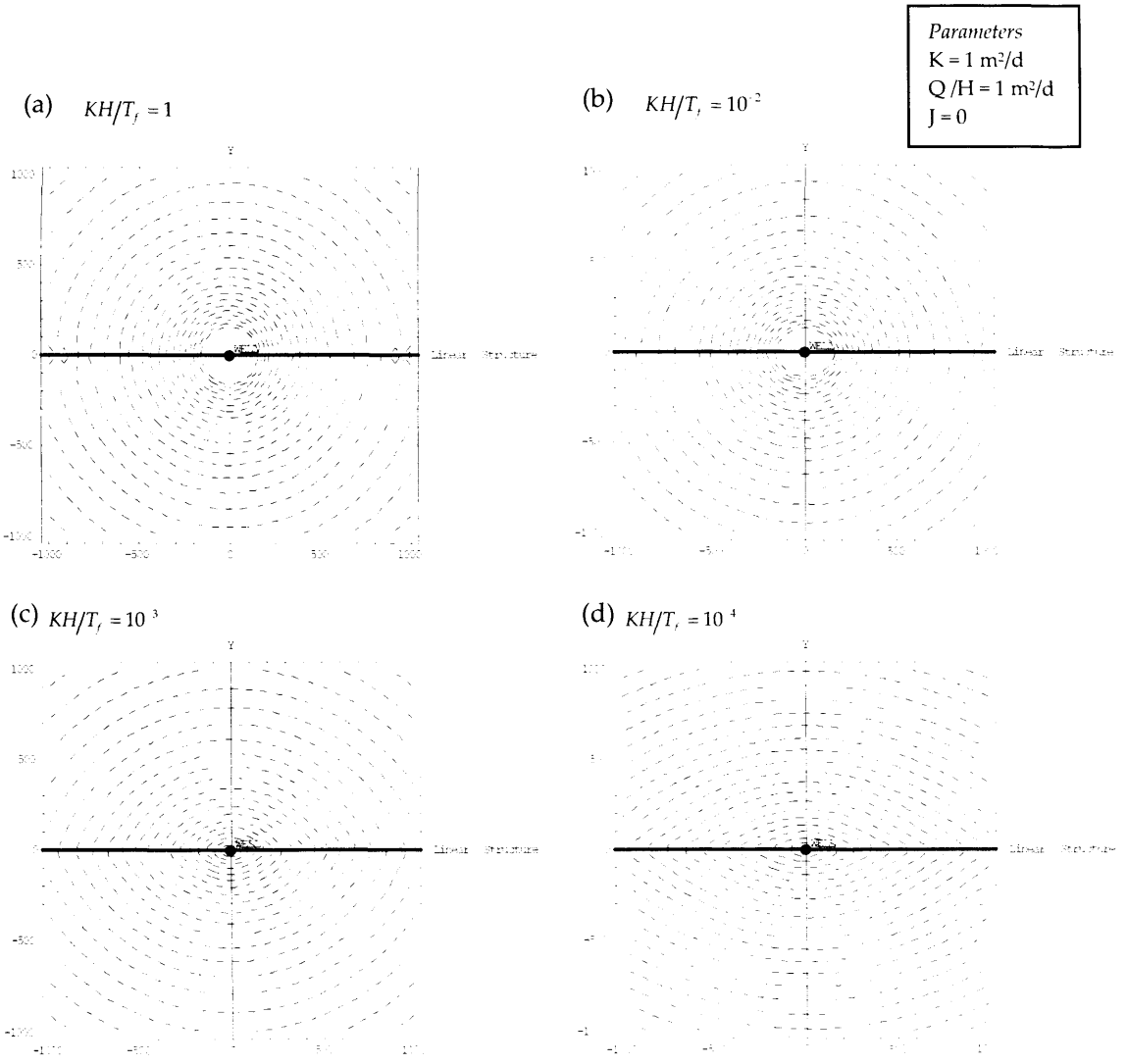

Figure 3.5 – Influence of the linear structure on the equipotentials imposed by a pumping well (case d=0, well located in the linear structure) for several values of the ratio KH/T_f. Units of x and y axes are metres.

apparent for highly contrasting conductivities $\left(KH/T_f \leq 10^{-3}\right)$, but that is largely due to the scale used. If equipotentials were drawn in a smaller domain surrounding the well, the elongation of the equipotentials is visible as soon as $KH/T_f > 0$. Anyway, highly contrasting conductivities such as $KH/T_f \leq 10^{-3}$ are the cases regarded as more interesting. The choice to site wells in discontinuities is based on the expectations of T_f being much larger than transmissivity of the country-rock. It is well known that hydraulic conductivity can vary by several orders of magnitude (Freeze and Cherry 1979), so it is not unlikely that the ratio KH/T_f may be quite small.

3.3.1.1 Pathline and total capture zone delineation

The capture zone can be delineated using the formulation for the stream function (equation 3.45) since it is known that along a streamline the stream function is constant. Mapping the stream function will provide a set of streamlines, allowing us to visualise which part of the x, y domain will contribute inflow to a well. This was accomplished using the *Mathematica Notebook*, for a domain centred at the well.

Figure 3.6 shows an example of the streamlines and equipotentials imposed by a well located in a linear structure, with a regional hydraulic gradient oriented parallel to the x-axis. For simplicity the effective porosity of the country-rock and of the linear structure were kept constant and equal to 2%.

Figure 3.6a is the stream function solution for a situation in which the linear structure is hydraulically indistinguishable from the country-rock. Thus, the capture zone is the same that would result from the Uniform Flow Equation (2.2). In figures 3.6b, 3.6c and 3.6d the ratios KH/T_f were kept as 10^{-3}. The orientation of the regional hydraulic gradient was made to vary from 0° (fig. 3.6b) to 45° (fig. 3.6b) and to 90° (fig. 3.6c).

The influence of the linear structure in fig 3.6b is to narrow the capture zone when compared to the homogeneous aquifer solution. The capture zone remains perfectly symmetrical with respect to the hydraulic gradient, since this is parallel to the linear structure. However, this symmetry is lost when the linear structure and the regional hydraulic gradient no longer coincide. Figure 3.6c is an example of that, with the capture zone distorted towards the side of the linear structure.

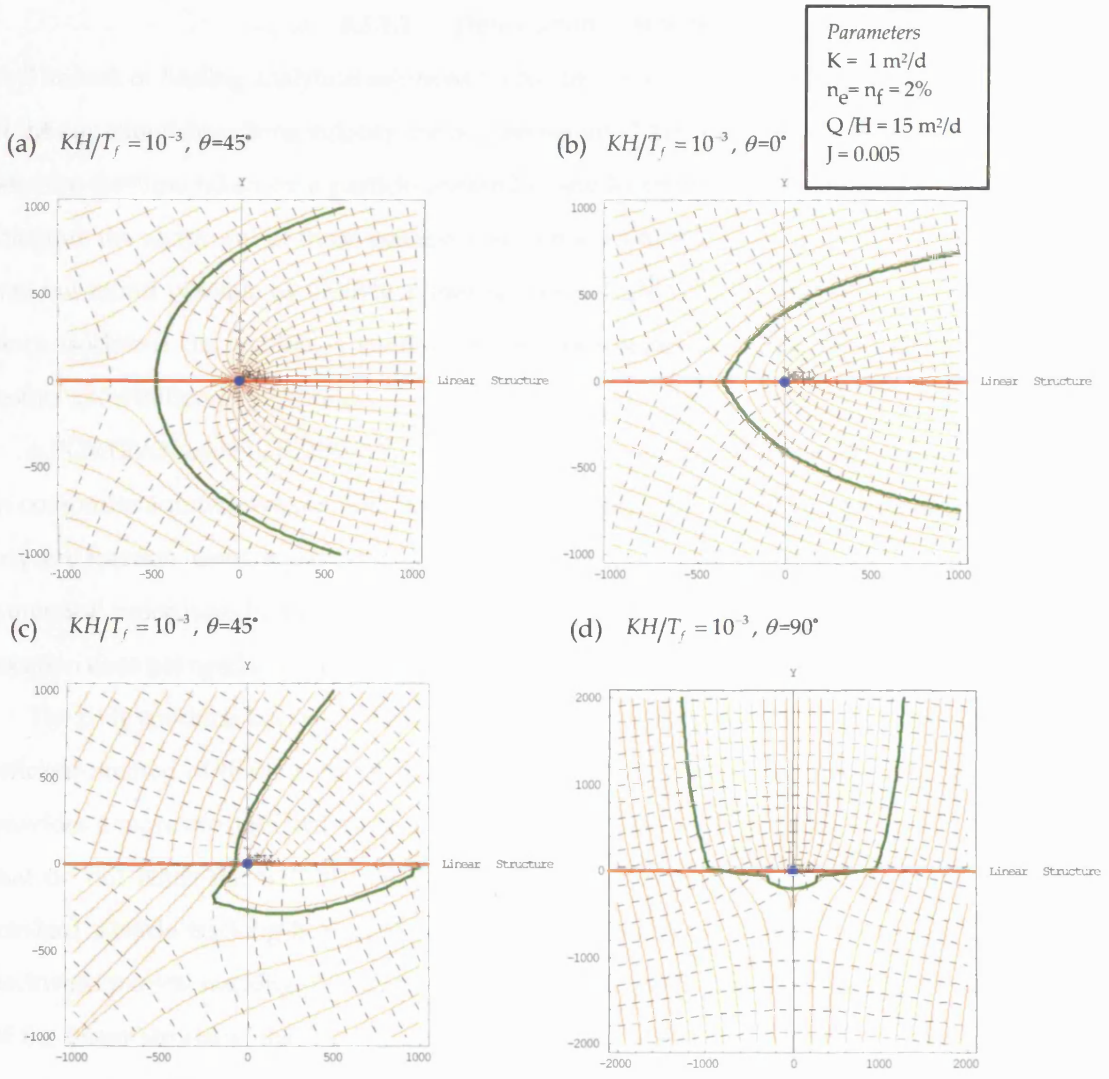

Figure 3.6 – Equipotentials, pathlines and capture zone of a well pumping a composite aquifer system (case d=0, well located in the linear structure), for several hydraulic gradient orientations. Dashed lines – equipotentials, red lines – pathlines, green lines – capture zone. Notice that scale in figure 3.6d is different from the other figures. Units of x and y axes are metres.

The discontinuity has a different influence when it is oriented perpendicular to the regional hydraulic gradient (fig. 3.6d). As expected, symmetry is recovered, but the width of the capture zone is much larger than in the homogenous aquifer case (fig.3.6a), although the distance from the well to the stagnation point is smaller than in the homogeneous case[1]. In this case, the effect of the feature is even more striking than when the hydraulic gradient is oriented at 0° (fig. 3.6b).

[1] Notice that the domain represented in fig. 3.6d is four times larger than the domain in fig. 3.6a to 3.6c.

3.3.1.2 Delineation of isochrones

The task of finding analytical solutions for isochrone delineation is impaired by the complexity of the equations describing velocity, namely equations (3.41) and (3.42). To find the equations that describe the time taken by a particle released at any location to reach the well, it is necessary to integrate the reciprocal of those equations with respect to x or y along a streamline. Such a task was not found possible by analytical means, so a particle tracking procedure was implemented. Since isochrone delineation is conducted for steady-state conditions, the tracking of particles results in definition of pathlines.

A FORTRAN code (GPZFAULT) was written with the purpose of conducting particle tracking in composite aquifer systems. The procedure takes advantage of the computation of velocity at any x, y location, using equations (3.41) and (3.42). This allows greater accuracy than achieved in numerical procedures based on a finite difference or finite elements grid, since the velocity at x, y location does not need to be interpolated from the flow rates at the cell boundaries.

The code conducts backward particle tracking, given that this procedure is a computationally efficient method of finding the particle paths. It is acknowledged that forward particle tracking provides a more accurate definition of the isochrones, since both particles that reach and particles that do not reach the well are tracked, thus better delineating the catchment area. However, forward particle tracking is a far lengthier and more computationally demanding process than backward particle tracking. When homogeneous media are involved, such as occurs on both sides of the linear structure, the loss of accuracy associated with backward tracking is not significant when compared to efficiency gains and can be attenuated using a larger number of particles.

It is important that the linear structure is assigned a width (w_f), allowing computation of its hydraulic conductivity (K_f) from transmissivity (T_f), since the value of K_f is required to compute velocities when the particle is in the linear structure. An obvious requirement for the flow solution still being valid is that the width w_f must be small so that flow in the linear structure can be regarded as always parallel to the linear structure walls. Boonstra and Boehmer (1986) and Boehmer and Boonstra (1987) consider that widths up to 10 metres should be valid for the model they studied. Although this thesis does not define a maximum acceptable width to the linear structure, what must be kept in mind is that the width must be negligible when compared to the scale of the study.

GPZFAULT releases the particles in a square surrounding the well, with square side equal to the linear structure width (w_f). Although in backward tracking particles are usually released in a circle surrounding the well, in the present case it was regarded as more appropriate to release the

particles at the linear structure / country-rock interface and at a similar distance in the linear structure, thus defining a square. Because in the absence of regional hydraulic gradient, flow in the linear structure is always parallel to the linear structure walls, particles that reach the interface would move parallel to it in the direction of the well. Therefore, particles that (in forward tracking) reach the square would stop and should be seen as reaching the well.

The particle tracking procedure implemented in GPZFAULT involves the following steps:

a) reads the input file with hydraulic parameters of linear structure and country-rock, pumping rate and width of the linear structure;

b) the code prompts for travel time and the number of time-steps to use;

c) particles locations are generated in a square centred in the well;

d) v_x and v_y are computed for every particle location using equations (3.41) and (3.42);

e) the advective velocity is computed from the v_x and v_y vectors, and its direction is reversed, since backward particle tracking is to be conducted;

f) each particle is moved for a time step $\Delta t = \frac{\text{travel time}}{\text{nº of time-steps}}$, according to a 4th order Runge-Kutta algorithm;

g) steps d) through f) are repeated for every particle until the input travel time is reached;

h) the final location of the ensemble of particles represents the isochrone.

A 4th order Runge-Kutta algorithm was chosen to solve the ordinary differential equations $dx = v_x dt$ and $dy = v_y dt$, allowing to find the new x and y coordinates for particles moved for a constant time step Δt. The use of constant time steps is computationally more efficient but it is also more prone to return inaccurate results in areas of strongly converging or diverging flow, such as near wells. The 4th order Runge-Kutta algorithm increases the accuracy of the solution, because it evaluates velocity four times for each time step: once at the initial particle location, twice at trial midpoints and once at a trial end point. A weighted velocity based on the values found at those four points is used to move the particle to the new x, y position. The algorithm is represented by the following equations for the x coordinate and similarly for the y coordinate (based on Spiegel and Liu (1999)):

$$x(t+\Delta t) = x(t) + (F_1 + 2F_2 + 2F_3 + F_4)/6 \tag{3.57}$$

$$\begin{cases} F_1 = \Delta t \cdot v_x(x,t) \\ F_2 = \Delta t \cdot v_x(x + \frac{F_1}{2}, t) \\ F_3 = \Delta t \cdot v_x(x + \frac{F_2}{2}, t) \\ F_4 = \Delta t \cdot v_x(x + F_3, t) \end{cases} \tag{3.58}$$

Although this algorithm results in enhanced accuracy when compared to any first order solution, inaccuracy may still result in the immediate vicinity of a pumping / injecting well. Use of a large number of time-steps reduces the possibility of errors occurring in those areas. In the cases presented below 100 to 500 time steps were used, ensuring that the results are stable.

When the regional hydraulic gradient coincides with the orientation of the linear structure, it is necessary to introduce a further step in the procedure. As seen in figure 3.5, when the ratio KH/T_f is less than unity, the linear structure works as a drain and particles will converge to it and then travel along it until the well is reached. However, in backward particle tracking, the particles released inside the linear structure would always travel along it and would never leave it, since flow in the discontinuity is parallel to its walls, with the v_y component being zero. Therefore, the effect of particles converging to the linear structure at large distances from the well would not be apparent. This problem only occurs when $\theta = 0°$, otherwise the regional hydraulic gradient introduces a component of v_y causing the particles to leave the linear structure.

In order to overcome this problem, when $\theta = 0°$ some particles are released exactly at the linear structure / country-rock boundary. These particles travel in the manner described above, using the relevant equations for determining velocity in the linear structure. However, at each time step a decision can be taken to shift the particle in Y direction (away from the linear structure) by 10^{-6} m. When the decision is favourable for shifting the particle, in the next step the particle will move according to the equations that describe velocity in the country-rock, where both v_x and v_y components exist, thus reproducing the effect of particles departing from the linear structure.

The decision to shift the particles is based on a random process in which particles leave the structure with probability in proportion to the ratio of the flow rate from the country-rock into the linear structure (q_r) and the flow rate along the linear structure (q_f). The threshold for accepting the shift is the generation (from a uniform distribution over $[0,1]$) of a random number $> \frac{q_f}{q_f + q_r}$.

Equation (3.41), with K_f replacing K, multiplied by the linear structure effective porosity is used to compute q_f at locations $(x, \left|\frac{w_d}{2}\right|)$, while q_r is computed from equations (3.41) and (3.42), multiplied by the effective porosity of the country-rock, at $(x, \left|\frac{w_d}{2} + 10^{-6}\right|)$ locations.

Figure 3.7 was built using the GPZFAULT code and shows the particles path for travel times of 1 day, 10 days and 50 days for several ratios of KH/T_f. The other parameters involved were kept constant throughout all the simulations: the values are given in figure 3.7. Effective porosity was

considered equal in the linear structure and country-rock since the variation of effective porosity in nature is far less important than variation of hydraulic conductivity values. Anyway, the shape and size of the isochrones is a function of the ratio $\frac{K}{n_e}\Big/\frac{K_f}{n_f}$, and it is invariant to whether the parameter that is changing is K or n_e. As a result, simulations for different KH/T_f ratios with constant n_e are also valid for an equal value of the ratio $\frac{K}{n_e}\Big/\frac{K_f}{n_f}$.

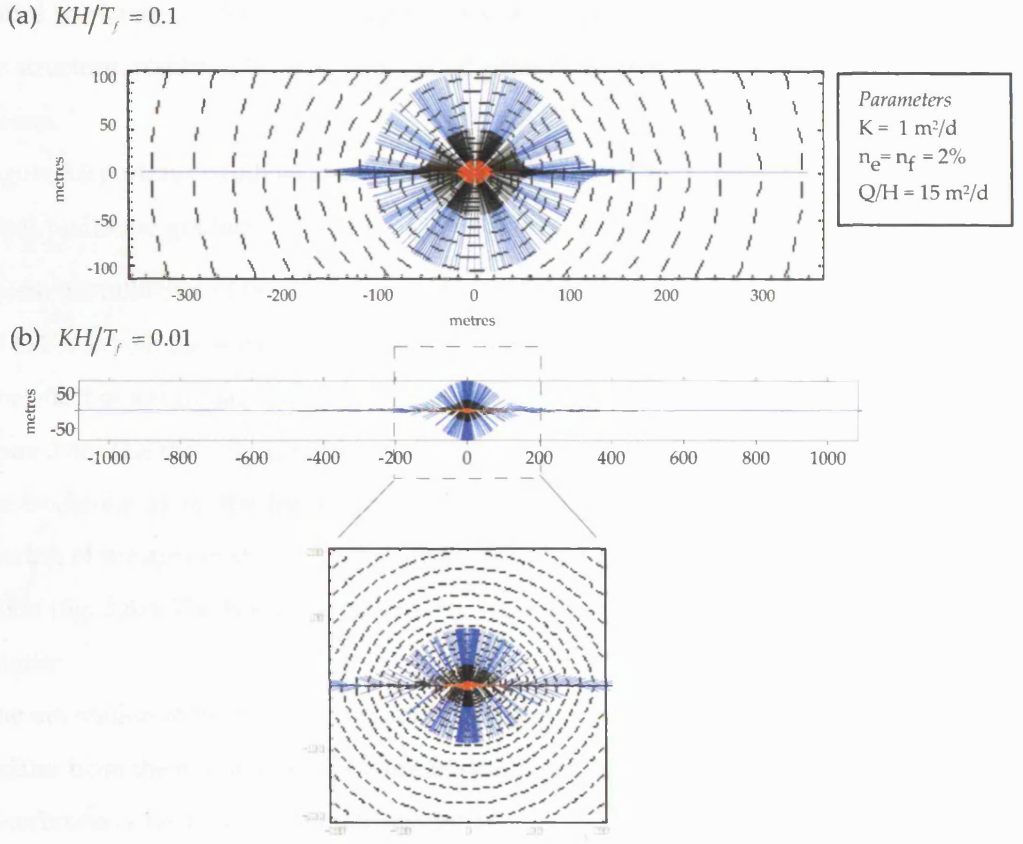

Figure 3.7 – 1-day (red), 10-day (black) and 50-day (blue) isochrones for a well pumping a composite aquifer system (case d=0, well located in the linear structure). Dashed lines represent the equipotentials. Note that different scales are used in a) and b).

Notice that no regional hydraulic gradient was considered in the simulations depicted in figure 3.7.

Figure 3.7a shows the isochrones for a ratio $KH/T_f = 10^{-1}$. Despite the hydraulic gradient being distributed almost radially, with no significant differences between the linear structure and country-rock, the large value of K_f causes the particles to travel much faster along the structure.

More interesting is the response in the country-rock. The shape of the isochrones in the country-rock is almost circular, showing that the velocity distribution is almost radial. However, it

is clear that for distances closer to the well (1 day travel time) there are already 'tails' developing along the linear structure, reflecting the effect of drainage imposed by the discontinuity. This effect causes considerable deviation from circular shapes near the well.

For contrast figure 3.7b shows a situation in which the equipotentials clearly deviate from the circular shape (cf. fig. 3.5 b). In this situation $KH/T_f = 10^{-2}$ and the much larger value of K_f causes the isochrones in the country-rock to deviate from circles for any of the simulated travel times. The 'tails' along the linear structure are now much more elongated, reflecting that the linear structure works as a drain of the country-rock at a much larger distance. Movement along the linear structure, resulting in highly elongated protection zones, now dominates the shape of the isochrone.

Figure 3.8 portrays pathlines delineated with GPZFAULT for several different orientations of a regional hydraulic gradient. The ratio KH/T_f varies from figure 3.8a through to figure 3.8e to represent the influence of the linear structure. Again, the effective porosity was kept constant and equal to 2% in both the linear structure and the country-rock.

The effect of a regional hydraulic gradient oriented parallel to the linear structure is displayed in figure 3.8b. The main features imposed by the existence of a linear structure are the elongation of the isochrone along the feature, resulting in the need to protect a large part of it, and the narrowing of the area to protect in the country-rock, when compared to the homogenous aquifer situation (fig. 3.8a). The isochrone is perfectly symmetrical with respect to the hydraulic gradient orientation.

The orientation of the hydraulic gradient becomes relevant to the shape of the isochrone when it deviates from the orientation of the linear structure. This is shown in figure 3.8c, where $\theta = 45°$. The isochrone is no longer symmetrical and becomes skewed to one of the sides due to faster movement along the linear structure. This skewness is inversely proportional to the ratio KH/T_f. In fact, the effect of the linear structure becomes dramatic for the case $KH/T_f = 10^{-2}$, with the isochrones being highly conditioned by the linear structure (fig. 3.8d)[1].

[1] Figure 3.8c through fig. 3.8f show wide blank spaces between pathlines starting at different sides of the linear feature. Such spaces should not be interpreted as if no flow occurs or as if particles released in those areas would not reach the well. The blanks are merely a consequence of the use of a backward particle tracking procedure and of the number of tracked particles. If a larger number of particles were to be tracked, those spaces would decrease, and they would not occur in a forward particle tracking procedure.

Finally, when the hydraulic gradient is oriented at a right angle to the linear structure ($\theta = 90°$) symmetry is recovered, but the effect of the discontinuity is again striking, with the shape of the isochrone being enlarged to both sides due to the v_x component in the linear structure. This widening of the protection zone can be dramatic and is a function of the ratio KH/T_f (fig. 3.8e and 3.8f).

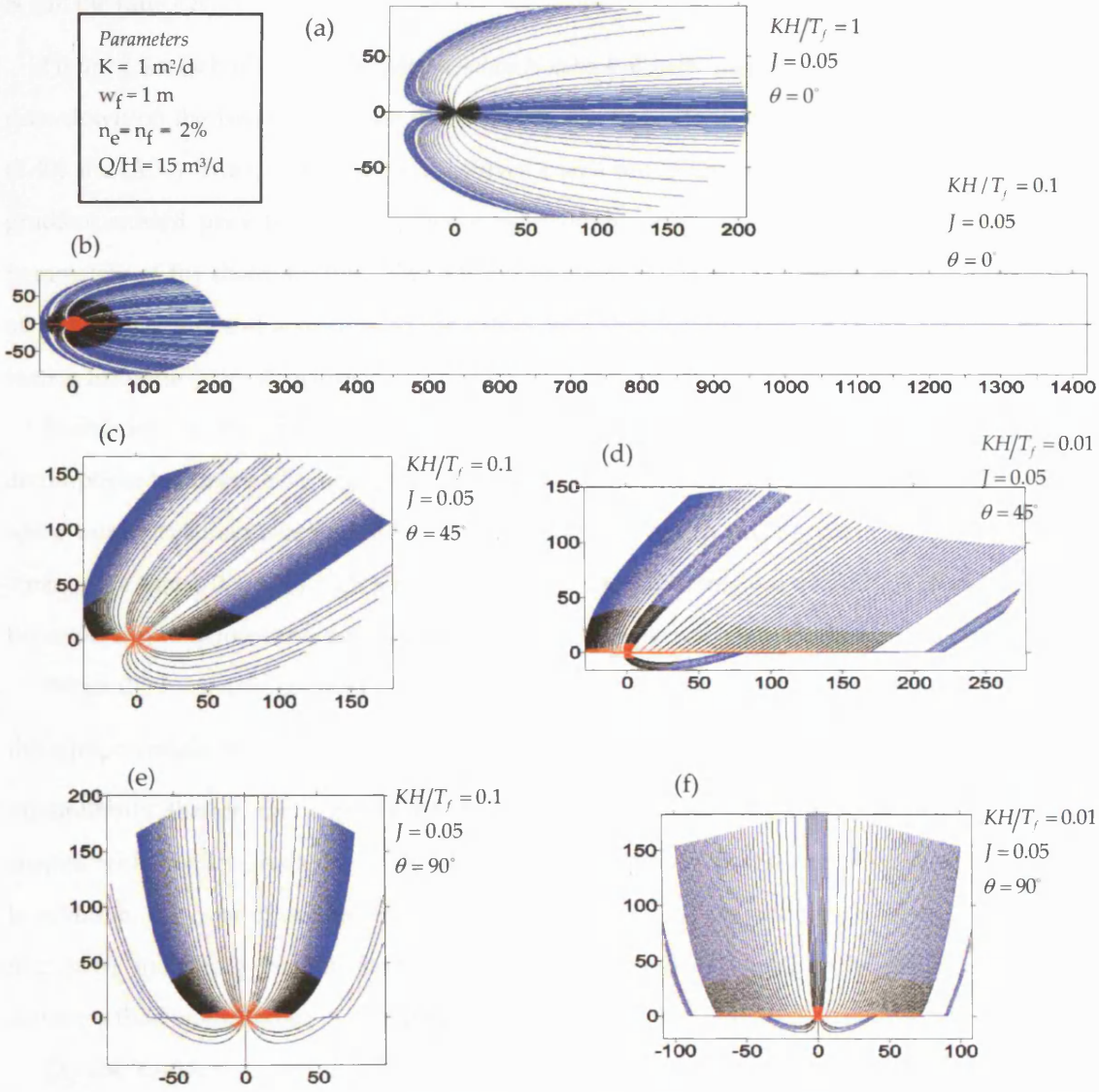

Figure 3.8 – 1-day (red), 10-day (black) and 50-day (blue) isochrones for a well pumping a composite aquifer system (case d=0, well located in the linear structure). The hydraulic gradient orientation (θ) and the ratio KH/T_f are the varying parameters. All other parameters are kept constant. Notice that the scale in b) is half the scale in the other figures. Units of x and y axes are metres.

3.3.2 Well located outside the linear structure (d>0)

In the situation where the pumping well is located in the country-rock (d>0), the influence of the linear structure in the flow field is a function not only of the ratio KH/T_f but also of the distance to the pumping well (d). The smaller the distance d the greater is the influence of the discontinuity in the overall groundwater flow pattern. Nevertheless, the major controlling factor is still the ratio KH/T_f .

Figure 3.9 was built using the *Mathematica Notebook* already mentioned, but now evaluation of drawdown on the two sides of the discontinuity has to be done independently, using equations (3.49) and (3.50). The situation shown involves a well pumping an aquifer in which no hydraulic gradient existed prior to pumping, hence representing solely the influence from the hydraulic parameters of the discontinuity. The other parameters involved were kept constant throughout all the simulations and according to the values indicated. The well is located at a distance $d = 25$ metres from the linear structure.

Evaluation of the inverse Fourier cosine transform in equations (3.49) and (3.50) was accomplished numerically, using the tools available in *Mathematica*. This procedure resulted in some numerical inaccuracies when $y = d$, the effect of which are apparent in the drawdown contours of figure 3.9. Although alternative methods for inverting the transforms must be sought, the effect is purely local and does not reflect itself on the overall shape of the equipotentials.

When the hydraulic contrast between country-rock and linear structure is small ($KH/T_f = 1$) the equipotentials tend to be circular (fig. 3.9a). Decreasing the ratio KH/T_f , that is, inserting a discontinuity that is more permeable than the surrounding medium, results in asymmetric shapes, with smaller gradients on the side of the discontinuity that is not being directly pumped. In addition, the cone of depression is elongated according to the orientation of the discontinuity (fig. 3.9b), indicating that the linear structure is allowing the water to be driven from larger distances than would occur in a homogeneous aquifer.

On the contrary, when $KH/T_f > 1$, thus decreasing the linear structure transmissivity, the equipotentials are nearly indistinguishable from those of a homogeneous aquifer, being circular in shape. Of course, the relative drawdown at each location is higher than would occur in a homogeneous aquifer, but in terms of gradients for the steady-state condition, the linear structure does not seem to be particularly influential (fig. 3.9c). Mention should be made that the use of very large values of KH/T_f is similar, in terms of the solution developed in section 3.2, to consider that the width of the linear structure goes to zero, i.e. that the linear structure vanishes.

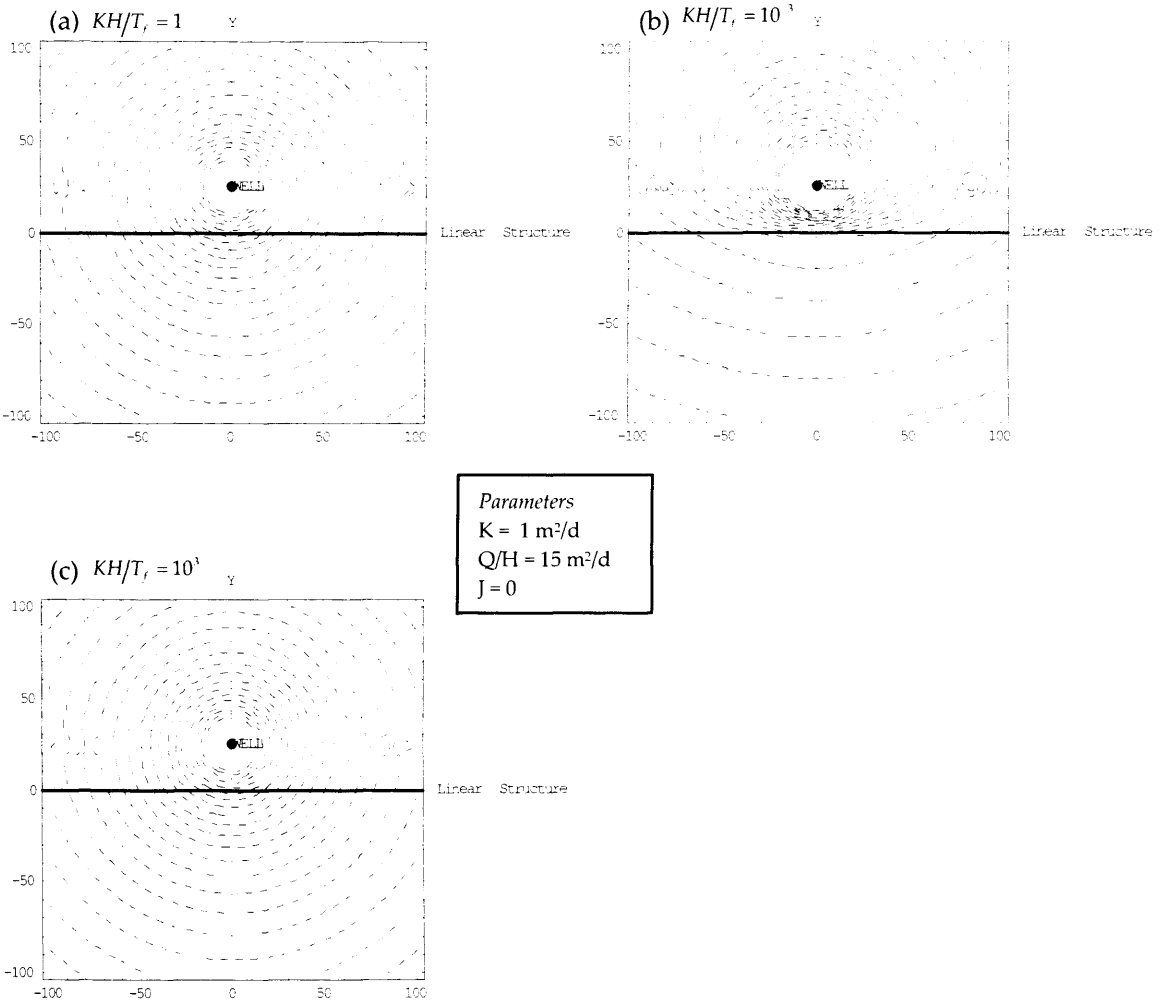

Figure 3.9 – Influence of the linear structure on the equipotentials imposed by a pumping well (case d>0, well located in the country-rock) for several values of ratio KH/T_f . Notice that numerical errors occur when y=d. Units of x and y axes are metres.

3.3.2.1 Pathline and capture zone delineation

Since the stream function was derived for the case $d > 0$ it is possible to use it to visualise the capture zone, much in the same manner as was done for the case $d = 0$, although the equations to be evaluated are now (3.55) and (3.56).

Figure 3.10 shows an example of the streamlines and equipotentials imposed by a well located in the country-rock at a distance $d = 200$ metres from the linear structure. There is a regional hydraulic gradient and, for simplicity, the effective porosities of the country-rock and of the linear structure were kept constant and equal to 2%.

Figure 3.10a is the stream function solution for a situation in which the linear structure is hydraulically indistinguishable from the country-rock. Thus, the capture zone is the same that

would result from the Uniform Flow Equation (2.2). In figure 3.10b, 3.10c and 3.10d the ratio of hydraulic conductivities, KH/T_f, was kept at a constant value of 10^{-3} while the hydraulic gradient orientation was made to vary from 0° to 90°.

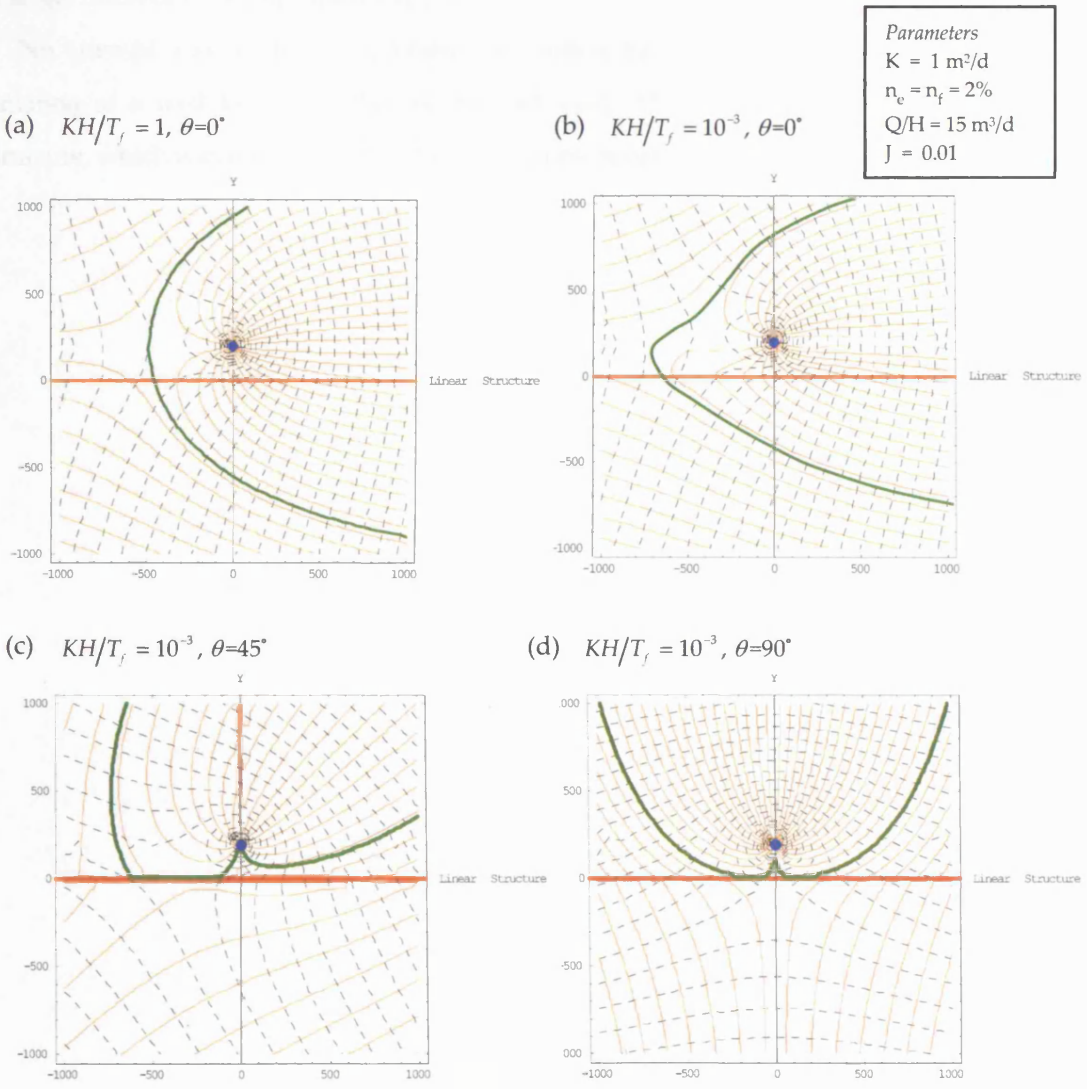

Figure 3.10 – Equipotentials, pathlines and capture zone of a well pumping a composite aquifer system (case d>0, well located in the country-rock). Dashed lines – equipotentials, red lines – pathlines, green lines – capture zone. In (c) numerical errors occur along the *y-axis*. Units of x and y axis are metres.

When the linear structure is more permeable and the regional hydraulic gradient is parallel to the linear structure, the capture zone is asymmetric, more elongated along the linear structure and less developed to the part of the aquifer that is not being directly pumped (fig. 3.10b). Asymmetry is also a prominent feature of the capture zone when $\theta = 45°$ (fig. 3.10c) with the capture zone being distorted towards the linear structure. The relevance of the situation with hydraulic gradient at right angles to the linear structure is not so obvious. In the case illustrated in figure

3.10d the linear structure has little influence on the shape of the protection zone. That is probably due to the stagnation point being located at a short distance form the linear structure. Obviously the influence of the linear structure increases when the stagnation point is located in the $y<0$ area at larger distances from the linear structure.

No attempt was made to implement the particle tracking procedure (GPZFAULT) for the situation of a well located in the country-rock ($d>0$). This was not possible due to the code structure, which was initially written for a well in the linear structure.

Chapter 4

DUAL AND MULTIPLE-POROSITY BEHAVIOUR: RELEVANCE TO PROTECTION ZONE DELINEATION

Genetic and tectonic history of rocks may lead to the development of regular patterns of fracture sets. This is commonly observed with the discontinuities defined by bedding planes and by schistosities, or with the arrangement of cooling joints in igneous rocks. This kind of fracture pattern has led some authors to treat those fractured media as having geometries that allow mathematical description.

One of the most common approaches in dealing with the hydrodynamic behaviour of fractured-rock aquifers takes advantage of those fracture pattern geometries and considers the aquifers as **dual-porosity media**. That is, the aquifers are regarded as two overlapping continua: the *fracture system* where most of the flow occurs; and the *rock matrix*, much less permeable than fractures, providing most of the storage capacity (fig. 4.1). Since both fractures and matrix are regarded as continua, it is then possible to find more or less complex analytical solutions for flow and solute transport.

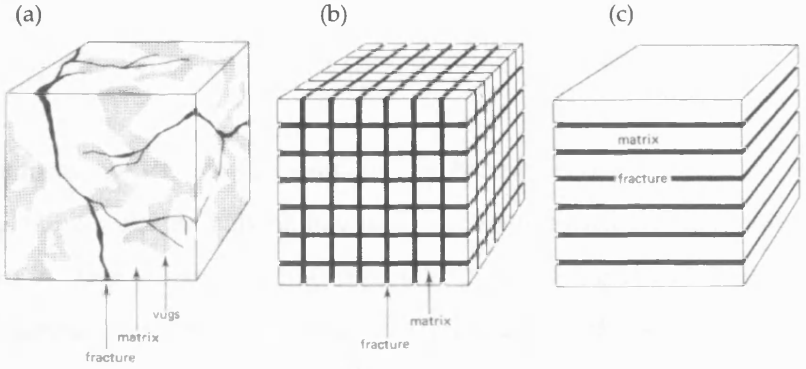

Figure 4.1 – Schematic illustration of the dual-porosity concept. a) naturally fractured rock formations, b) Warren-Root's idealized three-dimensional, orthogonal fracture system; c) idealized horizontal fracture system. From Kruseman and de Ridder (1994).

Dual-porosity models ultimately became of widespread use in oil reservoir engineering, where they were first enunciated and used, but are also used in groundwater flow studies, contaminant

transport analysis, underground waste repositories and even in geothermal energy studies. The model has been tested in those branches of science and technology and has proved, for some geologic conditions, remarkably useful and reliable.

In hydrogeologic studies the use of the dual-porosity concept is almost routine. In fact, most of the commercial software for interpretation of hydraulic aquifer tests includes options for analysis according to some dual-porosity analytical solution. As for the interpretation of tracer tests in fractured-rock aquifers, an analysis including a dual-porosity transport model is almost regarded as indispensable for interpreting the breakthrough curves, which often include long 'tails' that are easier to explain by including the diffusion of tracers into the matrix – **matrix diffusion**.

Despite the widespread use of dual-porosity models, their relevance to the delineation of protection zones has been largely neglected. No protection zones are known to have been delineated taking into account dual-porosity behaviour, despite some research studies indicating that such behaviour may have a considerable influence on the protection zone size and shape (Robinson and Barker 1999).

This chapter is concerned mostly with studying the influence of and applying the dual-porosity model to the delineation of protection zones in fractured-rock aquifers. Section 4.1 provides a brief review of the main concepts underlying the dual-porosity model. Section 4.2 presents an analytical solution for the delineation of protection zones around a single well located in a regional uniform flow field. Finally, sections 4.3 and 4.4 deal with multiple-porosity models, which are regarded as useful in understanding the hydraulic behaviour of hierarchical fracture systems.

4.1 A BRIEF REVIEW OF THE DUAL-POROSITY MODEL

The dual-porosity model was first proposed by Barenblatt et al. (1960) who recognised that although in fractured rocks the bulk of flow occurs in the fractures, the non-fractured blocks (the matrix) provide a large storage volume (fig. 4.2), thus playing a vital role in the hydraulic behaviour of fractured rock. Matrix and fractures (regarded as infinite length) are then treated as two coupled continua.

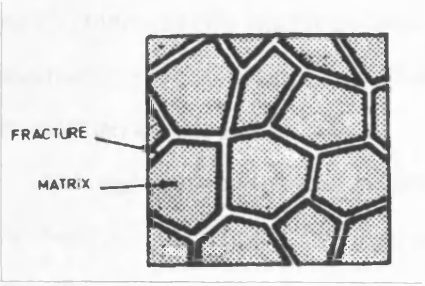

Figure 4.2 – Barenblatt et al. (1960) schematic representation of a fractured reservoir. From Chen (1989).

Obviously, this double continua approach is only acceptable provided a Representative Elementary Volume (REV) can be defined for the specified problem and domain[1]. The REV has to encompass simultaneously the porous block properties and the fracture properties (fig. 4.3a), so that if a representative volume is placed anywhere within the study domain it will always contain a persistent fracture phase and a matrix phase. Further, the size of the REV has to be such that the parameters representing the distribution of fractures and matrix within it are statistically significant (Bear et al. 1993). In that respect, the REV has to be much larger than the fracture spacing but much smaller than the domain of interest.

This concept of a REV common to two overlapping subsystems is not applicable to small-scale problems, where interest is in the hydraulic behaviour of a single fracture or of a small number of fractures, but as the scale increases so does the number of fractures encompassed by a representative volume and the dual-porosity approach becomes reliable (fig. 4.3b).

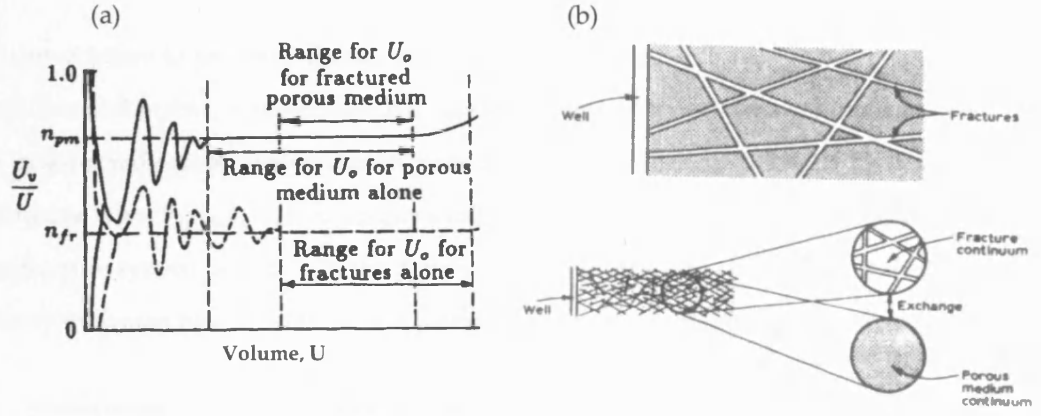

Figure 4.3– REV and dual-porosity concept. a) definition of a REV for a network of fractures and porous blocks. b) representation of two scales of study domain. Only for the larger domain it is possible to define a REV and to apply the dual-porosity concept. After Bear et al. (1993)

Two coexisting porosities and hydraulic conductivities are thus recognised: those of primary porosity and low conductivity in the matrix blocks; and those of low storage capacity and high

[1] See section 2.2.1 for a definition of Representative Elementary Volume (REV)

conductivity in the fractures. This concept makes it possible to explain flow and transport mechanisms as a re-equalization of the pressure differential between matrix and fractures (Kruseman and de Ridder 1994).

Although this model is an oversimplification of reality, since it requires the fracture system to be described, in practice, by some simple geometry, it allows us to account for the delay in the response to pumping or for the retardation of contaminants. These effects are caused by the matrix diffusion process by which water, solutes or heat can diffuse from/to the fractures into/from the matrix, due to the differences in potential that may arise between the two phases.

Several authors elaborated on the flow properties of such media, developing analytical solutions of the drawdown imposed by a well pumping a dual-porosity aquifer. Warren and Root (1963) were the first to develop such solutions and to apply them in oil engineering.

A basic assumption, common to any dual-porosity analytical solution, assumes that flow in the matrix is one-dimensional and perpendicular to the matrix – fracture interface. Obviously, this is a simplification of reality, valid only for large permeability contrasts between matrix and fractures. Some authors have used numerical solutions for situations considering more complex flow patterns in the matrix, but the problem is very complex.

A further assumption of earlier dual-porosity solutions was that flux between matrix and fractures is proportional to the difference in potential:

$$q \propto \left(\Phi_f - \Phi_m\right) \tag{4.1}$$

where Φ refers to potential (heads, concentrations or temperatures), f and m subscripts refer to fractures and matrix, respectively. The models using this type of flux solutions are often referred as **quasi-steady-state**. Later studies considered that exchanges between the two media are of **diffusive type** (fig. 4.4), which assumes that the potential at the blocks' surface is equal to that in the fracture system, with flux in the matrix being fully transient and described by the relevant law (Darcy for water, Fick for solutes and Fourier for heat) (Barker 1991).

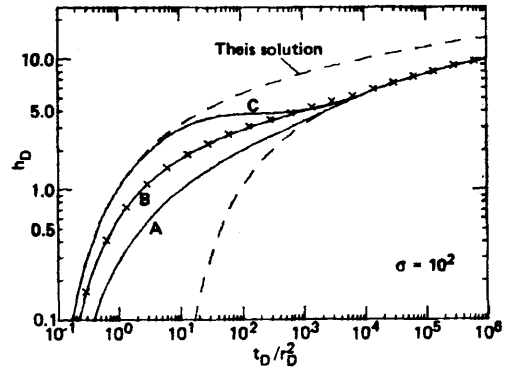

Figure 4.4 – Comparison between hydraulic heads according to diffusive type solutions and quasi-steady-state solution. Curve A - diffusive solution, sphere shaped blocks; Curve B - diffusive solution, slab shaped blocks, Curve C – quasi-steady state solution, slab shaped blocks. From Moench (1984). h_D r_D and t_D are dimensionless head, distance and time. σ is the ratio S_m/S and is kept constant at 10^2.

Both types of flux solutions, quasi-steady-state and diffusive, seem to find some support in the results of field tests, although the assumption implicit in the quasi-steady-state model does not have a physically sound support. Eventually, Moench (1984) was able to reconcile both types of solutions by including in the diffusive type model a **fracture skin**, a very low permeability mineral coating the surface of the fracture and causing delay in diffusion across the interface (fig. 4.5). Because the skin reduces gradients in the matrix blocks it gives rises to pressure responses similar to the ones predicted by the quasi-steady-state model. Nevertheless, it is acknowledged that the quasi-steady-state models are approximations to the more accurate diffusive models, but that they fail when relatively fast changes occur in the fractures (Barker 1991).

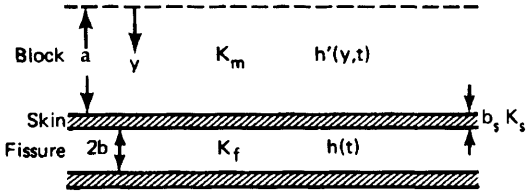

Figure 4.5 – Schematic diagram of fracture skin. From Moench (1984). K_s and b_s – hydraulic conductivity and thickness of fracture skin.

Although multiple solutions have been presented by several authors since the original Barenblatt et al. (1960) study, throughout the remaining of this chapter we shall refer to the flow solution presented by Barker (1985b), designated as the **Generalised Well Function**. This is a diffusive type model, described for a line source well, with no storage and no well losses, as:

$$\overline{s}(r,p) = Q\frac{K_0(\xi r)}{p\pi T_f} \tag{4.2}$$

where $\overline{s}$ is the Laplace transform of drawdown, K_0 is the modified Bessel function of the second kind, order zero and r is radial distance to the pumping well. T_f is transmissivity of the fracture system, p is the Laplace transform variable, Q is the well flow rate and ξ is given by:

$$\xi^2 = \frac{pS_f}{T_f}\left[1+\frac{S_m}{S_f}B(u)\right] \tag{4.3}$$

where B(u) is the block geometry function (BGF), $u = a\sqrt{\frac{pS_m}{T_m}}$ and a is a characteristic length.

The reason why this solution is favoured over others relates to the use of the BGF.

The shape of the matrix blocks is relevant to dual-porosity behaviour analysis. Most solutions consider that the blocks are constrained by horizontal fractures, defining slab shaped matrix blocks (fig. 4.6). Such an arrangement is not uncommon in nature, given that sedimentary rocks often show long parallel discontinuities that are arranged in sub-horizontal planes (the bedding planes). The same occurs with metamorphic rocks, where schistosity may also define long parallel

discontinuities. Therefore, this slab-shaped geometry has become widely used in dual-porosity studies (Kazemi 1969, Grisak and Pickens 1980, Bibby 1981, Barker 1982, Sudicky and Frind 1982).

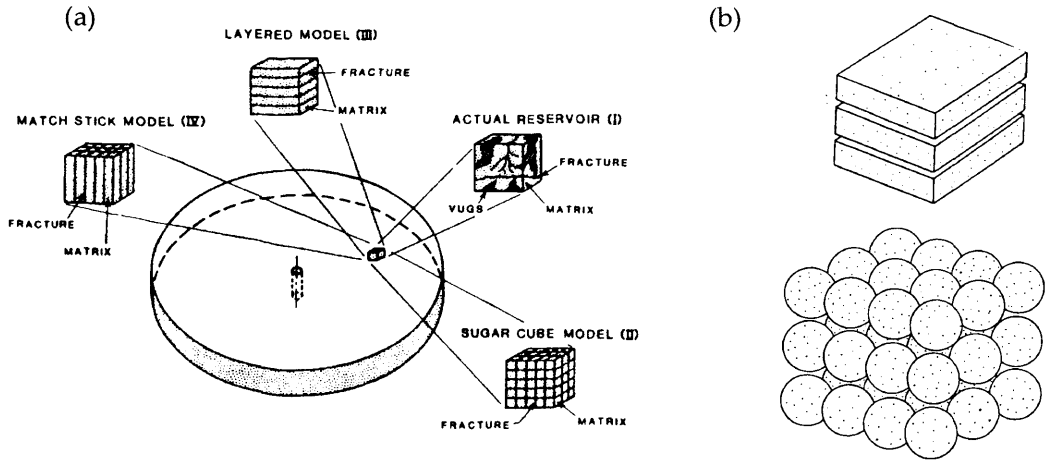

Figure 4.6 – Some examples of idealization of blocks in dual-porosity models. a) cube, slab and 'match stick' shapes (Kazemi and Gilman 1993); b) prismatic blocks and spherical blocks (Pinder et al. 1993).

However, other geometries may be more appropriate to describe fracture patterns. This is the case, for instance, with the cooling joints of plutonic rocks, that often show three mutually orthogonal sets, that have been approximated by some authors by cubes or spheres (Warren and Root 1963, Kazemi 1969, Gringarten and Witherspoon 1972, Moench 1984, Barker 1985a).

One other simple geometry is the cylinder, which can be used to approach the columnar jointing that often occurs in volcanic rocks as the result of the cooling process. A closely related geometry is the 'match stick' geometry) which has been used in the petroleum industry (Kazemi 1969), although it can be approximated by the infinite cylinders geometry (Barker 2003, pers. comm.).

The advantage of the generalised well function presented by Barker (1985) is that it remains unchanged whatever the shape of the blocks, provided an appropriate function (the BGF) is used to describe the matrix blocks.

BGFs are established for slabs, spheres, cylinders or mixtures of those geometries (table 4.1) enabling the use of equations (4.2) and (4.3) for several different fracture system geometries.

One other advantage of the generalised well function is that the BGF can be adapted to describe both the quasi-steady-state and the diffusive type models. Finally, the generalised well function can be made to represent the hydraulic behaviour of continuous porous media, provided the parameters are chosen appropriately (Barker 1985b).

Table 4.1 – Block geometry functions for some shapes of matrix blocks. Sources: Barker (1985a), Barker et al.(2000) and Barker (2003, pers. comm.) for the finite cylinder geometry.

Geometry	*BGF*, B(u)	*a – characteristic length**
Slabs	$\tanh(u)/u$	Half slab thickness
Infinite *cylinder*	$I_1(2u)/\left[uI_0(2u)\right]$	Half cylinder radius
Finite *cylinder*	$\frac{32}{\pi^2}\sum_{j=1}^{\infty}\sum_{n=1,3,5,\ldots}^{\infty}\frac{\nu_j^2+(n\pi\rho)^2}{(n\nu_j)^2\left[\nu_j^2+(n\pi\rho)^2+4u^2(1+R/L)^2\right]}$, where $J_0(\nu_j)=0$ is a Bessel function, R is the cylinder radius and *L* its length	$\frac{RL}{2(L+R)}$
Infinite (insulated) *hollow cylinder*	$\frac{1}{u}\left[\frac{K_1(Z_1)I_1(Z_2)-I_1(Z_1)K_1(Z_2)}{I_0(Z_1)K_1(Z_2)-K_0(Z_1)I_1(Z_2)}\right]$, where $Z_j=r_j u/a$ and I and K are modified Bessel functions	$\frac{r_2^2-r_1^2}{2r_1}$, r_2 – outer, and r_1 – inner radius
Sphere	$\coth(3u)/u-1/3u^2$	Half sphere radius
n-dimensional *sphere*	$I_{n/2}(nu)/\left[uI_{n/2-1}(nu)\right]$	*n*-sphere radius/n
Rectangular *parallelepiped*	$\frac{512}{\pi^6}\sum_{l=1}^{\infty}\sum_{m=1}^{\infty}\sum_{n=1}^{\infty}\left[\frac{\alpha_{lmn}}{\alpha_{lmn}+u^2}\right](lmn)^{-2}$, odd integers; $\alpha_{lmn}=(a\pi)^2\left[(l/X)^2+(m/Y)^2+(n/Z)^2\right]$	where $\frac{XYZ}{2(XY+YZ+XZ)}$, X, Y and Z are the sides of the parallelepiped
Cube	as rectangular parallelepiped with $X=Y=Z=6a$	
Discrete Mixture of *n* types of blocks	$\sum_{i=1}^{n}P_i B_i\left(\frac{ua_i}{a}\right)$, where P_i is the proportion of matrix volume occupied by blocks of type *i*	$\left(\sum_i^n \frac{P_i}{a_i}\right)^{-1}$
Continuous Mixture of *n* types of blocks	$\sum_{i=1}^{n}\int_0^{\infty}P_i(\beta)B_i\left(\frac{u\beta}{a}\right)d\beta$, where $P_i(\beta)d\beta$ is the proportion by volume of the composite block mixture occupied by blocks of shape *i* in the range β to $\beta+d\beta$	$\left(\sum_i^n\int_0^{\infty}\frac{P_i(\beta)}{\beta}d\beta\right)^{-1}$
Quasi-steady state	$\Theta/\left(\Theta+u^2\right)$, where Θ is a dimensionless parameter	-

*** a, the characteristic length, is the ratio of block volume to the area in contact with mobile fracture water**

Equations (4.2) and (4.3) are given in the Laplace transform space, which makes methods such as type curves unfeasible. However, the solutions in the Laplace transform space are much simpler and can be easily inverted numerically using any of the several available algorithms.

As for the transport solutions, one of the first analytical approaches for solute transport in a single fracture surrounded by a porous matrix was presented by Tang et al. (1981). This approach considers a non-dispersive transient transport in which dispersion along the fracture axis is ignored and a steady-state solution that includes all of the processes.

Although the Tang et al. (1981) solution is widely used, we shall we shall refer throughout this chapter to the solutions presented by Barker (1982), which are more versatile and applicable to more complex fracture geometries. Barker (1982) solutions were found with Laplace transforms, and are preferred over others, such as Sudicky and Frind (1982), who provide an inverted solution, because they are much simpler and the BGFs allow representing different fracture geometries without changing the general transport solution. The solution for 1-D transport is (Barker 1982):

$$\bar{C}(r,p)=\frac{C_0}{p}e^{-\left(\frac{v+\sqrt{4\chi D+v^2}}{2D}\right)r} \tag{4.4}$$

where $\bar{C}(r,p)$ represents solute concentration in the fractures and C_0 represents the constant inlet concentration and p is the Laplace transform variable. D is the longitudinal dispersion coefficient and v is a constant advective velocity. The parameter χ is defined as:

$$\chi=p\left[1+\phi_m\frac{a}{b}\mathrm{B(u)}\right] \tag{4.5}$$

where ϕ_m is matrix porosity, $u=a\sqrt{\frac{p}{D^*}}$, b is half-fracture aperture and a is a characteristic length. D^* is the matrix diffusion coefficient and B(u) is the block geometry function defined in table 4.1.

The solution for radial transport is also provided by Barker (1982), without considering dispersion in the fractures, as:

$$\bar{C}(0,y)=\frac{C_0}{p}e^{-\frac{\chi r^2}{2w}} \tag{4.6}$$

where $w=-\frac{Q(a+b)}{2\pi Hb}$ is related to steady radial flow velocity imposed by a pumping/injecting well in an aquifer of thickness H.

4.1.1 Limitations of the dual-porosity model

Although dual-porosity models have become widely popular as tools for a better understanding of flow and transport in fractured rocks, one should bear in mind their limitations, the most significant of which is oversimplification of the fracture system. Under some field conditions, such simplification may be acceptable, but probably not in general, and evidence of it should be sought for each case.

One other disadvantage of the dual-porosity models has to do with the difficulty in estimating some of the parameters that compose the solutions, namely the block size, or the effective fracture

apertures, or in some solutions, the thickness and permeability of the mineral coating the fracture surface.

Nevertheless, the extensive research conducted in the field of petroleum geology and, more recently, contaminant hydrogeology have demonstrated that interaction between fractures and matrix is highly significant and should not be ignored. This is both correct in terms of resources assessment and, more important to the subject of this thesis, in terms of retardation of contaminants in natural groundwater systems.

4.1.2 Multiple-porosity models

The dual-porosity model has become almost a routine tool to investigate and explain the hydraulic behaviour of fractured-rock aquifers, and so it was only natural that models that are even more complex were introduced to account for features of some particular fractured rocks. Research on the hydraulic response of carbonate aquifers has shown anomalous behaviour that could not be explained by dual-porosity models, thus leading to the development of triple-porosity models (Chen 1989).

In such models there are two types of continuous porous systems, one with good flow properties and another one with poor properties. No flow occurs between these two porous media. The third type of porosity is contributed by the fracture system. It has been proposed that such a model may be appropriate for describing fractured carbonate reservoirs (Sahimi 1995). Analytical solutions for such models have been provided by Closmann (1975), assuming quasi-steady-state flux conditions between the three involved media. Later Abdassah and Ershaghi (1986) found the equivalent analytical solution for the diffusive type flux.

The most relevant practical difference between the dual and the triple-porosity models is that instead of two parallel semi-log straight-line segments for the dual-porosity system, there are three parallel semi-log straight-line segments for the triple porosity system (fig. 4.7).

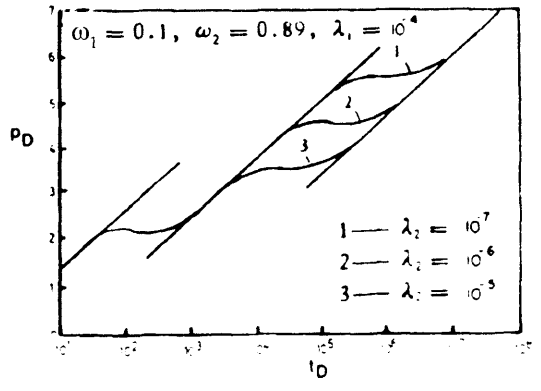

Figure 4.7 – Schematic representation of a semi-log plot for the triple porosity model, with three straight-line segments. From Chen (1989). Refer to original paper for meaning of symbols

Reportedly a general multiple-porosity, multiple-permeability model was formulated and rigorously solved by Liu and Chen in 1987, however the solution was not published (Chen 1989). Other authors (Bai et al. 1993) have addressed those same multiple-porosity, multiple-permeability models and were able to coupled it with deformation-dependent flow models, but the formulations obtained are numerical solutions, including a finite element solution for the dual-porosity model as a particular solution of the multiple-porosity, multiple-permeability model.

4.1.3 Dual-permeability models

The dual-porosity model, which accounts for diffusive flow and transport in the matrix, should only be used when the bulk matrix permeability is much less than that of the fracture system. This assumption is generally reasonable but there are circumstances under which the permeability of the matrix can be considerable and non-diffusive flow and transport in it should not be ignored. In such situation, the dual-porosity model may not be reliable and **dual-permeability** models should be considered[1].

Dual-permeability models, in which both fractures and matrix have considerable conductive properties, have been the subject of far less research than dual-porosity models. Still some studies addressed the hydraulic behaviour of naturally fractured reservoirs when the contrast between the two permeabilities is not significant (Chen 1989). Those studies usually involve the solution of the original Barenblatt et al.(1960) model.

Chen (1989) describes several studies, outlining the existence of solutions for some dual-permeability flow problems, subject to different boundary conditions. The solutions are generally numerical or involve quite complex functions, such as Quasi-Bessel functions. Nevertheless, such studies seem to address mainly the situation where the matrix porosity is less than or equal to fracture porosity ($K_m \leq K_f$), with the early straight-line segment of the drawdown curves moving closer to the late straight-line segment with decreasing K_f/K_m ratio.

Barker (1991) briefly mentions some dual-permeability related research, describing finite element models that represent the matrix while the fractures are represented as line elements.

[1] The term 'dual-permeability' or 'double permeability' is also used to describe a model in which major fractures are represented discretely and the majority of small fractures are represented as a continuum (Clemo and Smith 1997). This is not the meaning assigned to the term in this chapter, where the term 'dual-permeability' is intended for the case of significant flow and transport in the matrix.

These few studies apparently do not address the situation $K_f<K_m$, which is not surprising when the contrasting continuums are intact rock blocks (the matrix) and open fractures. However, if the contrasting continuums are different sets of fractures ordered in a hierarchical manner, it is possible that situations where $K_m>K_f$ develop. Under such circumstances, the dual-porosity approach is not valid and dual-permeability models must be used. This issue will be addressed in section 4.4.

4.2 INFLUENCE OF DUAL-POROSITY BEHAVIOUR TO DELINEATION OF GROUNDWATER PROTECTION ZONES

Delineation of groundwater protection zones is usually conducted considering only advective transport. This occurs for any of the analytical and semi-analytical solutions presented in chapters two and three and for the numerical models based on particle tracking. In any of those cases the reactive/decaying properties of contaminants and the dispersive features of solute transport are ignored.

Reactive/decaying properties are generally not considered because protection zones are chosen not to be dependent on the chemical or physical characteristics of any pollutant, otherwise multiple isochrones and capture zones would have to be delineated depending on the properties of the substances. Thus, in order to remain pragmatic about the usefulness of protection zones, reactive and decaying properties are ignored.

Dispersive behaviour would imply that there would not be a sharp protection zone boundary, but rather a wide boundary with width proportional to the dispersion coefficient (Grubb 1993). Fickian laws being applicable, the advective front represents the centre of the wide boundary, i.e. the result using advection is the mean of the results involving dispersive transport, and thus it is routine in analytical and semi-analytical solutions to ignore dispersion. Of course, this practice may be questionable for complex flow patterns such as those simulated with numerical methods.

While this practice of considering only advection seems reasonable for homogeneous and continuous aquifers, in situations involving uniformly fractured aquifers (such as dual-porosity aquifers) such practice might be disputable due to the non-negligible delay in transport caused by diffusion into the matrix.

Obviously diffusion into the matrix is a function of the chemical properties of pollutants, since the dual-porosity effect is dependent on a pollutant specific parameter, the matrix diffusion coefficient (D^*), which raises the same questions as considering reactive and decaying properties

of pollutants. However, for most solutes, the matrix diffusion coefficients will vary within a relatively narrow range, while the retardation inherent to the process of matrix diffusion will be a more relevant source of variability in the protection zone size. Since the retardation is linked not only to the matrix diffusion coefficient, but also to the fracture and matrix characteristics it is considered interesting to analyse the dual-porosity behaviour influence on the size and shape of protection zones.

4.2.1 Previous work

The problem of capture zone delineation in dual-porosity aquifers has been largely ignored, except for Robinson and Barker (1999) and some general remarks made in Barker et al. (1999).

Robinson and Barker (1999) acknowledge that the use of advection only may considerably underestimate the time of arrival of a pollutant, thus overestimating the area that needs to be protected. Those authors use the 1-D solute transport solution derived by Barker (1982) (equation 4.4), stating that, although it was intended to represent concentration build-up due to a fixed concentration source, it can also be interpreted as the cumulative probability of arrival of individual particles due to an instantaneous source. The probability of a location being included in an isochrone can be computed using that model and is illustrated by the cumulative probability curves represented in figure 4.8.

Robinson and Barker (1999) also make the important remark that the 1-D solution is valid for more complex flow patterns, both in 2-D and 3-D systems. This allows us to apply the same probability distribution curves (fig. 4.8) to more complex flow systems.

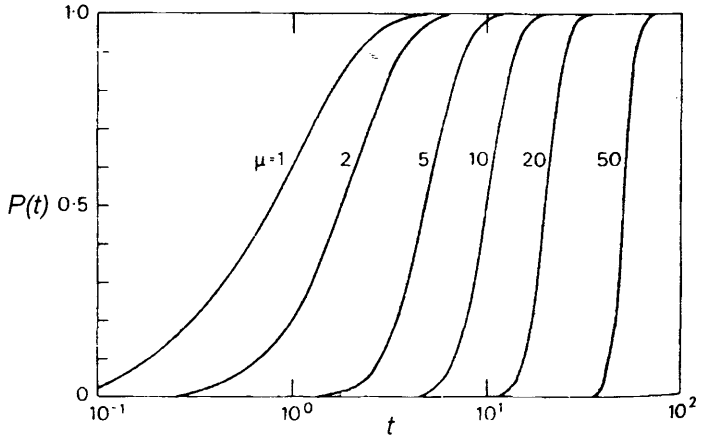

Figure 4.8 – Cumulative probability of arrival of individual particles due to an instantaneous source. Can also be interpreted as the breakthrough curves for a continuous source. P is the cumulative probability, t is time and in this figure $\mu = \frac{\phi_m}{ba}\frac{D^*}{v}x$. After Barker (1982).

A full appreciation of the dual-porosity influence in protection zones should include a radial flow pattern imposed on a regional uniform hydraulic gradient. As seen in chapter two, standard analytical solutions, such as the Bear and Jacobs (1965) solution, were derived for that hydrogeologic scenario and, consequently, assessment of the dual-porosity influence should be conducted under similar flow conditions.

4.2.2 Analytical solution

Isochrones refer to the time taken by a particle released at an x, y location to reach a pumping well. Because advection is the only driving mechanism, the isochrone can also be interpreted as relating to the time taken by a particle to go from an injection well to that same x, y location. That is, the pertinent equations are fully reversible, being indifferent as to whether the particles are being moved away from the source or towards the source.

For computational reasons, namely the definition of the boundary conditions, it is easier to evaluate the injection process, and, thus, the analytical solution is presented for a well injecting a contaminant into a dual-porosity aquifer.

Although the ultimate aim is to assess the influence of dual-porosity behaviour in the size of protection zones, it is necessary to determine the concentration variation with time. Later, and using the analogy enunciated by Robinson and Barker (1999), those equations can be reinterpreted in terms of probability.

4.2.2.1 Geometry and model assumptions

The geometry of the model is depicted in figure 4.9. It includes a well injecting a pollutant in a dual-porosity aquifer of thickness H. The fracture pattern is slab shaped, the slabs (matrix) having thickness $2a$, porosity ϕ_m and being separated by fractures of constant aperture $2b$. Flow occurs only in the fractures with velocity $v(x,y)$, and dispersion effects are not considered. A Cartesian coordinate system was adopted, with x-axis oriented parallel to the regional hydraulic gradient J. The well is located at the coordinate system origin.

The following assumptions are made:

- the matrix is homogeneous and saturated with immobile water;
- solute transfer between the fractures and matrix and within the matrix occurs by molecular diffusion in a direction perpendicular to the plane of the fractures;
- the solute concentration in water entering the fractures is constant and equal to C_0;

- initially the concentrations in the fractures and matrix is zero;
- the well injects water at a constant rate Q;
- hydrodynamic dispersion in the fractures is ignored;
- diffusion across the fracture width is negligible;
- steady-state flow conditions exist.

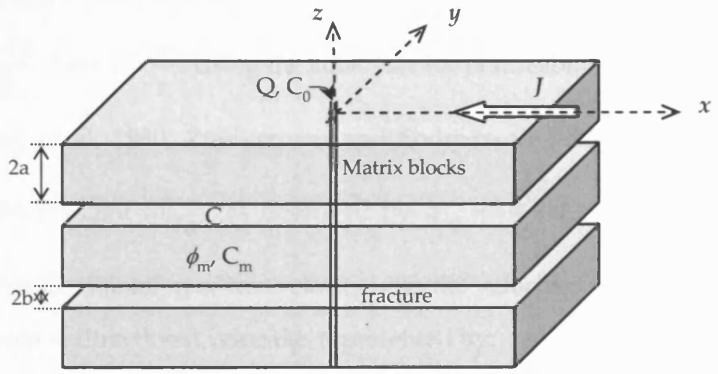

Figure 4.9 – Model geometry

4.2.2.2 Governing equations

Movement of solute in the fissures is defined by:

$$\frac{\partial C}{\partial t} = -\frac{\partial (v_x C)}{\partial x} - \frac{\partial (v_y C)}{\partial y} - D^* \frac{\phi_m}{b} \left(\frac{\partial C_m}{\partial z} \right)_{z=0} \tag{4.7}$$

where C represents concentration in the fractures, C_m concentration in the matrix and v_x, v_y are the x and y components of velocity.

Solute diffusion in the matrix is described by:

$$\frac{\partial C_m}{\partial t} = D^* \frac{\partial^2 C_m}{\partial z^2} \tag{4.8}$$

As a result of symmetry of the model there will be no diffusion across the centre of the matrix slabs:

$$\left. \frac{\partial C_m}{\partial z} \right|_{z=a} = 0 \tag{4.9}$$

The concentration at the interface fracture-matrix will be equal:

$$C(x,y,t) = C_m(x,y,0,t) \tag{4.10}$$

Initially the concentration at every location is zero:

$$C(x,y,0) = C_m(x,y,z,0) = 0 \tag{4.11}$$

The input concentration is constant and equal to C_0:

$$C(0,0,t) = C_0 \tag{4.12}$$

Because the flow conditions imposed by the well have reached steady-state, the mean velocity imposed by the well at radial distance r can be represented by (Barker 1982):

$$v = -\frac{Q(a+b)}{2\pi Hbr} \tag{4.13}$$

where Q is the constant pumping rate.

If $w = -\frac{Q(a+b)}{2\pi Hb}$ then $v = \frac{w}{r}$. Using the cubic law for permeability of a smooth fracture (Louis 1974, Witherspoon et al. 1980, Zimmerman and Bodvarsson 1996b)[1], the velocity due to the regional hydraulic gradient (v_{reg}) is described by $v_{reg} = -\frac{gb^2}{3\upsilon}J$, where g is gravity and υ is kinematic viscosity. Combination of this velocity with the velocities imposed by the injecting well (equation 4.13) leads to directional velocities represented by:

$$v_x = w\frac{x}{x^2+y^2} + v_{reg} \tag{4.14}$$

$$v_y = w\frac{y}{x^2+y^2} \tag{4.15}$$

4.2.2.3 Solving for concentration at any location

The solution of the problem can be found using Laplace transforms with respect to time (t), using p as the Laplace transform variable and with the transformed variable being represented with an over-bar, such as in $\bar{C}$.

The Laplace transforms of the equations for solute transport in the fissures (4.7) and in the matrix (4.8), using the initial condition represented by equation (4.11), are, respectively,:

$$p\bar{C} = -\left[\frac{\partial(v_x\bar{C})}{\partial x} + \frac{\partial(v_y\bar{C})}{\partial y}\right] - \frac{D^*\phi_m}{b}\frac{\partial\bar{C}_m}{\partial z}\bigg|_{z=0} \tag{4.16}$$

$$p\bar{C}_m = D^*\frac{\partial^2\bar{C}_m}{\partial z^2} \tag{4.17}$$

The solution of equation (4.17), solute transport in the matrix, using boundary conditions depicted by equations (4.9) and (4.10) is:

[1] For models considering deviations from the cubic law, that is relating hydraulic conductivity to fracture surface roughness, see for instance Brown (1987) and Zimmerman et al. (1992, 1996b).

$$\bar{C}_m = \cosh\left[\sqrt{\frac{p}{D^*}}(a-z)\right]\operatorname{sech}\left(a\sqrt{\frac{p}{D^*}}\right)\bar{C} \tag{4.18}$$

The first derivative of which, at z = 0, is:

$$\left.\frac{\partial \bar{C}_m}{\partial z}\right|_{z=0} = -\bar{C}\frac{pa}{D^*}\mathrm{B(u)} \tag{4.19}$$

where B(u) is the block geometry function (table 4.1) as defined by Barker (1985a), which for slabs is $B(u) = \dfrac{\tanh(u)}{u}$, and $u = a\sqrt{\dfrac{p}{D*}}$.

Using (4.19) in the equation that describes transport in the fractures (4.16) gives:

$$\frac{\partial\left(v_x\bar{C}\right)}{\partial x} + \frac{\partial\left(v_y\bar{C}\right)}{\partial y} = -\chi\bar{C} \tag{4.20}$$

where $\chi = p\left[1+\dfrac{a}{b}\phi_m B(u)\right]$.

Using the directional advective velocities provided by equations (4.14) and (4.15), and because the first derivatives of those velocities with respect to x and y cancel each other, equation (4.20) can be rewritten as:

$$\left(\frac{wx}{x^2+y^2}+v_{reg}\right)\frac{\partial\bar{C}}{\partial x} + \left(\frac{wy}{x^2+y^2}\right)\frac{\partial\bar{C}}{\partial y} = -\chi\bar{C} \tag{4.21}$$

It is possible to solve this equation for specific *x*, *y* locations, such as along the *x-axis* (y = 0, v_y = 0) and along the *y-axis*.

Along the *x-axis* equation (4.21) returns:

$$\left(\frac{w}{x}+v_{reg}\right)\frac{\partial\bar{C}}{\partial x} = -\chi\bar{C} \tag{4.22}$$

The solution of which, applying the Laplace transform of boundary condition (4.12), is:

$$\bar{C}(x,0) = \frac{C_0}{p}e^{-\frac{\chi x}{v_{reg}}}\left(1+\frac{v_{reg}x}{w}\right)^{\frac{w\chi}{v_{reg}^2}} \tag{4.23}$$

Particles released along the *y-axis* will follow paths defined by the stream function, which can be adapted from Grubb (1993) as:

$$\psi = \frac{b}{b+a}H\left[v_{reg}y + w\tan^{-1}\left(\frac{y}{x}\right)\right] \tag{4.24}$$

Since the concentration along the *y-axis*, $\bar{C}(0,y)$, is independent of *x* it is possible to express equation (4.21) using only the derivative with respect to *y* and replacing *x* with the expression resulting from the stream function (equation 4.24). Equation (4.21) returns after some manipulation:

$$\left[\frac{w}{y}\sin^2\left(\frac{H\frac{b}{b+a}v_{reg}y-\psi}{H\frac{b}{b+a}w}\right)\right]\frac{\partial\bar{C}}{\partial y}=-\chi\bar{C} \tag{4.25}$$

The solution of which, applying the Laplace transform of boundary condition (4.12), and acknowledging that the stream function for a particle released along the *y-axis* is given by $\psi = H\frac{b}{b+a}\left(\frac{\pi}{2}w+v_{reg}y\right)$, is:

$$\bar{C}(0,y)=\frac{C_0}{p}\left[\cos\left(\frac{yv_{reg}}{w}\right)\right]^{\frac{\chi w}{v_{reg}^2}} \tag{4.26}$$

Equations (4.23) and (4.26) retrieve the concentration along the *x-axis* and *y-axis*, respectively, of a solute injected at the well, provided the Laplace transform can be inverted. Although analytical inversion is not possible, several algorithms exist that conduct accurate numerical inversion of Laplace transforms.

While the equations above concern injection of a solute at a well located at the coordinate axis origin, they can also be interpreted as the concentration of a solute at a pumping well with the solute source being located along the *x-axis* or *y-axis*.

Finally, the equations above are valid for block shapes other than slabs, provided the block geometry function, B(u), is defined accordingly (table 4.1).

4.2.3 Probability of an area being included in a protection zone

Robinson and Barker (1999) state that the curves in figure 4.8, describing the concentration build-up at a point in a dual-porosity environment, can also be interpreted as the cumulative probability of an individual particle to reach a pumping well. The same reasoning allows us to rewrite equations (4.23) and (4.26) as:

$$\bar{P}(X\le x,0)=\frac{1}{p}e^{-\chi\left[\frac{x}{v_{reg}}-\frac{w}{v_{reg}^2}\ln\left(1+\frac{v_{reg}x}{w}\right)\right]} \tag{4.27}$$

$$\bar{P}(0,Y\le y)=\frac{1}{p}\left[\cos\left(\frac{yv_r}{w}\right)\right]^{\frac{\chi w}{v_{reg}^2}} \tag{4.28}$$

Since probabilities are now involved, C_0 was set to 1, so that the equations above can be interpreted as the cumulative probability distributions.

The equations above represent the probability that particles released at locations *(x,0)* and *(0,y)* will reach the well within time *t*. That is, they represent the probability of the isochrone *t* to

encompass locations $(x,0)$ and $(0,y)$. As such, the protection zone must now be regarded as related to probability.

A *Mathematica Notebook* was written to implement equations (4.27) and (4.28), with the Laplace transforms being inverted numerically using the *Numerical Inversion Mathematica Add-on* (Mallet 2000). The Stehfest algorithm was chosen to perform the numerical inversions.

The retardation effect caused by diffusion into the matrix is not only a function of the fracture characteristics but also of the diffusion coefficient (D*), which is pollutant specific, ranging from non-diffusing substances (such as particles) to highly diffusing elements, such as deuterium ($D^* = 1.67\times10^{-9}$ m²/s) (Maloszewski et al. 1999). Therefore, the dual-porosity influence on the size of the protection zones is pollutant dependent.

Nevertheless, if a range of values of D* is used it is possible to envisage that influence. Such is shown in figure 4.10, where limit values of 3×10^{-9} m²/s and 3×10^{-10} m²/s were input into equations (4.27) and (4.28) to compute the 100-day isochrone. Slabs compose the block geometry and the matrix porosity was made to vary so that its influence can be shown for several matrix to fracture porosity $(\phi_m a/b)$ ratios. Other parameters were kept constant and as shown in figure 4.10. The locations of the purely advective isochrones, along the *x-axis* (including the stagnation point) and *y-axis*, were computed with the Bear/Jacobs solution (equation 2.3).

The influence of dual-porosity behaviour can be dramatic, with the Bear/Jacobs solution clearly overestimating the region that needs to be protected, particularly along the x-axis direction. When considering the dual-porosity behaviour, breakthrough occurs much later, reducing substantially the size of the isochrone.

Notice that the term multiplied by χ in equations (4.27) and (4.28) above coincide with the advection time along the *x-axis* and *y-axis* for particles captured (or released) by a pumping (or injecting) well. Hence the equations above corroborate the Robinson and Barker (1999) remark of invariance of transport solution with respect to flow path, and that the 1-D dual-porosity transport solution can be applied to more complex flow patterns. That is, the equations above can be written simply from the 1-D solute transport equations as suggested by Robinson and Barker (1999).

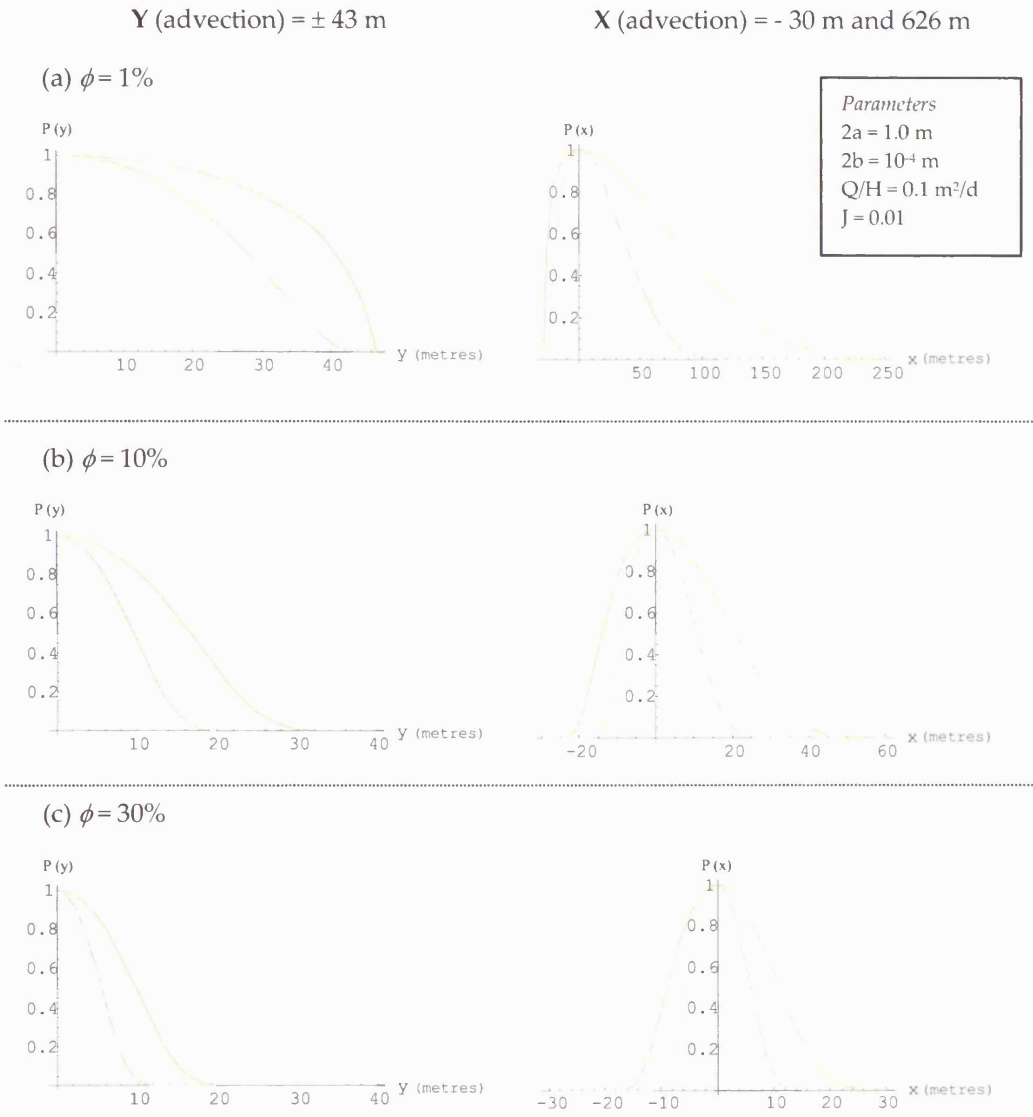

Figure 4.10 – Probability of a particle reaching a well within t = 100 days, starting at location (0, y) or (x, 0). Green - $D^*=3\times10^{-9}m^2/s$; red - $D^*=3\times10^{-10}m^2/s$. The values of Y (advection) and X (advection) are the limit values of Y and X if no dual-porosity effect was considered. Notice that a), b) and c) are at different scales.

Using that same remark about invariance of the transport solution, it is possible to write the equation for the probability of any x, y location being part of a protection zone as:

$$\overline{P}(X \le x, Y \le y) = \frac{1}{p} e^{-\chi t_a}$$

$$t_a = \begin{cases} \dfrac{x}{v_{reg}} + \dfrac{w}{v_{reg}^2} \ln\left[\dfrac{\sin\left(\tan^{-1}\dfrac{y}{x}\right)}{\sin\left(\dfrac{v_{reg}}{w} y + \tan^{-1}\dfrac{y}{x}\right)} \right] & y \neq 0 \\ \dfrac{x}{v_{reg}} - \dfrac{w}{v_{reg}^2} \ln\left(1 + \dfrac{v_{reg} x}{w}\right) & y = 0 \end{cases} \qquad (4.29)$$

where t_a is the advection time as provided by Bear and Jacobs (1965) solution (equation 2.3) or by Barker and MacDonald (1990).

Equation (4.29) gives the probability contours of a protection zone in a two-dimensional aquifer domain.

A FORTRAN code, designated as **GPZDUALP**, was written that implements equation (4.29) and also computes the *t*-isochrone for a single porosity aquifer. GPZDUALP was used to depict the influence of the dual-porosity behaviour on the size of protection zones on a 2-D domain (fig. 4.11). Again, two values of matrix diffusion coefficient were used and probabilities were computed for a 50-day isochrone[1].

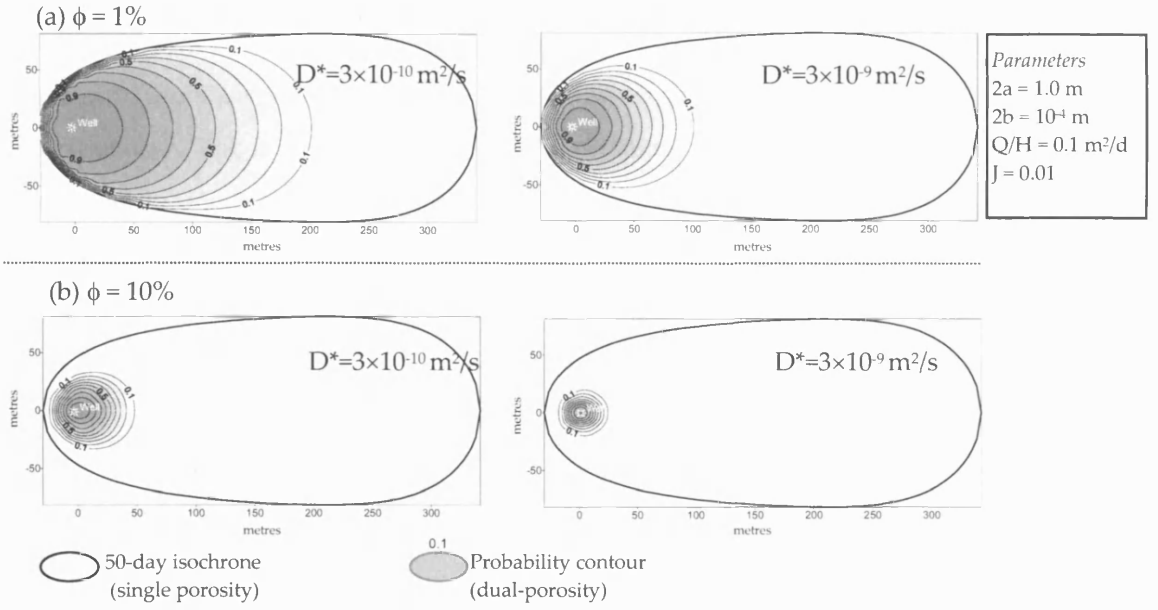

Figure 4.11 – 50-day probability related protection zone of a well pumping a dual-porosity aquifer. a) matrix porosity set to 1%; b) matrix porosity set to 10%. Two values of matrix diffusion coefficient were used, $D^*=3\times10^{-10}$ m²/s and $D^*=3\times10^{-9}$ m²/s. Also shown the 50-day isochrone for a single porosity aquifer computed, according to equation (2.3).

It is clear that travel velocities are several times lower than indicated by the purely advective model. Even if the most conservative probability values are used (lower values of P_x resulting in larger areas to protect), the retardation inherent to transport in dual-porosity aquifer imply the

[1] Bear in mind that although the probabilities shown in fig. 4.11 were computed based on interpreting relative concentrations as cumulative probabilities (see equations 4.27 and 4.28), it is not possible to interpret fig. 4.11 as relative concentrations of a solute injected at the well. The probabilities were computed along each flow path from every location to the well (a 1-D path) and, as such, do not take into acount the dilution factor that would occur for a solute injected at the well.

need to protect smaller areas than indicated by the Bear/Jacobs solution[1]. As expected, the effect is more acute with increasing ratio $\phi_m a/b$, since this implies larger matrix storage capacity and increased retardation.

It can be concluded that the dual-porosity behaviour should not be overlooked when delineating protection zones. The decrease in size of the area that needs to be protected is so striking that it cannot be ignored.

The fact that the dual-porosity effect is pollutant specific withdraws effectiveness from an analysis aiming to constrain the protection zone due to retardation in the matrix. It is not wise to use equation (4.29) to obtain definitive dimensions of the isochrones, even if a range of values of D* is used. The method described above should be used cautiously to evaluate the possibility of decreasing the size of the area to protect, since there are pollutants that simply do not diffuse into the matrix (Robinson and Barker 1999). In this respect the use of the single porosity solution is precautionary. Still, it is argued that the above equations provide a valuable tool that can be of assistance in implementing a procedure for delineating protection zones in dual-porosity environments.

4.3 A MULTIPLE-POROSITY MODEL FOR FLOW AND TRANSPORT IN FRACTURED ROCK AQUIFERS

Dual-porosity models are frequently used for interpretation of pumping and tracer tests in hard-rock aquifers, such as granites, schists and quartzite aquifers. However, it is not obvious that sound blocks of hard-rocks like granites and quartzites may show matrix porosity large enough to justify apparent dual-porosity behaviour. Instead, such behaviour may be due to several sets of fractures with different hydraulic properties co-existing in the same aquifer.

This section is concerned with understanding the hydraulic behaviour of hard-rock aquifers in which fractures can be regarded as hierarchical systems. For hierarchical fracture system **(HFS)** it is understood a scale-dependent medium of the form illustrated in figure 4.12, which can result from several processes, such as (National Research Council 1996):

[1] Notice that this comparison, as well as the ones depicted in figures 4.10 and 4.11, implies that the Bear and Jacobs solution is computed using the fracture porosity as the kinematic porosity, since it is along fractures that particles move. Nevertheless, it is possible to speculate that the Bear and Jacobs solution can retrieve much smaller protection zones provided an effective porosity, $\phi_{ef} = (\phi_m a + b)/(a + b)$, equal to the sum of matrix and fracture porosity, is chosen as the kinematic porosity. The comparison between the dual-porosity model and the Bear and Jacobs solution with such kinematic porosity has still to be done, although it can be easily argued that there is no physical reasoning supporting that approach, since water and solutes are moving towards the well only along fractures.

- fracture sets formed in successive geologic events;
- fracture geometry and location constrained by pre-existing fractures (such as often happens in sedimentary rocks);
- fracture density inversely correlated to fracture length, which creates fracture systems with a small number of long fractures , but with a large number of short fractures;
- fracture sets formed due to tension between two or more interacting faults.

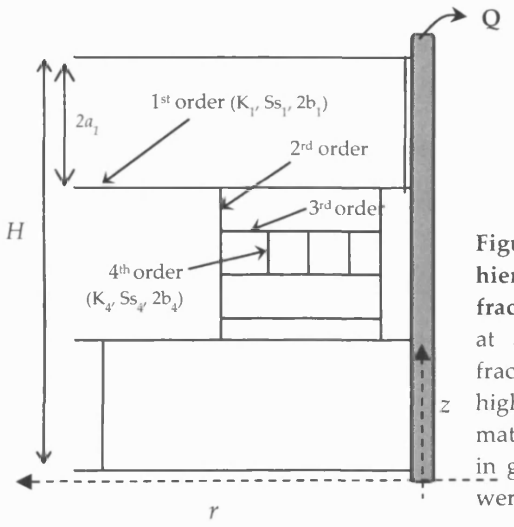

Figure 4.12 – Vertical section illustrating a hierarchical fracture system with 4 orders of fractures. A vertical well (shaded rectangle) pumps at a constant rate Q from 1st-order horizontal fractures. Higher order fractures connect to the next higher and next lower order fractures. In the mathematical model each order of fractures exists, in general in its own 3-D space. (Not all fractures were drawn).

Sedimentary and metamorphic rocks, in which persistent bedding or schistosity connect smaller but more profuse fractures, may be good examples for which HFS models can be appropriate.

In the remainder of this section hard-rock aquifers are considered, with matrix porosity and permeability set to zero. However, the analysis is equally valid if the non-fractured rock (matrix) is regarded as the highest order medium, providing storage and releasing water to a lower order fracture set.

4.3.1 Radial flow model – analytical solution

(Based on a note by J. A. Barker (2001), pers. comm.)

The analytical solution developed for the flow model is based on the generalized well function (Barker 1985b), which provides a unified solution for the most relevant aquifer tests models involving confined aquifers. The generalized well function enables single porosity as well as dual-porosity models to be analysed with the same equations, and, thus, provides the obvious choice

for developing a multi-porosity model, by allowing the generalized well function to be used for n porous media.

The generalized well function is defined in the Laplace space, because analytical inversion of the Laplace transforms used in its derivation is difficult and would certainly result in very complex equations. There are several routines that conduct accurate numerical inversion of Laplace transforms, and therefore it is possible to use the usually much simpler Laplace space equations.

J. A. Barker (2001, pers. comm.) provided the analytical solution presented in this subsection. The research conducted specifically within the framework of this thesis is related to analysis of some properties of the solution, to its implementation in a computer code and to comparisons with a numerical model (section 4.3.2 and subsequent sections).

4.3.1.1 Geometry and model assumptions

The geometry of the model is depicted in figure 4.12. It includes a well pumping in a multiple-porosity aquifer of thickness H. There are several sets of fractures that are designated according to the order they connect to each other. The 1st-order is the only one connected to the well, and thus the only one that directly provides water to the well. The 2nd-order fractures are limited by the 1st-order set and encompass the 3rd-order sets and so on. According to this designation, it is obvious that fracture size decreases with increasing fracture order.

The fracture pattern in figure 4.12 is slab-shaped, fractures of every order are separated by blocks of thickness $2a_i$, have storativity S_i, transmissivity T_i and constant aperture $2b_i$. Radial flow occurs only in the 1st-order fractures (larger fractures), since these are the only ones providing water directly to the well. In the $i>1$ order fractures all flow is in direction perpendicular to the plane of the $(i-1)^{th}$ fractures. A radial coordinate system was adopted, with the well located at the coordinate system origin.

The following additional assumptions are made:

- the aquifer is fully confined, of uniform thickness and infinite extent;
- the well fully penetrates the aquifer and there are no well-losses or well-storage;
- the pumping rate is constant and before pumping the piezometric level is horizontal,
- Darcy's law apply throughout the system;
- any elementary volume of the aquifer is assumed to contain a large number of fractures of any order.

4.3.1.2 Governing equations

Let $s_1(r,t)$ be the average drawdown in the 1st-order fracture system at distance r from the well, at time t after the start of pumping. The flow equation in the 1st-order fracture set, the ones directly pumped by the well, is given by:

$$S_1 \frac{\partial s_1}{\partial t} = \frac{T_1}{r}\frac{\partial}{\partial r}\left(r\frac{\partial s_1}{\partial r}\right) - q_2(r,t) \tag{4.30}$$

where $q_2(r,t)$ represents discharge from the 2nd-order fractures into the 1st-order fractures per unit area of the aquifer.

Drawdown $s_2(r,\vec{z}_2,t)$, in the 2nd-order fracture set, at distance r from the well and at distance $\vec{z}_2$ from the lower order fractures is given by:

$$S_2 \frac{\partial s_2}{\partial t} = T_2 \frac{\partial^2 s_2}{\partial z_2^2} - q_3(r,\vec{z}_3,t) \tag{4.31}$$

or generalizing for i[th]-order fractures:

$$S_i \frac{\partial s_i}{\partial t} = T_i \frac{\partial^2 s_i}{\partial z_i^2} - q_{i-1}(r,\vec{z}_{i-1},t) \tag{4.32}$$

where $\vec{z}_i = \{\vec{z}_2,\vec{z}_3,...,\vec{z}_n\}$ and $q_i(r,\vec{z}_i,t)$ is obtained by applying Darcy's law at the block surfaces, with A_i being the fracture area per unit area of the aquifer:

$$q_i(r,t) = -A_i K_i \frac{\partial s_i(r,a_i,t)}{\partial z_i} \tag{4.33}$$

As a result of symmetry of the model there will be no-flow across the centre of any fractures of order higher than 1:

$$\left.\frac{\partial s_i}{\partial z_i}\right|_{z_i=0} = 0 \qquad i>1 \tag{4.34}$$

Drawdown at the interface between fractures of successive orders will be equal:

$$s_i(r,a_i,t) = s_{i-1}(r,a_{i-1},t) \tag{4.35}$$

Initially drawdown at every location is zero:

$$s_i(r,\vec{z}_i,0) = 0 \tag{4.36}$$

4.3.1.3 Solving for drawdown at any location

Only the main steps of the derivation are given in this sub-section, with a full derivation being included in Appendix A.

The solution of the problem is found using Laplace transforms with respect to time (t), with p as the Laplace transform variable and with the transformed variable being represented with an over-bar, such as in $\overline{s}_1$.

The solution with two hierarchical levels, $i = \{1, 2\}$, corresponds to the dual-porosity solution and was derived by Barker (1985b), in terms of the generalized well function. For a line source well with no storage and no well losses the solution is:

$$\overline{s}_1(r,p) = Q\frac{K_0(\xi r)}{p\pi T_1} \tag{4.37}$$

where K_0 is the modified Bessel function of the second kind, order zero, and

$$\xi^2 = \frac{pS_1}{T_1}\left[1+\frac{S_2}{S_1}B(u)\right] \tag{4.38}$$

where $u = a\sqrt{\frac{pS_2}{T_2}}$ and B(u) is the block geometry function defined for slabs as $B(u) = \frac{\tanh(u)}{u}$.

Equation (4.37) is still valid to describe drawdown at the 1st-order fractures, regardless the number of fracture orders that may exist, because the 1st fracture set receives water only from the 2nd-order fractures, due to the hierarchical assumption. The difference from the dual-porosity model is that with increasing number of hierarchical orders, the contribution coming from the 2nd-order fractures now has to take into account the supply of water to those same 2nd-order fractures.

That is, what is changing is parameter ξ, that includes contribution from 2nd-order into 1st-order fractures. If we accept that slabs of decreasing size separate high order fractures, then it is possible to compute flow from each fracture order into the preceding one. This is accomplished by generalising equations (4.33) and (4.38), in which case flow in the 1st-order fractures is still described by equation (4.37) but ξ_1 (the 'influence' of 2nd-order fractures) must also include the effect of all higher order fractures.

The Laplace transform of equation (4.32) combined with equation (4.33) and using the initial condition given by equation (4.36) is:

$$S_i p\overline{s}_i = T_i\frac{d^2\overline{s}_i}{dz_i^2} - K_{i-1}A_{i-1}\left.\frac{d\overline{s}_{i-1}}{dz_{i-1}}\right|_{z_{i-1}=a_{i-1}} \tag{4.39}$$

which for the highest order (nth) becomes:

$$\frac{d^2\overline{s}_n}{dz_n^2} = \frac{pS_n\overline{s}_n}{T_n} \tag{4.40}$$

The solution of this equation, applying boundary conditions provided by equation (4.34) and (4.35), is:

$$\overline{s}_n = \overline{s}_{n-1}\cosh\left(z_n\sqrt{\frac{pS_n}{T_n}}\right)\Big/\cosh\left(a_{n-1}\sqrt{\frac{pS_n}{T_n}}\right) \tag{4.41}$$

Applying the first derivative of (4.41) in the equation of flow in the (n-1) order (equation 4.39) allows retrieving:

$$S_{n-1}p\overline{s}_{n-1} = T_{n-1}\frac{d^2\overline{s}_{n-1}}{dz_{n-1}^2} - K_n A_n \overline{s}_{n-1}\sqrt{\frac{pS_n}{T_n}}\tanh\left(a_{n-1}\sqrt{\frac{pS_n}{T_n}}\right) \tag{4.42}$$

which after algebraic manipulation can be transformed into:

$$T_{n-1}\frac{d^2\overline{s}_{n-1}}{dz_{n-1}^2} = S_{n-1}p\overline{s}_{n-1} + pS_n\frac{\tanh(u_n)}{u_n} \tag{4.43}$$

where $u_n = a_{n-1}\sqrt{\frac{pS_n}{T_n}}$ for large values of n (for general u_i see equation 4.50 below). Further simplification and rearrangement leads to:

$$\frac{d^2\overline{s}_{n-1}}{dz_{n-1}^2} = \overline{s}_{n-1}\frac{pS_{n-1}}{T_{n-1}}\left[1+\frac{S_n}{S_{n-1}}\mathrm{B}(u_n)\right] \tag{4.44}$$

Equations (4.40) and (4.44), representing flow in two consecutive levels, are equivalent equations if:

$$\xi_i^2 = p\frac{S_i}{T_i}\left[1+\frac{S_{i-1}}{S_i}\beta_{i-1}\mathrm{B}(u_{i-1})\right] \tag{4.45}$$

and

$$\beta_{i-1} = 1+\frac{S_{i-2}}{S_{i-1}}\beta_{i-2}\mathrm{B}(u_{i-2}) \tag{4.46}$$

In such case, equations (4.40) and (4.44) can be rewritten in a similar form:

$$\frac{d^2\overline{s}_n}{dz_n^2} = \overline{s}_n\xi_n^2 \tag{4.47}$$

taken into account that $\beta_n = 1$, and that $\frac{S_{n+1}}{S_n} = 0$, which implies $\xi_n^2 = \overline{s}_n\frac{pS_n}{T_n}$.

Since equation (4.39) is recursive and always returns equations similar to (4.47), this can be generalised to:

$$\frac{d^2\overline{s}_i}{dz_i^2} = \overline{s}_i\xi_i^2 \tag{4.48}$$

If the same generalisation is done for recursive equation (4.46) and the value of β_i is replaced into equation (4.45), this can be generalised to:

$$\xi_i^2 = p\frac{S_i}{T_i}\left\{1+\frac{1}{S_i}\sum_{j=i+1}^{n}S_j\left[\prod_{l=i+1}^{j}\mathrm{B}(u_l)\right]\right\} \tag{4.49}$$

where u_i is redefined as:

$$u_i = \xi_i a_{i-1} \tag{4.50}$$

$$\mathrm{B}(u_i) = \frac{\tanh(u_i)}{u_i}, \text{ for slabs at every hierarchical level} \tag{4.51}$$

As expected for a multiple-porosity system, the effect of each order of fractures is included in the effect of the immediately preceding order (equation 4.49). Therefore, the solution for drawdown imposed by a well pumping a multiple-porosity aquifer is:

$$\overline{s}_1(r,p) = Q\frac{\mathrm{K}_0(\xi_1 r)}{p\pi T_1} \tag{4.52}$$

where ξ_1 is defined according to equation (4.49). Thus, the solution is still the generalized well function provided by equations (4.37) and (4.38), with an effective block geometry function defined as:

$$B_{eff}(u) = \frac{1}{S_2}\sum_{i=1}^{n} S_{i-1}\left[\prod_{l=2}^{i}\mathrm{B}_l(u_l)\right] \tag{4.53}$$

where the subscript l on B_l indicates that the block shape at each hierarchical level may not be the same. Although in the formulae above, slab shaped blocks were used, any other shape is applicable provided the necessary adjustments are made in equation (4.51). See table 4.1 for definition of other BGFs.

4.3.2 Equivalence to dual-porosity behaviour

Analogy with the dual-porosity solution can lead to further simplification of the BGF equation. It appears that only the 2nd-order fractures have a direct influence on the conductive fractures (1st-order) flow behaviour. Higher fracture orders (i>2) are only relevant for the conductive fractures because they increase the amount of water that these receive from 2nd-order fractures. Thus, the hydraulic parameters and geometry of sets higher than two are irrelevant to the conductive fractures.

Therefore, hydraulically, the hierarchical model is similar to a dual-porosity model, equations (4.37) or (4.52), with $\xi^2 = p\frac{S_1}{T_1}\left[1+\frac{S_2}{S_1}\mathrm{B}_{\mathrm{eff}}(\mathrm{u})\right]$. The effective BGF, $\mathrm{B}_{\mathrm{eff}}(u)$, can then be expressed in terms of u_2 only, by algebraic manipulation of equations (4.49) and (4.50):

$$\mathrm{B}_{\mathrm{eff}}(\mathrm{u}) = \frac{u_2^2}{p}\mathrm{B}_2(u_2) \tag{4.54}$$

This equation has the same number of unknowns as the equivalent dual-porosity equation. For instance, for slab-shaped 2nd-order blocks, the effective BGF of a hierarchical fracture system is simply $B_{eff}(u) = \frac{u_2}{p}\tanh(u_2)$.

Appendix A gives some additional properties of the effective BGF, $B_{eff}(u)$.

Equivalence to standard dual-porosity solutions can also be sought by finding the *'effective storage'* of the hierarchical fractures system, with the parameter ξ expressed now as $\xi^2 = p\frac{S_1}{T_1}\left[1+\frac{S_{eff}}{S_1}B\ (u_2)\right]$. The equations to analyze in order to determine the 'effective storage' are (4.38) and (4.49) which give S_{eff} as:

$$S_{eff} = S_2 + \sum_{i=2}^{n} S_{i-1}\left[\prod_{l=2}^{i} B_l(u_l)\right] \tag{4.55}$$

Using this definition, the solution of 1-D flow in a multiple-porosity aquifer is equivalent to the dual-porosity model, with matrix storage provided by equation (4.55). Notice that, due to the dependence of u_l on p, the effective storage is not a constant and varies with time, outlining that the contribution of each level to flow occurs at different times.

For early times, that is large values of p and u, the BGF at each level can be approached by $B_l(u_l) = \frac{1}{u_l}$ and the 'effective storage' will be represented by:

$$S_{eff} = S_2 + \sum_{i=2}^{n} S_{i-1}\left[\prod_{l=2}^{i} \frac{1}{u_l}\right] \tag{4.56}$$

which obviously converges to S_2 as $u_1 \to \infty$ (or $t \to 0$), since the 2nd-order fractures are the first to contribute flow to the conductive 1st-order fractures.

For very large times, the limit as $t \to \infty$ can be studied using the limit as $p \to 0$ and therefore the BGF at each level, B_l will converge to 1, allowing to find the following 'quasi-steady-state' solution for the 'effective storage':

$$S_{eff} = \sum_{i=2}^{n} S_i \tag{4.57}$$

which shows that for late-time behaviour, the 'equivalent matrix storage' tends to a constant value: the total storage.

4.3.3 One-dimensional transport model – analytical solution

Analytical solutions for one-dimensional solute transport in dual-porosity medium were developed by several authors, including Barker (1982) which derived a solution in Laplace space, and Sudicky and Frind (1982) which inverted analytically the Laplace transforms. The two solutions are obviously equivalent, but the simplicity of the Laplace space solution makes it preferable. Further, Barker (1982) also derived the solution for radial transport of a solute injected at a well.

Since the multiple-porosity model is just a generalization of the dual-porosity model, it should be possible to find a solution for one-dimensional solute transport in a multiple-porosity medium.

Using the same model geometry and assumptions as Barker (1982), the solution for one-dimensional transport when there are two hierarchical levels ($i=2$) is the same as the dual-porosity solution derived by Barker (1982) as:

$$\bar{C}_1(r,p) = \frac{C_0}{p} e^{-\frac{v+\sqrt{4\chi D+v^2}}{2D} r} \tag{4.58}$$

where $\bar{C}_1(r,p)$ represents solute concentration in the 1st-order fractures and C_0 represents the inlet constant concentration in the system (notice that Laplace transform variables are used). D is the longitudinal dispersion coefficient in the main fractures and v is constant advective velocity, also acting only in the 1st-order fractures. The parameter χ is defined as:

$$\chi = p\left[1+\frac{\phi_2}{b_1} a_1 B(u)\right] \tag{4.59}$$

where ϕ_2 is porosity of the 2nd-order medium, $u = a_1\sqrt{\frac{p}{D_2^*}}$ and B(u) is the block geometry function already defined for slabs as $B(u) = \tanh(u)/u$.

Comparison of this transport situation with the flow model discussed in the previous section, indicates that, again, parameter χ must change to account for a larger number of hierarchical orders. Equation (4.58) remains valid for describing solute concentration in the first order fractures, the ones where advection and longitudinal dispersion have an effect. Since solute in these main fractures only diffuse to the 2nd-order fractures, any changes that need to be made are related to the parameter χ, which includes the effect of diffusion into higher order fractures.

Subject to the conditions that water flow in the higher order fractures obeys Darcy's law while solute transport follows Fick's laws, the mathematical descriptions of water flow and solute transport are the same (Barker 1985a). This can be seen in the similarity of the ξ and χ parameter

description in both equations (4.38) and (4.59), provided the correspondence indicated in table 4.2 is made:

Table 4.2 – Correspondence between water flow and solute transport models (adapted from Barker (1985a)

Transport mechanism	
Water flow	*Solute transport*
Drawdown (s)	Concentration (C)
Specific storage (Ss)	Porosity (ϕ)
Hydraulic conductivity (K)	Diffusion coefficient (D*)

Therefore, the solution to one-dimensional solute transport in a multiple-porosity system is still equation (4.58), with the parameter χ defined using the effective block geometry function, adapted from equation (4.49):

$$\chi_i = p\left\{1+\sum_{j=i}^{n}\left[\prod_{l=i}^{j}\frac{\phi_{l+1}}{b_l}a_l \mathrm{B}(u_{l+1})\right]\right\} \tag{4.60}$$

$$B(u)=\sum_{j=2}^{n}\left[\prod_{l=2}^{j}\frac{a_l}{b_l}\phi_{l+1}B_l(u_l)\right] \tag{4.61}$$

$$u_i = \chi_i a_{i-1} \tag{4.62}$$

where the subscript l on B_l indicates that the block shape at each hierarchical level may not be the same. For example:

$$B_i(u_i)=\frac{\tanh(u_i)}{u_i}, \text{ for slabs at each level} \tag{4.63}$$

4.3.4 MULTIPOROSITY code

The multiple-porosity solutions described in the previous sections were implemented in a computer code designated MULTIPOROSITY. The code was written in FORTRAN and performs all computations in that programming language, including the numerical inversion of the Laplace transform. However, input and output to MULTIPOROSITY is accomplished in an EXCEL workbook via a DLL (Dynamic Link Library) that involves programming in VISUAL BASIC. The EXCEL interface facilitates data input and visualisation of results.

MULTIPOROSITY has two modules: one using the flow solution presented in section 4.3.1 to compute drawdown imposed by a pumping well, and a second module based on the one-dimensional transport solution (section 4.3.3) to compute the solute concentration at time t and distance r from the source.

In order to simplify the formulation used and its implementation on the computer code, the following simplification was made to the radial flow model: storativity of each fracture is regarded as constant throughout all fracture orders, i.e. $S_i/S_{i-1}=1$, while the ratio between successive fracture spacing can vary freely. This increases versatility to data input, while still considering storage capacity variation at each fracture level, as a function of decreasing fracture spacing a_i.

In the radial flow module, both input formats (with and without constant S_i/S_{i-1}) were used.

Input for the one-dimensional transport model includes the **inlet pulse duration**. This allows analysis of situations in which the contaminant source is continuous, by setting the sampling time lower than the pulse duration, or situations in which the contaminant source is a pulse, by setting the sampling time later than the inlet pulse duration.

Both MULTIPOROSITY modules allow different block geometries (slabs, spheres or cylinders) at each hierarchical level.

4.3.5 Radial flow model type-curves and relevance of the number of fracture sets

Using a hierarchical fractured system in which the value of *S* of each fracture (regardless of fracture order) was kept constant and assuming that fracture spacing varies according to $a_i/a_{i-1}=0.2$, a number of simulations were made. The aim was to generate a series of type-curves for the flow model and to test the influence of the number of fractures orders.

The maximum number of hierarchical orders admitted was five and the minimum was two. In all cases $T_1 > T_2 = T_3 = T_4 = T_5$. Fracture spacing begins at 10 m for a_i and decreases by a factor of 0.2 for each successive fracture order. Obviously fracture spacing such as the one of order 5 (0.016 m) are not realistic and were used only for comparison purposes (table 4.3).

Table 4.3 – Parameters used in the generation of type-curves for the multiple-porosity radial flow model

Parameter	*Value*
Flow rate (Q)	10^{-4} m^3/s
Distance to the well (r)	0.35 m
Aquifer thickness (H)	10 m
Transmissivity T_1	1.99×10^{-6} m^2/s
Transmissivity $T_2= T_3= T_4= T_5$	6.80×10^{-7} m^2/s
Storativity ($S_1= S_2= S_3= S_4= S_5$)	5×10^{-5}
Half fracture spacing ($a_1= 5a_2= 25a_3= 125a_4= 625a_5$)	5 m

Figure 4.13 shows drawdown plots for the radial flow model. Progressive deviation from Theis type curve with increasing number of fracture sets is significant. It is important to mention that when using only two fracture sets (or even three) the effect is similar to dual-porosity, since the transition between two parallel straight lines is smooth. Only when using four and five fracture sets is the transition more sudden. All orders of fracture seem to be influential, and therefore higher orders should not be ignored.

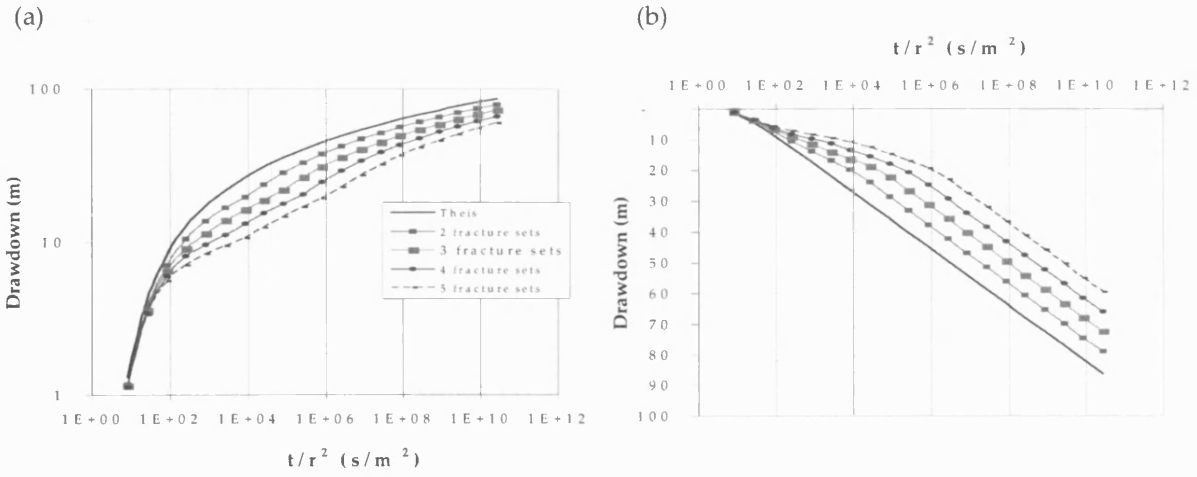

Figure 4.13 – Log-log (a) and semi-log (b) plots of drawdown in multiple-porosity networks.

The drawdown derivative type-curves (Bourdet et al. 1983) can also be computed on the basis of the formulation presented above. Modern pumping test analysis has been considerably enhanced by the use of the derivative plot, which provides a graphic presentation of $\log\left(t\frac{ds}{dt}\right)$ versus $\log t$. This analysis is very helpful in identifying situations that resemble dual-porosity behaviour. According to Horne (1997), dual-porosity behaviour results in derivative curves similar to the ones shown in figure 4.14.

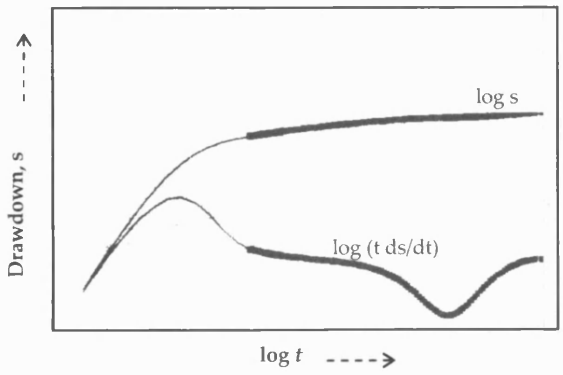

Figure 4.14 – Dual-porosity behaviour in a derivative plot. After Horne (1997).

For the multiple-porosity model, the drawdown derivative plots (fig. 4.15) show a gradual change from almost the Theis type-curve (for two fracture sets) to curves with well-defined minimum for four and five fracture sets. The shape of the derivative curves resembles the typical dual-porosity curves (fig. 4.14) for all simulations, even if attenuated for simulations with only two and three fracture sets.

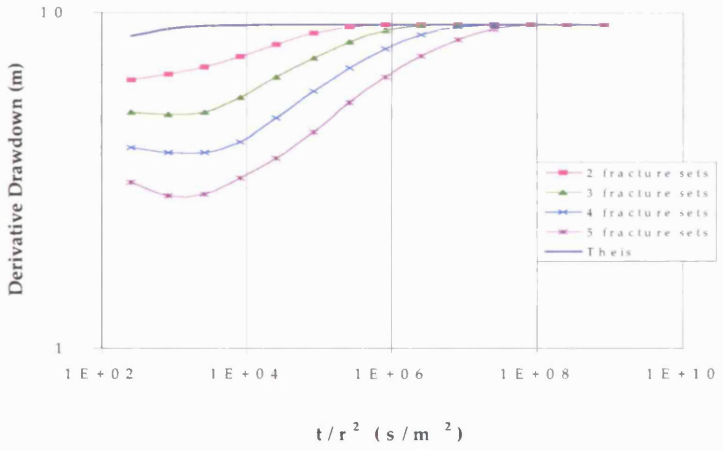

Figure 4.15 – Derivative of drawdown in multiple-porosity networks.

4.3.6 One-dimensional transport model type-curves

MULTIPOROSITY was also used to generate type-curves for the multiple-porosity transport model presented in section 4.3.3, both for situations involving a continuous source and for situations involving a pulse source. A sampling distance (r) of 20 metres was arbitrarily chosen and type curves were generated for a hierarchical fracture system with up to five fracture orders. The situation involving a single fracture set was generated for comparison purposes only, and it coincides with one-dimensional transport with advection and longitudinal dispersion but without any matrix diffusion effect.

Table 4.4 shows the parameters used in the type-curves generation. To simplify the situation, constant values of porosity, diffusion coefficient and fracture aperture were used for all fracture sets. A common assumption of longitudinal dispersivity equal to distance/10 was used, bearing in mind that the conclusions are valid for any other value of dispersivity, which influences only solute dispersion in the 1st-order fractures.

Table 4.4 – Parameters used in the type-curve generation for the multiple-porosity transport model

Parameter	*Value*
Advective velocity (v)	6×10^{-5} m/s
Longitudinal dispersion (D)	12×10^{-5} m²/s
Diffusion Coeff. ($D_2^*=D_3^*=D_4^*=D_5^*$)	1×10^{-10} m²/s
Porosity ($\phi_2=\phi_3=\phi_4=\phi_5$)	0.1
Fracture aperture	1×10^{-3} m
Half fracture spacing ($a_1= 5a_2= 25a_3= 125a_4= 625a_5$)	10 m
Contaminant pulse duration (only for fig. 4.16b)	2×10^{6} s

Figure 4.16 shows the relative concentration variation up to 4×10^{6} seconds (46.3 days). The effect of diffusion into the higher fracture levels is dramatic, with solute concentration decreasing drastically with increasing number of fracture levels. When compared to the simple advection-dispersion model (one fracture set), the effect is particularly striking when there are two levels of fractures involved (the dual-porosity model). The influence of further fractures orders of becomes progressively attenuated.

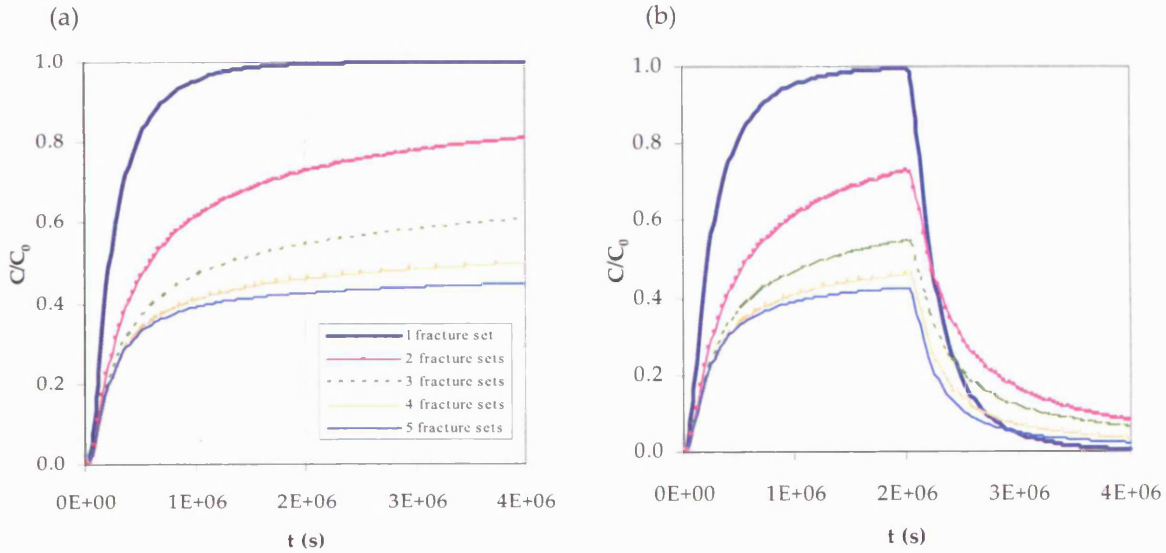

Figure 4.16 – Change in relative concentration according to the one-dimensional multiple-porosity model. a) continuous contaminant source, b) finite-period pulse contaminant source.

This behaviour can best be understood by resorting to the computation of the time to diffuse across each hierarchical level, according to:

$$t_{d_i} = a_i^2 \phi_i / D_i^* \tag{4.64}$$

For the fracture system characterised in table 4.4, similar values of porosity and diffusion coefficient were adopted, while fracture spacing was set to decrease by a constant factor of 5 between consecutive fracture orders. Consequently, the time to diffuse across 5th-order fractures is

only of 0.74 days, with t_d increasing by a factor of 25 for consecutive higher orders of fractures, up to a maximum of 793 years to diffuse across the 2nd-order.

Therefore, in the simulations depicted in figure 4.16 diffusion occurred completely only across orders four (t_d = 18.5 days) and five (t_d = 0.75 days). The time necessary to diffuse across the 2nd level explains that the major influence to the breakthrough curves shape is from that hierarchical level.

4.4 RELIABILITY OF THE MULTIPLE-POROSITY MODEL AND MULTIPOROSITY CODE

To test the reliability of the multiple-porosity model and of the code in which the model was implemented it was decided to compare the results of the multiple-porosity model with the analytical solutions of a dual-porosity model, thus studying the discrepancies between the two solutions. In addition, the analytical multiple-porosity results are compared with the results of a numerical discrete fracture network model in which the fractures are arranged in a manner to resemble a hierarchical fracture system. Finally, this section also considers the conditions under which the multiple-porosity model is no longer valid.

4.4.1 Adequacy of the dual-porosity assumption for analysis of multiple-porosity flow problems

To test the acceptability of studying multiple-porosity media using a classic dual-porosity analysis, the module PTFIT of code BGSPT was used (Barker and MacDonald 2000). That program attempts to fit the well function to a set of drawdown data by automatic variation of the aquifer parameters. It allows both single-porosity and dual-porosity systems to be analysed.

Table 4.5 shows the comparison between the parameters obtained with PTFIT and the parameters used in the multiple-porosity simulation (that is to say, PTFIT was calibrated against synthetic data generated with the MULTIPOROSITY code)[1]. Also shown is the Root Mean Square deviation[2] (RMS), which, to a point, is a measure of the acceptability of the PTFIT solution.

---

[1] The results from PTFIT were multiplied by the 1st order fracture spacing to convert from $Ss_{(matrix)}$ and $K_{(matrix)}$ into S_2 and T_2. The parameters not listed in table 4.5, such as pumping rate, distance to the well and aquifer thickness were the same as listed in table 4.3, section 4.3.5. Notice that T_1 and S_1 were not estimated by PTFIT: they were provided as fixed values.

[2] The Root Mean Square (RMS) is a measure of the deviation between observed and predicted drawdown and is given by $RMS = \sqrt{\sum_{i=1}^{n}(\Delta s_i)^2/n}$, where Δs is the drawdown difference and n is the number of drawdown observations.

Table 4.5 – Comparison between hydraulic parameters obtained for MULTIPOROSITY with PTFIT and parameters used in analytical simulation

	Dual-porosity model (PTFIT) best-fit				*MULTIPOROSITY*
Parameter	*2 fracture sets*	*3 fracture sets*	*4 fracture sets*	*5 fracture sets*	
T_1 (m²/s)	1.99×10^{-6}	1.99×10^{-6}	1.99×10^{-6}	1.99×10^{-6}	$T_1 = 1.99\times10^{-6}$ m²/s
S_1	5.0×10^{-5}	5.0×10^{-5}	5.0×10^{-5}	5.0×10^{-5}	$S_1 = 5.0\times10^{-5}$
T_2 (m/s)	6.81×10^{-7}	6.17×10^{-7}	5.00×10^{-7}	3.95×10^{-7}	T_2 (T_3, T_4, T_5) = 6.80×10^{-7} m²/s
S_2	5.01×10^{-5}	2.97×10^{-4}	1.56×10^{-3}	7.78×10^{-3}	S_2 (S_3, S_4, S_5) = 5.0×10^{-5}
RMS	0.026	0.118	0.543	0. 990	

The values of T_2 and S_2, as well as the RMS deviation, obtained for systems with two and three fracture sets can be regarded as reasonable (table 4.5). The same does not happen for four and five fracture sets. Obviously, it is not realistic to consider five different fracture sets and spacing as small as a_5 (0.016 m). However, such behaviour can also be generated for, say, three fracture sets with increasing S in each fracture set. Thus, in these cases the dual-porosity model cannot replicate the hydraulic behaviour of multiple-porosity models.

It is also interesting to note that the value estimated for T_2 using PTFIT decreases with increasing number of orders of fractures.

The percentage error in the fit of the dual-porosity model (fig. 4.17) reveals that change in the drawdown is more sudden and complex than can be generated by a dual-porosity model. A similar error pattern was envisaged for four fracture sets, although with lower absolute errors.

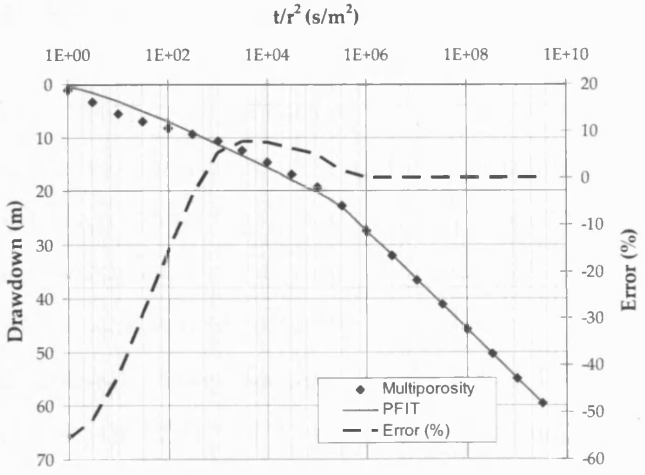

Figure 4.17 – Best-fit obtained with a dual-porosity model (PTFIT) for MULTIPOROSITY network with 5 fracture sets.

4.4.2 Numerical modelling of hierarchical fracture systems

In order to verify the formulation for the multiple-porosity model developed in the previous section, it was decided to conduct numerical modelling of hierarchical fracture systems (HFS). The results of constant rate pumping tests performed on those networks are then compared against the multiple-porosity analytical formulation to check the adequacy of this model.

The hierarchical fracture networks were generated with FRACMAN (Dershowitz et al. 1995), a 3-D discrete fracture network software suite developed by Golder Associates to model the geometry of discrete features, including faults, fractures, paleochannels, karsts and stratigraphic contacts[1].

Flow simulations were conducted in the FRACMAN networks using the finite elements code MAFIC (Miller et al. 1999), also developed by Golder Associates, to simulate transient flow and solute transport through 3-D rock masses with discrete fracture networks.

Besides verifying the multiple-porosity analytical solution, the numerical simulations were also used to test the MULTIPOROSITY code.

4.4.2.1 Generating HFS networks

FRACMAN was used to generate fracture networks that can be regarded as hierarchical. The generation volume was a cube of 200 m x 200 m x 200 m. Fractures were randomly generated using the Poisson Rectangle Model. This model generates fractures that are rectangles and probably it is the best approximation to theoretical media such as the parallel plate models of dual-porosity systems. Due to computer limitations, the number of fracture sets was limited to a maximum of three.

Three distinct fracture networks were created:

- network HFS1 – consisting of only one set of two horizontal fractures (fig. 4.18a). Both fractures extend much further than the limits of the modelling region, and therefore are seen as infinite for purposes of this study. The result of any constant rate aquifer test conducted in this network should be the Theis type curve;
- network HFS2 – consisting of two fractures sets (fig. 4.18b). The first set being the same two horizontal fractures as in HFS1, and the second set being smaller ('finite') vertical fractures, with an area of 20 m x 20 m and density (Area/Volume) of 0.1. The total number of fractures

[1] For further details on discrete fracture network (DFN) models refer to section 5.1.

in this network is 1070. This network attempts to simulate a HFS with two orders of fractures;

- network HFS3 – consisting of three fracture sets (fig. 4.18c). Sets one and two being the same two sets as in HFS2, and the third set being even smaller vertical fractures, with an area of 10 m x 10 m and density (Area/Volume) of 0.1. This third set is orthogonal to the preceding ones. The total number of fractures is now 2291. The third fracture set was generated only in a volume of 40 m x 40 m x 200 m in the centre of the modelling domain, due to computational constrains. Caution was taken that there was no direct intersections between sets 1 and 3, to make sure that set 3 is 'limited' by set 2. This network simulates a HFS with three fracture orders.

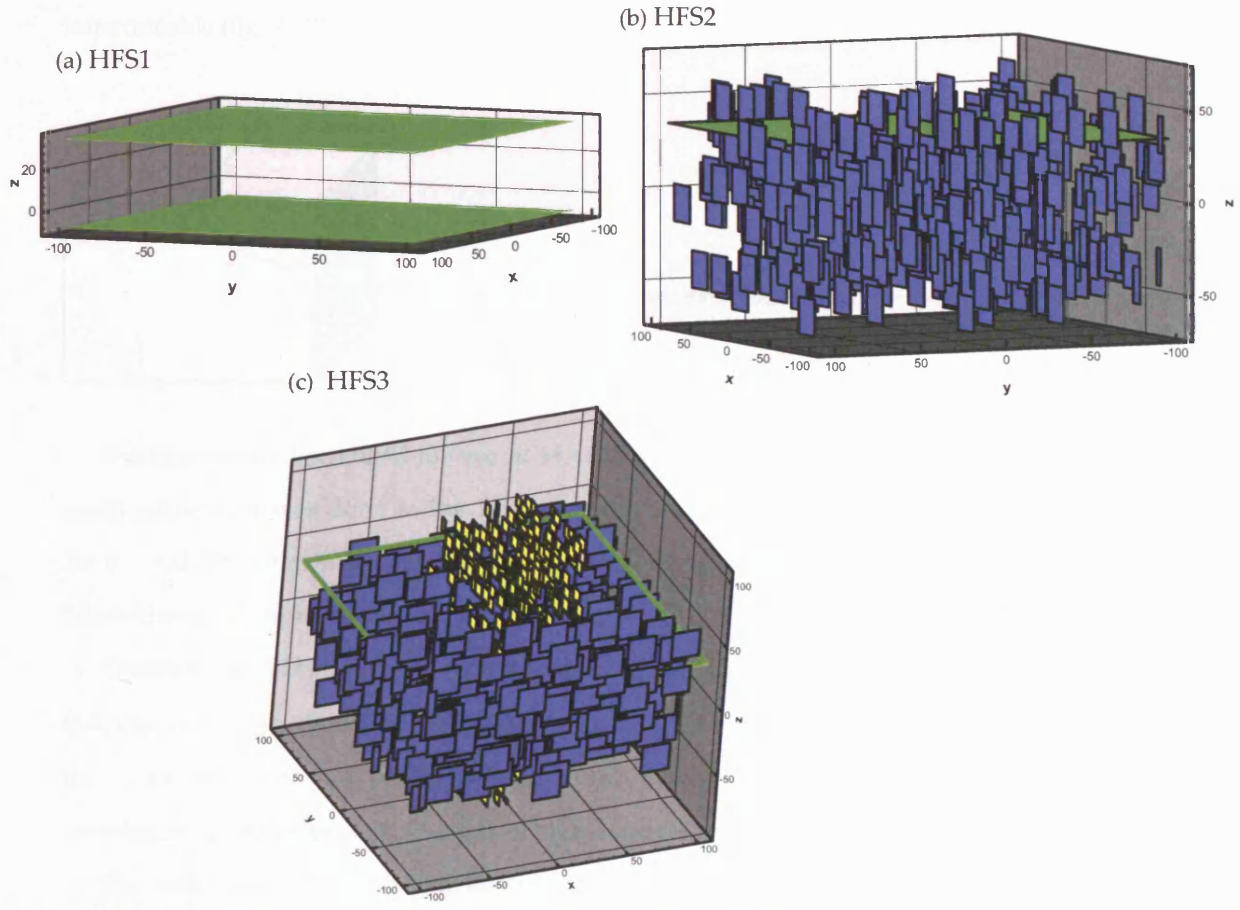

Figure 4.18 – Fracture networks generated with FRACMAN. Green – 1st order fractures, blue - 2nd order fractures, yellow - 3rd order fractures. Not all fractures were drawn. To aid the perception of the 3-D structure, in b) only one fracture plane of set one was drawn and in c) only the trace of one fracture of set one was represented. The second fracture of set one is located as in a). x, y and z in metres.

According to the designation followed hereafter, fractures from set 1 are 1st-order fractures, fractures from set 2 are 2nd-order fractures and fractures from set 3 are 3rd-order fractures.

The hydraulic characteristics of the two fractures of set 1 were kept constant in all simulations as $T_1 = 8.5 \times 10^{-7}$ m²/s and $S_1 = 5 \times 10^{-5}$ (for each fracture). For sets 2 and 3, transmissivity and storativity were varied so that situations were created in which they are either lower or higher than the corresponding properties of set one. Finally, for each scenario the standard deviation of T and S was set to zero, so that T and S are the same for all fractures of the same set.

4.4.2.2 Boundary conditions and fracture discretization

Flow simulations were conducted with MAFIC. The vertical boundaries of the simulated domain were set to constant-head boundaries, while the horizontal boundaries were set to impermeable (fig. 4.19).

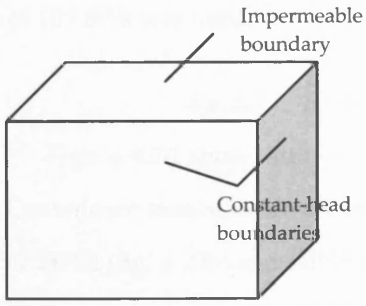

Figure 4.19 – Boundary conditions. Boundaries not visible were given the same boundary conditions depending on being vertical (constant-head) or horizontal (impermeable) faces of a cube.

Fractures were discretized for use in MAFIC according to the usual rules in FRACMAN, but mesh refinement was done in the 10 metres surrounding a vertical well located at coordinates X = 0, Y = 0. The refinement aims to decrease the occurrence of numerical errors where hydraulic heads change abruptly.

Constant rate pumping tests were simulated in the fully penetrating well. Care was taken so that the well intersects only 1st-order fractures, thus ensuring that no water is taken directly from the other sets and that the behaviour of the network is truly hierarchical (i.e. drawdown propagates in sequence from 1st-order to higher orders).

The well has a radius of 0.35 m and measurements of drawdown were made at the well and at four other points on the network. The purpose of those four points was mostly to confirm that the cone of depression did not reach the constant head boundaries. The aquifer test radius of influence was first estimated according to the well-known relation:

$$R_i = \sqrt{\frac{2.25Tt}{S}} \tag{4.65}$$

where T and S are the transmissivity and storage coefficient of a confined, isotropic and homogenous aquifer. Although this relation may not be strictly applicable to fractured environments, it is regarded as acceptable for network HSF1, which should return the Theis solution. Using the T and S parameters for that fracture network (T_1 = 8.5x10^{-7} m^2/s and S_1 = 5x10^{-5} for each fracture) it can be computed that the domain boundaries (at 100 m from the well) will be reached by the cone of depression 72 hours after the beginning of pumping. For that reason the aquifer tests duration was set to a maximum of 50 hours.

In the higher order fracture networks, where transmissivity is similar to HFS1 but where storage is increased by the higher order fractures, it is not possible to use the above equation, but care was taken that drawdown observed in the four control points was negligible.

Having verified that drawdown observed is not affected by constant-head boundaries, only the measurements in the well are presented henceforth. In all simulations a constant pumping rate of 10^{-4} m^3/s was used.

4.4.2.3 Fit between MAFIC data and multiple-porosity model

Figure 4.20 shows drawdown and derivative drawdown plots for the three HFS networks. Drawdown measurements were made at the well face. Notice that the derivative drawdown plots of HFS2 (fig. 4.20b) and HFS3 (fig. 4.20c) networks closely resemble the derivative plots generated by the dual-porosity model (fig. 4.14) and by the multiple-porosity model (fig. 4.15).

Figure 4.21 shows the fit obtained with the MULTIPOROSITY code to the pumping test results. The fit was done visually, but it is equally good for any of the three networks. HSF1 results (Theis type-curve) are reproduced accurately (fig. 4.21a) by the MULTIPOROSITY code. The data produced for networks involving two (HFS2) and three (HFS3) fracture sets fits equally well, thus proving that the multiple-porosity analytical solution is able to reproduce the hydraulic behaviour of complex fracture networks.

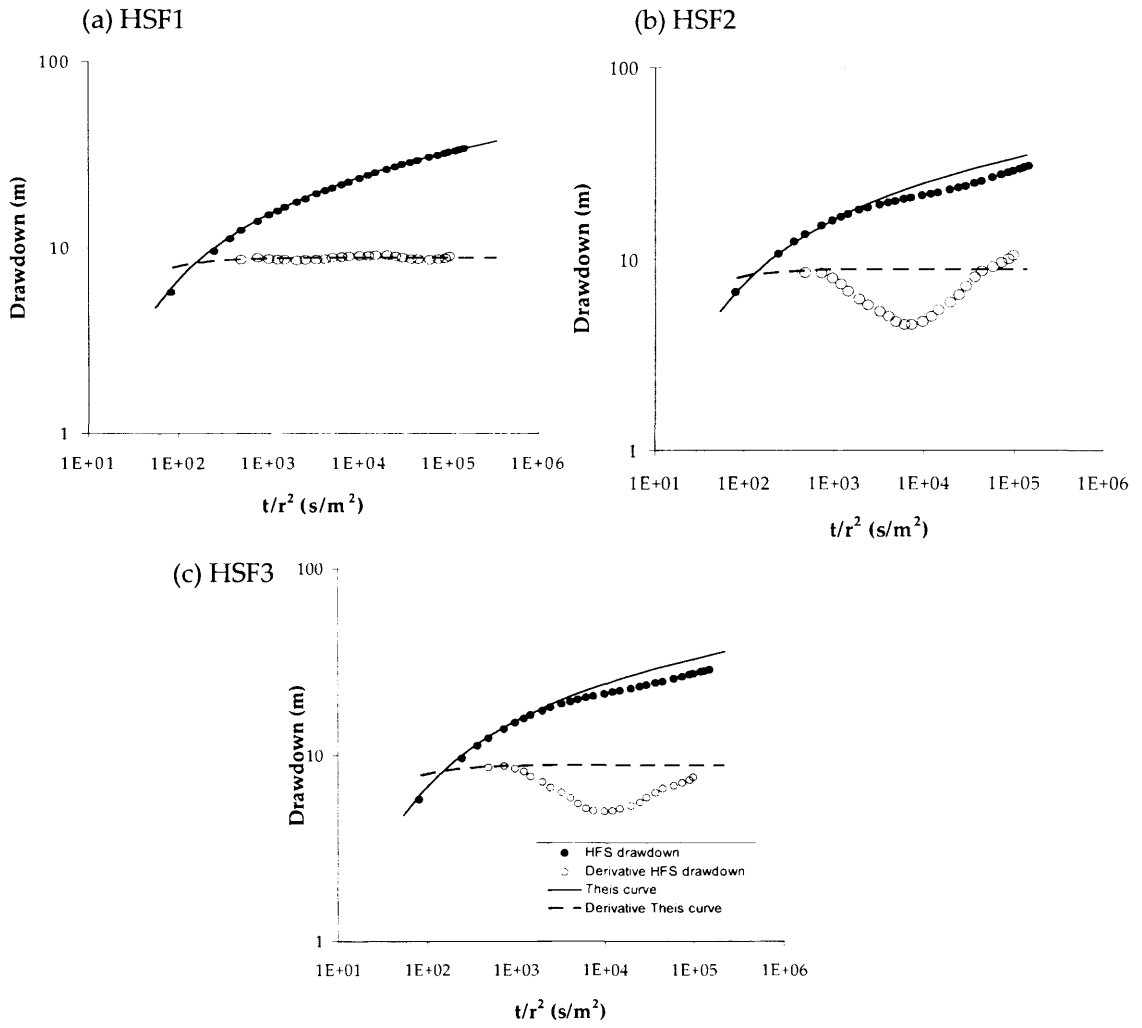

Figure 4.20 – Log-log plots and derivative plots of drawdown in networks HFS1 (a), HFS2 (b) and HFS3 (c).

Table 4.6 compares the parameters obtained with the MULTIPOROSITY code with the hydraulic parameters effectively used in the generation of the hierarchical fracture systems. The comparison is favourable and allows us to conclude that both the multiple-porosity analytical solution and the MULTIPOROSITY code are reliable and valid in describing the behaviour of hierarchical fracture systems.

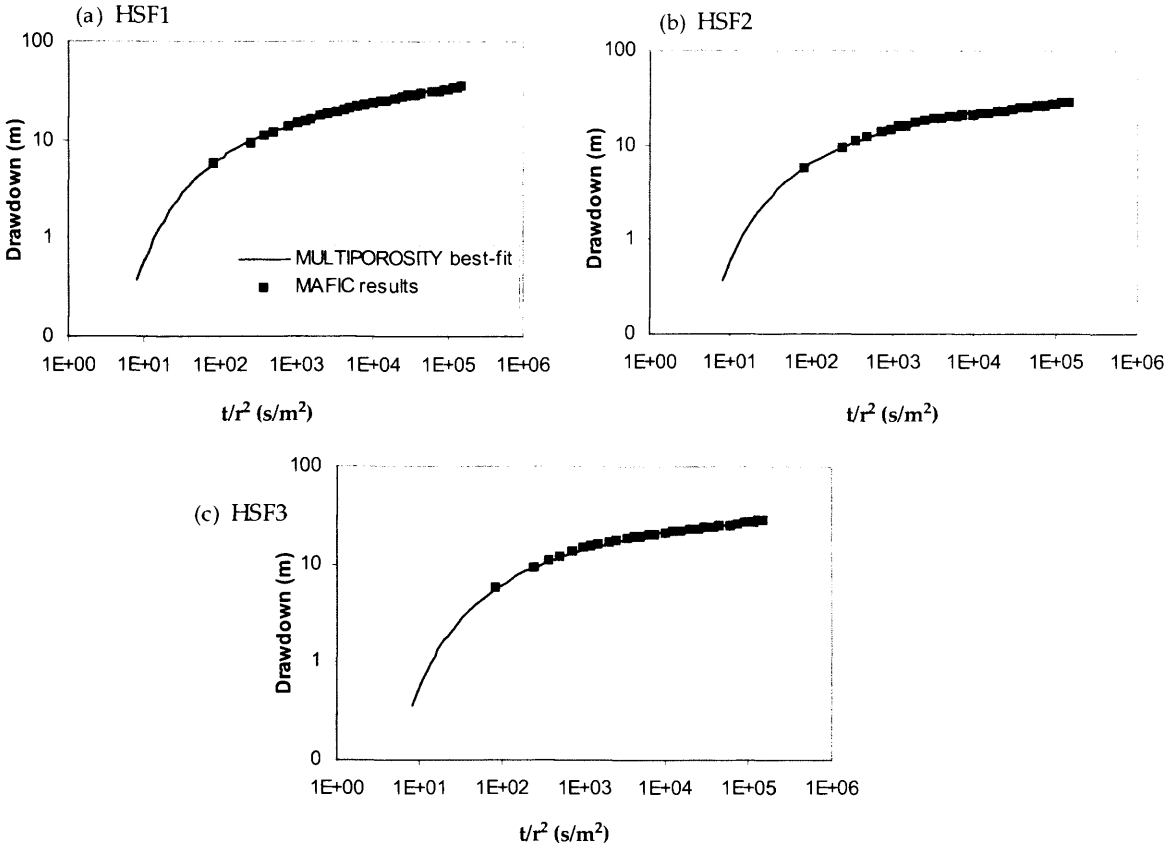

Figure 4.21 – Comparison of MAFIC pumping test results and multiple-porosity model. a) HFS1, b) HFS2, c) HFS3.

Table 4.6 – Comparison between parameters obtained with MULTIPOROSITY and parameters actually used in MAFIC simulations

Parameter	*MAFIC*	*MULTIPOROSITY*
T_1 (m²/s)	1.7×10^{-6}	2×10^{-6}
S_1	10^{-4}	10^{-4}
T_2 (m²/s)	6.8×10^{-9}	4.3×10^{-9}
S_2	5×10^{-4}	10^{-2}
T_3 (m²/s)	6.8×10^{-9}	4.3×10^{-10}
S_3	5×10^{-4}	2×10^{-2}

Further simulations conducted in MAFIC, namely with distinct values of ratios S_i/S_{i-1}, where storativity is equal in the several fracture sets ($S_1 = S_2 = S_3$), or even with storativity decreasing with increasing fracture order ($S_2 < S_3$), were also acceptably reproduced by the MULTIPOROSITY code. Of course, the effect caused by multiple-hierarchical levels decreases for these situations, with the drawdown curves approaching the Theis type-curve. The situation is different whenever transmissivity of fractures sets increases with increasing fracture order ($T_1 < T_2 < T_3$) in which case the multiple-porosity model no longer duplicates the MAFIC results.

4.4.3 Situations for which the multiple-porosity model is not valid

In all simulations studied in section 4.4.2, T_1 is greater than transmissivity of any other fracture set ($T_1>T_i$, i>1). This situation is in agreement with the assumption normally made in dual-porosity models, where $K_{fractures} >> K_{matrix}$. However, there is no reason to assume that higher order fractures should always have lower transmissivity than 1st-order fractures. Often in geological systems, horizontal fractures are the most persistent, but are also the ones subjected to higher lithostatic pressure. This pressure may cause fracture closure, thus diminishing its transmissivity when compared, for instance, with shorter vertical joints.

A series of simulations were conducted in network HFS2 for which several ratios of T_2/T_1 were used (fig. 4.22). In all cases, S_2 was kept below S_1.

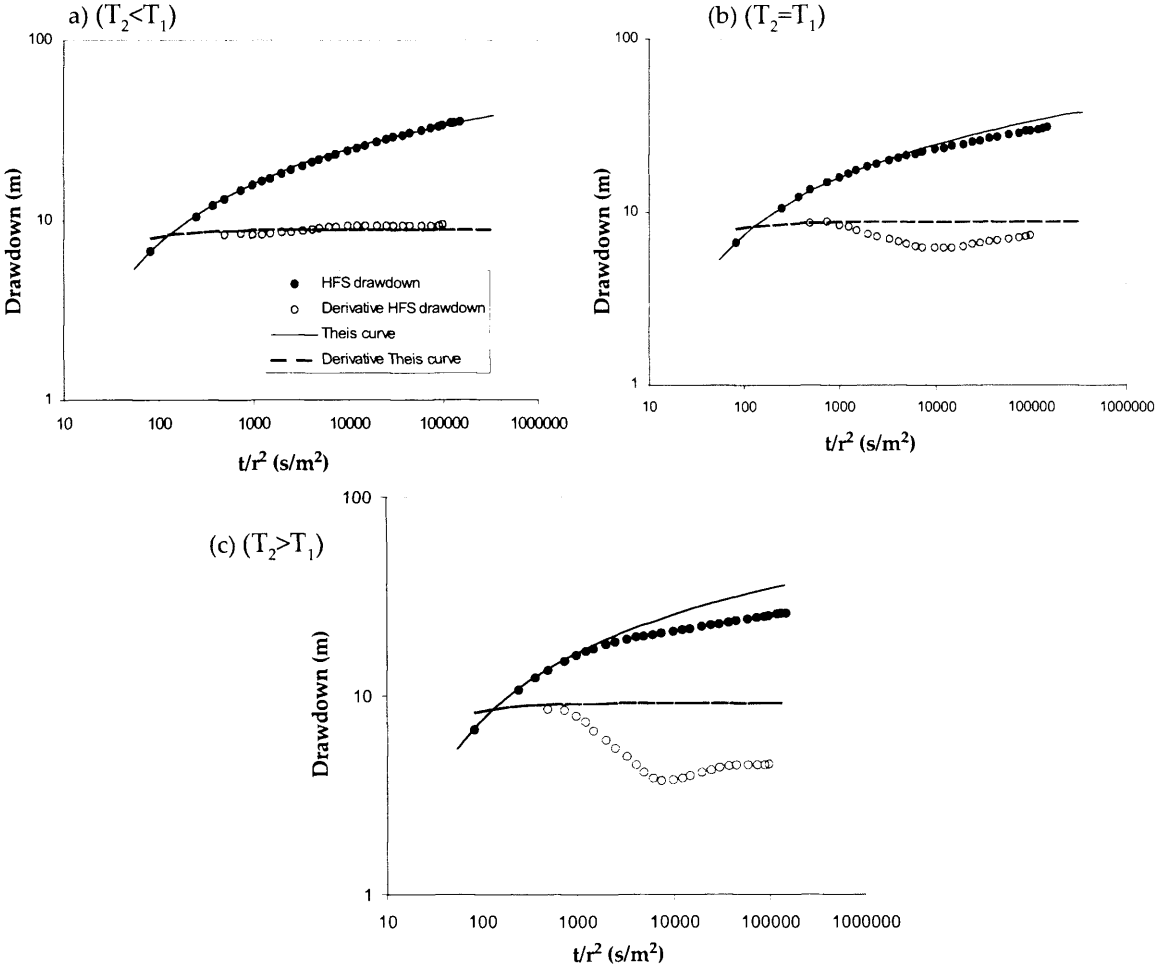

Figure 4.22 – Log-log plots and derivative plots of drawdown in network HFS2 for varying ratios of T_2/T_1. In all cases $S_2<S_1$.

The increase in T_2 causes a deviation from the theoretical Theis curve as well as an increasing departure from the dual-porosity behaviour, since the drawdown derivative does not fully recover from the minimum. The drawdown derivative curves have peculiar shapes that resemble the type-curves for intersection of linear impermeable boundaries (Horne 1997), which is not the case. No other similar type curves were found in the literature.

A semi-log analysis (fig. 4.23) of the cases $T_2 = T_1$ and $T_2 > T_1$ suggests that the drawdown curve can be fitted by two straight lines.

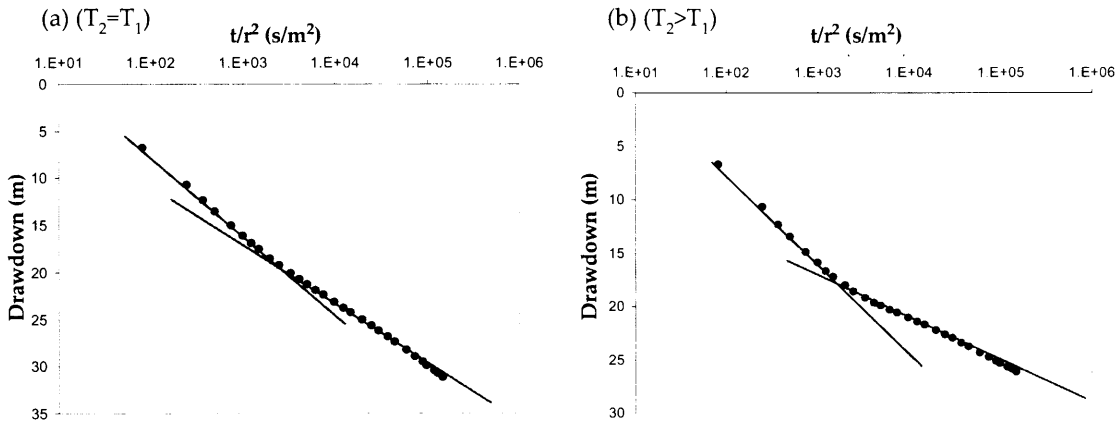

Figure 4.23 – Semi-log plot of drawdown in network HFS2 and straight line fit.

Dual-porosity and multiple-porosity models cannot explain this hydraulic behaviour. In these models, flow from the matrix into the fractures is regarded as one-dimensional and, therefore, the increment in matrix hydraulic conductivity (K_{matrix}) has the effect of reducing the time over which the dual-porosity effect is visible.

To understand how drawdown evolves in 2nd-order fractures a transient finite differences model was built within an Excel workbook (fig. 4.24a). The aim was to sample drawdown in several locations of a 2nd-order fracture at any given time, both for 1-D and 2-D flow in the 2nd-order fractures. The model was able to replicate the hydraulic behaviour illustrated in figure 4.22 and figure 4.23 (even though it included a much smaller number of 2nd-order fractures) and accordingly it was considered as valid.

Figure 4.24 shows two views of the same 2nd-order fracture plane, extending from X = -200 m to X = +200 m, and located at Y = 20 m and having a width (or spacing between 1st-order fractures) of 40 metres (the 1st-order fractures are intersected by the well at Z = ±20 m). The fracture was made to terminate against the 1st-order fractures. Widths were investigated but the pattern of behaviour did not change. The same hydraulic parameters were used in the generation of both 1-D and 2-D

simulations, always keeping $T_2 > T_1$. Both views were taken at the same time since the beginning of the test.

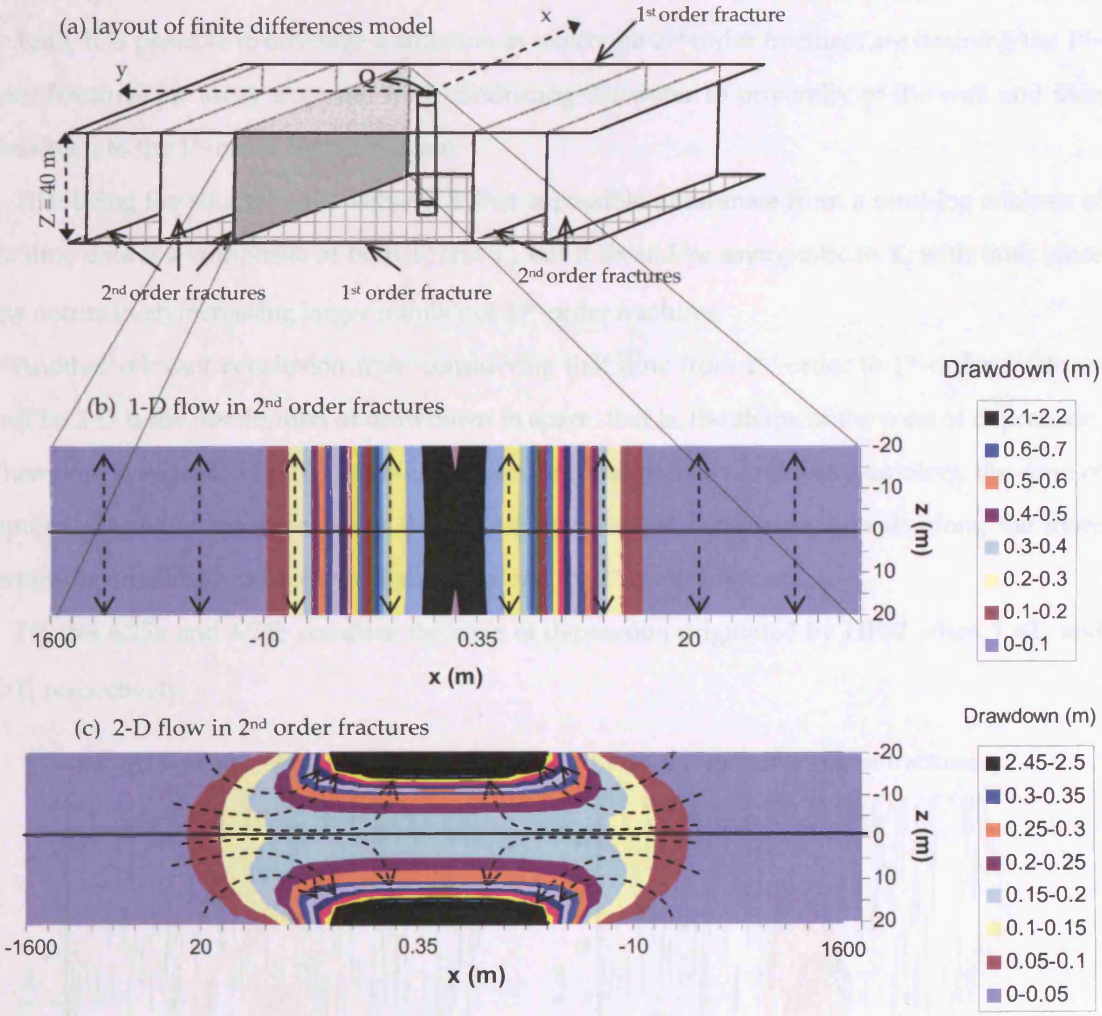

Figure 4.24 – Discrete fracture model built in EXCEL workbook. a) Layout of model. Fracture planes were discretized using finite differences. Not all 2nd-order fractures are drawn. Drawdown contours were made in the plane of shaded 2nd-order fracture considering b) 1-D flow and c) 2-D flow inside the fracture and between 1st and 2nd-order fractures. Arrows indicate flow direction. Notice that scale in the x-axis is not linear.

Figure 4.24b illustrates the situation in which flow is regarded as 1-D, and it is clear that a pseudo-steady-state was reached since flow does not occur longitudinally along the 2nd-order fractures. This agrees with existent models for dual-porosity (and for leaky) aquifers, where $K_2 << K_1$.

Figure 4.24c shows the situation in which flow inside the 2nd-order fractures is allowed to be two-dimensional. The flow pattern is now considerably more complex. In addition, overall, drawdown is now smaller than in 1-D flow. In fact drawdown now propagates in distance more

rapidly along the 2nd-order fractures than along the larger 1st-order fractures, T_2 being larger than T_1. Therefore, even though the well does not intersect 2nd-order fractures, these fractures are conducting water to a distance near to the well and then releasing it to the 1st-order fractures. At the limit, it is possible to envisage a situation in which the 2nd-order fractures are draining the 1st-order fractures far away from the well, conducting the water to proximity of the well and then releasing it to the 1st-order fractures again.

That being the situation, the value of T that is possible to estimate from a semi-log analysis of late time data is a composite of both T_2 and T_1, but it should be asymptotic to T_2 with time, since flow occurs in an increasing larger number of 2nd-order fractures.

Another relevant conclusion from considering that flow from 2nd-order to 1st-order fractures must be 2-D is the distribution of drawdown in space, that is, the shape of the cone of depression. When flow is regarded as 1-D, such as happens in dual-porosity and leaky aquifers, the cone of depression is truly isotropic, but if flow is 2-D the cone of depression extends along the more permeable fractures and becomes elongated along the 2nd-order fractures.

Figures 4.25a and 4.25b compare the cone of depression originated by HFS2 when $T_2<T_1$ and $T_2>T_1$ respectively.

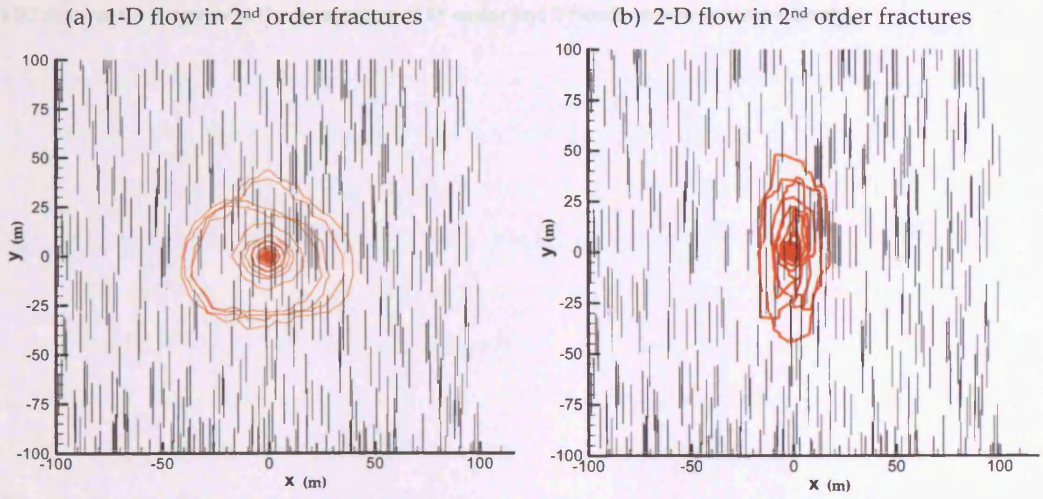

Figure 4.25 – Shape of the cone of depression for HFS2 under different T_2/T_1 ratios. Traces represent the 2nd order fractures. The 1st order fractures are horizontal and perpendicular to the 2nd order, coincide with the plan view.

MAFIC models flow along fractures as 2-D and so it was decided to perform, for comparison purposes, a simulation with $T_2<T_1$, because this approximates 1-D flow along 2nd-order and into 1st-order fractures. In the situation similar to the dual-porosity behaviour, the cone of depression is

close to isotropic and, in a plan view it, approximates a circle. For the situation in which $T_2>T_1$ the cone is affected by anisotropy and ellipses are shown in a plan view.

Therefore, drawdown distribution both in time and in space for a HFS with T increasing with hierarchy shows a pattern that cannot be reconciled with multiple-porosity or Theis analysis.

Obviously, it is possible to do a partial interpretation. A Cooper - Jacob analysis of the $T_2>T_1$ situation was applied to both straight lines of the semi-log chart. Results are compiled in table 4.7 including, for comparison purposes, the parameters used in the simulation. Attention is drawn to the fact that S_2 seems to be underestimated, with error increasing proportionally to the ratio T_2/T_1.

Table 4.7 – Comparison between hydraulic parameters obtained with Cooper-Jacob analysis and parameters used in numerical simulation (The results of the Cooper-Jacob analysis have been divided by two, since this was the number of first order fractures).

		$T_2<T_1$		$T_2=T_1$		$T_2>T_1$	
	Parameter (*)	Cooper-Jacob	MAFIC	Cooper-Jacob	MAFIC	Cooper-Jacob	MAFIC
Early time	**T_1 (m²/s)**	1.02×10^{-6}	8.50×10^{-7}	1.02×10^{-6}	8.50×10^{-7}	1.02×10^{-6}	8.50×10^{-7}
	S_1	4.92×10^{-5}	5.00×10^{-5}	3.68×10^{-5}	5.00×10^{-5}	3.78×10^{-5}	5.00×10^{-5}
Late time	**T_2 (m/s)**	-	6.80×10^{-9}	1.41×10^{-6}	8.50×10^{-7}	2.12×10^{-6}	6.80×10^{-5}
	S_2	-	1.00×10^{-5}	7.95×10^{-6}	1.00×10^{-5}	5.70×10^{-7}	1.00×10^{-5}

(*) T_1, S_1 and T_2, S_2 in Cooper-Jacob column mean the best-fit parameters in early and late time data respectively. In MAFIC column they represent the parameters of 1st-order and 2nd-order fractures, respectively.

Chapter 5

PROTECTION ZONES FOR FRACTURE NETWORKS I

OVERVIEW AND STATISTICAL CONTINUUM METHOD

Previous chapters dealt with fractured-rock aquifers in an essentially similar way – the methods used for delineating the protection zones were based on the overlapping of two continuous porous media. In chapter three, the two continua were the single linear feature and the surrounding country-rock, while in chapter four the continua were a network of infinite fractures and the matrix blocks limited by those fractures.

However, most fractured-rocks will exhibit fracture patterns that are not described by the relatively simple geometries and solutions used in those chapters. Generally, fractured-rock aquifers show fracture patterns with some randomness in terms of fracture geometry and hydraulic characteristics. The fractures are usually small in area compared to the study scale, but their (finite) size may have a major impact in the flow and transport properties of the aquifers. Finally, the fact that the hydraulic properties of the fractures are not constant will cause flow and transport to occur mostly through a small number of fractures, with most fractures being less important or even non-conductive (National Research Council 1996).

These fractured-rock aquifers with fracture patterns exhibiting some degree of randomness will be designated hereafter as **fracture networks** (fig. 5.1) and, under the circumstances described above, it is not at all obvious that an Equivalent Porous Medium assumption is suitable for such media. In fact, extensive studies conducted since the beginning of the 1980's, mainly related to radioactive wastes disposal, have shown that a REV (a necessary condition for assuming EPM) may be defined only for large scales or not defined at all.

A review of the techniques usually applied for delineation of protection zones in fractured rocks was included in section 2.2. Very few studies have attempted to deal with the transport features of fracture networks when delineating protection zones (Bradbury and Muldoon 1993, 1994, Robinson and Barker 1999, Rayne et al. 2001), the most common approach being the straightforward application of the techniques developed for continuous porous media.

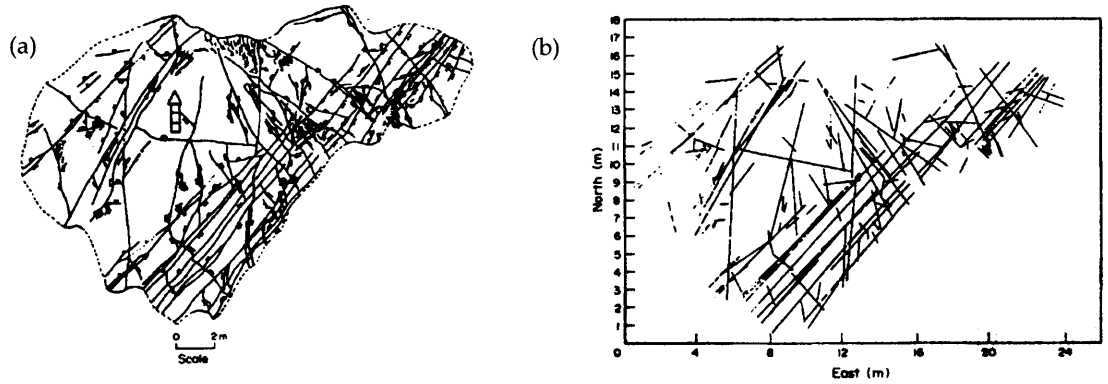

Figure 5.1 – Sample fracture network. a) original fracture trace map; b) schematic representation of the fracture network in a). From National Research Council (1996).

This lack of studies has to do with the complex hydraulic behaviour of fracture networks. Flow and transport in fracture networks has been one of the most active areas of research in the past decades, with considerable resources directed towards understanding those phenomena. Those efforts were mainly related to radioactive waste disposal sites, and the achievements are outstanding in terms of the development of tools for modelling fractured-rock aquifers. However, the complexity of those tools and the associated financial costs make them poorly amenable for use in relatively low-budget hydrogeologic studies such as protection zone delineation.

Because delineation of protection zones in fracture networks must take into account the solute transport features imposed by the fracture patterns, one should not ignore that:

a) a REV may not exist or may exist only at scales above the scale of study;
b) dispersion will always occur at fracture intersections;
c) the fracture pattern has a random nature;
d) the laws that describe solute transport in continuous porous media, such as Fick's laws, may not be adequate to describe transport in fracture networks.

It is important to know what tools are available that allow a valid representation of solute transport in fracture networks and then try to adapt those tools to the more restricted problem of delineation of protection zones. However, mention should be made to a recent report by Marschall and Elert (2003) detailing the use of several modelling approaches to simulate groundwater flow in the Äspö Hard Rock Laboratory, a fractured rock research facility in Sweden. The authors conclude:

A wide spectrum of flow modelling approaches was seen in Task 4, including 2D and 3D representations of the site, stochastic and deterministic approaches and homogeneous and heterogeneous distributions of hydraulic properties. At the end of the flow modelling exercise, a consistent picture of the hydraulic conditions at the site was not achieved.

This chapter, as well as chapter six, is mostly concerned with contributing to the development of tools for delineating protection zones that, while encompassing an acceptable representation of the solute transport in fracture networks, also acknowledge the existence of limited data and resources. Such tools should further recognise the existence of considerable uncertainty about the flow and transport conditions and, therefore, a probabilistic approach should be an option.

Due to the amount of work developed, protection zones in fracture networks are addressed in this thesis in chapters five and six. In chapter five, section 5.1 provides a review of the main methodologies used for modelling solute transport in fracture networks, while section 5.2 describes the research conducted in order to adapt one of those methods, the Statistical Continuum Method, to delineation of protection zones. Chapter six is concerned with a new approach to modelling solute transport in fracture networks. The approach is based on a Continuous Time Random Walk. Sections 6.1 and 6.2 describe the one-dimensional analytical solutions, while sections 6.3 and 6.4 describe the semi-analytical implementation of the method in a two-dimensional environment. Section 6.5 applies this technique to delineation of groundwater protection zones and section 6.6 presents a summary of the work developed in chapters five and six.

5.1 A REVIEW OF METHODS FOR MODELLING FLOW AND SOLUTE TRANSPORT IN FRACTURE NETWORKS

The two most common modelling approaches to simulate flow and transport processes in fracture networks are **Discrete Facture Network Models** and **Continuum (deterministic or stochastic) Models**. These techniques are often regarded as opposite, with the continuum approach representing the fracture network as an equivalent porous medium and the discrete models considering flow through each individual fracture.

However, as Hsieh (2002) reminds us, both modelling approaches share the same underlying physical principles, with laws such as conservation of mass and Darcy's law being the governing equations in any case. Quoting Hsieh (2002):

In principle, a discrete-fracture model may be set up to appear like a continuum model by using 3 sets of mutually perpendicular and regularly spaced fracture sets that extend throughout the model domain, thus mimicking a finite-difference grid. Conversely, a continuum model may be set up to appear like a discrete-

fracture model by using a fine grid with a highly variable distribution of hydraulic conductivity (K) such that grid cells with high K are connected in a fashion to mimic fracture network.

Both these approaches have advantages and disadvantages relative to each other and in relation to their applicability as routine hydrogeologic tools. In an attempt to take the best out of each concept, **hybrid models** have been developed in the past few years. This approach tries to couple the use of Discrete Fracture models, which are more robust in terms of physical description of the flow and transport phenomena, with the more computationally efficient and less data demanding Continuum models.

These three approaches to fracture network modelling will be briefly reviewed in this section. As mentioned before, this is a very active area of research and a more thorough description of the available techniques, beyond the scope of this thesis, should be sought elsewhere, for instance in Bear et al. (1993), Sahimi (1995) and National Research Council (1996).

5.1.1 Discrete Fracture Network (DFN) models

The idea of representing fractured rocks by sets of lines or planes representing individual fractures is easy to understand and appealing. **Discrete Fracture Network (DFN)** models aim to simulate realistically the discontinuity of the system, by including the geology and geometry of fracture networks into a groundwater simulation (fig. 5.2). Every fracture is simulated as having its own hydraulic properties, such as permeability and transport aperture, so that in effect, every fracture is simulated as an individual aquifer (Doe 2002).

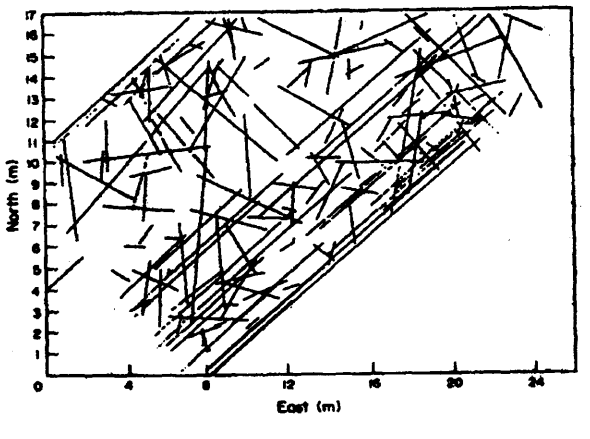

Figure 5.2 – DFN model of network depicted in figure 5.1. From National Research Council (1996).

This notion of representing fractures as individual conductors draws on the works of Snow (1968, 1969) and on the cubic law. Snow's work was based on the representation of fractures as parallel plates with permeability proportional to the cube of spacing (aperture) between the plates. In his studies, Snow considered fractures as infinite and of constant aperture, but since then many models have been developed that considered more realistic finite fractures, with homogeneous or heterogeneous hydraulic properties in each fracture set.

The highly sophisticated DFN models used nowadays draw not only on Snow's work but also on the development, mainly since the 1970's, of statistical measures of fracture geometry and hydraulic properties, and on stochastic hydrogeology which integrate the uncertainty in field information.

DFN modelling suffered a major boost during the 1980's and 1990's through application at waste disposal sites, such as Stripa, Äspo Hard Rock Laboratory and Sellafield (Rouleau and Gale 1987, Cacas et al. 1990a, Cacas et al. 1990b, Herbert 1993, Dershowitz and Eiben 1999, Outters and Shuttle 2000). These studies promoted the use of DFN models as practical tools, able to simulate not only the hydraulic behaviour of fractures, but also allowing matrix blocks to be considered as: impermeable; as a source of added storage (the dual-porosity concept); or as a permeable medium (dual-porosity and dual-permeability).

DFN models may be two-dimensional or three-dimensional. In the first case, fractures are represented by lines characterised by some aperture and/or transmissivity (fig. 5.3a). The 3-D models, mostly developed in the 1990's taking advantage on the increased computational capacity, represent fractures as disk-shaped or polygonal planes intersecting in a 3-D domain (fig. 5.3b). Although the 2-D models had a fundamental role in studies aiming to understand the hydraulic behaviour of fractured rocks, it is known that a realistic representation of field conditions must be done with 3-D models, since the 2-D DFN models often fail to adequately represent the connectivity of the system.

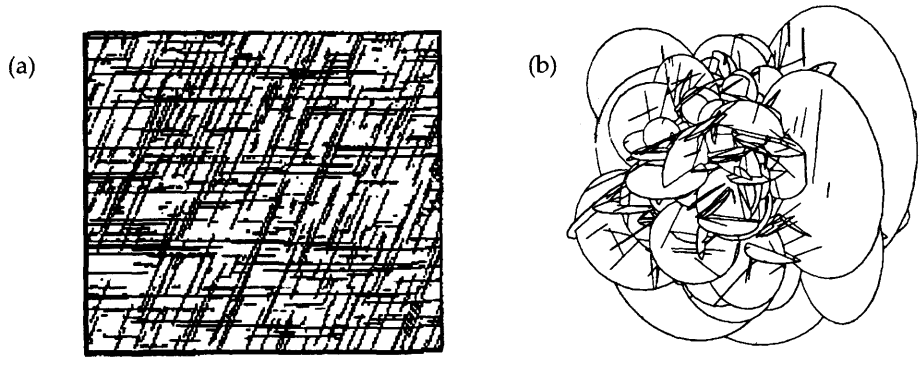

Figure 5.3 – Discrete Fracture Networks. a) two-dimensional network; b) three-dimensional network of disk-shaped fractures. From Sahimi (1995).

In essence, the 2-D and 3-D DFN modelling approaches are very similar, both relying on the random generation of fractures, by resorting to some stochastic process that uses the statistics on fracture geometry and hydraulic properties collected in the field. The data on fracture density, length, orientation and transmissivity and/or aperture, distributed according to some established probability density functions, are used to generate individual fractures that together simulate the fracture network. Because the process is stochastic, multiple realisations of the fracture system must be conducted, so that the outcome of the study will be the probability of an event occurring.

Various stochastic processes have been used to generate fractures (Dershowitz et al. 1995). Two of those processes that will be mentioned in subsequent sections are the **Poisson Process** (defining networks to which we will refer later as Poisson networks) and the **Levy-Lee Process** (Levy-Lee networks).

The Poisson process is probably the most used to generate the location of fractures and its popularity has to do with the simplicity of the Poisson distribution, which is characterised by a single parameter, but it also builds on the fact that fieldworks indicated the Poisson distribution as commonly observed for fracture spacing along a scanline (Priest and Hudson 1976). Networks are created by randomly generating fracture mid-point locations until the scanline density of the input data is reached. These networks result in a single characteristic length scale (provided the average lengths for each set are not dramatically different) (fig 5.4a).

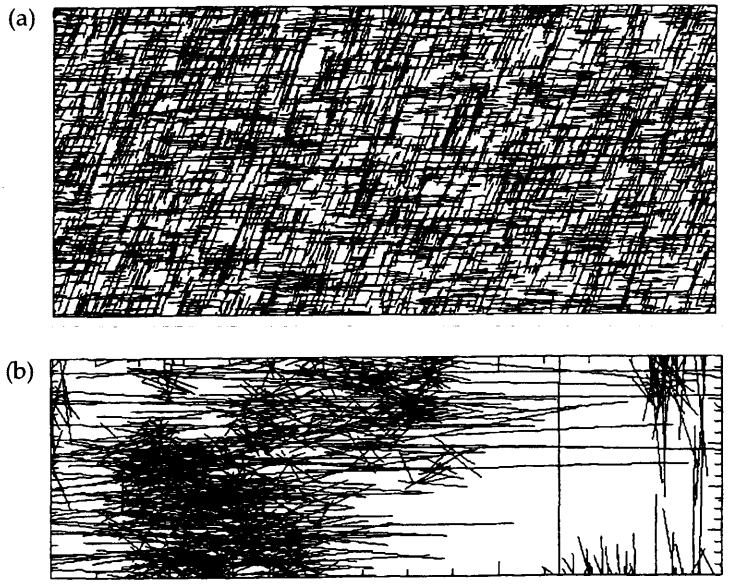

Figure 5.4 – Two networks generated by different stochastic processes. a) Poisson network; b) Levy-Lee network. After Parney (1999).

The Levy-Lee process aims to generate fracture networks with a range of length scales and that may show fractal properties (Dershowitz et al. 1995, Parney 1999). The Levy-Lee process is a

random walk where each step of the walk determines the mid-point location of a fracture. The length and orientation of the fracture are then a function of the distance from the previous fracture mid-point. This random walk results in a large number of small steps and a small number of larger steps. The large steps create long widely spaced fractures with small orientation variations, and the small steps result in clusters of small closely spaced fractures, of widely varying orientations (fig 5.4b).

Once the discrete fracture network is generated, the use of DFN models to simulate groundwater flow and transport is relatively straightforward and similar to any other program of numerical groundwater flow modelling. The fractures are discretized according to some procedure (for instance, the code FRACMAN used in section 4.3 discretises each fracture using finite elements) and the flow solution is found by computing the hydraulic heads at the nodes, given consideration to boundary conditions and hydraulic properties of the elements. Transport is usually simulated by particle tracking, with particles being moved by advection along fractures, and dispersion being allowed at fracture intersections. Interaction with the rock blocks may also be modelled in some codes, using for instance matrix diffusion, but most commonly, the matrix is regarded as impermeable.

There are two views regarding the usefulness of DFN models. A first view considers that such models should be used solely as a tool for concept evaluation, allowing for a better understanding of the hydraulic behaviour of fractured rocks and eventually in the definition of effective parameters to be used in continuum models. A second view considers that DFN models are practical tools for site-specific simulations. This later view led to the use of DFN models in waste repositories and seems to be gaining support in more conventional studies such as in hydrogeologic characterisation for civil engineering purposes (Fouché et al. 2003, Lawrence et al. 2003).

The fact is that DFN models have some clear advantages in modelling fractured rocks, particularly in what regards solute transport. They provide a robust and physically sound representation of a discontinuum medium and involve few assumptions when modelling flow and solute transport. They avoid the need of a REV, and do not involve the concept of effective hydraulic parameters. Equally important is that no particular law of solute transport is considered, allowing for simulation of Fickian and non-Fickian transport behaviour.

However, DFN models have some important constraints that are thought to hamper their use as practical tools in routine hydrogeologic studies, namely:

a) they demand for a considerable amount of information regarding the fracture geometry and hydraulic properties of fracture sets. It is necessary to define probability distributions for fracture density, fracture length, fracture orientation and sometimes fracture shape. This information may prove difficult to obtain or being available only after geologic and structural studies that require considerable time and financial resources. Even more illusive to obtain are distributions of aperture and/or of transmissivity for each fracture set;

b) even if all the necessary information is gathered, it is known that only a small percentage of fractures are responsible for conducting most of the flow, with the majority of fractures being irrelevant or inactive. This effect of channelling is usually not considered in DFN models (National Research Council 1996);

c) DFN models have proved extremely difficult to calibrate and condition on field data. Even if extensive pumping tests and tracer tests are conducted in any site, it is very difficult to use that information to constrain the DFN realisations;

d) DFN modelling has a high computational burden (Herbert and Lanyon 1995). Because multiple realisations need to be conducted, in which every possible fracture has to be modelled individually, the computational requirements are very demanding. Even with the exponential increase in computational capacity the use of DFN models is usually restricted to local-scale areas.

Research has been done in order to reduce the computational requirements and to develop processes of conditioning the realisations on field data. In recent years, one-dimensional **pipe models** have been adopted in an attempt to reduce the computational requirements (Cacas et al. 1990a, Cacas et al. 1990b, Dershowitz and Fidelibus 1998, 1999, Adams and Parkin 2002). The fracture network is first generated in a 3-D environment and then it is collapsed to a system of 1-D pipes, so that flow in each fracture plane is reduced to a single representative pipe centred in the middle of the fracture plane or to an arbitrary number of pipes (fig. 5.5).

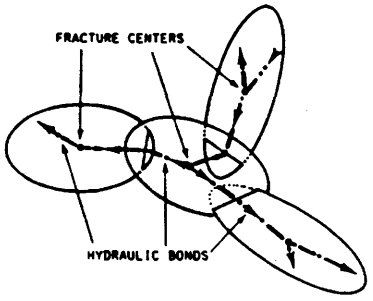

Figure 5.5 – Conversion of a 3-D fracture network into 1-D pipes. From Cacas et al. (1990b)

Pipe models have been applied to field situations, and although they are becoming more and more sophisticated using graph theory algorithms to identify pathways, their use is very restricted and still constrained by the computational burden (Outters and Shuttle 2000).

Strategies for conditioning the discontinuum models usually involve some kind of inversion techniques, such as **simulated annealing** (Mauldon et al. 1993, Sahimi 1993, Nakao et al. 2000). This inversion technique is an optimization algorithm that finds lattice configurations that are functionally equivalent to the observed system (National Research Council 1996). In practice, simulated annealing is used to find an appropriate fracture pattern of connected fractures given some experimental information (fig. 5.6). Although this methodology seems very promising, the fact is that the computational burden involved is very high and it does not seem that in the near

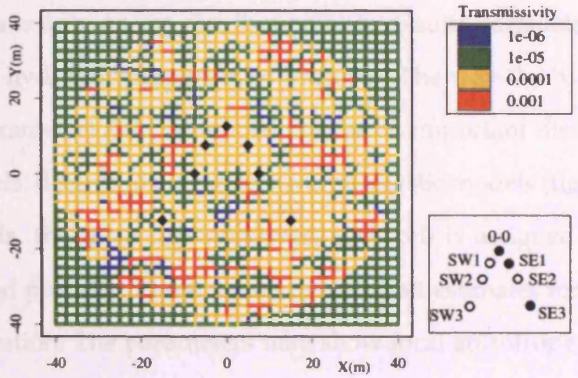

Figure 5.6 – Example of a network optimised using simulated annealing. Transmissivity associated to each line segment (bond) provide the best fit to a hydraulic test monitored in six wells. From Nakao et al. (2000).

future it will be a practical alternative.

Despite all the difficulties to its practical application, DFN models are invaluable tools for contaminant hydrogeology and capture zone definition problems, although they probably should not be applied directly for modelling specific sites. Nevertheless, DFN models provide the results to which any other method should be compared. With this purpose, a 2-D DFN model will be used throughout this chapter.

5.1.2 Continuum models

The most common approach to model flow and transport behaviour of fractured-rock aquifers is simply to assume that these media behave as a continuous porous medium and use the well-known analytical and numerical methods for modelling continuous porous media – the EPM

assumption. These models are designated as **Continuum** models, as **Equivalent Porous Medium** models or **Homogeneous Porous** models.

The widespread use of continuum models has little to do with the reliability of such tools when applied to fractured rocks, being mostly the result of the simplicity. Nevertheless, there are some conceptual arguments that favour the use of continuum models, especially when fracture density is considerable so that an EPM approach seems reasonable.

The principle underlying the use of continuum models is that the heterogeneity of the rock can be represented using a limited number of homogeneous regions (or cells in numerical models). At the scale of interest, the hydraulic properties of each region are described by volume-averaged coefficients: hydraulic conductivity and effective porosity. This discretization into cells avoids the need to consider every fracture, making it a lot simpler to build an aquifer model.

Therefore, the emphasis is now on the distribution of hydraulic parameters in the cells rather than on the geometric and hydraulic properties of fractures. The way the hydraulic conductivity (or any other hydraulic parameter) field is defined creates an important distinction between two groups of continuum models: deterministic models and stochastic models (fig. 5.7).

In **deterministic models**, the most common ones, each cell is assigned a constant value of conductivity, storativity and porosity. These values are the best estimates for that area and are to be optimized during calibration. The parameters may show local anisotropy, but homogeneity is maintained in each cell. This is the approach used in models that became the standard for flow and transport modelling in continuous porous mediums, the best known of which is MODFLOW and associated codes (McDonald and Harbaugh 1988, Pollock 1989).

Stochastic models acknowledge uncertainty in the hydraulic parameters and attempt to find flow and transport solutions that encompass that uncertainty. Several authors have advocated this approach because only tenuous connections have been found between fracture geometries and hydraulic conductivity fields, and thus it seems appropriate to discard geometric information and focus on the statistical structure of the conductivity field (Niemi 1994, Hendricks-Franssen 2000). This is accomplished by generating spatially variable hydraulic conductivity fields based on the distribution of parameters inferred from field tests[1]. The hydraulic parameters are envisaged as random variables that are spatially correlated and characterised by mean, variance and a correlation structure (that is, the degree of spatial continuity of the K field, usually found by geostatistical analysis of the field data).

[1] Although any other parameters could also be modelled as random, generally only stochastic hydraulic conductivity or transmissivity fields are generated, because these parameters show larger variation than any other hydraulic parameter.

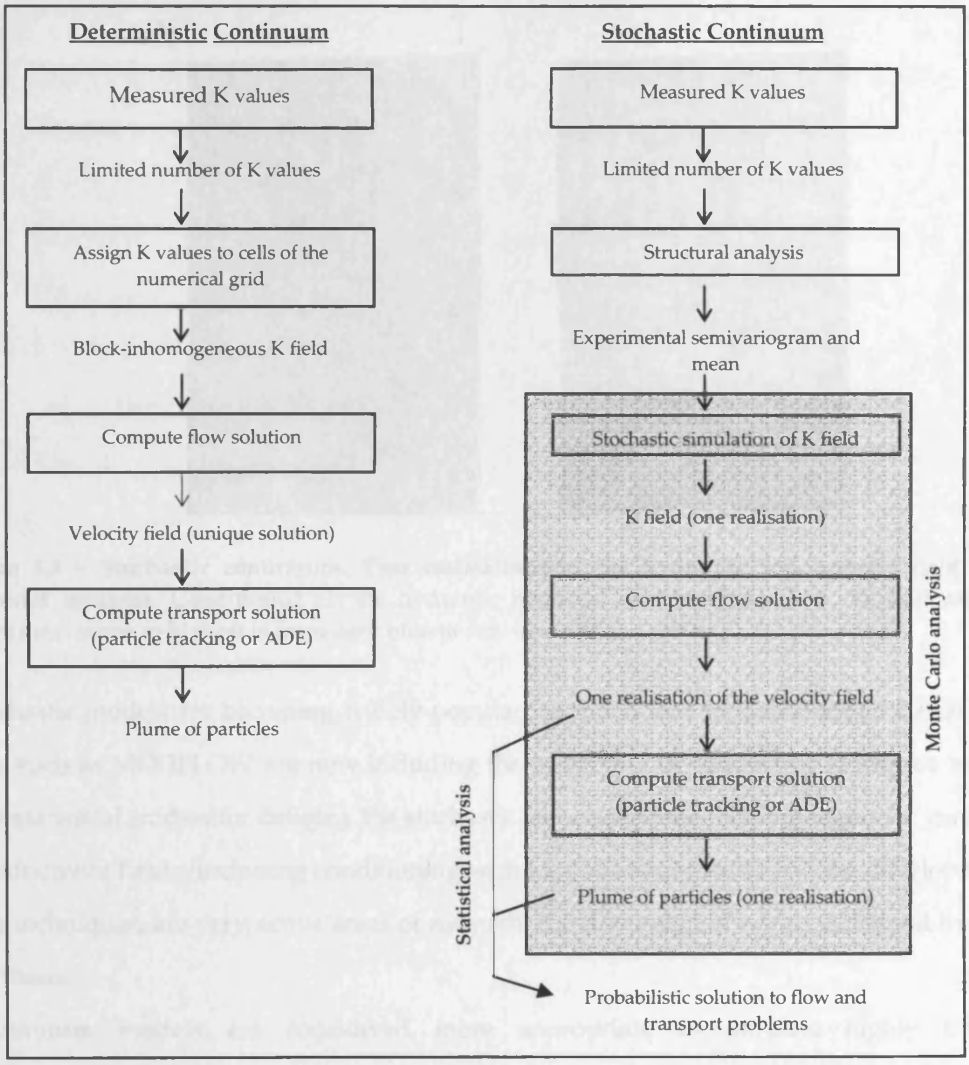

Figure 5.7 – Illustrative procedures of deterministic and stochastic continuum models. ADE is the Advection-Dispersion Equation.

Having established the stochastic parameters, the flow solution can be obtained in one of two ways:

a) using the stochastic equations for flow, in which case the result is immediately obtained in probabilistic terms, with a measure of uncertainty resulting;

b) by conducting Monte Carlo analysis, by means of which multiple realisations of the hydraulic conductivity field are generated (fig. 5.8), with a constant value for each cell in each realisation. The flow and transport solution are obtained for each realisation and a probabilistic study is conducted to obtain results in terms of probability and uncertainty.

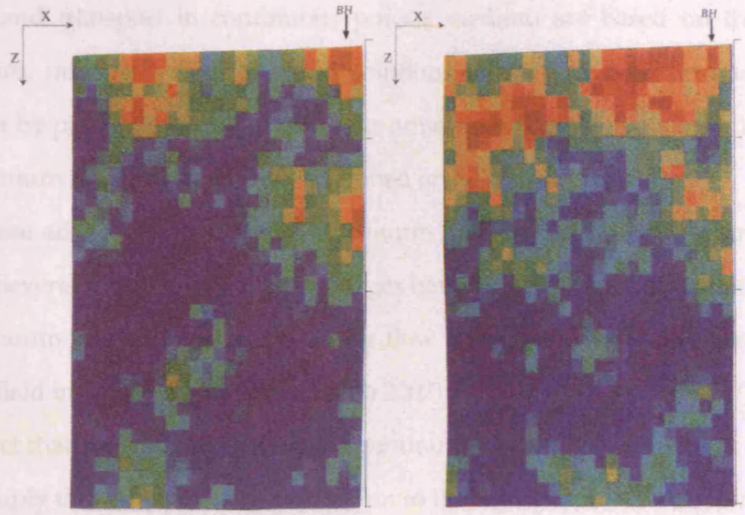

Figure 5.8 – Stochastic continuum. Two realisations of the hydraulic conductivity field in a fractured medium. Conditioned on the hydraulic response of a borehole (BH). Vertical section. Scale from lowest to highest is from dark blue to red. From Niemi (1994).

Stochastic models are becoming widely popular, so much that well-established deterministic models such as MODFLOW are now including the possibility of conducting stochastic analysis. The geostatistical studies for defining the stochastic parameters, the methodologies for generating the conductivity fields (including conditioning with local measurements) and the development of inverse techniques, are very active areas of research, the discussion of which is beyond the scope of this thesis.

Continuum models are considered more appropriate to simulate highly fractured environments, with well-connected fractures, for large scale studies. Rocks that have suffered multiple tectonic events and/or those with significant matrix permeability are the best candidates (National Research Council 1996). The application of stochastic continuum models to simulate flow and transport in fractured environments have reportedly been quite successful in reproducing the flow and solute transport features, comparing favourably with the field data and with DFN models (Ando et al. 2003, Ohman and Niemi 2003).

Amongst their advantages are:

a) their simplicity allows large areas to be modelled;

b) they are implemented in well-established finite-differences or finite-elements codes, modelling aquifers with multiple types of flow boundaries and physical limits. This is a clear advantage over DFN models, where the definition of complex physical limits is difficult;

c) flow and transport in continuous porous medium are based on thoroughly tested theories, making it simple to find solutions to the flow and the transport problems (either by particle tracking or using the advection-dispersion equation);

d) continuum models are easily conditioned on field data.

Despite all these advantages, the use of continuum models to simulate fractured-rock aquifers is controversial. Several fundamental disadvantages have been pointed out, specifically:

a) continuum models tend to simulate a flow field that is more diffused than the actual flow field in a fracture network (Hsieh 2002);

b) the fact that a reasonable equivalent continuum to the flow behaviour is attained, does not imply that an equivalent continuum to the transport behaviour is also adequate. In fact, it is established that the EPM assumption is more easily accepted for flow than for transport behaviour (Endo et al. 1984, Guérin and Billaux 1994);

c) continuum models rely on the possibility of defining a REV to which effective parameters can be assigned, but extensive field and theoretical studies have demonstrated that often in fractured rocks a REV can only be defined for very large scales or not defined at all (Bear et al. 1993, National Research Council 1996);

d) the stochastic approach is scale dependent. Because the conductivity fields include spatial correlation, considering different scales will lead to different results (Niemi 1994);

e) the link between geometry of the fracture system and solute transport is lost;

f) continuum models rely on Fick's 2nd law to simulate solute transport. However, it is known that often transport in fractured rocks shows anomalous behaviour, not compatible with Fickian transport (Berkowitz and Scher 1995);

g) channelling effects cannot be reproduced in continuum models.

h) the geostatistical analysis necessary to implement the stochastic continuum require a considerable amount of field information, which seldom is available.

Therefore, despite their advantages, the use of continuum models in fractured-rock aquifers is hampered by several fundamental problems. It is important to remember that several studies have shown that for a continuum model to be able to reproduce accurately the solute transport features observed in the field, discretization has to be so high that the model ends-up resembling a DFN model (National Research Council 1996, Parney 1999).

Nevertheless, the advantages of continuum models should not be neglected, particularly for routine hydrogeologic studies, such as delineation of protection zones. Their simplicity motivates

the use of a deterministic model throughout this chapter to obtain flow solutions, although the transport problem will be solved by other methods.

5.1.3 Hybrid models

DFN models provide a physically sound description of flow and solute transport in fractured rocks, but their use is restricted to small-scale domains, while the Continuum models are not so reliable in describing those phenomena, but are simple and versatile enough to allow modelling large-scale domains. The two modelling techniques have complementary abilities, and several authors suggested their joint use when modelling fractured-rock aquifers, thus giving rise to **hybrid models.**

Several hybrid modelling techniques have been proposed, but most are based on the use of a DFN model at a small-scale to collect information about the hydraulic properties of the fracture network.

An early (Long et al. 1982, Robinson 1984) and now well established technique relies on the definition of porous-medium equivalents to a small-scale DFN domain by computing the directional hydraulic conductivity, K(Θ), of the network for several orientations of an uniform hydraulic gradient. The polar plot of $1/\sqrt{K(\Theta)}$ as a function of gradient direction, Θ, should be a perfect ellipsoid if the medium is behaving as an EPM with respect to flow properties (fig. 5.9). The deviation from the ellipsoid is a measure of the deviation from an equivalent continuum.

Using this $1/\sqrt{K(\Theta)}$ plot technique it is possible to compute a permeability tensor that can then be used in a continuum porous medium model to compute the flow solution using an anisotropic coefficient in each cell of the numerical continuum domain.

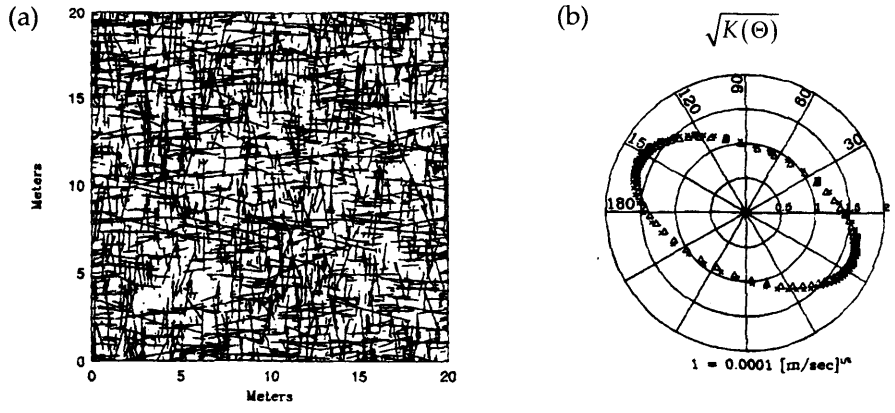

Figure 5.9 – Finding equivalent continuum properties. Representation of the average flux through a fracture network (a) in terms of a directional $\sqrt{K}$ ellipse (b). From National Research Council (1996).

Although other methods for computing the effective transmissivity of a fractured network have been proposed (e.g. Hestir and Long 1990, Zimmerman and Bodvarsson 1996a), the use of $1/\sqrt{K(\Theta)}$ ellipsoids to upscale from a small-scale fracture domain to a large-scale continuum domain is the most commonly used, and can be implemented with any DFN model, in two and three dimensions. However, the use of ellipsoids has proved successful only for modelling flow. Attempts were made to use similar techniques to define tensors of effective porosity and dispersivity, which would allow modelling transport in a large-scale continuum (Herbert and Lanyon 1995). Effective porosity and dispersivity show considerable variability with respect to hydraulic gradient orientation and ellipsoids become very difficult to establish, even if the continuum approximation to the flow properties is acceptable (Endo et al. 1984, Guérin and Billaux 1994). In fact, Barker (2002) has demonstrated analytically that for a fracture network composed of infinite fractures, directional effective porosity cannot, in general, be described by a tensor.

Consequently, this approach still has to prove its validity for simulating the transport features of fracture networks, although its strength in modelling flow seems to be well established.

Other authors (Robinson and Barker 1999) have suggested a slightly different approach, which would include the use of a stochastic continuum. In this case, values of directional conductivity and effective porosity would still be computed in a small-scale DFN domain, using multiple realisations. The values retrieved would be fitted to continuous distributions, which would then become the input to the stochastic continuum. Transport in the large-scale domain would be simulated using a Monte Carlo procedure to generate multiple realisations of the flow field, where particle tracking would then be conducted to find the distribution of particles at any given time. See section 2.2 for further details on this methodology.

The **hierarchical model** (also known as the dual-permeability model) provides a completely different approach (Clemo 1989, Smith et al. 1990, Smith and Schwartz 1993, Clemo and Smith 1997). This methodology has the potential to model far larger volumes of fractured rock than can be accommodated with DFN models. The approach recognises a hierarchy amongst fractures, preserving dominant fractures as discrete fractures (primary fractures) and modelling flow and transport in the more numerous smaller–scale fractures by using a lumped parameter representation, forming what the authors call a network block (fig. 5.10). No assumptions are made about equivalent continuum behaviour in these network blocks, nor is the definition of a REV necessary. Rather, each network block has unique properties, reflecting the influence of

smaller fractures. Together, the combination of primary fractures and network blocks forms what the authors designate as a dual-permeability medium.

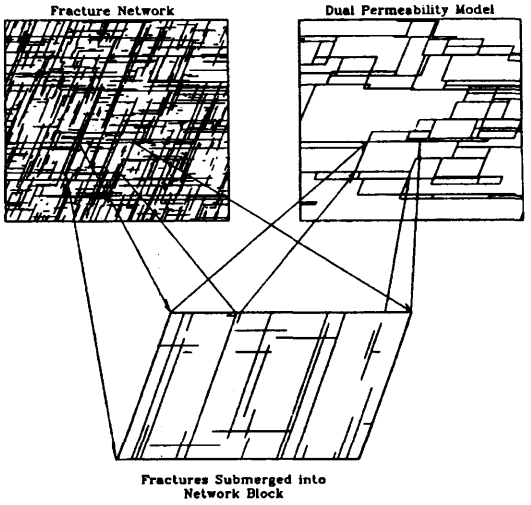

Figure 5.10 – Schematic representation of hierarchical (or dual-permeability) model for a fracture network. Primary fractures are retained as individual discrete fractures. Most fractures are submerged into network blocks. From Smith and Schwartz (1993).

The hierarchical model is appropriate to model solute transport in fracture networks where fractures have a broad range of scale lengths. The methodology was implemented in a 2-D domain, but no work is known in relation to its efficiency and reliability in a 3-D domain.

Schwartz and Smith (1988) suggest yet another hybrid tool to upscale from local scale DFN models into regional scale aquifers. The methodology proposed is known as the **Statistical Continuum Method** and particle tracking is at its core. Solute transport is modelled by first collecting statistics on particle movement in a subdomain using a DFN model and then using these statistics in a continuum model to simulate transport at a larger scale. Particle tracking is also used in the continuum model, so there is never a need to assign numerical values to a dispersion tensor. This upscaling technique has several advantages and will be described thoroughly in the next section.

5.1.4 Approach adopted in this thesis

The description of the different approaches to model flow and solute transport in fracture rocks shows that no single method seems to be suitable for all purposes. Although DFN models provide the most reliable solutions to the transport problem, they cannot be used directly in the delineation of protection zones, which usually require modelling large-scale domains. The use of continuum models to simulate solute transport in fracture networks lacks some consistency and has several drawbacks, but has the considerable advantage of being able to model large areas.

The strategy followed in this chapter is based on hybrid models, which combine the reliability of DFN models with the simplicity of Continuum models. The next section will demonstrate the use of the Statistical Continuum Method, while chapter six will be devoted to the development of an analytical and a semi-analytical procedure for modelling solute transport in fracture networks at the catchment scale.

5.2 APPLICATION OF A HYBRID METHOD FOR DELINEATION OF PROBABILISTIC PROTECTION ZONES

Solute transport modelling in fracture networks is closely associated with the concept of randomness. This is easily perceived in discrete modelling methods, where the location of a particle (or solute) at time t is determined by the random geometric arrangement of the fracture network and by the directions taken by particles at every fracture intersection. Therefore, and although advection is the single driving force, particles' location will vary between realisations of the network and even in each single realisation. The result of the modelling process will be a plume of particles regardless the particles being released at the same location. Although this effect is easier to understand when dealing with solute transport in discrete fracture network (DFN) models, it also occurs for stochastic continuum and hybrid models.

The spread of the particles can be interpreted as a dispersive effect or as the probability of a particle being at a certain location at time t. That is, the t isochrone no longer is a single surface line, but rather is distributed over a wide area according to some probability function. It is then advisable to define **probabilistic protection zones**.

The aim of this section is to delineate probability contours for groundwater protection zones using a hybrid procedure to upscale from a small-scale Discrete Fracture Network (DFN) domain to a regional scale continuum domain.

This study applies the Statistical Continuum Method (SCM) whereby the statistics of movement in a DFN model are used to replicate advective movement in a larger continuum domain. For this purpose the SCM has been somewhat modified and generalised so that it can use the flow solution of a standard continuum finite difference model, MODFLOW (McDonald and Harbaugh 1988). The SCM, albeit still experimental and requiring validation against field situations, has several advantages, namely (National Research Council 1996):

- it allows upscaling of particle movement without the need to explicitly account for every fracture that would occur at a regional scale;
- makes no assumption about Fickian behaviour on solute transport;

- particle tracking is conducted in the DFN domain and then the continuum model mimics the particles movements without the need for considering dispersion tensors.

5.2.1 Previous studies on the Statistical Continuum Method

The Statistical Continuum Method attempts to merge the accuracy of discrete models when representing the physics of flow and transport, with continuum models that have fewer limitations on domain size but that may not accurately represent the physics of the transport process in a fractured medium.

The method was first enunciated by Schwartz and Smith (1988). It consists in using particle tracking in which physical transport is simulated in terms of velocity and velocity variation. Statistics describing the particle movement come from observing the actual pattern of particle movement in a discrete sub-domain. This sub-domain should be a small but representative piece of a much larger continuum. Particle motion in the continuum then mimics movement in the discrete subdomain (fig. 5.11).

Schwartz and Smith (1988) conducted particle tracking in a small two-dimensional DFN with two orthogonal fracture sets and collected statistics of movement in each of the four possible directions. The statistics collected were:

a) frequency of particle movement in each direction;

b) frequency distributions of fracture lengths between intersections (for each direction);

c) frequency distributions of velocity in each direction[1];

These statistics were collected for several hydraulic gradient orientations so that a matrix could be created with those distributions as variables for each orientation. Particle motion in the larger continuum domain was then conducted by first finding a solution to the groundwater flow problem with a continuum model. Sampling of the hydraulic gradient orientation at each particle location is done and the relevant statistics of movement applied. Particle tracking in the continuum starts by sampling the direction of movement from the orientation distribution, then the length of movement is generated from the relevant probability distribution and finally a velocity for that direction is generated from the probability distribution of velocity. Each particle is moved in this manner until the end of the required travel time.

[1] Although velocity will be used throughout this section for consistency with previous works on the SCM, what in fact is sampled in the SCM is the absolute value (norm) of velocity vector, that is, a scalar value - speed. Orientation is considered separately.

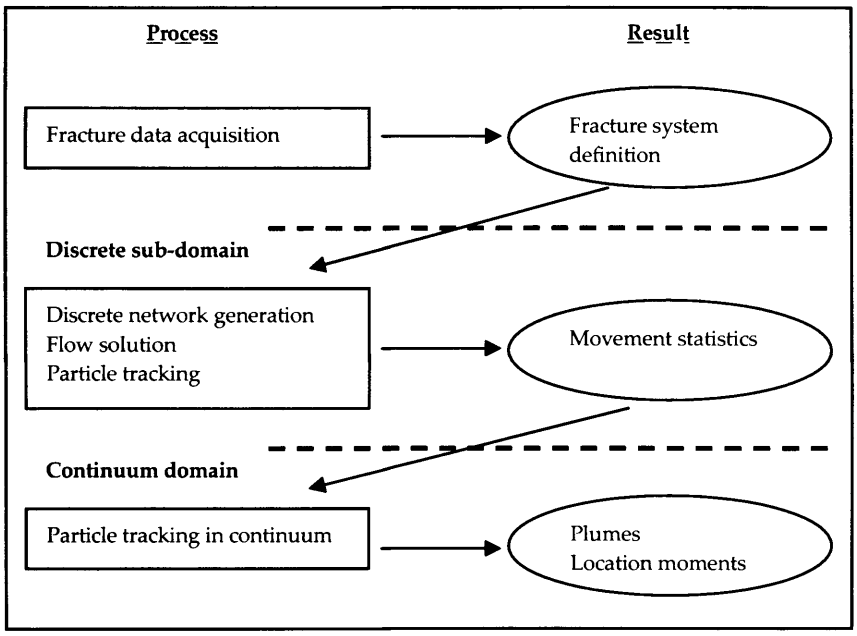

Figure 5.11 – Flow chart for the Statistical Continuum Method. From Parney (1999).

The SCM has undergone some changes since 1988. Namely, Smith et al. (1990) included statistics for autocorrelation of velocity in the same direction. That same work concluded that the most suitable distribution for path-length, velocity and standard deviation of velocity was the two-parameter gamma distribution. Parney and Smith (1995) included one important modification by redefining path-length as the continuous distance a particle travels within a single fracture, rather than the distance between fracture intersections. This modification allows a more reliable simulation of transport and at the same time decreases the computational effort necessary in the continuum model (fig. 5.12). Parney and Smith (1995) also recognised the existence of a correlation between path-length and velocity.

Parney's PhD thesis (1999) presents a systematic analysis of the potential of the SCM. Again, two fracture sets were used, although they were allowed to be non-orthogonal. The thesis compared solute transport simulated according to the SCM, using several different probability distributions for path-length and velocity, with the solute transport simulations of a DFN model. Parney (1999) applied the model under uniform flow conditions and used the 1st and 2nd spatial moments of the ensemble of particles to compare the results from the SCM and the DFN. The study concluded that, although a precise match was never achieved, the moments from the SCM were within one standard deviation of the moments from the DFN, which was considered as a reasonable approximation.

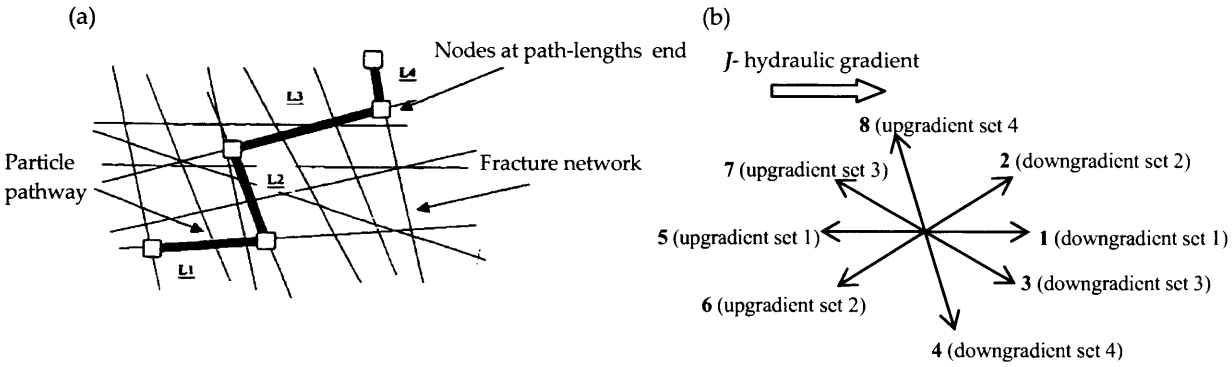

Figure 5.12 – Definition of path-length and movement direction. a) path-length is the distance a particle travels along a fracture between the fracture intersection in which it enters and the intersection through which it exits (Parney 1999); b) for the 4 fracture sets in fig. 5.2a there are 8 possible directions of movement, since the particles are allowed to travel locally against the regional hydraulic gradient.

However, the most important part of Parney's thesis is dedicated to generalising the method to three-dimensions, using the FRACMAN/MAFIC (Dershowitz et al. 1995, Miller et al. 1999) package to model flow in the DFN. Although the SCM did not prove as reliable as in two-dimensions, it was also possible to reach an approximation to one standard deviation of the moments from the DFN model.

The most relevant conclusions of Parney's thesis were:

- no single distribution of path-length and velocity always provides the best results, but the three-parameter gamma distribution tends to return the most consistent results;
- the use of autocorrelation in velocity and correlation between path-length and velocity do not provide systematically better approximations and frequently cause larger deviations than SCM without correlation structures;
- for well-connected **Poisson networks** with fractures of similar scale length, the method can be applied both in 2-D and 3-D models, with results within one standard deviation of the mean results in the DFN;
- for fracture systems close to the percolation threshold or for fracture sets of different scale length, i. e., **Levy-Lee networks**, the method performed poorly.

5.2.2 Generalization and implementation of the method

The results obtained by Parney (1999) are encouraging and seem to confirm the SCM as a reliable tool for modelling solute transport in fractured rocks at catchment scale. Therefore, it may be a suitable method to delineate groundwater protection zones in fractured rock aquifers, as long as the following improvements are made:

a) generalise the method so that it can account for any number of fracture sets;
b) improve the fit of the 1st and 2nd spatial moments of particles' location to increase the reliability of the movement of particles in the continuum domain;
c) link the SCM to a standard groundwater modelling program, so that it can recognise the groundwater flow solution and conduct the particle tracking according to the statistics collected in the DFN domain;
d) create a computer code that is able to use the SCM output to compute contours of probability of a given location being part of a protection zone.

These improvements have been made as part of this thesis and the methodology was implemented in a 2-D flow domain. Although 3-D modelling would provide simulations that are more realistic, there are several drawbacks regarding the use of a 3-D DFN model to collect statistics of movement. Namely, these models are computationally very intensive and their use is still somewhat complex. Further, Parney (1999) used a modified version of MAFIC to collect the statistics in the 3-D flow domain. It was not possible to obtain the modified MAFIC code, hence the restriction to 2-D modelling.

An important motivation for using 3-D fracture networks is that vertical fractures are essential to ensure that the fracture network is connected (Robinson and Barker 1999). Reliable 2-D DFN modelling only occurs in well-connected fracture networks, implying that the methodology followed in this section is not valid for fracture networks close to the percolation threshold. Anyway, and since the methodology is used to model solute transport at the catchment scale, it is considered that, once connectivity is guaranteed, the vertical movements are less important than horizontal movements because they are constrained by aquifer thickness.

The method was implemented in a computer code with three modules that operate successively to delineate the probabilistic protection zones. Module STATMOV runs the DFN code and collects the statistics of particle movement; module SCPATH conducts particle tracking in the catchment scale continuum using the MODFLOW groundwater flow solution; PROBCONT uses the output of SCPATH to compute the probability of each cell of the continuum domain to be part of the groundwater protection zone.

The DFN code chosen to simulate transport in the small scale domain was the Stochastic Discrete Fracture (SDF) model (Rouleau and Gale 1987, Bradbury and Muldoon 1993), a 2-D DFN model that is able to generate random fracture networks, solve the groundwater flow problem, and conduct particle tracking to simulate solute transport by advection.

Throughout the remainder of this section, the fracture network illustrated in figure 5.13 and with the statistics indicated in table 5.1 will be set as the **base case**.

Table 5.1 – Fracture statistics for the base case network

Fracture set	*Fracture orientation*	*Fracture density (m^{-1})*	*Fracture length*		*Fracture aperture (m)*	*Transmissivity (m) **
			Mean (m)	*Stand. Dev. (m)*		
set 1	N110°, 15°NE	0.6	4.0	2.2	5×10^{-5}	6.7×10^{-3}
set 2	N145°, 65°E	0.6	2.7	2.2	5×10^{-5}	6.7×10^{-3}
set 3	N20°, 55°W	1.2	3.3	2.2	1×10^{-4}	5.3×10^{-2}

*** Transmissivity of individual fractures, computed according to the cubic law for plane fractures.**

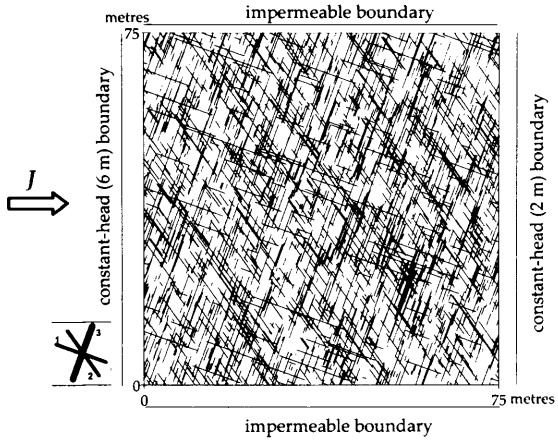

Figure 5.13 – Sample realisation of the discrete subdomain (75m×75m) with boundary conditions. In the smaller square, thickness of fractures is proportional to fracture aperture.

The fracture density and aperture of set three are responsible for a high anisotropy of the fracture system.

The simulations presented hereafter refer to this base case fracture network, except where mentioned otherwise.

5.2.2.1 Gathering statistics of particle movement in the discrete fracture sub-domain

Module STATMOV gathers the statistics by forcing multiple runs of SDF. STATMOV also provides the parameters necessary to build the network and the boundary conditions to allow computation of the velocity field. At each SDF run, a realisation of the fracture network is built. A number of particles are released at x, y locations and their path tracked in order to gather the required statistics of movement. Each SDF realisation allows tracking a maximum of 200 particles.

STATMOV was built so that it computes statistics for any number of fracture sets in the discrete fracture domain (in SDF the maximum number of fracture sets is 5), both in the *regional up-gradient* and in the *regional down-gradient* direction. The statistics collected, ***for each possible direction of movement*** (twice the number of fracture sets), are:

- percentage of times each direction is chosen by the ensemble of particles, resulting in a uniform distribution of directional choices;

- mean, variance and skewness of path-length;
- mean, variance and skewness of velocity. These parameters are normalised by the hydraulic gradient. This normalization converts mean velocity into the mean ratio K/n_e and allows one to compute mean, variance and skewness of velocity for any hydraulic gradient value. For simplicity, the mean ratio K/n_e will be designated hereafter as 'velocity'. Because velocity may vary by orders of magnitude, it is presented in terms of its negative logarithm.

Three-parameter gamma distributions both for path-length and for velocity seem to provide the most reliable SCM results, although under certain circumstances other distributions, such as the lognormal, can retrieve better results (Parney 1999). The three-parameter gamma distribution uses the mean, standard deviation and skewness of the data (Johnson et al. 1994). However, in the course of this study it became obvious that the differences in applying three or two-parameter gamma distribution are negligible, and therefore a two-parameter gamma distribution (using mean and standard deviation) was used to fit path-length and velocity retrieved from the base case network (fig. 5.14). Notice that the Kolmogorov-Smirnov test indicates as acceptable, with probability ($1-p_{KS}$) above 90%, the hypothesis of the data being distributed according to a gamma distribution[1].

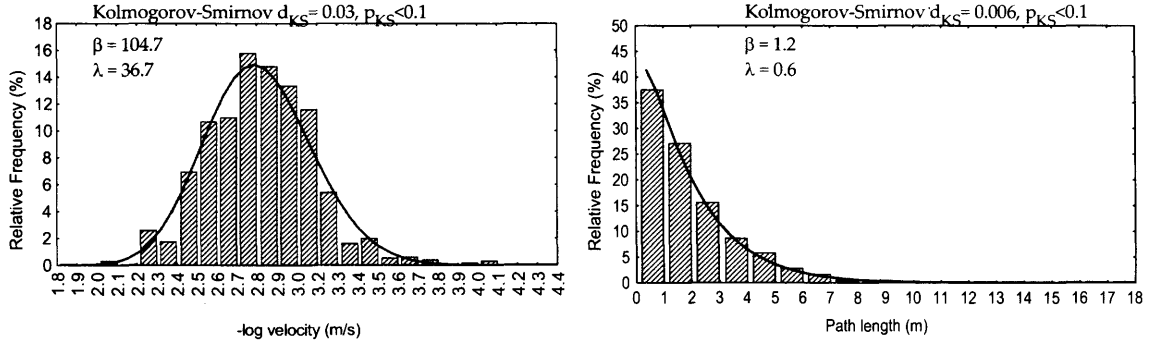

Figure 5.14 – Gamma distribution fit to the values of –log velocity and path-length. Fracture set 1, down-gradient. Other fracture sets fit to the same distribution type. Sample size: 4691.

The two-parameter gamma distribution is defined as:

$$p_X(x) = \frac{\lambda e^{-\lambda x}(\lambda x)^{\beta-1}}{\Gamma(\beta)} \qquad -\infty < x < \infty \tag{5.1}$$

[1] The Kolmogorov-Smirnov test used in fig. 5.14 is a goodness-of-fit test for any continuous statistical distribution. The cumulative relative frequencies of the sample and the distribution are matched up, the maximum difference is found (d_{KS}) and compared to a critical value for acceptance, for a given level of significance (p_{KS}) and bearing in mind the total number of observations. Thus, the p_{KS} value refers to the level of acceptance that the sample is distributed according to the tested distribution: a small value of p_{KS} indicates that the sample follows the tested distribution with probability $1-p_{KS}$. The value p_{KS} is computed by setting the critical value equal to d_{KS} and using the total number of observations to retrieve p_{KS} from the Kolmogorov-Smirnov distribution.

where $\Gamma(\beta)$ is the gamma function. The distribution is dependent on the **shape** (β) and **scale** parameters (λ) (Johnson et al. 1994). As the shape parameter β approaches infinity, the gamma distribution converges to the normal distribution (fig. 5.15).

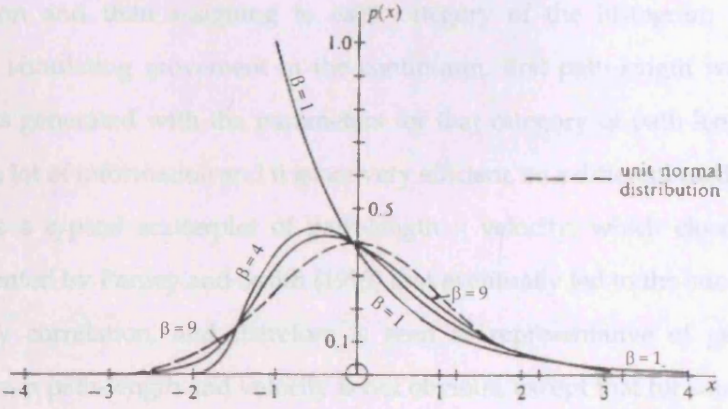

Figure 5.15 – Standardized (λ=1) Gamma distributions. Increasing β leads to convergence with the normal distribution. From Johnson et al. (1994).

The shape and scale of the gamma distribution are estimated using the statistics for path-length and velocity. The following moment estimators were applied (Weisstein 1999):

$$\beta = \frac{\bar{\mu}^2}{\sigma^2} \tag{5.2}$$

$$\lambda = \frac{\bar{\mu}}{\sigma^2} \tag{5.3}$$

where $\bar{\mu}$ and σ^2 are mean and variance, respectively.

Other distributions, such as the normal, the log-normal and the exponential were tested, since their shape can be, under some circumstances, quite similar to the gamma distribution (fig. 5.16). However, the Kolmogorov-Smirnov test proved, in most cases, those to be worse than the gamma distribution.

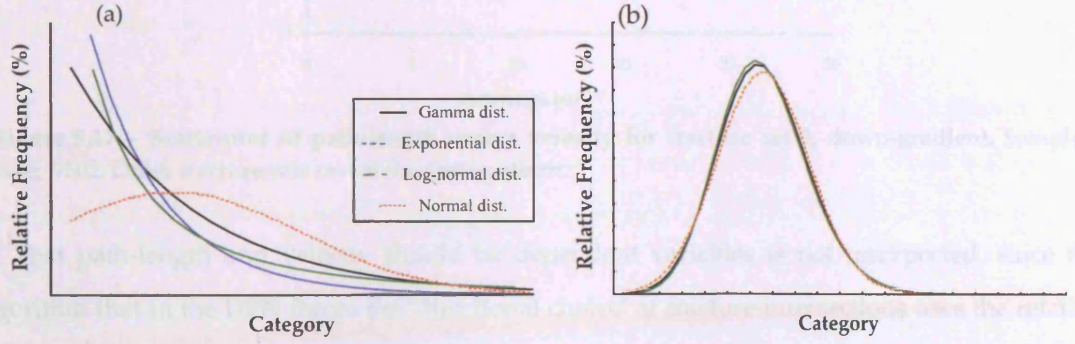

Figure 5.16 – Similarity between gamma, exponential, log-normal and normal distributions. a) low shape (β = 1.2) value ; b) high shape (β = 105) value.

5.2.2.2 Correlation between path-length and velocity

Despite Parney's (1999) conclusion that a correlation between path-length and velocity does not improve the accuracy of the method, a subroutine was included to allow the use of that correlation as an option. Parney modelled that correlation by building a histogram of the path-length distribution and then assigning to each category of the histogram a distribution of velocities. When simulating movement in the continuum, first path-length was generated and then velocity was generated with the parameters for that category of path-length. This method requires storing a lot of information and it is not very efficient, so a different method is used.

Figure 5.17 is a typical scatterplot of path-length × velocity, which closely resembles the scatterplots presented by Parney and Smith (1995) that eventually led to the adoption of the path-length × velocity correlation, and therefore is seen as representative of general behaviour. Correlation between path-length and velocity is not obvious, except that for small values of path-length there is a large variance of velocity, with that variance decreasing with increasing path-length. The decrease in variance is also linked to a decrease in the negative logarithm of mean velocity (i.e. increase in mean velocity).

Bivariate frequency plots of path-length and velocity (fig 5.18) indicate that those variables should be treated jointly and use should be made of bivariate gamma distributions. However, these are complex distributions, which are not easily handled in terms of fitting or estimation of parameters.

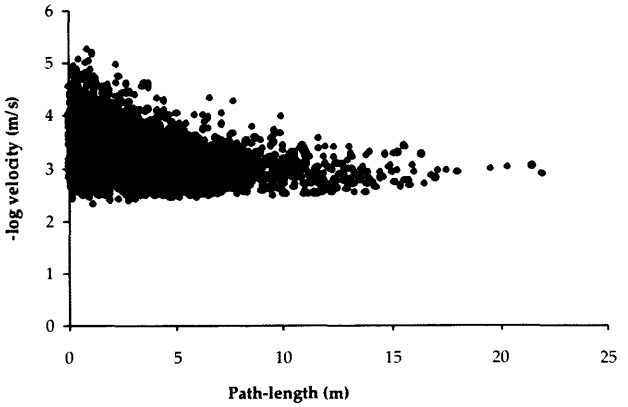

Figure 5.17 – Scatterplot of path-length versus velocity for fracture set 3, down-gradient. Sample size: 9502. Other fracture sets reveal the same pattern.

That path-length and velocity should be dependent variables is not unexpected, since the algorithm that in the DFN forces the 'directional choice' at fracture intersections uses the relative proportion of flow rate in each of the intersecting fracture segments as the probability that the particles may travel along each of those segments. Since higher speeds coincide with higher flow

rates, once a particles enters a high velocity fracture it is likely to continue along it, thereby imposing large path-lengths.

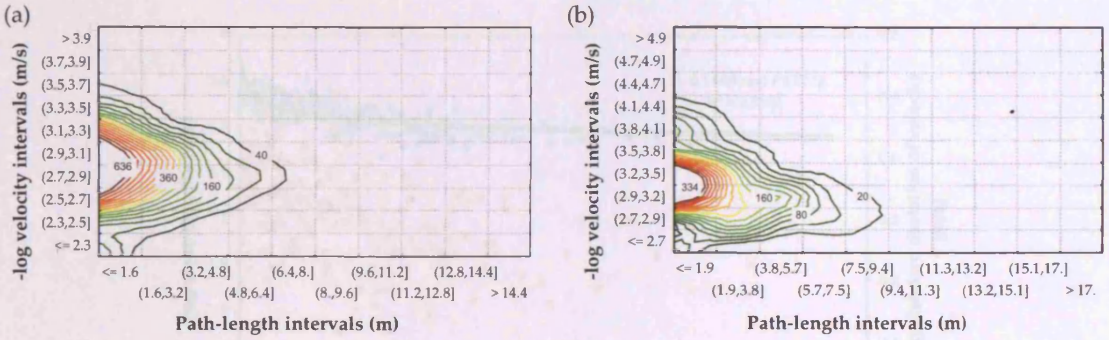

Figure 5.18 – Two examples of frequency plots of path-length and velocity. The two variables seem to behave coherently according to a bivariate distribution. a) fracture set 1, down-gradient, sample size: 4691; b) fracture set 3, down-gradient, sample size: 9502.

Partial distributions of velocity for several ranges of path-length (fig. 5.19) indicate that although gamma distributions can always fit the velocity data, the shape and scale parameters are not constant and tend to increase with path-length. That is, it is necessary to vary the gamma distribution parameters with path-length, implying that skewness of the distribution decreases for higher velocities.

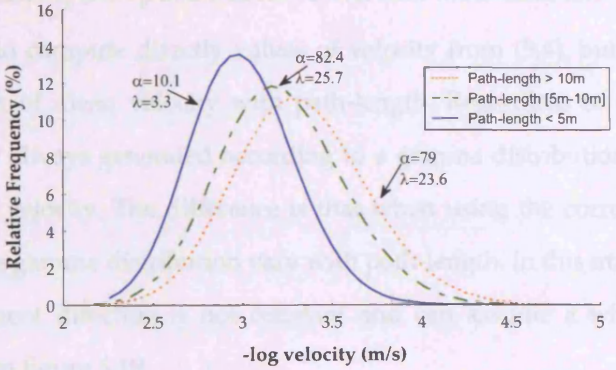

Figure 5.19 – Gamma distribution fit to partial distributions of velocity for several ranges of path-length. Fracture set 3, down-gradient.

The possibility that the smaller dispersion at higher path-lengths is due to a low number of samples cannot be disregarded. In that case, only mean velocity would vary with increasing path-length. Figure 5.20 shows scatterplots of mean and standard deviation of velocity versus path-length.

Figure 5.20 also shows a non-linear regression between mean velocity and path-length. Similar plots for several different fracture sets indicate that the best fit is provided by:

$$mean\ velocity = c_0 - c_1 \ln(path\text{-}length) \tag{5.4}$$

where c_0 and c_1 are constants.

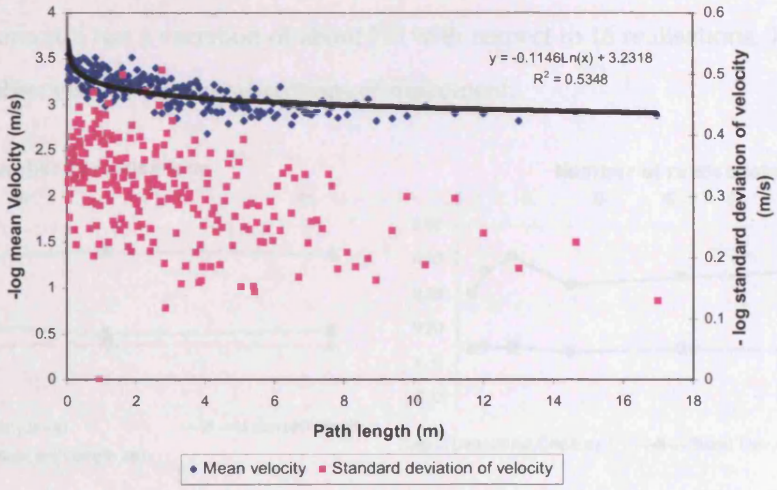

Figure 5.20 – Scatterplot of mean and standard deviation of velocity versus path-length. Also shown the best-fit regression between mean velocity and path-length. Fracture set 3, down-gradient, sample size: 9502. Other fracture sets reveal the same behaviour.

The correlation coefficient is usually very small, in fact most of the time insignificant, due to the large dispersion for small path-lengths. Nevertheless, equation (5.4) was implemented in modules STATMOV, that computes c_0 and c_1, and SCPATH, that uses the correlation.

It is not intended to compute directly values of velocity from (5.4), but just to characterize a tendency for variation of mean velocity with path-length. Regardless of the use or not of the correlation, velocity is always generated according to a gamma distribution using the mean and standard deviation of velocity. The difference is that when using the correlation, the shape and scale parameters of the gamma distribution vary with path-length. In this manner, the distribution used for each movement direction is not constant and can assume a whole range of gamma distributions, such as in figure 5.19.

5.2.2.3 Number of realisations

The accuracy of any calculations involving Monte Carlo procedures, such as collecting the statistics of movement from multiple realisations of some process, is dependent on the stabilisation of the parameters to be studied, that is, on the number of realisations involved. In the present case, the number of necessary realisations is dependent on the number of fracture elements sampled by each particle. Therefore, the maximum number of particles allowed by SDF (200 particles) was used in each realisation. The sampling area was as large as admissible in SDF for the prescribed fracture density.

Figure 5.21 depicts an example in which the parameters collected by STATMOV were plotted against the number of realisations on the DFN domain.

All parameters seem to stabilise quickly, except for the standard deviation of velocity, which with 32 realisations still has a variation of about 7% with respect to 16 realisations. This pattern of behaviour was observed for all other directions of movement.

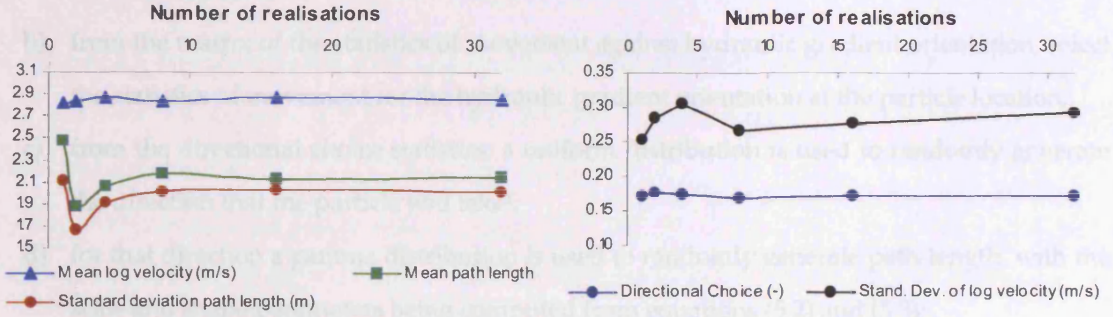

Figure 5.21 – Stabilisation of movement statistics with number of realisations. Fracture set 1, down-gradient. About 25000 movements were sampled in each realisation.

More realisations should be conducted to ensure stabilisation of the standard deviation of velocity. Due to computer limitations, the number of realisations was kept at 32. A sensitivity analysis showed that the results of the SCM are almost indistinguishable when considering 8, 16 or 32 realisations.

Figure 5.21 illustrates just a sample situation and similar analyses should be conducted for every different modelling situation and for each movement direction.

Because the statistics of movement must be determined for several hydraulic gradient orientations, code STATMOV rotates the hydraulic gradient orientation by 15° increments and again performs multiple runs of SDF as explained above, in order to build a matrix of statistics for directional choice, path-length and velocity against hydraulic gradient orientation.

5.2.2.4 Modelling solute transport in the catchment scale continuum domain

Module SCPATH uses the statistics gathered in the discrete fracture sub-domain to simulate particle tracking in the larger continuum domain. The first step is to solve the groundwater flow problem to get values of hydraulic gradient at each point of the continuum domain, since that is the only parameter required by SCPATH. Program MODFLOW, via the interface PMWIN (Chiang and Kinzelbach 2001), is used to obtain solutions to the groundwater flow problem. SCPATH then uses the finite difference grid information and flow rate at each cell face to compute

the hydraulic gradient at each location, much in the same manner as MODPATH does it (Pollock 1989): interpolation using the flow rates at each cell face.

Once the flow solution is established, SCPATH conducts particle tracking according to the following procedure:

a) compute the hydraulic gradient orientation and magnitude at the location where particles are to be released;

b) from the matrix of the statistics of movement against hydraulic gradient orientation, select the statistics of movement for the hydraulic gradient orientation at the particle location,;

c) from the directional choice statistics, a uniform distribution is used to randomly generate the direction that the particle will take[1];

d) for that direction a gamma distribution is used to randomly generate path-length, with the scale and shape parameters being computed from equations (5.2) and (5.3);

e) velocity can be generated by two processes: If velocity is seen as independent of path-length, the statistics (mean and standard deviation) of velocity are used to randomly generate velocity according to a gamma distribution; if a correlation is assumed, then equation (5.4) is used to generate the mean velocity, after which a gamma distribution with shape and scale according to equations (5.2) and (5.3) is used to randomly generate the velocity of the particle;

f) velocity (or more accurately the ratio K/n_e) is multiplied by the hydraulic gradient value to give the advective velocity;

g) the particle is moved to the end of the path-length and, knowing the path-length and velocity of the particle, travel time is computed;

h) steps c) through g) are repeated until the end of the time-step or until the particle changes cell. When either of these occurs, the hydraulic gradient is computed at the new particle location and steps b) through g) are repeated. The choice of small time steps is important to ensure accuracy of the tracking procedure, since it is directly related to the number of readings of the hydraulic gradient orientation and size;

i) steps a) through h) are repeated until the end of the prescribed travel time and a new particle is then selected to move.

SCPATH also includes an option to conduct 'standard' particle tracking in the continuum domain. It uses the same hydraulic parameters on which the MODFLOW flow solution was

[1] A subroutine ensures that the particles changes direction every time a directional choice is made, and that the particles are not allowed to 'choose' the same direction consecutively.

computed and, contrary to MODPATH, includes the possibility of using anisotropy in effective porosity. This option allows us to compare 'standard' particle tracking with the results of particle tracking conducted according to the statistics of movement. The use of directional effective porosities is more realistic, since anisotropy in porosity is certain to occur in fractured rocks.

5.2.3 Comparison of SCM with porous media models and DFN models[1]

To test the reliability of the SCM and simultaneously to test the computer code, a comparison was made between solute transport in the discrete fracture sub-domain and solute transport simulated using SCM.

The fracture network illustrated in figure 5.13 and table 5.1 was used as the base case. Backward particle tracking was conducted, with particles released at random at coordinates x = 75 m, y = [20 - 55 m].

No rotation of the hydraulic gradient was conducted in this case, since the purpose was to assess the reliability of SCM under uniform hydraulic gradient conditions.

The statistics were used in a continuum domain of same size and boundary conditions, with a uniform hydraulic gradient equal to 0.053, the same as used in the DFN domain (fig. 5.13). Comparison between the DFN results and the SCPATH results was accomplished through:

- ability of SCPATH to reproduce the statistics that resulted from the DFN simulation;
- plots of location of particles at given times;
- comparison of the 1st and 2nd spatial moments about the mean of particles' location.

5.2.3.1 Duplicating the statistics of movement in the discrete fracture network

An essential condition is that SCPATH is able to reproduce the statistics of directional choice, path-length distribution and velocity distribution. Nevertheless, it is not expected that the results of SCPATH match exactly the parameters of a single realisation of the discrete fracture domain since the parameters used in SCPATH are the result of statistics gathered in 32 realisations.

Figure 5.22 compares directional choices made in the discrete domain and in the Statistical Continuum. It is obvious that the match is good, although there are more choices of directions 1 (down-gradient fracture set 1) and 6 (up-gradient fracture set 3) and corresponding lower number of choices of the directions 2 (down-gradient fracture set 2) and 3 (down-gradient fracture set 3).

[1] This section aims to assess the reliability of the SCM and of the codes for the sample case under study (fig. 5.13, table 5.1). For a systematic analysis of reliability of the Statistical Continuum Method refer to Parney (1999).

These differences cannot be due to the use of one single realisation of the discrete domain since the same errors are found when comparing the results of SCM with the values that were used to generate the fracture directions. The discrepancy is due to the need of ensuring that particles actually change direction every time a directional choice is made, and that particles are not allowed to take the same direction consecutively. Thus, in SCPATH directional choice is not a completely random event because it is constrained by the preceding choice. However, the magnitude of the error involved, as seen from figure 5.22, is irrelevant.

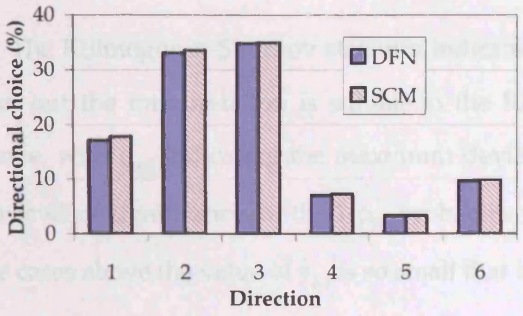

Figure 5.22 – Comparison of directional choices made in the DFN and in the SCM.

As for path-length distribution (fig. 5.23), again, there seems to exist deviation between the results of SCM and the discrete domain, but the statistics of SCM follow the ones collected with STATMOV, which probably means that the difference is due to only one realisation of the discrete domain being used for comparison.

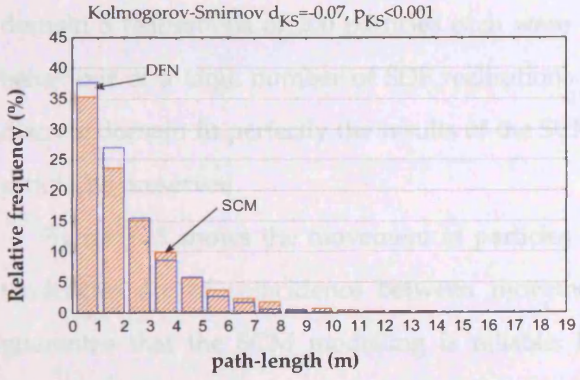

Figure 5.23 – Comparison of path-lengths generated by the DFN and by the SCM. Fracture set 1, down-gradient.

Figure 5.24 shows the comparison for velocity, generated without correlation between path-length and velocity, and the fit is good enough, with the differences being probably due to a single realisation of the discrete domain being represented.

Although differences occur, the statistics of movement in the DFN domain are reproduced by SCPATH.

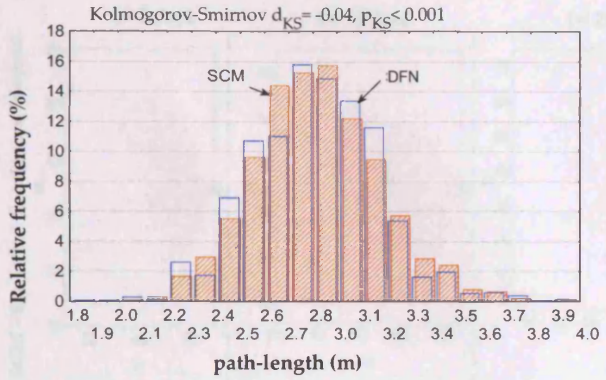

Figure 5.24 – Comparison of velocity generated by the DFN and by the SCM. Fracture set 1, down-gradient.

The Kolmogorov-Smirnov statistics indicated in figures 5.23 and 5.24 refer to the two-sample test, but the interpretation is similar to the Kolmogorov-Smirnov statistics used in figure 5.14 above, with d_{KS} indicating the maximum deviation between the two samples and p_{KS} indicating the level of significance (or the 1-p_{KS} probability that samples come from the same population). In the cases above the value of p_{KS} is so small that indicates that the two samples come from the same population with probability above 99%. Thus, the differences between the SDF and the SCM seen in those plots are statistically negligible.

5.2.3.2 Location of particles in time

Plumes of particles were tracked, both in the discrete domain and in the statistical continuum domain. In SCPATH 1000 particles were tracked in one single realisation while in the discrete domain 5 realisations of 200 particles each were used. Since SCPATH reproduces the statistical behaviour of a large number of SDF realisations it is not expected that the 5 realisations of the discrete domain fit perfectly the results of the SCM. However, the main tendencies of movement should be preserved.

Figure 5.25 shows the movement of particles in the discrete domain and in SCM. The main tendencies are of coincidence between movement of the two clouds of particles, a strong guarantee that the SCM modelling is reliable. However, it is also obvious that longitudinal dispersion seems to be underestimated in the SCM. The reasons for this can be fully appreciated when using the spatial moments of the plumes.

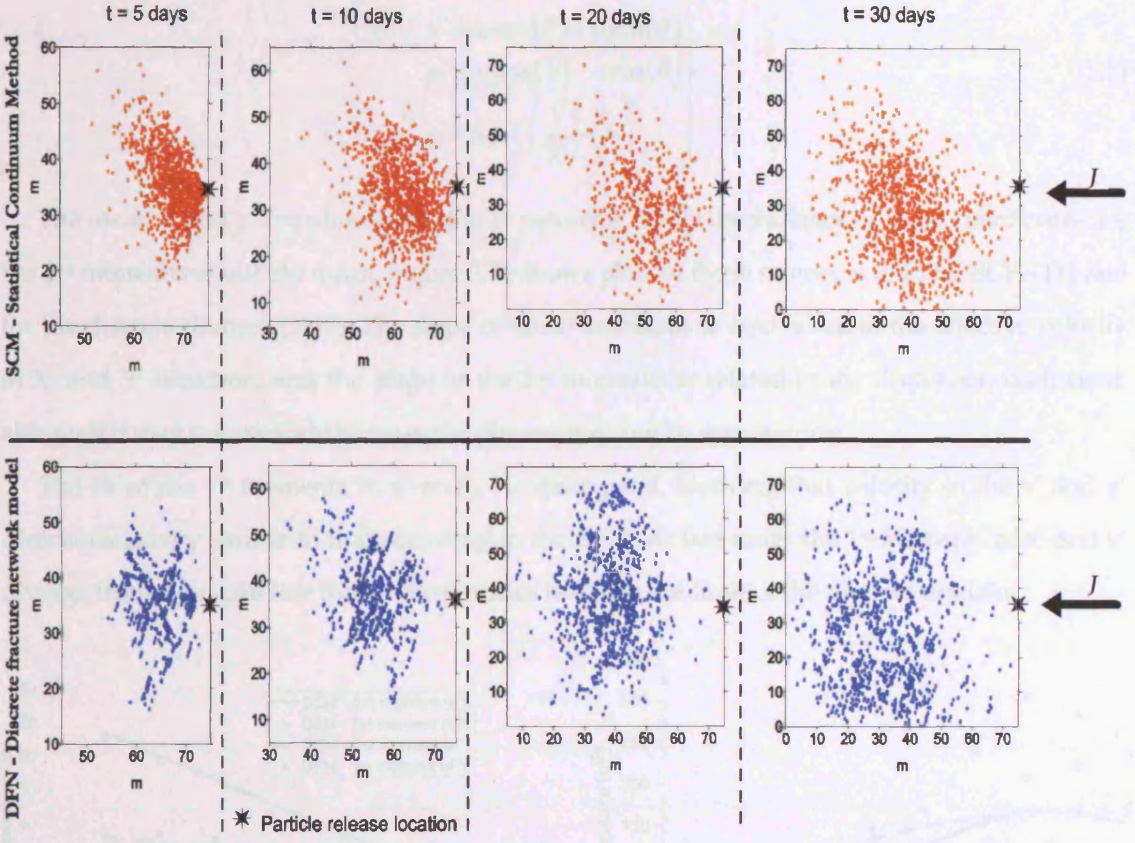

Figure 5.25 – Plumes of particles tracked using SCM and DFN models. Correlation path-length/velocity not used. 1000 particles instantaneously released at $X_0 = 75$m, $Y_0 = 37.5$m. Uniform hydraulic gradient from right to left. Notice that scale varies.

5.2.3.3 Spatial moments

Smith et al. (1990) and Parney (1999) used the spatial moments of particle locations to assess the reliability of the SCM method, and the same approach is used in this study. The DFN and SCPATH results were compared by plotting the first (mean) and second (variance) moments about the mean particle location.

The mean $\bar{X}$ and $\bar{Y}$ coordinates of the ensemble of particles allow definition of the main direction of movement, knowing the X_0 and Y_0 initial location of particles. The segment $\overline{(\bar{X}\bar{Y})(X_0Y_0)}$ defines the longitudinal direction of movement and is regarded as the new x'-axis. All x, y particle locations are rotated into the new coordinate system according to (Spiegel and Liu 1999):

$$\left.\begin{aligned} x' &= x\cos(\theta) + y\sin(\theta) \\ y' &= y\cos(\theta) - x\sin(\theta) \\ \varphi &= \tan^{-1}\left(\frac{\bar{Y} - Y_0}{\bar{X} - X_0}\right) \end{aligned}\right\} \quad (5.5)$$

The mean x′ and y′ coordinates are the 1st moments, while the variance of those coordinates are the 2nd moments about the mean. Figure 5.26 shows plots of those moments both for SCPATH and for the discrete domain (SDF). The slope of the 1st moments is equivalent to the effective velocity in X′ and Y′ direction, and the slope of the 2nd moments is related to the dispersion coefficient, although it may not coincide because the plumes may not be symmetrical.

The fit of the 1st moments in x′ and y′ is quite good, showing that velocity in the x′ and y′ directions is very similar to that occurring in the DFN. At late times the 1st moments of x′ and y′ diverge from a straight line due to the particles reaching the limit of the discrete domain.

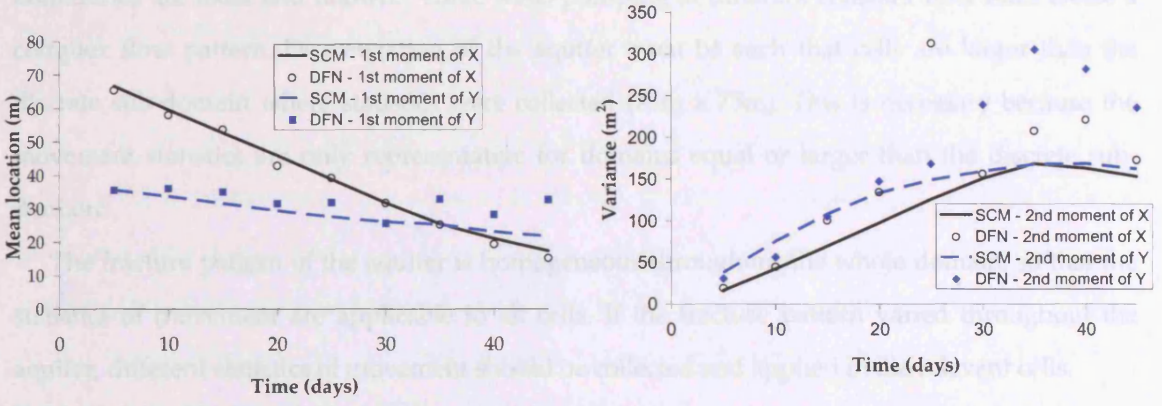

Figure 5.26 – Spatial moments of x′ and y′. Particles released at $X_0 = 75$m, $Y_0 = 37.5$m.

As for the 2nd moments, dispersion in the y' direction shows a good fit until particles start leaving the fracture domain. After 30 days, dispersion in the y' direction in the DFN domain is larger than in SCM. The DFN model identifies the lateral boundaries as impermeable, and so the particles are deflected back into the domain, while SCPATH does not identify the boundary as impermeable and consequently the particles leave the domain, decreasing lateral dispersion.

Comparison of dispersion in the x' direction is not as good as in the y' direction. Both in the DFN and in SCPATH particles were released at location $X_0 = 75$ m and $Y_0 = 37.5$ m. SCPATH uses precisely this location and generates the first element starting from that point. In the discrete domain, particles are shifted to the closest node of the previously generated network. Therefore, in the DFN and in SCPATH particles do not start exactly at the same location.

This effect should be averaged in multiple realisations of the DFN but, since every realisation of the discrete domain has a different starting location, there will be an apparent dispersion even for $t = 0$. This provides a possible explanation for the less good fit between 2nd moments of x' and y'. Nevertheless, the overall tendency of dispersion in x' and y' is well represented in SCM.

5.2.4 Solute transport at the catchment scale

The ultimate aim of the Statistical Continuum Method is to simulate solute transport in fractured aquifers at scales for which discrete fracture network models become impractical. To achieve this purpose MODFLOW output provides the flow solution that is required as input to SCPATH, according to the procedure described in section 5.2.2.4.

Figure 5.27 shows the layout used as a sample problem to test SCPATH at the catchment scale. A confined fractured aquifer has lateral impermeable boundaries, while heads at the left and right boundaries are fixed and known. Three wells pumping at different constant flow rates create a complex flow pattern. Discretization of the aquifer must be such that cells are larger than the discrete sub-domain where statistics were collected (75m x 75m). This is necessary because the movement statistics are only representative for domains equal or larger than the discrete sub-domain.

The fracture pattern of the aquifer is homogeneous throughout the whole domain, so that the statistics of movement are applicable to all cells. If the fracture pattern varied throughout the aquifer, different statistics of movement should be collected and applied in the relevant cells.

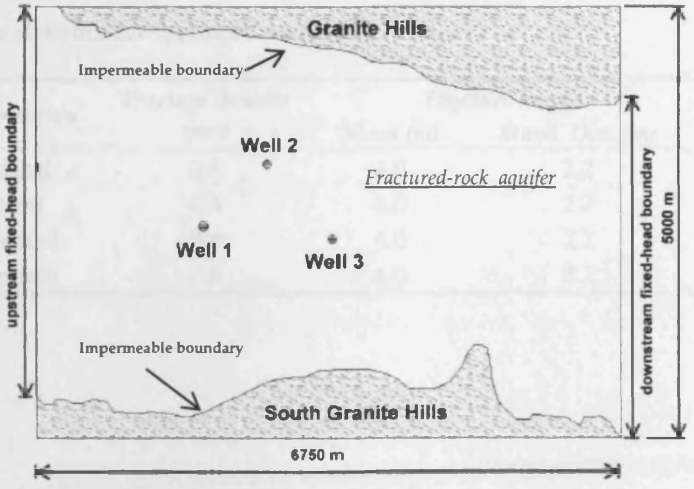

Figure 5.27 – Layout of the aquifer used as sample case

5.2.4.1 Solute transport in an 'isotropic' fracture network

The simulations conducted in section 5.2.3 considered a uniform flow field, with a constant hydraulic gradient applied throughout the entire modelling domain. Identification of the hydraulic gradient orientation at any location is essential for application of SCPATH, since that is the single parameter retrieved from the continuum flow model and used in SCPATH. Therefore, it is important to test the reliability of SCPATH under complex flow conditions.

The sample case aquifer was assumed as an equivalent porous medium with constant K and n_e in each cell. PMWIN computed the flow solution and backward particle tracking was conducted using PMPATH. In the discrete sub-domain, statistics of particle movement were gathered for an almost isotropic fracture system (fig. 5.28, table 5.2).

The statistics of movement were used with the flow solution computed by PMWIN. If SCPATH is identifying the hydraulic gradient properly and conducting particle tracking correctly, then there should be close correspondence between the path-lines delineated with the packages PMWIN/PMPATH and SCPATH, because the fracture system is well connected and is almost isotropic. The location of the isochrones should not coincide, because there was no concern in computing the flow and transport solutions using K and n_e parameters equivalent to those resulting from the isotropic fracture network. However, the aim of this simulation was to check whether SCPATH uses the flow solution correctly and reaches the same solution of path-lines and capture zones as an equivalent porous medium, when the fractured system is 'isotropic'.

The characteristics of the 'isotropic' fracture system are shown in the table 5.2 and a sample realisation of the network is illustrated in figure 5.28.

Table 5.2 – Fracture statistics for 'isotropic' network

Fracture orientation	*Fracture density* (m^{-1})	*Fracture length*		*Fracture aperture (m)*
		Mean (m)	*Stand. Dev. (m)*	
N40°, vertical	0.6	4.0	2.2	5×10^{-5}
N-S, vertical	0.6	4.0	2.2	5×10^{-5}
N120°, vertical	0.6	4.0	2.2	5×10^{-5}
N100°, vertical	0.6	4.0	2.2	5×10^{-5}

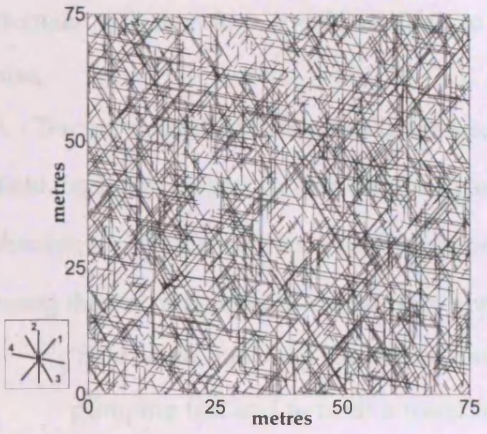

Figure 5.29 – Sample realisation of the discrete subdomain (75m×75m) of 'isotropic' fracture network.

Figure 5.29 shows the groundwater flow solution used, the path-lines computed using the equivalent porous medium model and the path of the particles tracked by SCPATH. It can be seen that the paths delineated using both methods are very similar, although dispersion is inevitable when using SCPATH. Thus, SCPATH is dealing correctly with a non-uniform hydraulic gradient.

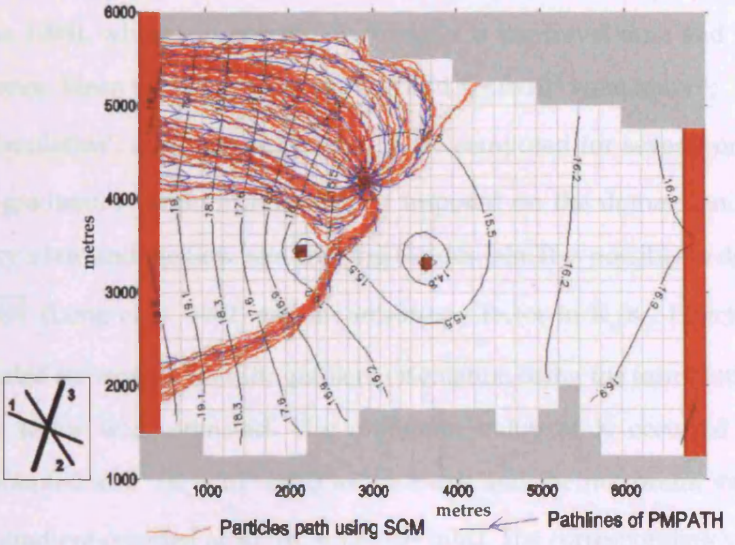

Figure 5.28 – Pathlines delineated in an aquifer with an 'isotropic' fracture network. 1000 particles were backtracked from the well.

5.2.4.2 Solute transport in an 'anisotropic' fracture network

From this point onward, the fracture network used is again the base case as described in table 5.1 and illustrated in figure 5.13, that is, a highly anisotropic system. This was considered more challenging for simulating transport at the catchment scale. Section 5.2.3 already established the reliability of the SCM for this fracture network at a scale equivalent to that of the DFN sub-

domain and, therefore, it only remains to test the ability of SCPATH in upscaling to catchment size.

The previous section was not concerned with the values of K and n_e used to generate the flow field, because isochrones were not compared. However, the K and n_e used in every cell must be consistent with the characteristics of the fracture system. Therefore, K and n_e must be computed using the fracture network model. Two approaches were used:

- 'field' data, meaning the use of data that one would gather in a real situation: K from a pumping test and n_e from a tracer test. For this purpose, a pumping test was simulated in the DFN for a single realisation of the base case network. The Thiem equation was used to compute the value of K. All DFN nodes were used as observation wells and the mean value of K was adopted. This results in an isotropic K. Tracer tests were also simulated in the DFN with particles being dropped at one boundary and the time of arrival at the other boundary being used to compute the value of n_e according to the equation $n_e = \frac{qt}{L}$ (Guérin and Billaux 1994), where q is specific discharge, t is the travel time and L is the effective travel distance. Mean values of $K = 4 \times 10^{-3}$ m/d and $n_e = 6 \times 10^{-5}$ were found[1];
- 'integral simulation', meaning that K and n_e are computed for several orientations of the hydraulic gradient. A uniform flow field is imposed on the domain and K is computed using Darcy's law and the flow rate crossing the domain. It is possible to define an ellipsoid of $1/\sqrt{K(\Theta)}$ (Long et al. 1982) and an anisotropy factor in K_x/K_y. Effective porosity was also computed for every hydraulic gradient orientation using the formulation above and an anisotropy factor was estimated. The minimum value of K occurred for a hydraulic gradient oriented at 0° ($K_x = 10^{-3}$ m/d) to the *x-axis* and the maximum value occurred for hydraulic gradient oriented at 90° ($K_y = 5.8 \times 10^{-3}$ m/d). The corresponding values of effective porosity found were $(n_e)_x = 6 \times 10^{-5}$ and $(n_e)_y = 9 \times 10^{-5}$, for the $\Theta = 0°$ and $\Theta = 90°$ orientations, respectively.

The main practical difference between the two approaches is that the second method allows us to account for anisotropy in K and n_e. When computing the flow solution with PMWIN, every cell of the finite difference domain was allocated the same parameters. Notice that the concepts of "anisotropy in n_e" and "directional n_e" are only adequate because this effective porosity must be

[1] The value of effective porosity is far below the usual values found on field situations. Nevertheless, and since all values of porosity and the statistics of movement were derived from the same network, the analysis is still valid.

understood here as a "**kinematic porosity**". This quantity can be defined as the ratio between the volume of circulating water and the total volume of rock (de Marsily 1986); that is, it represents the portion of the porosity corresponding to the mobile fraction of water. Kinematic porosity should not be confused with the porosity ratio, i.e. the percentage of voids in a rock volume, which is not directional dependent.

Figure 5.30 shows the flow solution found with PMWIN, both for the situation considering isotropic behaviour (fig. 5.30a) and for the situation considering anisotropy in K (fig. 5.30b). Also shown are the path of particles released at the wells and backtracked in order to define the capture zones. For the isotropic case the particle tracking program PMPATH was used, but in the anisotropic case the pathlines were found with the option of SCPATH that incorporates anisotropy in kinematic porosity n_e, which is not possible in PMPATH.

Notice that the capture zones depicted in figures 5.30a and 5.30b are strikingly different not only due to the anisotropy included in 5.30b, but also because the flow solutions were not calibrated to any field data; such calibration would force the flow solutions to be more alike and consequently the capture zones would be more similar.

As described in section 5.2.2.4, these flow solutions supply the information that must be used by the SCPATH code to simulate solute transport according to the Statistical Continuum Method. SCPATH computes the hydraulic gradient value and orientation for every cell of the finite difference domain and then applies the matrix of movement statistics vs. hydraulic gradient orientation to conduct particle tracking. Therefore, the only information that is retrieved from the continuous porous medium model is the hydraulic gradient at every cell.

Figure 5.31 compares the capture zones delineated according to the SCM procedure with the capture zones shown in figure 5.30 which were delineated using an EPM approach.

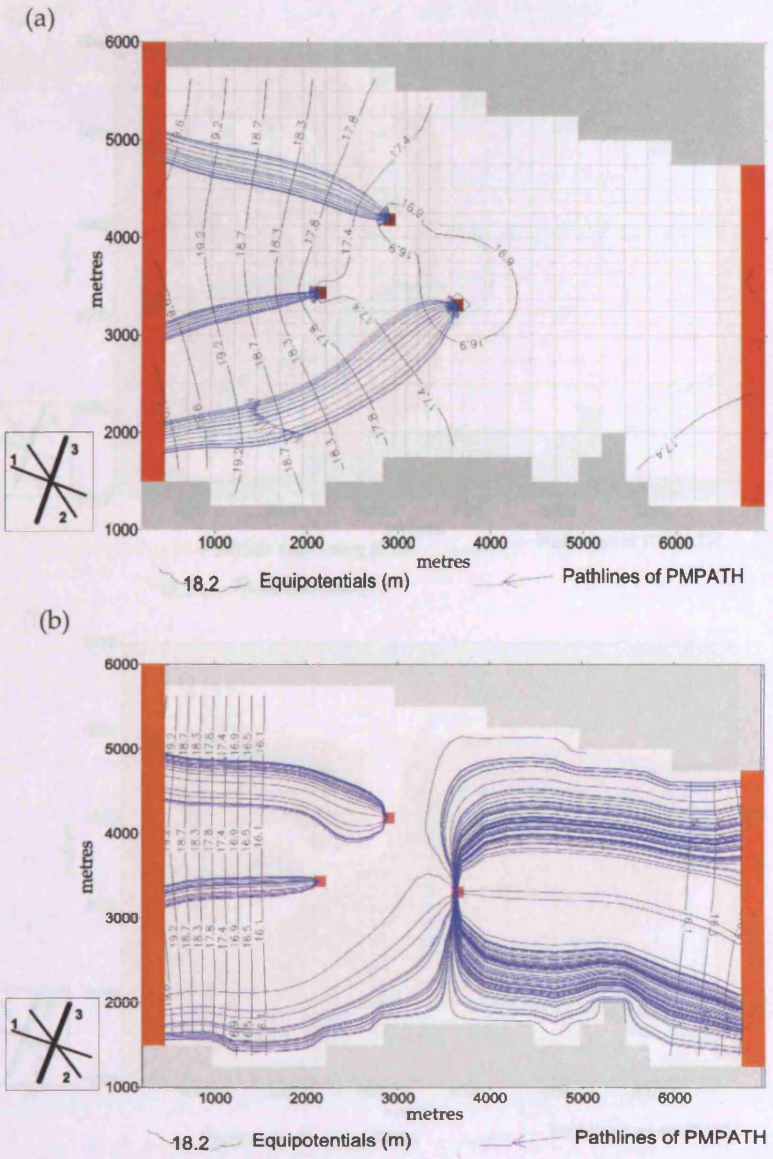

Figure 5.30 – Capture zones of three wells in an aquifer with an 'anisotropic' fracture network, according to an EPM approach. *a) Flow solution computed with K_x=K_y; b) Flow solution computed with K_y/K_x=5.8.* 1000 particles were backtracked from each well. The small squares shows the orientation of the fracture sets that compose the aquifer.

If the flow solution obtained with an isotropic K is used (fig. 5.31a), the pathlines are completely different when delineated with SCPATH and when delineated assuming EPM conditions (PMPATH used), due to the highly anisotropic behaviour and discontinuous character of the fracture system. Dispersion is higher and the main flow direction is imposed by the most permeable fracture set (number 3), oriented at N20°E. The results of SCPATH seem to be consistent with the imposed flow field and with the anisotropy of the fracture system, which is in favour of the reliability of the method.

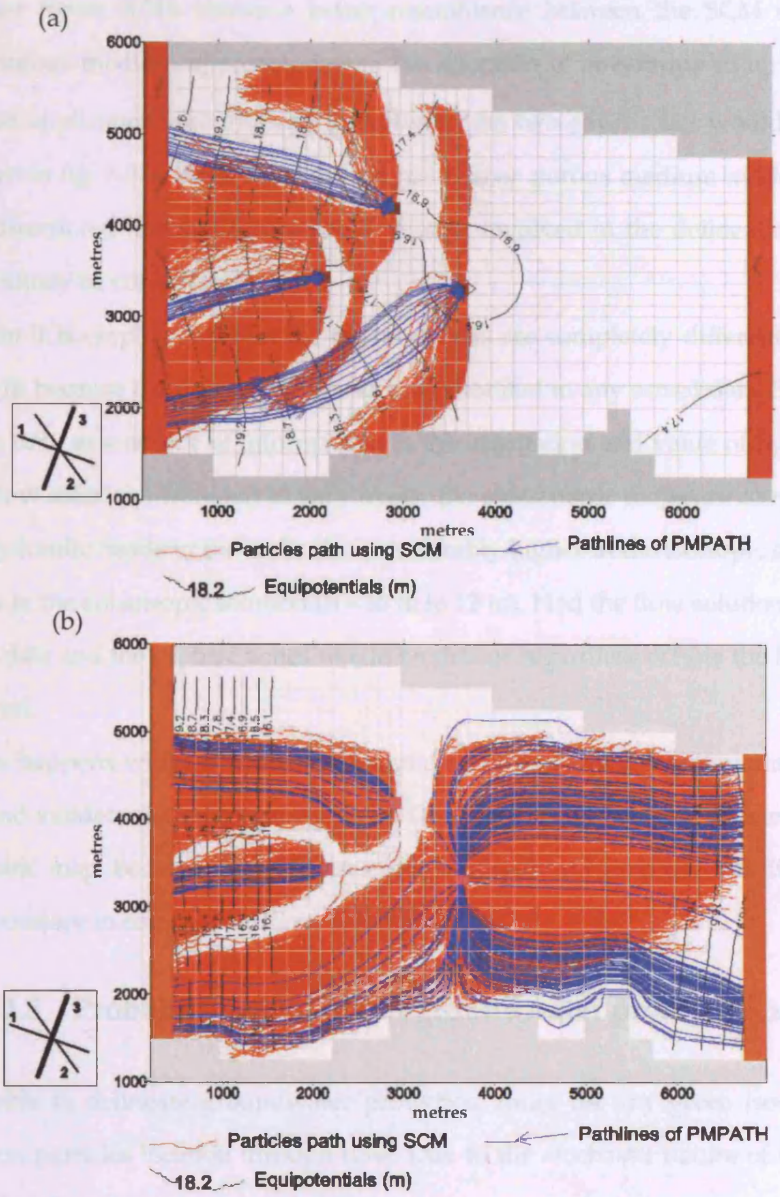

Figure 5.31 – Comparison between capture zones delineated by the SCM approach and by the EPM approach. ***a) Flow solution computed with K_x=K_y; b) Flow solution computed with K_y/K_x=5.8..*** **Notice that the aquifer is composed by an 'anisotropic' fracture network.** 1000 particles were backtracked from each well. In SCM the tracking of particles was limited to 10000 days, which explains why some of the paths do not reach the limit of the capture zone.

Figure 5.31b compares the groundwater capture zones delineated using the flow solution that considers anisotropy in K. In this case the continuous porous media capture zone was computed considering also anisotropy in n_e. As for the pathlines delineated with SCPATH, they indirectly encompass both the anisotropy in K and the anisotropy in n_e, and they are consistent with the hydraulic gradient and anisotropy of the fracture network. The pathlines delineated by both methods are now more similar, the main differences resulting from the dispersion imposed by the fracture network.

Notice that figure 5.31b shows a better resemblance between the SCM solution and the continuous porous medium approach due to the adoption of anisotropy in n_c. However, in the most common applications the discrepancy between the two approaches would be more akin to the one shown in fig. 5.31a, since the standard continuous porous medium models do not permit to consider directional kinematic porosity. The error involved in the delineation of the capture zone can obviously be considerable.

Once again it is emphasized that the capture zones are completely different between figures 5.31a and 5.31b because the flow solution was not calibrated to any actual data. SCPATH uses the flow solution only as a source of information on the orientation and value of hydraulic gradient, but as both flow solutions were left to vary freely, the piezometric maps are completely different. In fact, the hydraulic heads in the wells are considerably higher in the isotropic solution (h = 16 m to 17 m) than in the anisotropic solution (h = 10 m to 12 m). Had the flow solutions been calibrated to any 'field' data and the capture zones would be similar regardless of how the flow solution had been computed.

As always happens with the process of groundwater modelling, the existence of reliable data to calibrate and validate the model is essential. In the present case, what is relevant is the existence of a piezometric map, because the SCM uses only the hydraulic gradient and discards any other parameter necessary to compute the flow solution.

5.2.5 Probability contours of groundwater protection zones

It is possible to delineate groundwater protection zones for any given isochrone using the information on particles location through time. Due to the stochastic nature of the movement of particles, such delineation must be probabilistic.

In order to quantify uncertainty the module PROBCONT computes the probability of any cell of the continuum domain being part of an isochrone *t*. The procedure is similar to the method used by van Leeuwen (2000) although backward particle tracking is used. PROBCONT checks the path of every particle and computes the probability as follows:

- whenever each particle *i* reaches a cell *j* before time *t* a value of $Z_i = 0$ is assigned to the cell. Whenever the travel time to each cell is above *t*, a value of $Z_i = 1$ is assigned;
- the sum of Z_i values at each cell *j* is divided by the total number of particles *n* reaching the cell to find the probability P(j, t) that particles crossing that cell will take longer than time *t* to reach the well, according to $P(j,t) = \frac{1}{n}\sum_{i=1}^{n} Z_i$.

The result is the probability that any particle passing out of that cell will take longer than time *t* to reach the well. For instance, the 75% contour for the 50-day isochrone indicates that 75% of the particles crossing that contour will take longer than 50 days to reach the well, thus defining the 0.75 probability of the well being totally protected.

PROBCONT was used with the SCPATH output, both when considering isotropy in K and when considering anisotropy in K and n_e. The groundwater protection zones were delineated for a ten-year isochrone.

Figure 5.32 shows the probability contours for the isotropic K flow solution. There is considerable difference between the protection zones delineated with PMPATH and the protection zones delineated with SCM, both in the orientation and in size of the protection zones. The protection zones delineated by the SCM are marked by particles travelling primarily along fractures that are more permeable (fracture set 3).

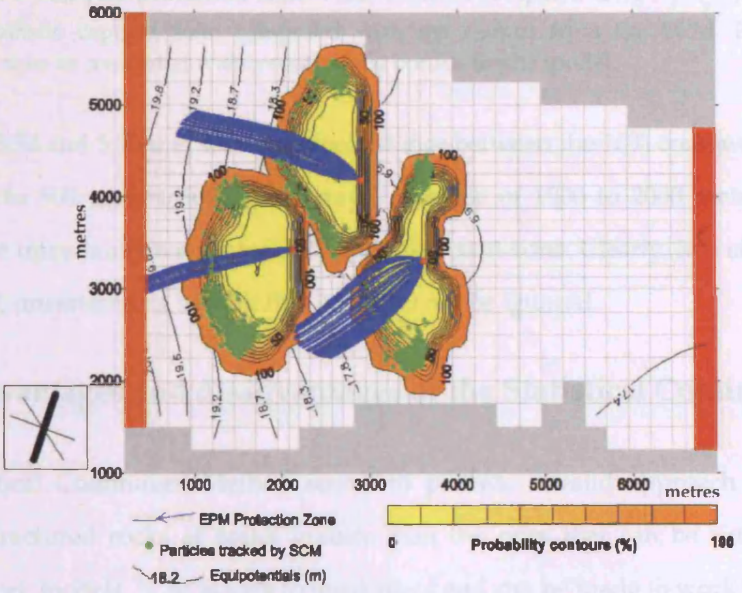

Figure 5.32 – Ten-year protection zone. *Flow solution computed with* K_x=K_y. Contours represent the probabilistic capture zone computed with the output from the SCM. Blue lines realise the protection zone as computed with a continuous porous media model.

Figure 5.33 shows the groundwater protection zone delineated when considering anisotropy in K and n_e. The uncertainty contours seem to be consistent both with the piezometric surface and with the fracture anisotropy, with lateral dispersion being very high despite the steep hydraulic gradient parallel to x.

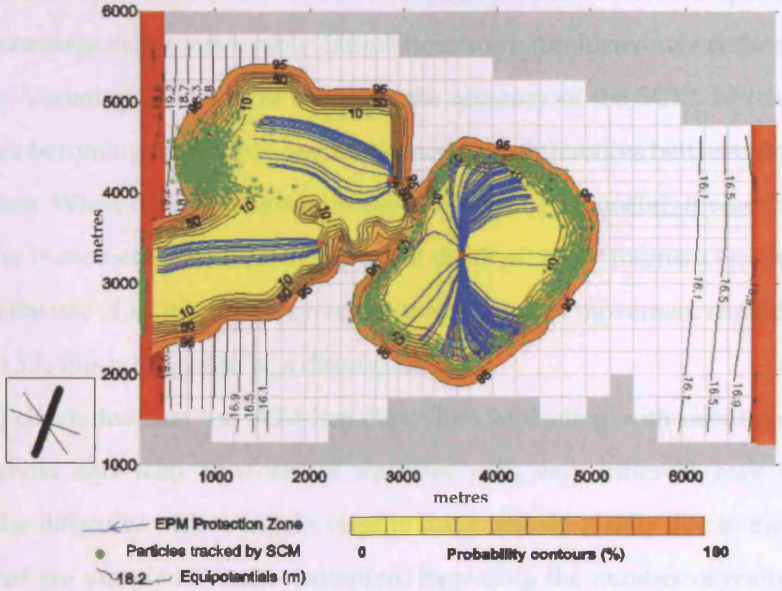

Figure 5.33 – Ten-year protection zone. ***Flow solution computed with*** K_x/K_y***=5.8.*** Contours represent the probabilistic capture zone computed with the output from the SCM. Blue lines realise the protection zone as computed with a continuous porous media model.

In figures 5.32 and 5.33 it is seen that the distance between the 10% contour and 100% contour can be of up to 500 metres, for a total travel distance of 1000 to 2000 metres. This is a good measure of the uncertainty associated with the protection zone. Clearly, in a situation such as the case modelled, uncertainty is so high that it should not be ignored.

5.2.6 Advantages and disadvantages of the Statistical Continuum Method

The Statistical Continuum Method seems to provide a valid approach to simulate solute transport in fractured rocks at scales greater than the ones that can be simulated by discrete fracture network models. SCM is easy to implement and can be made to work in conjunction with standard finite difference flow models, so that probability contours of protection zones can be computed for aquifers at the catchment scale.

The spatial moments of plumes delineated with the SCM are reliable, especially the first moment (mean location of the centre of the plume). The method seems to provide a less accurate representation of dispersion (fig. 5.26), which is probably due to the simplifications inherent to the method. However, part of the discrepancies observed in figure 5.26 are related to the way SCM was implemented (a subroutine should be included to force particles to ignore movement directions that will cause the particle to enter an inactive cell).

In the simulations shown, the fracture sets have constant orientation and aperture, although usually those parameters vary considerably. Simulations were conducted where those parameters were left to vary. Variations in aperture enhances the accuracy of the SCM, which results from directional choices becoming more clear due to the increased differences between flow rate in the several fracture sets. When fracture orientation was the varying parameter, it was concluded that the fit between the 1st moments was equally good, but the fit of the 2nd moment was worse.

SCM requires the use of a DFN model on which the statistics of movement should be collected. As seen is section 5.1, this is judged to be a disadvantage.

Parney (1999) concluded that the SCM has difficulties in dealing with networks close to the percolation threshold and with networks of fractures with very different scale lengths. It is considered that the difficulty with networks close to the threshold is only due to the low number of movements that are sampled in each realisation. Increasing the number of realisations or the discrete domain size should be enough to overcome this difficulty. As for the different length scales, this probably cannot be solved by increasing the sub-domain due to the large number of fractures that would have to be modelled. It is worth mentioning that the several distinct modelling approaches to the groundwater flow in the Stripa fractured rock test site, all indicated that large discrete fractures, fracture zones or faults, must be modelled explicitly whatever the modelling approach is (National Research Council 1996) and possibly that is also the case for the Statistical Continuum Method.

Notice that the statistics of movement were collected in a domain to which impermeable boundaries were assigned to top and bottom edges (fig. 5.13). Such boundaries were adopted in order to ensure that the overall hydraulic gradient is oriented at 0° with the *x-axis* (that is, all flow entering the domain from the right boundary will leave it through the left boundary). Thus, in this setup there is no ambiguity on the hydraulic gradient orientation, which is fundamental to the application of the Statistical Continuum Method since the hydraulic gradient orientation is used to conduct solute transport in the continuous large-scale model.

However, it can be argued that different boundary conditions should be used at the top and bottom edges of the domain, namely linearly varying head boundaries. Because the small-scale domain on which the statistics of movement are collected is not continuous, those varying head boundaries will not coincide with flow lines, and therefore flow and particles will be able to cross them (whenever a fracture intersects the boundary), introducing ambiguity on the hydraulic gradient orientation. Nevertheless, it is recognised that the adoption of impermeable boundaries,

by constraining the area in which flow can occur, may affect the statistic of movement. This influence can be studied in, at least, two distinct manners: a first method would adopt the linearly varying head boundaries and compare the statistics thus collected with those gathered when adopting impermeable boundaries; the second method would adopt impermeable boundaries at increasing distances and would compare the statistics collected in each of the geometries adopted.

Chapter 6

PROTECTION ZONES FOR FRACTURE NETWORKS II

CONTINUOUS TIME RANDOM WALKS

Techniques such as Discrete Fracture Network (DFN) models and hybrid methods have increased our understanding of the hydraulic behaviour of fractured-rocks environments. However, the widespread application of those methods to model solute transport has been constrained by their complexity. Hydrogeologic studies in fractured rocks would be considerably simplified if techniques similar to those used for continuous porous media could be applied to fractured rocks. In particular, the use of dispersion tensors would expedite solute transport modelling in fractured-rock aquifers.

However, several features obstruct the use of dispersion tensors in discontinuous media. Amongst those features are:

- dispersion is not necessarily described by a tensor. Even if the flow behaviour of fracture networks can be described using $1/\sqrt{K(\Theta)}$ ellipsoids (Long et al. 1982), it may be extremely difficult to describe effective porosity, tortuosity and dispersivity according to tensors (Endo et al. 1984, Guérin and Billaux 1994). Consequently, concepts such as 'longitudinal' and 'transverse' dispersion coefficients may be meaningless in fractured rocks (National Research Council 1996);
- solute movement in fractured rocks occurs along well-defined directions, the fracture orientations. As a result, dispersive movement in fractured rocks cannot be analogous to molecular diffusion, since movement in every direction is not possible;
- dispersion may not occur according to Fick's laws. Tracer tests, have shown that dispersivity is not constant, increasing with scale of observation (Bear et al. 1993). Some authors give empirical correlations between dispersivity and distance (Ross 1986, Neuman 1993) and consider those correlations as the result of a 'scale effect', while others assume that Fickian behaviour is not applicable (Berkowitz and Scher 1997, Painter 1999);

- there may not exist a Representative Elementary Volume (REV) to which effective transport parameters can be assigned (Clemo and Smith 1997). This is particularly the case for geologic environments where fracture lengths may be distributed as fractals, in which case no REV will exist (Painter 1999). This may also be the case for low density fracture systems (Lee et al. 1994).

These features, together with the considerable uncertainty inherent to hydraulic parameters in fractured rocks, make solute transport very difficult to simulate. Techniques based on solute transport, such as delineation of groundwater protection zones, reflect the same problems.

It is recognised that DFN models, although able to deal with the features listed above, are very complex to use and alternatives should be sought. Even hybrid techniques such as the Statistical Continuum (section 5.2) can be hard to implement and benefit would result from their simplification.

This chapter studies a different methodology for modelling solute transport in fractured rocks. The methodology is designated as **CTRW** and it attempts to model solute transport by a process similar to the methods used in continuous porous media, that is, by using dispersivities, while still maintaining the main features imposed by the fracture network characteristics. The CTRW is based on a random process, but contrary to Fickian transport, it does not assume that macroscopic dispersion is a process similar to molecular diffusion (Rasmuson 1985), i.e. that solute concentration in space follows a normal distribution (Fetter 1999). Therefore, Fickian behaviour is not an assumption.

This chapter is organised as follows: section 6.1 presents the reasoning for adopting a CTRW and depicts its differences to the random process used in continuous porous media; section 6.2 presents analytical solutions for solute transport according to a 1-D CTRW; sections 6.3 and 6.4 use those 1-D solutions to build procedures for 2-D solute transport and, finally, section 6.5 applies the 2-D CTRW to the delineation of groundwater protection zones.

6.1 BROWNIAN MOTION AND CTRW: TWO STATISTICAL MODELS FOR SIMULATING SOLUTE TRANSPORT

Dispersion in fracture networks occurs at various levels, since there is dispersion at each individual fracture, at fracture intersections, and at the scale of the network (Sahimi 1995). For the remainder of this section, we will be dealing with dispersion at fracture intersections; transport in each individual fracture is assumed purely advective.

6.1.1 Brownian motion, random walks and solute transport

Solute transport involving hydrodynamic dispersion is usually regarded as a process similar to molecular diffusion, following Fick's 2nd law:

$$\frac{\partial C}{\partial t} = D\frac{\partial^2 C}{\partial x^2} \tag{6.1}$$

where D can be regarded as a coefficient of molecular diffusion or hydrodynamic dispersion, depending on the phenomenon that is being studied.

The physical basis for the diffusion equation (6.1) is Brownian motion (fig. 6.1), that is, the movement of small particles suspended in a fluid and subjected to continual molecular impacts (Chung 1979). Brownian motion can be represented by a random process $\{X(t), t \geq 0\}$ with the following properties (Hsu 1996):

a) X(t) has stationary independent increments (designated hereafter as *path-lengths*);

b) path-lengths X($t+\Delta t$)-X(t) follow a normal distribution;

c) X(0) = 0;

d) $E[X(t)] = vt$, where v is the drift coefficient (velocity).

Consequently, Brownian motion is represented by a normal distribution process with mean vt and variance represented by $\sigma^2(t)$.

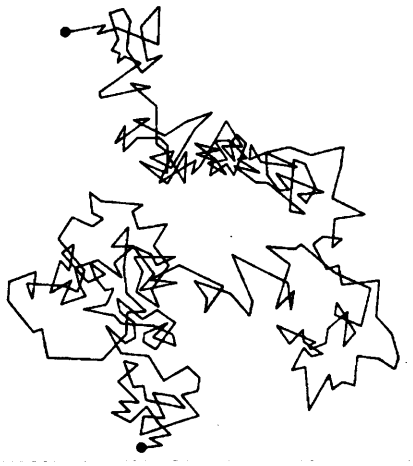

Figure 6.1 – Illustration of Brownian motion. A particle immersed in a fluid is submitted to molecular impacts and moves in every possible direction. Length of movement to each impact is described by a normal distribution and the overall movement shows a drift.

Einstein in 1905 gave a physical description of Brownian motion of a particle in a fluid as:

$$\frac{\partial C}{\partial t} + \frac{\langle \delta x \rangle}{\tau}\frac{\partial C}{\partial x} = \frac{\langle \delta x^2 \rangle}{2\tau}\frac{\partial^2 C}{\partial x^2} - \frac{\langle \delta x^3 \rangle}{3!\tau}\frac{\partial^3 C}{\partial x^3} \cdots \tag{6.2}$$

where τ is the transition time (time to complete a path-length, δx), $\langle \delta x^n \rangle$ is the n^{th} spatial moment. It is assumed that the path-length, δx, is small compared to the typical scale length for variations in the concentration distribution (Bazant 2001).

If the 1st and 2nd spatial moments exist and it is established that:

$$v = \lim_{\tau \to 0} \frac{\langle \delta x \rangle}{\tau} \text{ and } D = \lim_{\tau \to 0} \frac{\langle \delta x^2 \rangle}{2\tau} \tag{6.3}$$

where v is drift (or advective velocity) and D is the diffusion coefficient and if $t/\tau \to \infty$, that is the time of observation is much above the transition time, the 3rd and higher moments can be ignored and equation (6.2) reduces to the advection-dispersion equation:

$$\frac{\partial C}{\partial t} + v\frac{\partial C}{\partial x} = D\frac{\partial^2 C}{\partial x^2} \tag{6.4}$$

which is consistent with Fick's 2nd law (equation 6.1).

The conditions that $t/\tau \to \infty$ and that each path-length can be decomposed in infinitely many independent smaller path-lengths are reasonable assumptions in Brownian motion which occurs at a molecular scale. Similarly, when particles are being moved in a continuous domain such as in a porous medium (e.g. sand aquifer), deviations from the mean trajectory are numerous and very fast, with any time of practical observation t being much higher than the transition time τ for each path-length. Hence, hydrodynamic dispersion in a continuous porous media aquifer can be treated as Brownian motion, following a normal distribution and described by equation (6.4).

This connection between Brownian motion and hydrodynamic dispersion enables Fickian solute transport to be modelled by discrete time random walks, in which the normal distribution is used to generate the distance of movement for prescribed times (de Marsily 1986). This is acceptable because movement can be subdivided in time-steps of any duration. It is assumed that particle movement is distributed according to a continuous law (normal distribution) scaled with respect to any time chosen (fig. 6.2).

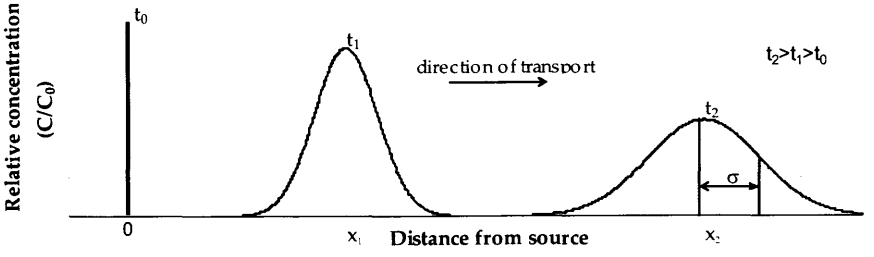

Figure 6.2 – Transport and spread of a solute due to advection and dispersion. Notice that the evolution of the solute with time is predicted by a normal distribution, so that in the y-axis relative concentration could be replaced by probability.

However, in fractured rocks it is not possible to subdivide each movement into as many small independent path-lengths as desired, since particles are likely to move along some fractures for a considerable time (fig. 6.3). Path-lengths then coincide with fracture segments and transition times τ (the time to travel along a fracture segment) can be such that in real-world problems $t/\tau \to \infty$

will only be acceptable if t goes to infinity. The result is that dispersion in fractured media cannot disregard the 3rd and higher order terms in equation (6.2) (except for large times, frequently above those of interest in hydrogeology problems); consequently the advection-dispersion equation (6.4) is not adequate.

Furthermore, there is no reason to consider that $X(t+\Delta t)-X(t)$ (the path-length, fig. 6.3) are distributed according to a normal law, since several field studies have shown that fracture length tends to follow skewed distributions (e.g. lognormal, exponential, etc.).

Therefore, Brownian motion and consequently Fick's 2nd law are not necessarily adequate for describing solute transport in fractured environments. A different process must be adopted to represent transport in fracture networks

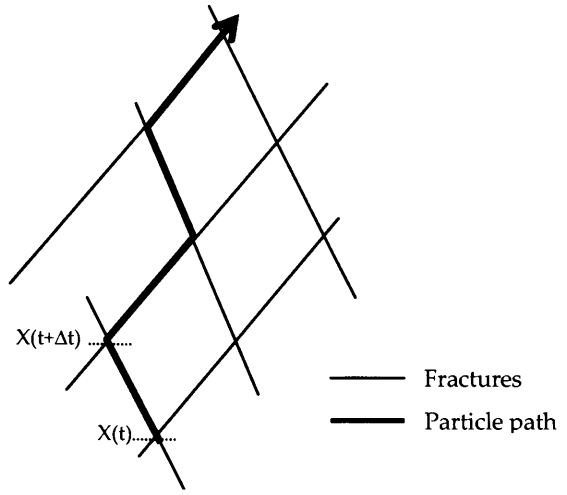

Figure 6.3– Random walk in a fracture network. The path taken by a particle is constrained by the geometry of the fracture network and the length of each movement is constrained by the location of fracture intersections. The random walk occurs only according to fracture orientation and the time to cross each fracture segment may not be negligible compared to the observation time.

Because each step, that is each movement along a path-length, will have different time duration, related to the length of the fracture segment and the flow rate in it, it is necessary to treat transition times also as a continuous variable with some known distribution. Thus, joint use of continuously distributed time-steps and continuously distributed path-lengths should be made, resulting in what is known as a **Continuous Time Random Walk**.

6.1.2 Continuous Time Random Walks

Continuous Time Random Walk **(CTRW)** theory (Montroll and Weiss 1965, Scher and Lax 1973, Klafter and Silbey 1980) has been used since the 1960's in several branches of physics to model anomalous diffusion, although it also covers Fickian behaviour as a limit case.

For a particle released at the origin at time $t = 0$, the general form of the CTRW is (Bazant 2001):

$$X(t) = \sum_{n=0}^{N(t)} \Delta x_n \tag{6.5}$$

where $N(t)$ is a random process (a transition time continuous distribution) and Δx_n are independent identically distributed length increments.

The probability of a particle being at x at time t can be expressed as the sum over all step numbers, n, of the product of: a) the probability that a certain number of steps will occur in time t; and b) the probability that this number of steps will cause a displacement of x:

$$P(x,t) = \sum_{n=0}^{\infty} P(n,t) P_n(x) \qquad t > 0, \; -\infty < x < \infty \tag{6.6}$$

where **P(x,t)** is the probability of a particle being in x at time t, **P(n,t)** is the probability of taking n steps in time t and $\mathbf{P_n(x)}$ is the probability of a particle being at x in n steps. Distributions **P(n,t)** (hereafter designated continuous distributions of transition times) and $\mathbf{P_n(x)}$ (designated continuous distributions of path-length) must be found in order to determine the CTRW (fig. 6.4).

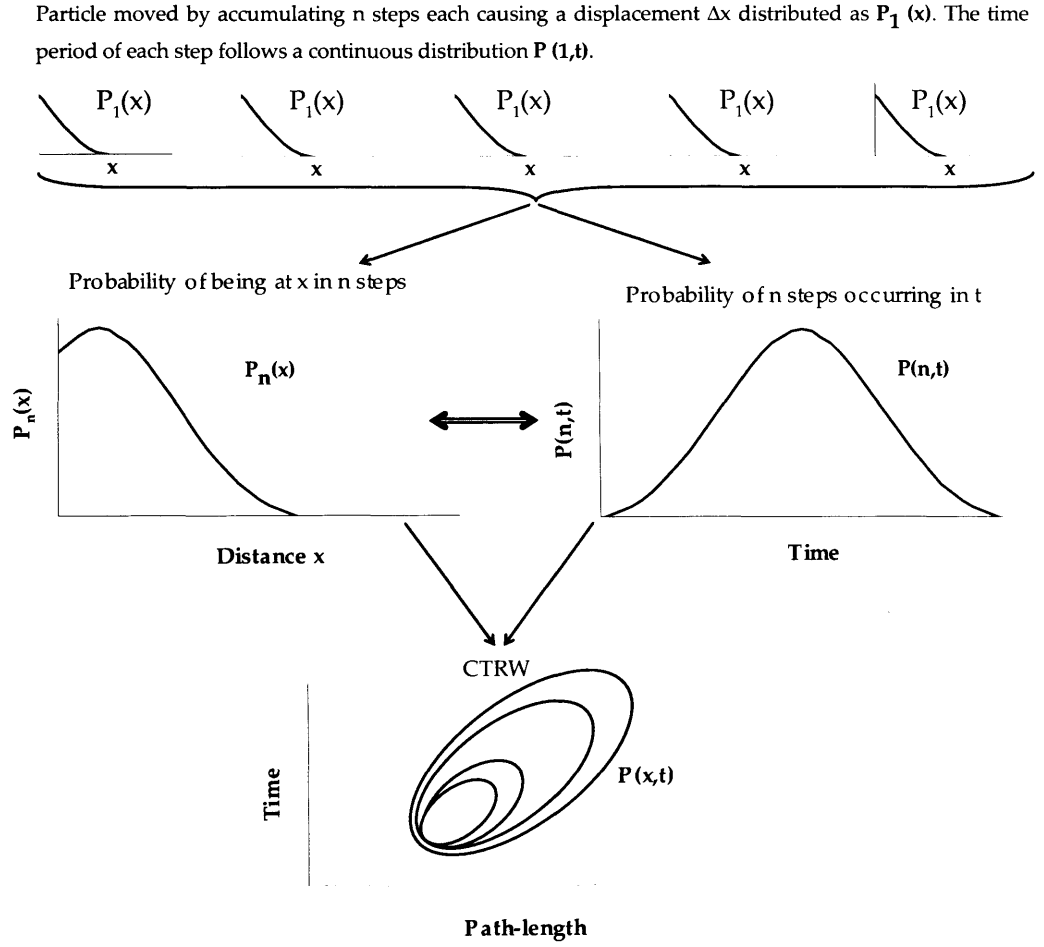

Figure 6.4 – The process of definition of a CTRW. The accumulation of steps of length $P_1(x)$ causes a movement that allows to reach x in n steps, $P_n(x)$. The time necessary to reach x is a function of the time necessary for n steps to occur, P(n,t). The joint probability of P(x,t) and P(n,t) defines a CTRW.

The main property of this random process is that it does not necessarily follow the central limit theorem, which states that the sum $X_1 + \ldots + X_n$ of n independent random variables X will converge to a normal distribution regardless of the distribution of the individual X_i's. Under some circumstances, the Continuous Time Random Walk instead of converging to a normal distribution will converge to a **Stable law** (the generalized central limit theorem). These are distributions that can be highly skewed and for which the 2nd spatial moment may not exist[1] (Uchaikin and Zolotarev 1999). Thus, stable laws (fig. 6.5) permit the simulation of anomalous transport, i.e. transport in the which the spread of the solutes is not proportional to $\sqrt{t}$, without having to resort to the **scale effect** of dispersivity (in which it is assumed that dispersivity is not constant and varies with the scale of observation).

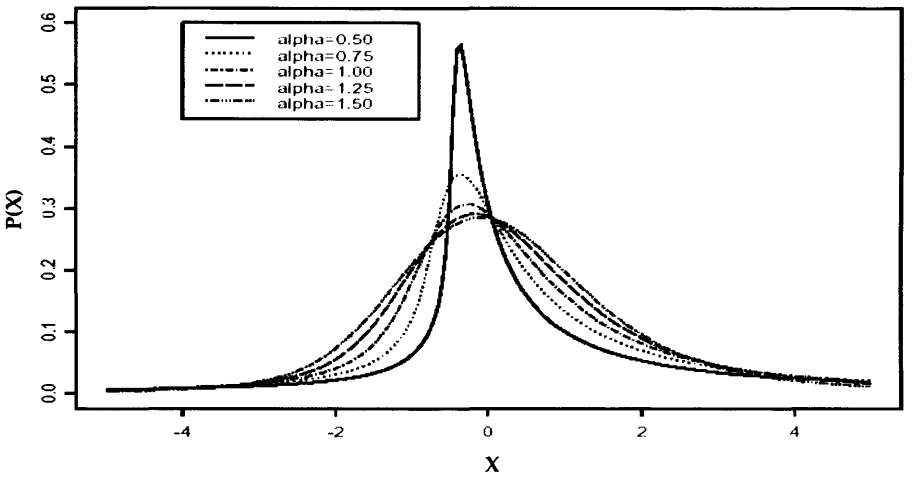

Figure 6.5 – Some examples of stable distributions. From Nolan (1999).

CTRW theory was first applied to calculate impurity conduction in semiconductors (Scher and Lax 1973) but it was also used to analyze properties of amorphous semiconductors (Montroll and Scher 1973). In recent years, research has been conducted in order to apply CTRWs to solute transport exhibiting non-Fickian behaviour. Applications in this domain include numerical studies of transport in fracture networks (Berkowitz and Scher 1995, 1997, 1998, Margolin and Berkowitz 2000, Delay and Bodin 2001, Grubert 2001) and analyses of tracer tests conducted at the

[1] The term stable comes from the fact that the shape of the distribution remains unchanged after addition of random variables distributed according to a stable distribution. Stable distributions encompass a wide range of known probability distributions (including the normal), but only three have closed form expressions: the normal, the Cauchy and the Lévy distribution.
The classical central limit theorem says that the normalized sum of independent, identical terms with a finite variance converges to a normal distribution. The generalized central limit theorem shows that if the finite variance assumption is dropped, the only possible resulting limits are stable laws (Nolan, 1999).
Under some circumstances, the mean of stable laws may also be undefined, such as when the 'alpha - index of stability' (one of the parameters characterizing stable distributions) equals 1. See figure 6.5.

field scale (Kosakowski et al. 2001) and at the laboratory scale (Berkowitz et al. 2000, Levy and Berkowitz 2003). The CTRW theory has been shown to account for both Fickian and non-Fickian behaviour, and the Advection-Dispersion Equation (6.4) as well as a Fractional Advection-Dispersion Equation have been derived based on the CTRW (Benson 1998, Barkai et al. 2000, Schumer et al. 2001, Gorenflo and Mainardi 2003).

Those studies are mostly concerned with transport that is anomalous at large times, that is, transport that never converges to Fickian behaviour (fig. 6.6). In addition, those studies usually apply the CTRW to amorphous materials or fracture networks where fractures are oriented randomly.

Although also based on a CTRW, the solute transport modelling technique that will be presented in this chapter is essentially different from the studies above. The methodology developed takes into account the geometric features implied by fracture orientation, thus not requiring that the medium is amorphous or that fractures are oriented at random.

Solutions for 1-D solute transport according to CTRW are presented in the following section (6.2) while 2-D solute transport in fracture networks will be addressed in sections 6.3 and 6.4. It is considered that the methodologies developed here are innovative and provide an efficient way of modelling solute transport in complex media, such as fractured-rock aquifers.

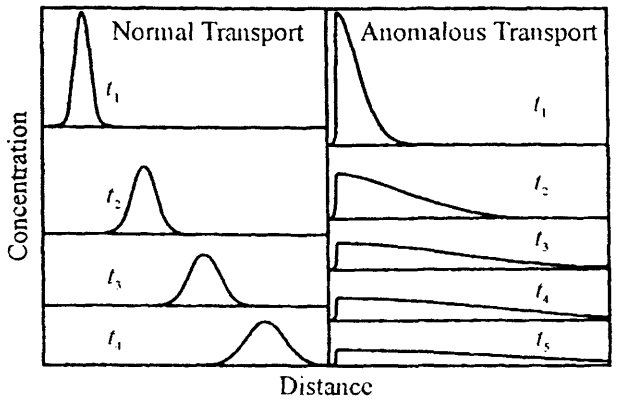

Figure 6.6 – Illustration of the contrast between normal and anomalous transport modelled with a CTRW. From Berkowitz and Scher (1997).

6.2 SIMULATION OF 1-D SOLUTE TRANSPORT ACCORDING TO A CTRW ANALYTICAL MODEL

Fracture length has been identified as following various distributions laws (Bonnet et al. 2001), but often the step length of a single particle movement (fig. 6.7) is assumed to follow either a

power-law decay or an exponential decay (Berkowitz 2001). Power law decay leads to stable laws and non-Fickian behaviour even for late times. Particle movement resulting from accumulation of steps following an exponential decay leads to the normal distribution and, as a result, follows Fickian behaviour for late times (Margolin and Berkowitz 2000). However, while Fickian behaviour is not reached, solute transport is anomalous (*pre-asymptotic*) and a scale effect may be apparent.

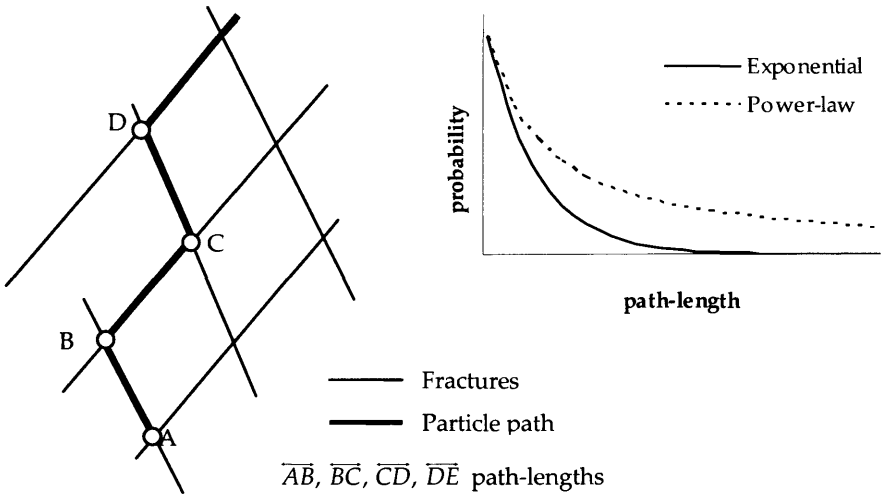

Figure 6.7 – Ensemble of path-lengths defining continuous distributions. Path-lengths are the fracture segments between changes of direction of the particle path at fracture intersections. The ensemble of fracture segments (AB, BC, CD, ...) can be distributed following exponential or power-law decays.

The CTRW solutions are dependent on the distribution of path-length, $\mathbf{P_n(x)}$, and distinct solutions will be found when considering that path-length are distributed according to exponential distributions or power-laws. In the following sections, analytical solutions for the 1-D CTRW will be evaluated for the two situations: section 6.2.1 will deal with exponentially distributed path-lengths and section 6.2.2 will concern power-law distributed path-lengths.

6.2.1 Solute transport with exponential path-lengths

The evaluation of the CTRW (equation 6.6) requires determining:

a) $\mathbf{P_n(x)}$, the continuous probability distribution of a particle reaching x in n steps (for simplicity we shall refer to it as the probability distribution of path-lengths);

b) **P(n,t)**, the continuous probability distribution of n steps occurring in time t (for simplicity we shall refer to it as the probability distribution of transition times).

6.2.1.1 Continuous distributions composing the CTRW

A good way to obtain a realistic distribution of step lengths (or path-lengths[1] as described in section 5.2) and transition times (time to complete a path-length) is to generate a Discrete Fracture Network and sample the paths and travel times taken by particles released at some points. This has in fact been done in section 5.2 and the results will be used to determine the relevant distributions composing the CTRW.

Continuous distribution of path-lengths, $P_n(x)$

When studying the distribution of path-lengths in the SCM (see fig. 5.14) it was concluded that two-parameter gamma distributions provided the best fit to individual path-lengths (that is, the probability of reaching x in one step, $\mathbf{P_1(x)}$). However, it was noticed that the shape parameter (β) was always close to one. In those conditions, the two-parameter gamma distribution coincides with the exponential distribution.

Figure 6.8 shows a sample of the path-length histograms as well as the distribution fitted, for the fractured network described by table 5.1 and illustrated in figure 5.13 of section 5.2. The exponential distribution provides a very good fit[2] with the Kolmogorov-Smirnov statistics indicating a probability above 99% ($1\text{-}p_{KS}$) that the data is distributed according to the chosen distribution. Other fracture networks studied showed similar behaviour and other studies (Parney 1999) show that the gamma distribution with $\beta \approx 1$ (i.e. the exponential) can describe the path-length distribution accurately.

The exponential distribution (fig. 6.9) is frequently applied for describing phenomena involving some kind of waiting time or transition time (Chung 1979). Its *probability density function* (in our case coinciding with $\mathbf{P_1(x)}$) is:

$$P_1(x) = \lambda e^{-\lambda x} \qquad x > 0 \tag{6.7}$$

the mean being

$$\bar{\mu} = \frac{1}{\lambda} \tag{6.8}$$

and the variance

$$\sigma^2 = \frac{1}{\lambda^2} \tag{6.9}$$

[1] Path-length is understood as the length between changes in direction of a particle at fracture intersections, not to be confused with the length of the fracture.

[2] For further insight into the interpretation of Kolmogorov-Smirnov test see section 5.2.2.1.

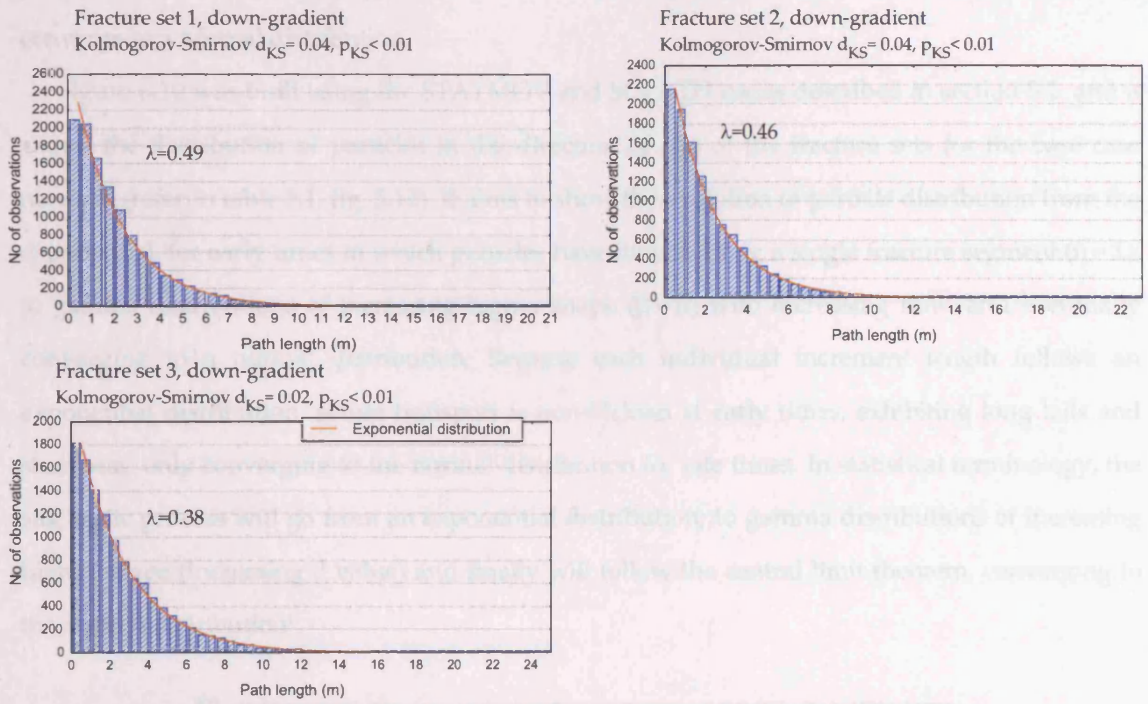

Figure 6.8 – Path-length histograms and best fit with the exponential distribution. Total number of movements was 11689 in each fracture direction. Notice that path-length is measured as the distance that a particle travels in one fracture. Refer to table 5.1 and fig. 5.13 for characteristics of the fracture network.

The probability density function and the 1st and the 2nd moments about the mean depend on a single parameter, λ, which corresponds to the inverse of the mean path-length.

Having defined $\mathbf{P_1(x)}$ it is possible to use it to compute $\mathbf{P_n(x)}$ the probability of reaching x by accumulating n steps distributed as $\mathbf{P_1(x)}$.

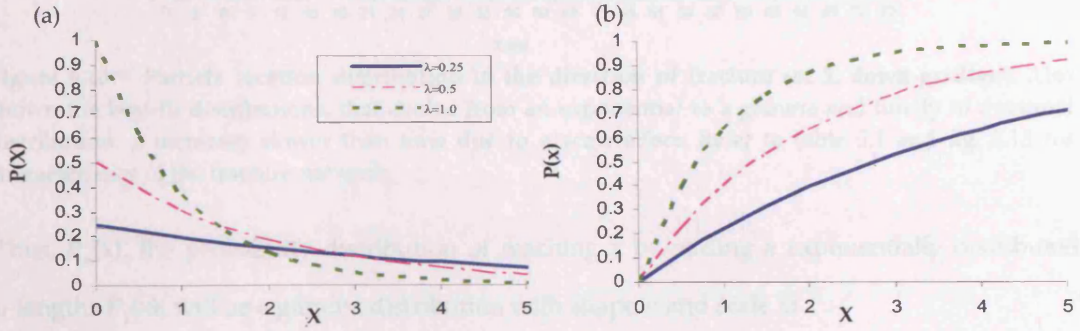

Figure 6.9 – Exponential distribution. a) probability density function; b) cumulative density function

One of the main properties of the exponential distribution is that the sum of n exponentially distributed variables with the same λ will be a gamma distribution, $P(x) = \frac{\lambda e^{-\lambda x}(\lambda x)^{\beta-1}}{\Gamma(\beta)}$, with

parameters $\beta = n$ and unchanged λ (Johnson et al. 1994). If n is large then the distribution will converge to a normal distribution.

Figure 6.10 was built using the STATMOV and SCPATH codes described in section 5.2 and it shows the distribution of particles in the direction of one of the fracture sets for the base case network (refer to table 5.1, fig. 5.13). It aims to show the evolution of particle distribution from the exponential, for early times in which particles have moved along a single fracture segment ($n = 1$), to gamma distributions of increasing higher shape ($\beta = n$) with increasing time, and eventually converging to a normal distribution. Because each individual increment length follows an exponential distribution, solute transport is non-Fickian at early times, exhibiting long tails and skewness, only converging to the normal distribution for late times. In statistical terminology, the stochastic process will go from an exponential distribution, to gamma distributions of increasing higher shape (increasing β value) and finally will follow the central limit theorem, converging to the normal distribution[1].

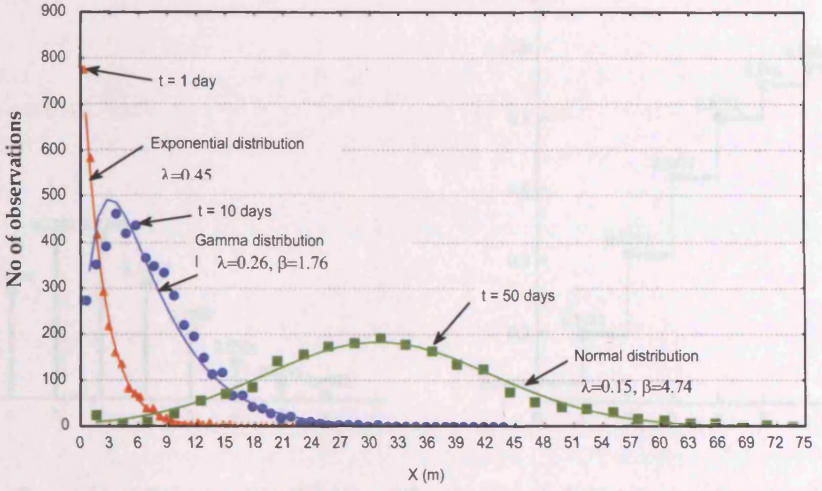

Figure 6.10 – Particle location distribution in the direction of fracture set 3, down-gradient. Also shown the best-fit distributions, that evolve from an exponential to a gamma and finally to a normal distribution. β increases slower than time due to a scale effect. Refer to table 5.1 and fig. 5.13 for characteristics of the fracture network.

Thus, $\mathbf{P_n(x)}$, the probability distribution of reaching x by adding n exponentially distributed path-lengths $\mathbf{P_1(x)}$, will be a gamma distribution with shape n and scale λ:

[1] Notice that in fig. 6.10 the shape parameter (β) increases at a slower rate than time, when it should increase at exactly the same rate, since the gamma should result from the sum of $n = t$ exponential distributions defined for $t = 1$ day. The difference in increasing rates is due to the data being sampled from a 2-D network, so that the particles are not always travelling along the fracture set represented in fig. 6.10 and actually follow other paths in the chosen time intervals. Thus, for $t = 10$ days the particles travelled along $n<t$ path-lengths in the direction sampled, and the gamma distribution has shape corresponding to the sum of $n<t$ exponentials. If a 1-D solute transport model was chosen to explain the data in fig. 6.10 a scale effect (dispersivity varying with distance) would be necessary to explain the distribution of particles in time.

$$P_n(x) = \frac{\lambda e^{-\lambda x}(\lambda x)^{n-1}}{\Gamma(n)} \qquad x>0 \qquad (6.10)$$

Continuous distribution of transition times, P(n,t)

As for the continuous distribution of transition times (essentially a waiting time problem), it was assumed a Poisson Process, which is often regarded as a good description of phenomena involving waiting times. A Poisson Process (fig. 6.11) with step rate γ has the following properties (Hsu 1996):

- X(0) = 0
- X(t) has independent increments
- the number of events in any interval $[t, t+\Delta t]$ is Poisson distributed according to:

$$P[X(t+\Delta t) - X(t) = n] = e^{-\gamma t}\frac{(\gamma t)^n}{n!} \qquad t \geq 0,\ n = 0,\ 1,\ 2,...$$

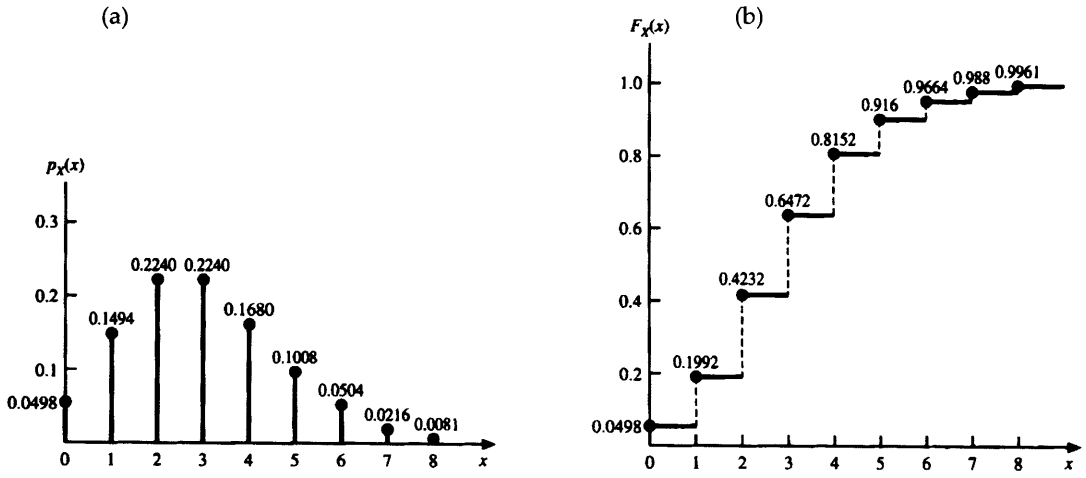

Figure 6.11 – Example of Poisson distribution with γ=3. a) probability density function; b) cumulative density function. From Hsu (1996).

The first and second properties are certainly followed in the case under consideration. As for the third property, it was tested by the same procedure used for $\mathbf{P_n(x)}$. Figure 6.12 was obtained by a process analogous to figure 6.8, using the STATMOV module to sample the time taken by particles to travel along fracture segments (path-lengths) of a fracture network. It also shows the fit obtained with the Poisson distribution. Although there are some deviations from the distribution, the fit is good enough to be accepted as a reliable model for the transition time distributions. It should be mentioned that some authors have already adopted the Poisson Process for describing this type of phenomena (Schumer et al. 2003).

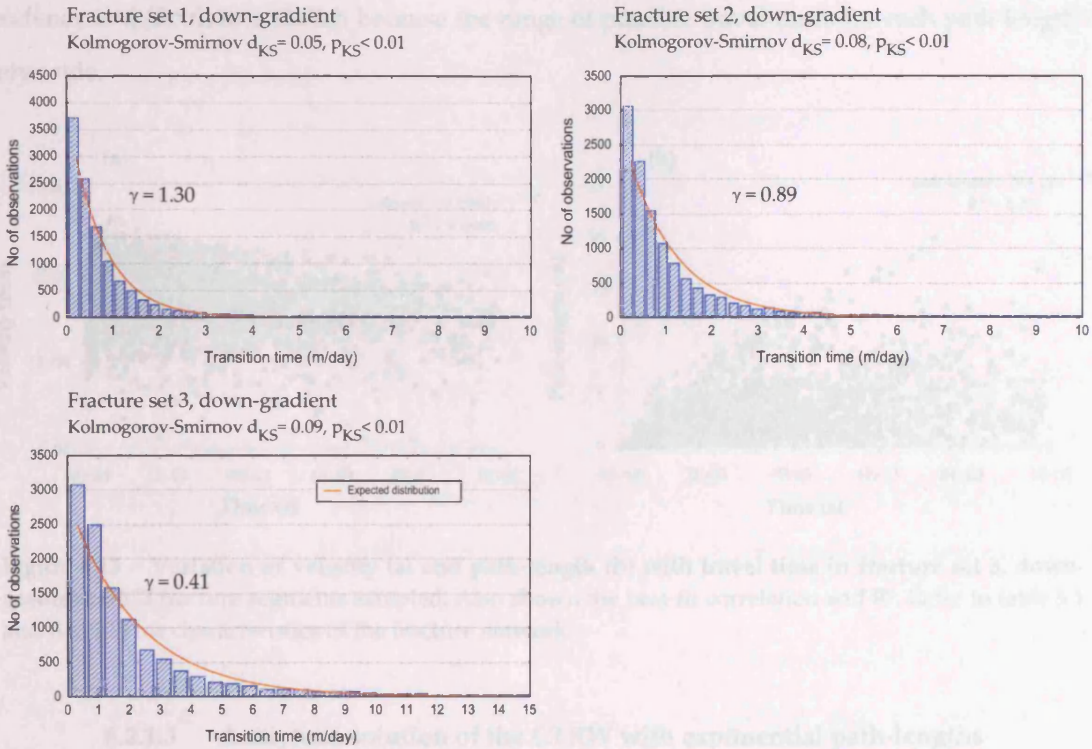

Figure 6.12 – Transition time histograms and best fit with the exponential distribution. Transition time is the time taken to complete a path-length. Notice that a Poisson Process is a renewal process with exponentially distributed intervals. Sample size: 11689 in each fracture direction. Refer to table 5.1 and fig. 5.13 for characteristics of the fracture network.

Thus, the Poisson process gives the probability of n steps occurring in time t, **P(n,t)**:

$$P(n,t) = e^{-\gamma t}\frac{(\gamma t)^n}{n!} \qquad n \geq 0,\ t \geq 0 \tag{6.11}$$

which depends on a single parameter, γ.

6.2.1.2 Independence between continuous distribution $P_n(x)$ and P(n,t)

The CTRW process requires independence between the two distributions (**$P_n(x)$** and **P(n,t)**) that compose it. However, intuition would lead to think that a correlation should exist between path-length, **$P_1(x)$**, and the time, **P(1,t)**, to complete that path-length. Figure 6.13 shows scatterplots of time versus velocity (fig. 6.13a) and time versus path-length (fig. 6.13b). This later figure shows that it is not possible to establish a correlation between path-length, **$P_n(x)$**, and the time for a particle to travel along it, **P(n,t)**. This occurs because path-length is positively correlated with velocity (see section 5.2.2.1), but it is not possible to envisage a correlation between travel time and velocity (fig. 6.13a), implying that the path-length is independent of the transition time taken to complete that distance. Although very small fractures show a short travel time, the overall

tendency is difficult to establish because the range of possible travel times for each path-length is very wide.

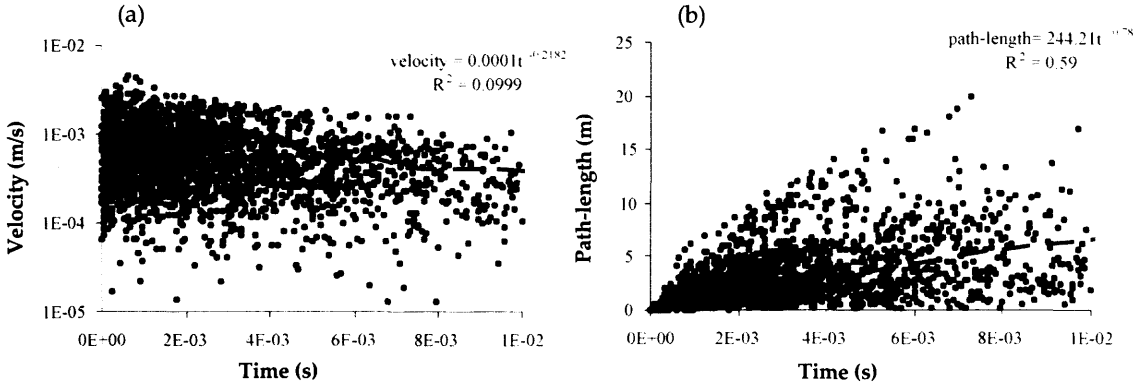

Figure 6.13 – Variation of velocity (a) and path-length (b) with travel time in fracture set 3, down-gradient. 9673 fracture segments sampled. Also shown the best-fit correlation and R^2. Refer to table 5.1 and fig. 5.13 for characteristics of the fracture network.

6.2.1.3 Analytical solution of the CTRW with exponential path-lengths

Having established the distributions for transition time **P(n,t)**, and for path-length, $\mathbf{P_n(x)}$, it remains to establish the CTRW for one-dimensional movement using equation (6.6). The probability $\mathbf{P_n(x)}$ of being at x in n steps is given by equation (6.10), $P_n(x) = \frac{\lambda e^{-\lambda x}(\lambda x)^{n-1}}{\Gamma(n)}$ and the probability **P(n, t)** of n steps occurring in time t is given by equation (6.11), $P(n,t) = e^{-\gamma t}\frac{(\gamma t)^n}{n!}$, the Poisson Process.

Replacing **P(n, t)** and $\mathbf{P_n(x)}$ in equation (6.6) returns:

$$P(x,t) = \sum_{n=1}^{\infty} e^{-\gamma t}\frac{(\gamma t)^n}{n!}\frac{\lambda e^{-\lambda x}(\lambda x)^{n-1}}{\Gamma(n)} + \delta(x)e^{-\gamma t} \qquad (6.12)$$

Notice that the term multiplied by the Dirac delta function, $\delta(x)$, represents the probability that the particle is still located at the origin. That is, it represents the probability that no step occurs in time t, with the particle still at x=0, in which case P(x, t) is given simply by the Poisson Process (equation 6.11) with n=0.

Algebraic manipulation of (6.12) leads to:

$$P(x,t) = \sqrt{\gamma t \lambda x}\frac{e^{-\gamma t-\lambda x}}{x}\sum_{n=1}^{\infty}\frac{(\gamma t \lambda x)^{n-1/2}}{n!\Gamma(n)} + \delta(x)e^{-\gamma t} \qquad (6.13)$$

The equivalence between the gamma functions and modified Bessel functions of the first kind of order n (I_n) (Spiegel and Liu 1999), states that:

$$I_{-k}(x) = \sum_{n=0}^{\infty} \frac{(x/2)^{2n-k}}{n!\Gamma(n+1-k)} \tag{6.14}$$

Using the relation provided by (6.14) and the fact that for integer values of n, $I_{-n}(x) = I_n(x)$, equation (6.13) can be expressed in terms of the modified Bessel functions as:

$$P(x,t) = \sqrt{\frac{\lambda\gamma t}{x}} e^{-\lambda\left(\frac{\gamma t}{\lambda}+x\right)} I_1\left(2\sqrt{\lambda\gamma t x}\right) + \delta(x)e^{-\gamma t} \qquad t \geq 0,\ x \geq 0 \tag{6.15}$$

where $I_1(x)$ is the modified Bessel function of the first kind of order one.

Equation (6.15) is the probability density function for a CTRW involving exponentially distributed path-lengths and a Poisson Process. It describes one-dimensional transport of particles at time t after their instantaneous release from a common source. Movement along the fracture is governed by two parameters λ and γ, which are themselves related to advection and dispersion along the fracture.

Notice that the product γt represents the number of mean steps occurring in time t, while the product λx is the number of mean steps[1] contained in x. Consequently, $\gamma\lambda tx$ is the square of the number of mean steps needed to reach x in time t. A hydrogeological interpretation to this product will be given later.

Figure 6.14 shows the probability distribution of particles for several values of x and t. Particles go from a highly skewed distribution, resembling an exponential, to an increasingly less skewed one, finally converging to the normal distribution. That is, particles progress from non-Fickian behaviour, showing long tails at early times that progressively vanish, to Fickian behaviour.

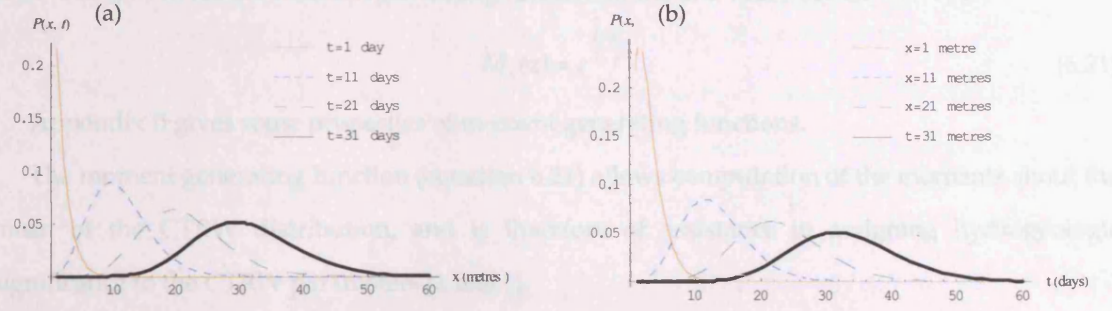

Figure 6.14 – Probability distribution of 1-D CTRW with exponentially distributed path-length (λ=1, γ=1). The shape of the distribution evolves from highly skewed to a normal distribution. a) probability distribution for constant time; b) probability distribution for constant distance.

[1] A mean step has length $1/\lambda$ and period $1/\gamma$.

6.2.1.4 Hydrogeological meaning of the CTRW parameters (λ and γ)

The moment generating function of the CTRW distribution (6.15) can be computed, given that x≥0, from (Hsu 1996):

$$M_x(z) = \int_0^\infty e^{zx} P(x,t)dx \tag{6.16}$$

where z is a real variable[1].

Using (6.15) into (6.16) and after some algebraic manipulation:

$$M_x(z) = e^{-\gamma t}\sqrt{\lambda\gamma t}\int_0^\infty \left[\frac{e^{-x(\lambda-z)}}{\sqrt{x}} I_1\left(2\sqrt{\lambda\gamma t x}\right) + \delta(x)e^{-\gamma t}\right]dx \tag{6.17}$$

Using the series expansion of the modified Bessel function, equation (6.17) becomes:

$$M_x(z) = e^{-\gamma t}\sqrt{\lambda\gamma t}\sum_{n=0}^{\infty}\frac{\left(\sqrt{\lambda\gamma t}\right)^{2n+1}}{n!\Gamma(n+2)}\int_0^\infty x^n e^{-x(\lambda-z)}dx + e^{-\gamma t} \tag{6.18}$$

The integral can be carried out explicitly:

$$\int_0^\infty x^n e^{-x(\lambda-z)}dx = \frac{\Gamma(n+1)}{(\lambda-z)^{n+1}} \tag{6.19}$$

Replacing (6.19) into (6.18) and using the recursive property of the gamma function, the moment generating function becomes:

$$M_x(z) = e^{-\gamma t}\sum_{n=0}^{\infty}\frac{1}{\Gamma(n+2)}\left(\frac{\lambda\gamma t}{\lambda-z}\right)^{n+1} + e^{-\gamma t} \tag{6.20}$$

Given that $\Gamma(n+2) = (n+1)!$ and that the sum $1+k+\frac{k^2}{2!}+\frac{k^3}{3!}+\ldots = e^k$ (Spiegel and Liu 1999), then the solution for the moment generating function of the one-dimensional CTRW is:

$$M_x(z) = e^{\frac{t\gamma z}{\lambda-z}} \tag{6.21}$$

Appendix B gives some properties of moment generating functions.

The moment generating function (equation 6.21) allows computation of the moments about the mean of the CTRW distribution, and is therefore of assistance in assigning hydrogeologic significance to the CTRW parameters (λ and γ).

The n^{th} moment of the distribution can be computed from:

$$E(X^n) = \frac{d^n}{dz^n}M_x(z)\bigg|_{z=0} \tag{6.22}$$

[1] The moments of a distribution can be evaluated by two methods. Either by using direct integration of the distribution or by use of the moment generating function (equation 6.16). The two methods will be used in this section according to convenience. If the moment generating function of X is finite in an open interval about zero, then this function completely determines the distribution of X. The n^{th}-derivative of the moment generating function evaluated at zero is the n^{th} moment of the distribution. See Appendix B for further information on moment generating functions.

Therefore, the mean of the distribution, i.e. its 1st moment, is:

$$\bar{\mu} = E(X) = \frac{t\gamma}{\lambda} \tag{6.23}$$

The variance of the distribution, i.e. its 2nd moment about the mean, is given by:

$$\sigma^2 = E\left(X^2\right) - (\bar{\mu})^2 = 2\frac{t\gamma}{\lambda^2} \tag{6.24}$$

Advective velocity (v), or the drift coefficient, can be computed from the mean, according to:

$$v = \frac{d\bar{\mu}}{dt} = \frac{\gamma}{\lambda} \tag{6.25}$$

The dispersion coefficient (D) and dispersivity (α) can be computed from the variance of the distribution:

$$D = \frac{1}{2}\frac{d\sigma^2}{dt} = \frac{\gamma}{\lambda^2} \tag{6.26}$$

and

$$\alpha = \frac{1}{2}\frac{d\sigma^2}{d\bar{\mu}} = \frac{1}{\lambda} \tag{6.27}$$

Although the distribution can be highly skewed, converging to the normal distribution only at late times, implying that non-Fickian behaviour characterizes solute transport, dispersivity (α) is a constant value equivalent to the mean path-length. Hence, no scale effect occurs.

Using the definition of the Peclet number, $P_e = \frac{vl}{D}$ where l is a characteristic length (Fetter 1999), and equations (6.25) and (6.26) it can be shown that the products γt and λx both represent the Peclet number if the mean travelled distance is taken as the characteristic length. Thus, the product $\gamma\lambda tx$ is the square of the Peclet number for the mean location x in time t.

Equations (6.25) and (6.27) allow description of the one-dimensional CTRW using hydraulic parameters such as dispersivity and advective velocity in the direction of the fracture orientation. Equation (6.15) can be rewritten in more familiar hydrogeological terms as:

$$P(x,t) = \frac{1}{\alpha}\sqrt{\frac{vt}{x}}e^{-\frac{(vt+x)}{\alpha}} I_1\left(\frac{2\sqrt{vtx}}{\alpha}\right) + \delta(x)e^{-\frac{vt}{\alpha}} \tag{6.28}$$

Figure 6.15 illustrates a contour plot of variation of probability, P(x, t), with respect to time and distance for a fixed value of velocity and dispersivity, showing that the function is well behaved.

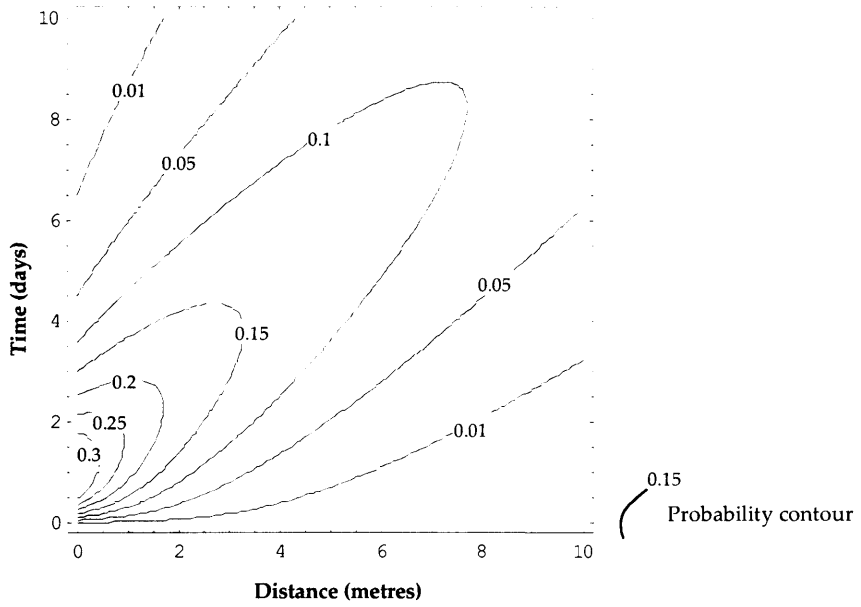

Figure 6.15 – Probability variation with time and distance of the 1-D CTRW with exponentially distributed path-lengths (v = 1, α =1).

Notice that skewness, the 3rd moment about the mean, of the one-dimensional CTRW is given by:

$$E\left[\frac{(x-\mu)^3}{\sigma_X^3}\right] = \frac{3}{\sqrt{2t\gamma}} \tag{6.29}$$

being inversely proportional to $\sqrt{t}$. Therefore, distortion of the CTRW distribution decreases with time, showing that it converges to Fickian behaviour for large times. For a more formal demonstration of convergence between the 1-D CTRW and Fickian behaviour see Appendix C.

6.2.2 Solute transport with power-law steps

Berkowitz (2001) suggests that the distribution of path-lengths may show exponential decay, as modelled in the previous section, or power-law decay, in which case the transport solution never converges to Fickian behaviour (Margolin and Berkowitz 2000, Berkowitz 2001). The sum of power-law distributed variables does not obey the central limit theorem and does not converge to a normal distribution, rather converging to stable distributions (the generalized central limit theorem). Also, Nolan (2002), Benson (1998) and Meerschaert and Scheffler (2000) suggest that the sum of variables following a Pareto distribution, related to the power-law distribution, will result in anomalous diffusion, converging to stable laws.

Power-laws are often related to fracture networks with fractal geometry (Bonnet et al. 2001). However, fracture networks may have power-law distributions for fracture length without showing fractal geometry (fig. 6.16), such as happens with the Levy-Lee networks generated by Parney (1999).

Nevertheless, and since fracture networks in which fractures are distributed as fractals seem to be common in nature (Bonnet et al. 2001), suggesting that path-lengths might be distributed according to power-laws (or Pareto distributions), it is regarded as interesting to evaluate the corresponding one-dimensional CTRW.

The CTRW with power-law distributed path-lengths is the subject of analysis in this section, following the same strategy adopted for the previous section: definition of the continuous distributions composing the CTRW; evaluation of the CTRW equation and hydrogeological meaning of parameters.

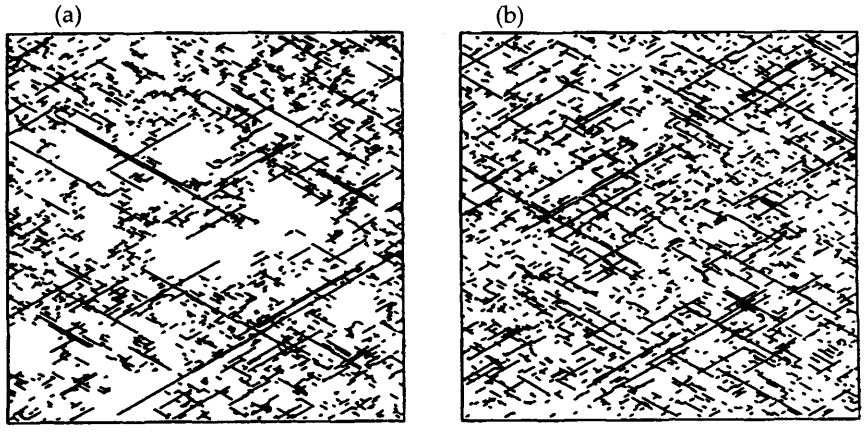

Figure 6.16 – Two examples of networks with fracture lengths following a power-law distribution. A small number of long fractures co-exist with a large number of short fractures. a) fractal network; b) non-fractal network. After Bonnet et al. (2001)

6.2.2.1 Continuous distributions composing the CTRW

To evaluate the 1-D CTRW with power-law distributions it is necessary to find the two terms composing the general CTRW equation (6.6), that is, $\mathbf{P_n(x)}$, the distribution of path-lengths, and, $\mathbf{P(n,t)}$, the distribution of steps. In the case analysed in section 6.2.1, those distributions could be studied using DFN models (see fig. 6.8 and fig. 6.12). No such tool was available to generate fracture networks in which path-lengths follow a power-law.

Continuous distribution of path-lengths, $\mathbf{P_n(x)}$

A power-law distribution is represented by (Adamic 2000):

$$P(X = x) \propto x^{-(\beta+1)} \tag{6.30}$$

while the Pareto distribution is represented by[1]:

$$P(X \geq x) \propto x^{-\beta} \tag{6.31}$$

The two distributions above are equivalent, describing phenomena where large events are rare, but small ones are quite common. The difference is that the Pareto distribution represents $P(X \geq x)$ while the power-law represents $P(X = x)$ and is therefore the derivative of the former. For our purposes, the probability distribution as described by the Pareto function is more useful and we shall use it from now on. Its probability density function (fig. 6.17) is given by:

$$P(x) = \frac{\beta c^{\beta}}{x^{\beta+1}} \qquad x > c \tag{6.32}$$

The parameter β in the Pareto distribution (6.32) represents the shape of the distribution, while c represents the minimum value.

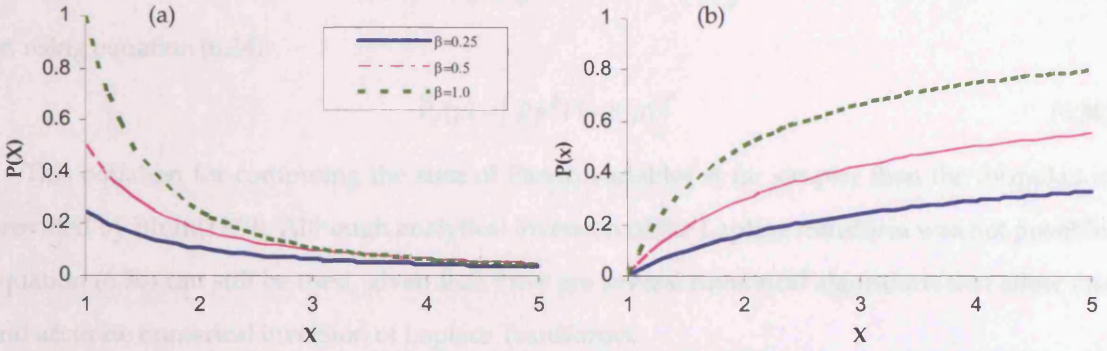

Figure 6.17 – Pareto distribution. a) probability density function; b) cumulative density function

For the first movement ($n = 1$) the probability of occurrence of an increment of length x, $\mathbf{P_1(x)}$, is given by the Pareto distribution (6.32). For simplicity, the minimum c is set to 1:

$$P_1(x) = \frac{\beta}{x^{1+\beta}} \mu(x-1), \qquad \beta > 0,\ x > 1 \tag{6.33}$$

where μ is the unit step function, included to guarantee that x>1.

The probability distribution required in the generic CTRW is $\mathbf{P_n(x)}$, i.e. the sum of n Pareto variables described by equation (6.33). Although many authors state that the sum of Pareto distributions converge to stable distributions, the solution for a sum of Pareto vectors seems to have been given solely by Blum (1970). However, the formulation obtained by Blum (1970) is very complex, requiring numerical procedures to evaluate the sums. Blum himself acknowledges that computational difficulties arise in attempts to compute the sum of Pareto variables for large

[1] Notice that in the Johnson et al. (1994) notation, equation (6.31) represents the Pareto (I) distribution.

values of n and certain ranges of x and β. Due to its complexity Blum's (1970) formulae is considered inappropriate for evaluating the CTRW.

Since in the Pareto distribution x is always positive, it is possible to apply the Laplace transform with respect to x, using p as the transform variable and depicting the transformed variable by an over-script as in $\overline{P}_1(p)$.

The Laplace Transform of (6.33) is:

$$\overline{P}_1(p) = \beta p^{\beta} \Gamma(-\beta, p) \tag{6.34}$$

where $\Gamma(-\beta, p)$ is the incomplete gamma function, defined as $\Gamma(-\beta, p) = \int_p^{\infty} z^{-\beta-1} e^{-z} dz$.

Using the convolution property of the Laplace transform the sum of n independent identically distributed random variables (see Appendix D) evaluates to:

$$\overline{P}_n(p) = \overline{P}_1(p)\overline{P}_1(p)....\overline{P}_1(p) = \left[\overline{P}_1(p)\right]^n \tag{6.35}$$

or, using equation (6.34):

$$\overline{P}_n(p) = \left[\beta p^{\beta} \Gamma(-\beta, p)\right]^n \tag{6.36}$$

This equation for computing the sum of Pareto variables is far simpler than the formulation provided by Blum(1970). Although analytical inversion of the Laplace transform was not possible, equation (6.36) can still be used, given that there are several numerical algorithms that allow fast and accurate numerical inversion of Laplace Transforms.

To test the reliability of equation (6.36) a small computer code was written in FORTRAN for generating vectors from a standard Pareto distribution (6.33) and add them for a specified number of n steps. The frequency histograms resulting from this numerical procedure are compared in figure 6.18 with the analytical solution (equation 6.36) for sums of $n = 1$ to $n = 5$ Pareto variables[1]. The comparison is highly favourable, indicating that equation (6.36) retrieves reliable sums of Pareto distributions.

[1] The Laplace transform was inverted numerically in *Mathematica* with the Add-on *NumericalInversion* (Mallet 2000), using the Stehfest algorithm.

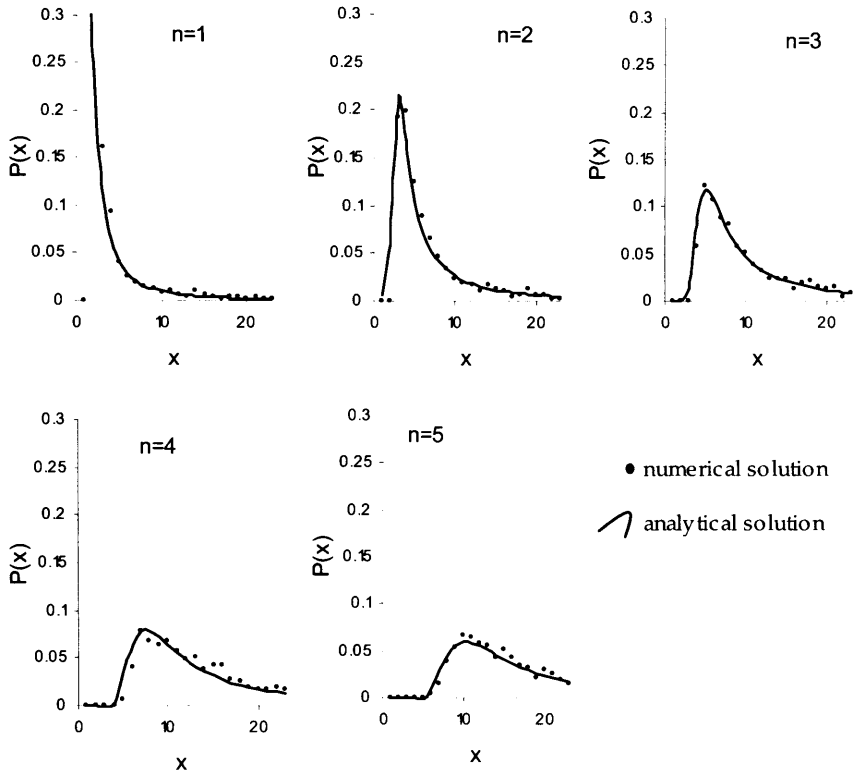

Figure 6.18 – Sum of Pareto distributed variables (β=1). Comparison between numerical and analytical solution for several values of n.

Continuous distribution of transition times, P(n,t)

In the absence of a DFN tool from which to sample the transition times to complete each path-length, the continuous distribution of transition times, **P(n,t)**, is regarded, as in section 6.2.1, as a Poisson Process, $P(n,t) = e^{-\gamma t}\frac{(\gamma t)^n}{n!}$.

Assuming a Poisson Process is disputable, since it is possible to argue that large travel times should correspond to the very long fractures inherent to Pareto distributions. This correlation would disrupt the possibility of using a Poisson Process. However, when modelling Levy-lee fracture networks Parney (1999) mentions that no correlation between travel time and path-length is apparent. Therefore, a Poisson Process may be a reasonable assumption, but still requiring confirmation through DFN modelling.

6.2.2.2 Analytical solution of the CTRW with power-law path-lengths

The Laplace transform with respect to x of the general CTRW (equation 6.6, with x≥0) is:

$$\overline{P}(p,t) = \sum_{n=0}^{\infty} P(n,t)\overline{P}_n(p) \tag{6.37}$$

Using equation (6.36) for the distribution of path-lengths and equation (6.11) (the Poisson Process) for **P(n,t)**, equation (6.37) becomes:

$$\overline{P}(p,t) = e^{-\gamma t} \sum_{n=0}^{\infty} \frac{\left[\gamma t \beta p^{\beta} \Gamma(-\beta, p)\right]^n}{n!} \tag{6.38}$$

Given that the sum $1 + k + \frac{k^2}{2!} + \frac{k^3}{3!} + \ldots = e^k$ (Spiegel and Liu 1999), equation (6.38), the one-dimensional CTRW with a power-law distribution of path-lengths, gives:

$$\overline{P}(p,t) = e^{-\gamma t\left[1-\beta p^{\beta}\Gamma(-\beta,p)\right]} \tag{6.39}$$

Equation (6.39) describes solute transport of particles at time t after their instantaneous release from a common source, with movement along the fracture being governed by two parameters: β and γ.

Figure 6.19 shows the shape of the distribution for several distinct values of t. The distribution remains highly skewed and does not seem to converge to a normal distribution and, consequently, to Fickian behaviour.

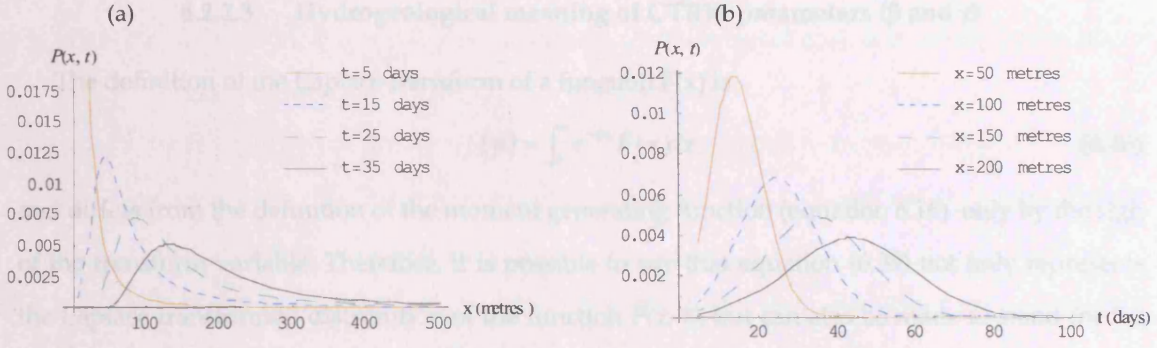

Figure 6.19 – Probability distribution of the 1-D CTRW with Pareto distributed path-lengths (β=1, γ=1). a) probability distribution with distance for constant time. The shape of the distribution remains highly skewed; b) probability distribution with time for constant distance.

A contour plot of variation of probability, **P(x, t)**, with respect to time and distance for a fixed value of velocity and dispersivity shows that the function is well behaved (fig. 6.20).

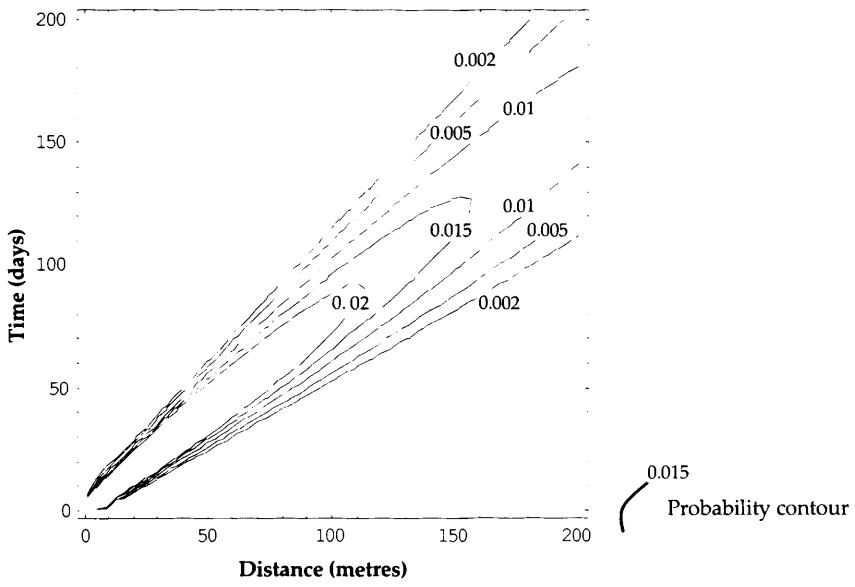

Figure 6.20 – Probability variation with time and distance of the 1-D CTRW with power-law distributed path-lengths (β = 5, γ =1).

6.2.2.3 Hydrogeological meaning of CTRW parameters (β and γ)

The definition of the Laplace transform of a function F(x) is

$$f(p) = \int_0^x e^{-px} F(x) dx \tag{6.40}$$

and differs from the definition of the moment generating function (equation 6.16) only by the sign of the transform variable. Therefore, it is possible to say that equation (6.39) not only represents the Laplace transformed distribution of the function *P(x, t)*, but can also be made to stand for the moment generating function, provided *p* is replaced by –z. Thus, the moment generating function of the CTRW (6.39) is simply:

$$M_x(z) = e^{-\gamma t\left[1-\beta(-z)^{\beta}\Gamma(-\beta,-z)\right]} \tag{6.41}$$

To obtain the spatial moments of equation (6.41) it is necessary to differentiate it with respect to z and then let z = 0, as was done in section 6.2.1.4 (see equation 6.22). However the 1st and 2nd derivatives of (6.41) each return a division by z = 0, so the limits of the function are indeterminate, unless restrictions are imposed on the value of β.

If it is assumed that β>1 it is then possible to find the limit of the first derivative of the moment generating function, retrieving the mean of the function as $\bar{\mu} = E(X) = \frac{t\beta\gamma}{\beta - 1}$. The second

derivative of the moment generating function can be determined as long as it is assume that β>2, with the variance of the distribution being $\sigma^2 = E(X^2) - (\bar{\mu})^2 = \frac{t\beta\lambda}{\beta - 2}$.

Advective velocity (v) can be computed from the mean, according to:

$$v = \frac{d\bar{\mu}}{dt} = \frac{\beta\gamma}{\beta - 1} \qquad \beta>1 \qquad (6.42)$$

The dispersion coefficient (D) and dispersivity (α) can be computed from the variance of the distribution:

$$D = \frac{1}{2}\frac{d\sigma^2}{dt} = \frac{\beta\gamma}{2\beta - 4} \qquad \beta>2 \qquad (6.43)$$

and

$$\alpha = \frac{1}{2}\frac{d\sigma^2}{d\bar{\mu}} = \frac{\beta - 1}{2\beta - 4} \qquad \beta>2 \qquad (6.44)$$

Therefore, the β value (the shape factor of the Pareto distribution) conditions the behaviour of the CTRW:

a) for β<1 both the mean and the variance of the CTRW are not defined;
b) for 1<β<2 the mean has a finite value, and the advective velocity of the particles is a constant. The variance of the CTRW is not defined;
c) for β>2 both the mean and the variance have finite values. Advective velocity, dispersion coefficient and dispersivity are all constant, not dependent on time. That is, no scale effect is apparent.

Since the 1st and 2nd moments of the 1-D CRW with power-laws distributed path-lengths are only defined for specific values of β, it is demonstrated that the CTRW does not necessarily converge to the normal distribution and, depending on the value of β, transport may be anomalous regardless of the scale of observation.

As for the hydrogeological meaning of the CTRW parameters (β and γ) and although they can be derived by manipulating the equations (6.42) to (6.44) above, the resulting formulae $\left(\gamma = \frac{2D}{4\alpha - 1}; \beta = \frac{4\alpha - 1}{2\alpha - 1}\right)$ are too complex to give insight into the hydrogeologic meaning of β and γ parameters. It can only be said that β is related to the mean path-length, $\bar{\mu}_L$, according to:

$$\beta = \frac{\bar{\mu}_L}{\bar{\mu}_L - 1} \qquad (6.45)$$

where μ_L is the mean path-length resulting from the Pareto distribution. As for γ, it is the step rate of the Poisson Process, or the inverse of the mean time to complete a step.

Finally, and still resorting to the solutions for velocity, dispersion coefficient and dispersivity it is possible to rewrite the 1-D CTRW with Power-law distributed path-lengths (equation 6.39) using those hydraulic parameters as: $\bar{P}(p,t) = \exp\left\{-\frac{2tv\alpha}{2\alpha-1}\left[\frac{2\alpha-1}{4\alpha-1} - p^{\frac{4\alpha-1}{2\alpha-1}}\Gamma\left(-\frac{4\alpha-1}{2\alpha-1}, p\right)\right]\right\}$. Again, this equation is too complex to be particularly insightful.

Throughout section 6.2 two analytical solutions for solute transport according to one-dimensional CTRWs were established. The two solutions differ in the distribution assumed for the path-lengths (the length of each individual movement); a first solution assumes exponentially distributed path-lengths (section 6.2.1) and a second solution assumes power-law distributed path-lengths (section 6.2.2). In both cases, it was admitted that the occurrence of steps was distributed according to a Poisson Process. The main difference resulting from the two analytical solutions is that the exponentially distributed path-lengths cause solute transport to be non-Fickian at early times, but eventually will tend to Fickian transport, while the power-law distributed path-lengths may give rise to anomalous transport regardless of the observation time.

The following sections, 6.3 and 6.4, will use those analytical solutions to build procedures for simulating solute transport in fracture networks according to two-dimensional CTRW. Section 6.5 will then apply the 2-D CTRW to delineation of groundwater protection zones.

6.3 A TWO-DIMENSIONAL CTRW FOR MODELLING SOLUTE TRANSPORT AND DELINEATE PROBABILISTIC PROTECTION ZONES

The analytical solutions for the random walks defined in section 6.2 are regarded as useful descriptions of one-dimensional solute transport in fractured-rock aquifers where Fickian behaviour is not necessarily an assumption. However, solute transport modelling in fracture networks requires considering higher dimensions, since fracture networks are, by definition, of dimension above one.

Evaluation of the general CTRW (equation 6.6) with movement occurring in multiple directions does not seem to be feasible, but the 1-D CTRW can be implemented in procedures that simulate a two-dimensional random walk, i.e. movement in a 2-D fracture network.

These procedures require the use of the relevant 1-D CTRW parameters in each fracture set direction. For the CTRW with exponentially distributed path-lengths (equation 6.28), those parameters are dispersivity (α) and advective velocity (v), while for the CTRW with power-law distributed path-lengths (equation 6.39), the parameters are step-rate (γ) and shape factor (β).

The 2-D CTRW was implemented in two different ways:

1. direct application of the analytical 1-D CTRW equations (6.28 or 6.39) enables retrieval of the distribution of probability along a certain fracture orientation, **P(x,t)**, at any desired travel time, for the whole domain under study. If this process is repeated for every fracture direction, a series of vectors will result. These vectors representing movement in each direction can then be added to find the distribution of the particles at time *t* (fig. 6.21). Thus, the procedure requires only a single step (of time duration equal to the total travel time) in each direction. This procedure shall be designated **'Explicit CTRW'** hereafter;
2. using the equations that describe the distribution of path-lengths, $\mathbf{P_n(x)}$, and the distribution of transition times, **P(n,t)**, multiple steps of known length and transition time are added until travel time *t* is reached. In this procedure, at each step, variates are generated for the path-length and for the duration of movement, and these are then added to the variates of the previous step (fig. 6.21). This implies the use of equations (6.7) and (6.11) for the CTRW with exponentially distributed path-lengths, and of equations (6.11) and (6.33) for the CTRW with power-law distributed path-lengths. This procedure shall be designated **'Implicit CTRW'**.

In both cases, the procedure relies on the generation of random numbers from known probability distributions. While the generation of random numbers from exponential and power--laws distributions is well documented, with algorithms being available for that purpose, the same cannot be said for the generation of random numbers from the 1-D CTRW distributions (equations 6.28 and 6.39).

Both methods are implemented and described in the remainder of this chapter. For purposes of evaluation of the reliability of the procedures, it is interesting to present first the procedures for the uniform flow case (section 6.3) and subsequently to generalize it to non-uniform flow cases, that is, to cases in which the hydraulic gradient varies in space (section 6.4).

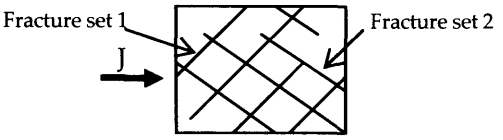

EXPLICIT 2-D CTRW

Step 1: Generate vectors x_1 and x_2 from 1-D CTRWs for desired travel time

Set 1 one-dimensional CTRW

P(x,t) for t = desired travel time

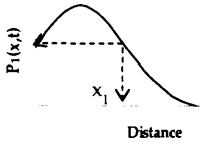

Set 2 one-dimensional CTRW

P(x,t) for t = desired travel time

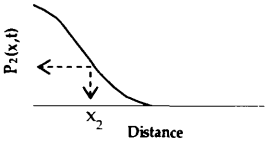

Step 2: Determine final particle location by adding x_1 and x_2

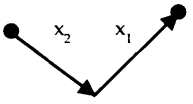

IMPLICIT 2-D CTRW

Step 1: Generate x_1 and x_2 vectors from the distribution of path-lengths, $P_n(x)$

Set 1 path-length, $P_n(x)$

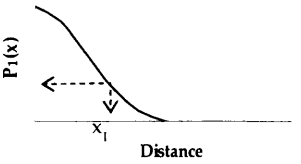

Set 2 path-length, $P_n(x)$

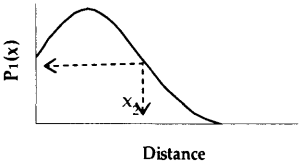

Step 2: Generate t_1 and t_2 from the distribution of transition times, P(n,t)

Set 1 transition times, P(n,t)

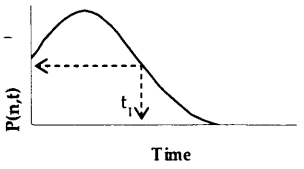

Set 2 transition times, P(n,t)

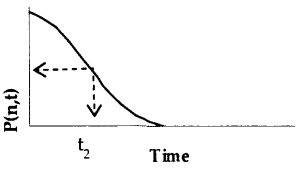

Step 3: Determine next particle location by adding x_1 and x_2 and travel time by adding t_1 and t_2

Step 4: Repeat steps 1 to 3 until the added travel times equal the desired travel time. The final particle location is the sum of all x vectors.

Figure 6.21 – Explicit and Implicit two-dimensional CTRW procedures. The procedures are exemplified for a fracture network with two fracture sets and, for simplicity, it was assumed that movement could occur only in the down-gradient direction.

6.3.1 Explicit two-dimensional CTRW (exponentially distributed path-lengths)

The Explicit CTRW procedure with exponentially distributed path-lengths is based on direct application of the analytical formulation describing the CTRW, i.e. equation (6.28). Since multiple fracture sets are now admitted, each possible movement direction (twice the number of fracture sets, since up-gradient movement is possible) will be distributed according to a 1-D CTRW, with

$P_j(x,t)$ distributions, and corresponding parameters v_j and α_j, where the subscript j refers to the movement direction. Because multiple directions can occur it would be necessary to determine the joint probability density function, which is notoriously difficult to evaluate.

Further, it is recognised that the probability of movement in each direction is not always the same, being a function of orientation and hydraulic characteristics of each fracture set. Therefore, an extra parameter, ρ_j, must be introduced that equals the frequency with which a particle moves in each direction. This parameter, ρ_j, is equivalent to the directional choice parameter defined in the SCM (section 5.2) and has domain $0 \le \rho_j \le 1$, $\sum_{j=1}^{2n} \rho_j = 1$, where n is the number of fracture sets.

The introduction of directional choice, ρ_j, implies the need to redefine advective velocity (v_j) in each fracture direction, which according to equation (6.25) is the product of step rate (γ_j) and dispersivity (α_j or $1/\lambda_j$). Because the probability of any direction being chosen is defined by ρ_j, the step rate[1] γ_j in that direction is also a function of ρ_j. The period of occurrence of a step, regardless of the direction, is:

$$\sum_{j=1}^{2n} \frac{\rho_j}{\gamma_j} \tag{6.46}$$

which allows us to retrieve the redefined step rate in each direction $\left(\gamma_j^T\right)$ as:

$$\gamma_j^T = \rho_j \Big/ \sum_{i=1}^{2n} \frac{\rho_i}{\gamma_i} \tag{6.47}$$

Using this new definition of directional step rate, the directional advective velocity (v_j) becomes:

$$v_j = \alpha_j \gamma_j^T \tag{6.48}$$

Similarly, the variance and mean of the 1-D CTRW can be redefined as:

$$\sigma_j^2 = 2tv_j\alpha_j \quad \text{and} \quad \bar{\mu}_j = v_j t \tag{6.49}$$

Thus, the Explicit CTRW procedure depends only on two hydraulic parameters, v_j and α_j, with the equation of the 1-D CTRW remaining as equation (6.28).

Given that the location of any particle in the two dimensional domain is the sum of differently oriented 1-D vectors, it is possible to define the location of particles for any time desired simply by generating random variates from the 1-D CTRW distributions and add those variates to find the x and y coordinates of the particles (see fig. 6.21).

[1] Notice that γ_j is used here with the same definition as in section 6.2 for the 1-D CTRW, that is, the number of steps per unit time in a given direction, as if movement in other directions was not possible.

The 2-D CTRW can then be defined as:

$$X = \sum_{j=1}^{2n} P_j(x,t)\vec{Z}_j \tag{6.50}$$

where $P_j(x,t)$ for the j^{th} direction is given by equation (6.28), $\vec{Z}_j$ represents a unit vector in the j^{th} movement direction and X represents the resulting particle location. Equation (6.50) can be rewritten, using the scaling and shift properties provided by the variance and the mean of the 1-D CTRW distribution, as:

$$X = \sum_{j=1}^{2n}\left\{\sigma_j\left[\frac{P_0(x,t)-t}{\sqrt{2t}}\right]+\overline{\mu}_j\right\}\vec{Z}_j \tag{6.51}$$

or:

$$X = \sum_{j=1}^{2n}\left\{\sqrt{v_j\alpha_j}\left[P_0(x,t)-t\right]+v_jt\right\}\vec{Z}_j \tag{6.52}$$

where $P_0(x,t)$ is a ***'standard'*** CTRW distribution, given by equation (6.28) with parameters $v_j = 1$ and $\alpha_j = 1$.

Equation (6.52) can be decomposed into x and y coordinates according to:

$$\begin{cases} x = \sum_{j=1}^{2n}\left\{\sqrt{v_j\alpha_j}\left[P_0(l,t)-t\right]+v_jt\right\}\cos\left(\theta_j\right) \\ y = \sum_{j=1}^{2n}\left\{\sqrt{v_j\alpha_j}\left[P_0(l,t)-t\right]+v_jt\right\}\sin\left(\theta_j\right) \end{cases} \tag{6.53}$$

where l refers to the generated variate and θ_j is the orientation of the j^{th} movement direction.

Equation (6.52) provides the means of simulating two-dimensional solute transport in a fracture network simply by generating variates that follow the 1-D CTRW and adding the vectors resulting from the scalar products of those variates with the corresponding movement direction.

Under uniform flow conditions, the Explicit CTRW procedure is just the application of equation (6.52) and involves the following steps:

1. vectors are generated from a 'standard' 1-D CTRW given by equation (6.28) with $v_j = 1$ and $\alpha_j = 1$ for each movement direction and for the required time t;
2. the x and y particle coordinates are found from equation (6.53), using the variates generated in 1).

This methodology, although not resulting from an analytical solution of the 2-D CTRW distributions, that would enable finding the probability at each location, allows us to generate particle plumes, which, if desired, can be contoured to find the corresponding probability distribution.

An algorithm was implemented to generate random variates following the 'standard' probability density function given by equation (6.28). The algorithm is based on the **cumulative probability function** of the 1-D CTRW and involves its numerical inversion.

Suppose that the cumulative probability function of a random variable x is known and denoted by F(x), then variates following its probability density function can be generated by:

1. generating P_i uniformly distributed in [0, 1] (P_i is the cumulative probability at x_i);
2. invert $P_i = F(x_i)$ to obtain the variate x_i that retrieves a cumulative probability P_i. Due to the complexity of the cumulative distribution it is not possible to achieve its inversion analytically. Therefore, a root-finding algorithm was used to obtain the values of x_i.

The ensemble of generated x_i variates will follow the f(x) probability density function, which in this case is the 'standard' 1-D CTRW.

The cumulative distributions[1] of the 1-D CTRW, both with exponentially and with power-law distributed path-lengths are given in Appendix E, in the Laplace space, which implies that the algorithm includes numerical inversion of the Laplace transform using the Stehfest algorithm.

Figure 6.22 illustrates the full Explicit two-dimensional CTRW procedure, including the use of the cumulative probability function to generate the random numbers.

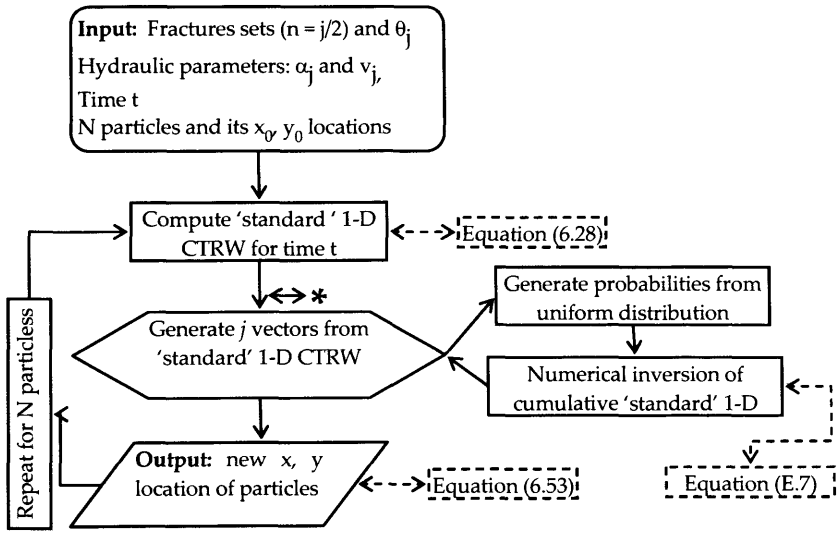

Figure 6.22 – Flow chart for the EXPLICIT two-dimensional CTRW procedure. The equations shown refer to the 1-D CTRW with exponential path-lengths, but the procedure is similar for the power-law path-lengths, except that the equation should change accordingly. The uniform hydraulic gradient is supposed to be known. *The meaning of the asterisk will be given in section 6.4.2.

[1] The use of the cumulative distribution function is required instead of the probability density function in order to ensure that for a given y (probability) there is only one valid x, which does not necessarily occur for probability density functions.

6.3.1.1 Implementation under uniform flow conditions

To test this methodology a FORTRAN code was written that implements the procedure to conduct particle tracking in a uniform flow field of known hydraulic gradient. The fracture network described as base case in sections 5.2 and 6.2 was again used with the relevant parameters being sampled with the STATMOV module described in section 5.2. Table 6.1 lists the parameters sampled for each direction of movement.

Table 6.1– Input parameters for the Explicit CTRW simulation (based on fracture network illustrated in fig. 5.13 and table 5.1)

Direction j	*Fracture set*	*Angle with x* θ (°)	*Dispersivity* α (m)	*Step rate* γ (d^{-1})	*Directional choice* ρ (-)
1	1	160°	2.08	1.30	0.17
2	2	125°	2.13	0.89	0.31
3	3	250°	2.70	0.41	0.32
4	1	340°	0.53	1.37	0.05
5	2	305°	0.83	1.07	0.06
6	3	70°	1.52	0.85	0.09

Particle tracking was conducted in a square domain of size 750 m × 750 m, with impermeable lateral boundaries and an hydraulic gradient of 0.0533 oriented from right to left. Particles were released at location $X_0 = 750$ m and $Y_0 = 0$ m. These are the same boundary conditions used in the discrete sub-domain on which STATMOV collected the relevant information, although the discrete subdomain was only of size 75 m × 75 m.

Figure 6.23 compares plumes of particles tracked using the Explicit CTRW procedure and the Statistical Continuum Method. The Explicit CTRW reproduces reasonably solute transport, both in terms of advection and dispersion. The plume evolves from highly skewed to normally distributed for late times, showing that longitudinal and transverse dispersivities would not provide an adequate description of the shape of the plume. Transport is anomalous for early times and tends to Fickian for late times.

The computation time for the CTRW was of about one minute on a PC equipped with a 1.3 GHz processor and 256 Mb RAM.

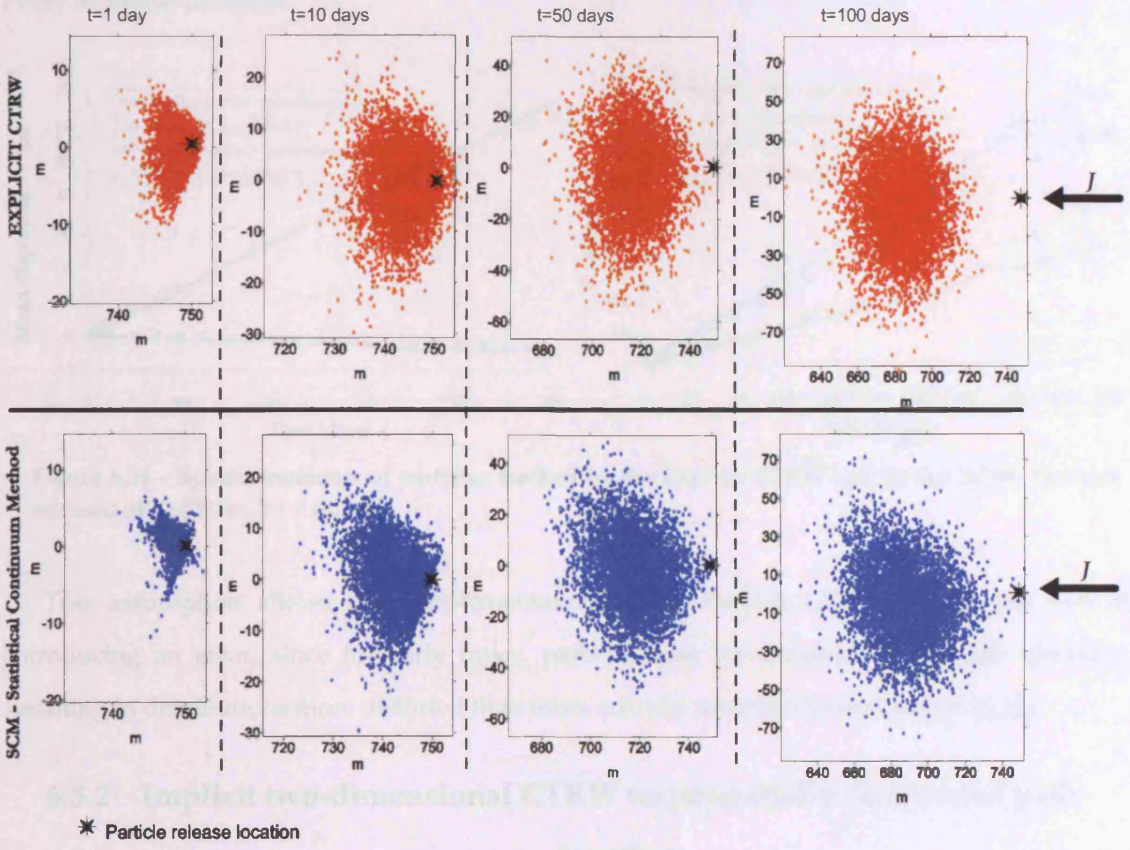

Figure 6.23 – Comparison of plumes of particles tracked by the Explicit CTRW and by the SCM. 5000 particles were instantaneously released at location $X_0 = 750$ m, $Y_0 = 0$ m. Notice that scale varies. Uniform hydraulic gradient oriented from right to left.

The 1st and 2nd spatial moments of the plumes are compared in figure 6.24. The Explicit CTRW procedure gives reliable approximations to the overall advective velocity of the plume, with the first moment closely resembling those resulting from the SCM procedure. As for the 2nd moment about the mean, which can be assimilated to overall dispersion, its fit to the SCM model is not as good as for the first moment, but still it is acceptable.

Notice that the plumes tracked by the CTRW procedure seem to converge to a bivariate normal distribution faster than the plumes tracked by the SCM. This is particularly obvious in figure 6.23, in which the plumes tracked by the SCM for 10 days are still marked by the fracture orientations, while that effect is no longer apparent for the particles tracked by the CTRW.

In fact, it seems that after 50 days the plume tracked by the CTRW is already close to a bivariate normal distribution, while the SCM still results in skewed plumes. This discrepancy between the two methods is due to the 2-D CTRW defined by equation (6.52) involving

movement in every possible direction regardless the travel time. That is, even for very early times the overall movement of the plume is averaged by considering that each particle has moved in every available direction.

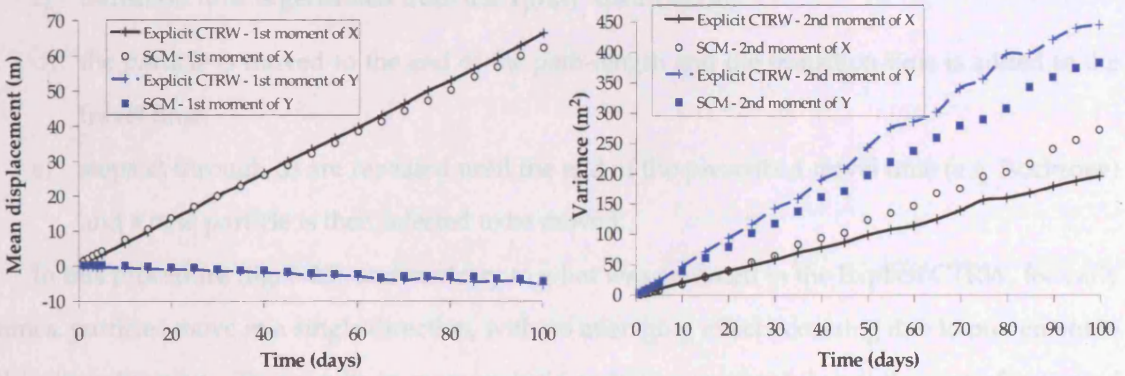

Figure 6.24 – Spatial moments of particles tracked by the Explicit CTRW and by the SCM. Particles released at X_0=750 m, Y_0=0 m.

This assumption allows easy implementation of the Explicit CTRW, but at the cost of introducing an error, since for early times, particles may have moved in a single direction, resulting in distributions more distorted than those actually retrieved from equation (6.52).

6.3.2 Implicit two-dimensional CTRW (exponentially distributed path-lengths)

The implicit CTRW procedure is based on the generation of variates following the path-length, $\mathbf{P_n(x)}$, and the transition time, $\mathbf{P(n,t)}$, distributions. In the CTRW with exponentially distributed path-lengths, it is thus required to generate variates following the distributions described by equations (6.7) and (6.11).

Since multiple fracture sets are now admitted, each possible movement direction will be distributed according to $P_{n,j}(x)$ and $P_j(n,t)$ distributions, and corresponding parameters γ_j and λ_j. Further, it is also necessary to take into account the probability of particles moving in each direction, ρ_j. This directional choice parameter must now be used directly and cannot be taken into account in an overall step-rate value, as was done in the Explicit CTRW procedure.

Consequently, the Implicit CTRW procedure requires three parameters to be known in each movement direction: the inverse of mean path-length (λ_j); the step rate (γ_j) and directional choice (ρ_j).

Solute transport in the fracture network can then be simulated using the following procedure:

a) using the ρ_j values, a uniform distribution is used to randomly generate the direction that the particle will take;

b) path-length is generated from the exponential $P_{n,j}(x)$ distribution;

c) transition time is generated from the $P_j(n,t)$ distribution;

d) the particle is moved to the end of the path-length and the transition time is added to the travel time;

e) steps a) through d) are repeated until the end of the prescribed travel time (e.g. isochrone) and a new particle is then selected to be moved.

In this procedure (fig. 6.25), and contrary to what was assumed in the Explicit CTRW, for early times, particles move in a single direction, with no averaging effect occurring due to movement in the other directions. This results in more realistic particle movement, but at the cost of increased complexity in the procedure.

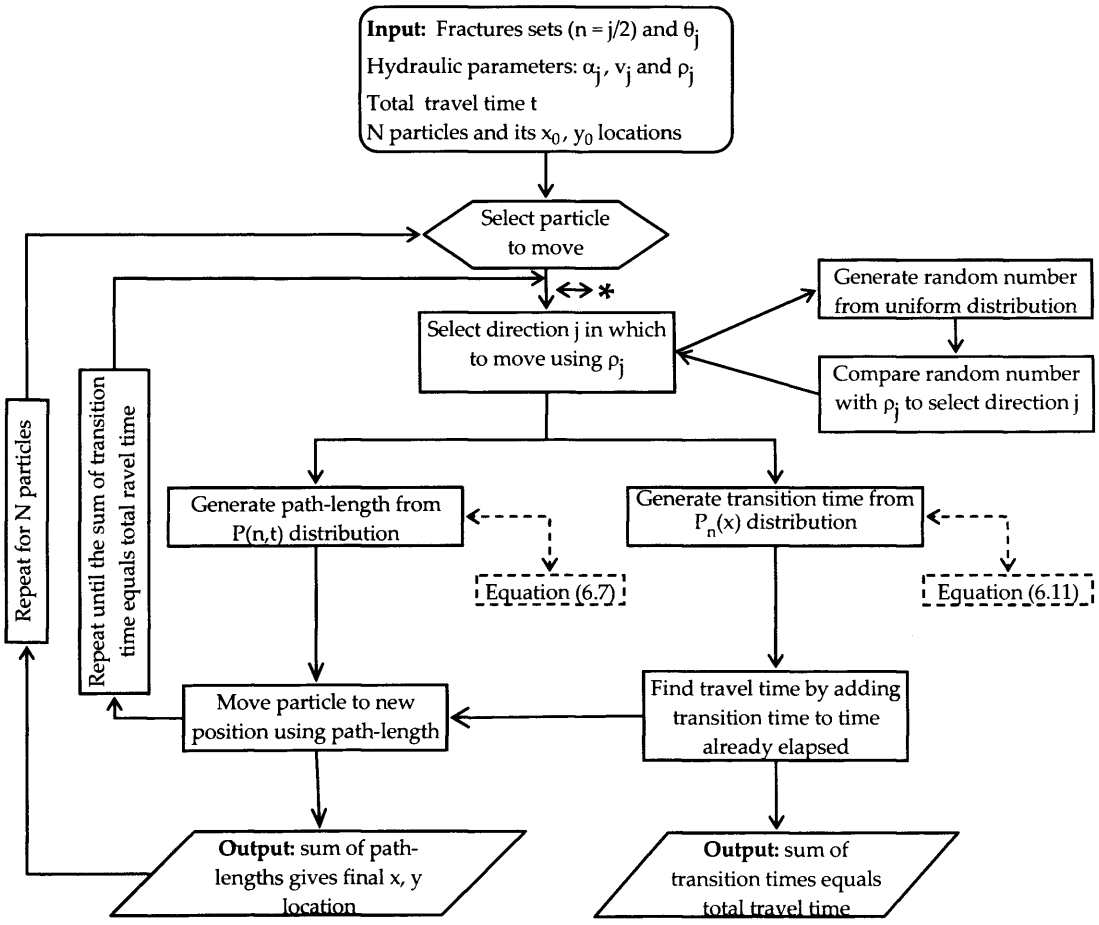

Figure 6.25 - Flow chart for the IMPLICIT two-dimensional CTRW procedure. The equations shown refer to the 1-D CTRW with exponential path-lengths, but the procedure is similar for the power-law path-lengths, except that the equation should change accordingly. The uniform hydraulic gradient is supposed to be known. *The meaning of the asterisk will be given in section 6.4.2.

6.3.2.1 Implementation under uniform flow conditions

The FORTRAN code on which the Explicit procedure was implemented also simulates solute transport using this Implicit CTRW procedure. The same modelling domain and the same fracture network were used to test the methodology, and thus the parameters used are again those shown in table 6.1.

Figure 6.26 shows plumes of particles that were tracked using the Implicit CTRW procedure, and the Statistical Continuum Method. The Implicit CTRW reproduces solute transport quite well, both in its advection and in its dispersion components. Again, the plume evolves from highly skewed to normally distributed for late times. The adoption of longitudinal and transverse dispersivities would not provide an adequate description of the shape of the plume. Once more transport is anomalous for early times and tends to Fickian for late times.

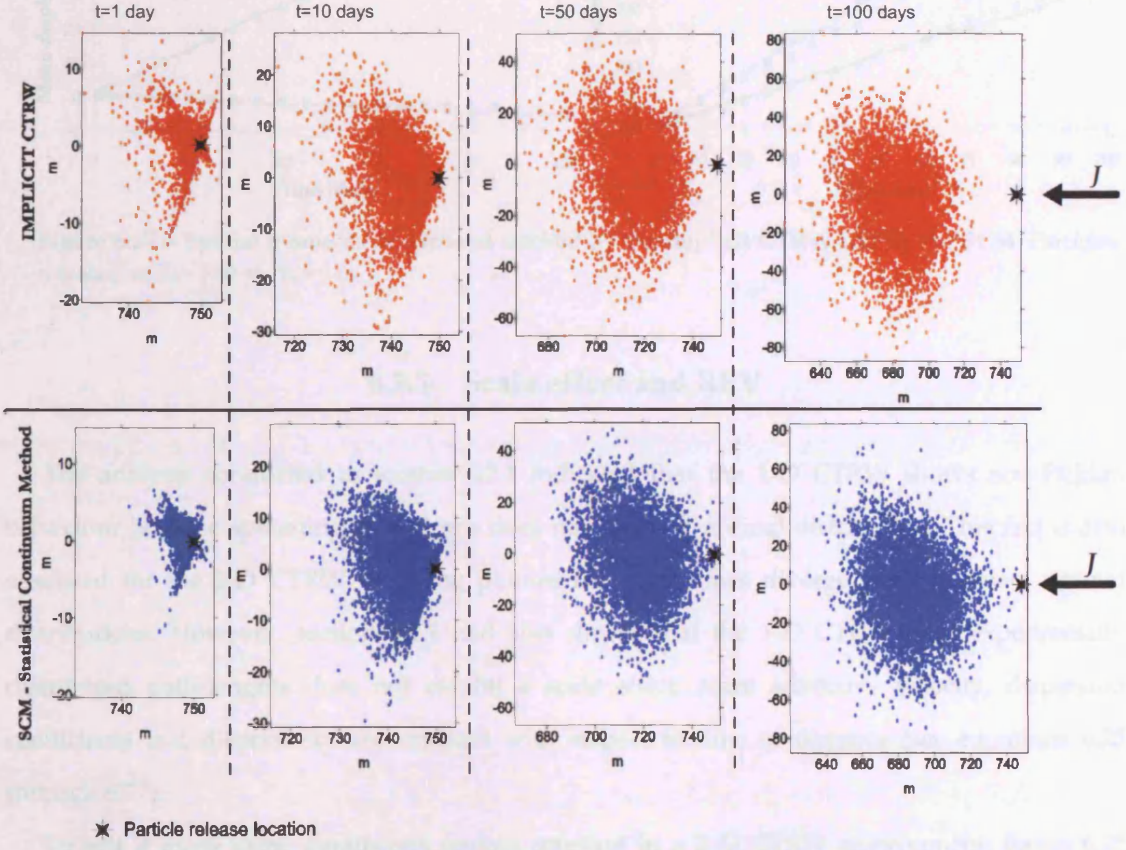

Figure 6.26 – Comparison of plumes of particles tracked by the Implicit CTRW and by the SCM. 5000 particles were instantaneously released at location $X_0 = 750$ m, $Y_0 = 0$m. Notice that scale varies. Uniform hydraulic gradient oriented from right to left.

The particles' 1st and 2nd spatial moments are compared in figure 6.27. The same remarks made for the Explicit CTRW are valid for the Implicit CTRW procedure, with more reliable descriptions of advection than of dispersion, but with improved 2nd moment fit when compared to the Explicit

CTRW procedure. Nevertheless, in both cases the comparison is favourable, outlining the validity of the Implicit CTRW procedure.

When compared to the Explicit CTRW procedure, the Implicit CTRW generates more distorted distributions, with the influence of individual fractures sets more clearly established at early times.

The computation time for the CTRW, for the 100-days travel time situation, was of about 10 seconds on a PC equipped with a 1.3 GHz processor and 256 Mb RAM.

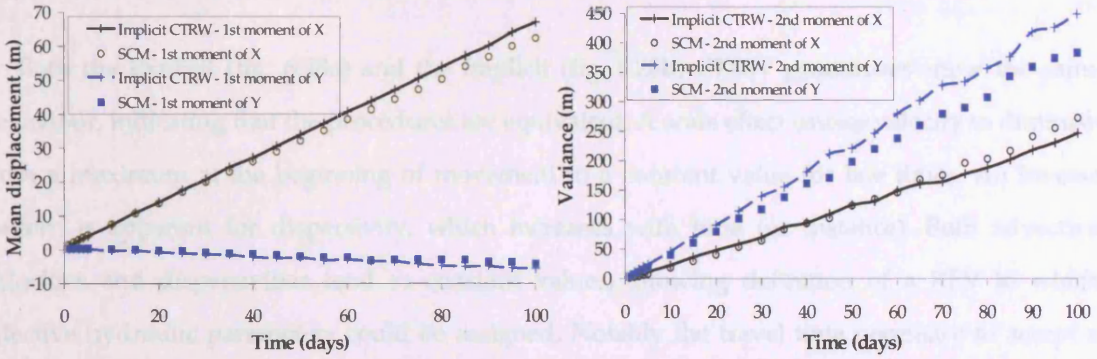

Figure 6.27 – Spatial moments of particles tracked by the Implicit CTRW and by the SCM. Particles released at $X_0 = 750$ m, $Y_0 = 0$ m.

6.3.3 Scale effect and REV

The analysis conducted in section 6.2.1 indicated that the 1-D CTRW shows non-Fickian behaviour because spreading of a plume does not follow a normal distribution. This fact is also observed for the 2-D CTRW since the plumes for short times diverge from bivariate normal distributions. However, section 6.2.1 had also shown that the 1-D CTRW with exponentially distributed path-lengths does not exhibit a scale effect, since advective velocity, dispersion coefficients and dispersivity are constant with respect to time or distance (see equations 6.25 through 6.27).

To test if those same parameters remain constant in a 2–D CTRW environment, figure 6.28 plots *apparent* advective velocity and *apparent* dispersivity for the plumes illustrated in figures 6.23 and 6.26. The term *apparent* is to underline that those parameters are computed assuming Fickian behaviour and that transversal and longitudinal movement can describe the shape of the plumes. Such distinction is necessary for comparison with the tendencies reported in the literature.

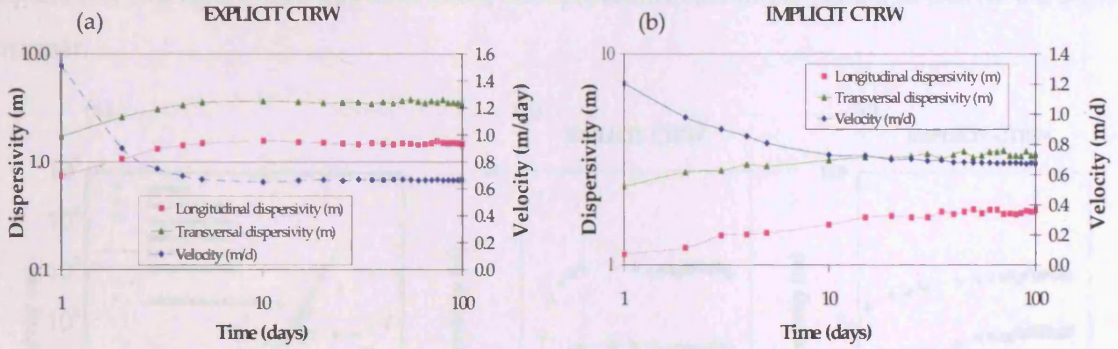

Figure 6.28 – *Apparent* velocity and *apparent* dispersivity variation with time, for particles tracked by: a) the Explicit CTRW; b) the Implicit CTRW.

Both the Explicit (fig. 6.28a) and the Implicit (fig. 6.28b) CTRW procedures show the same behaviour, indicating that the procedures are equivalent. A scale effect causes velocity to diminish from a maximum at the beginning of movement to a constant value for late times. An inverse pattern is apparent for dispersivity, which increases with time (or distance). Both advective velocities and dispersivities tend to constant values, allowing definition of a REV to which effective hydraulic parameters could be assigned. Notably the travel time necessary to accept a REV is much smaller in the Explicit CTRW (about 10 days) than in the Implicit CTRW (about 100 days). This inconsistency is, once again, the result of the averaging effect inherent in equation (6.52).

Nevertheless, in both cases, and although the 2-D CTRW does not have a real scale effect since dispersivity and velocity are constant in each direction of movement, an analysis using the Fickian model would indicate the existence of an *apparent* scale effect. Seemingly, this scale effect is similar to the behaviour usually resulting from the interpretation of tracer tests conducted at different scales and reported by several authors. Neuman (1995) has collected data from several sources and comparison with the scale effects resulting from the CTRW shows the same tendencies (fig. 6.29).

6.3.4 Two-dimensional CTRW with power-law distributed path-lengths

The Explicit and Implicit CTRW with power-law distributed path-lengths are implemented in the same manner as the CTRW with exponentially distributed path-lengths, except that the equations describing the distributions are different. The $P_{n,j}(x)$ and $P_j(n,t)$ distributions for the Implicit CTRW are now given by equations (6.33) and (6.11), respectively. In the Explicit CTRW, the equation to implement is equation (6.50) defined above, but with $P_j(x,t)$ now provided by

equation (6.39). Apart from this distinction, both procedures are implemented in exactly the same manner.

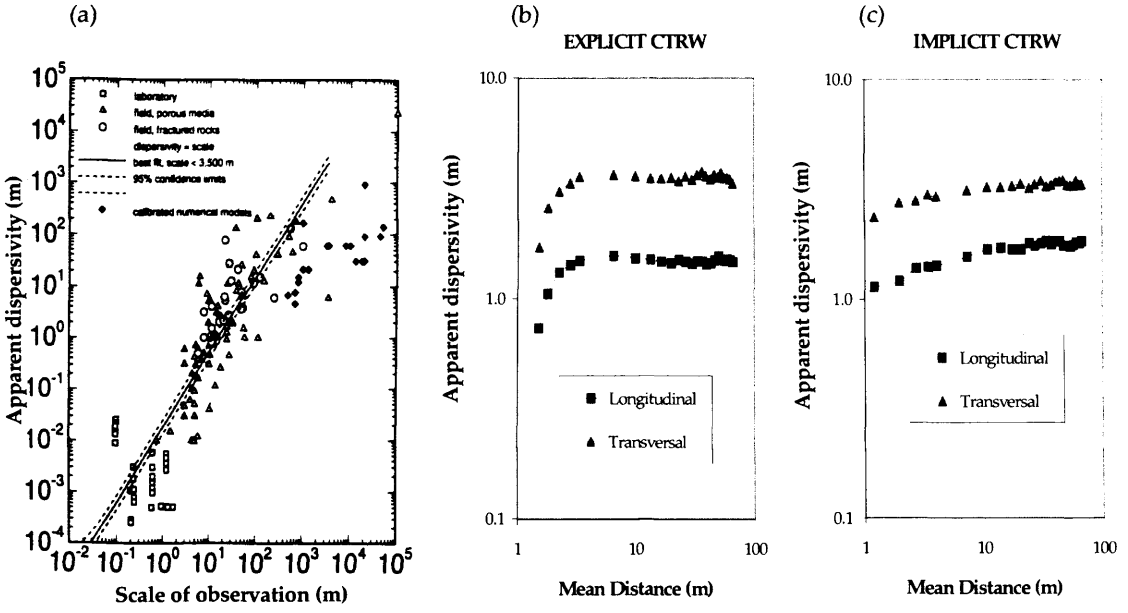

Figure 6.29 – Variation of apparent dispersivity with scale of observation. a) field data (Neuman 1995) ; b) Explicit CTRW; c) Implicit CTRW.

In this case, it is not possible to assess the reliability of the CTRW procedures, since no tool was available to model solute transport in a discrete fracture network in which fracture lengths were distributed according to power-laws. Therefore, no comparison could be made.

The generation of random variates from equation (6.39) was once again conducted via numerical inversion of the cumulative probability function (given in Appendix E). However, since in this case it was not feasible to find general solutions for the variance and mean of the 1-D CTRW (section 6.2.2.3), it is not possible to scale and shift a 'standard' distribution. These difficulties have led to considering the Explicit CTRW procedure with power-law distributed path-lengths less efficient than the corresponding procedure for the CTRW with exponentially distributed path-lengths.

Nevertheless, both the Implicit and Explicit procedures were implemented and some simulations were made, with the aim of studying the general behaviour of a 2-D CTRW with power-law distributed path-lengths. Table 6.2 shows the parameters used in the simulation, which in this case are γ_j, β_j and ρ_j. The parameters used were chosen arbitrarily, but the results achieved are thought, nonetheless, to be interesting. The modelled area and the boundary conditions were the same as used for the 2-D CTRW with exponentially distributed path-lengths.

Table 6.2 – Input parameters for the CTRW simulation with power-law distributed path-lengths.

Direction j	*Fracture set*	*Angle with x* θ(°)	*Step rate* γ(d^{-1})	*Shape factor* β(-)	*Mean path-length* $\overline{\mu}_i$ (m)	*Directional choice* ρ(-)
1	1	160°	1.30	1.92	2.08	0.17
2	2	125°	0.89	1.89	2.13	0.31
3	3	250°	0.41	1.59	2.70	0.32
4	1	340°	1.37	10.0	1.11	0.05
5	2	305°	1.07	10.0	1.11	0.06
6	3	70°	0.85	2.94	1.51	0.09

(fracture orientations based on fracture network illustrated in fig. 5.13 and table 5.1)

Figure 6.30 shows the plumes tracked using the Implicit procedure. The plumes are highly skewed at early times and no convergence to a bivariate normal distribution is apparent. Therefore, even for very late travel times such as t = 1000 days, it may not be possible to define a REV since the plumes are still correlated with the fracture orientations.

Plots of apparent velocity and dispersivity (fig. 6.31) show considerable instability that seems to attenuate with time. In this case, the existence of a scale effect until about 100 days cannot be regarded as apparent since it was already visible in the 1-D analytical evaluation of the CTRW (see section 6.2.2.3). No Representative Elementary Volume can be defined in this case, regardless the fact that velocity and dispersivity tend to a constant value, because the shapes of the plumes do not seem to be compatible with Fickian transport.

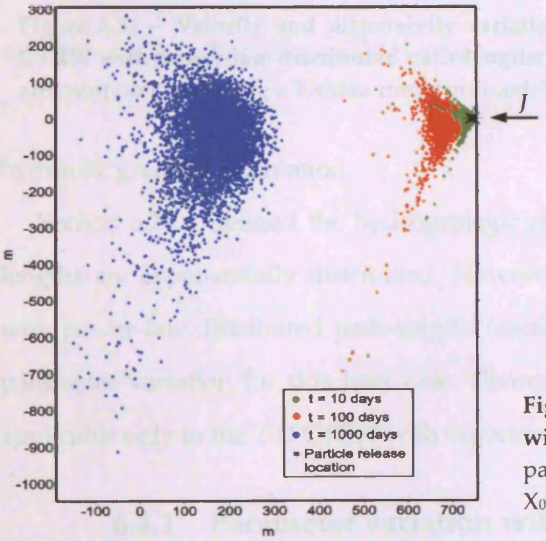

Figure 6.30 – Particles tracked by the Implicit CTRW with power-law distributed path-lengths. 5000 particles were instantaneously released at location X_0=750 m, Y_0=0m. Hydraulic gradient from right to left.

6.4 MODELLING SOLUTE TRANSPORT AT THE CATCHMENT SCALE ACCORDING TO A TWO-DIMENSIONAL CTRW (NON-UNIFORM FLOW CONDITIONS)

The application of the 2-D CTRW to situations in which the hydraulic gradient is not uniform is far more complex than application to uniform flow cases, be it in its Explicit or in its Implicit procedure forms. The added complexity results from the variability of the CTRW parameters with hydraulic gradient orientation. Therefore, in order to implement the CTRW under non-uniform flow conditions it is necessary to characterize the variation of the relevant parameters with

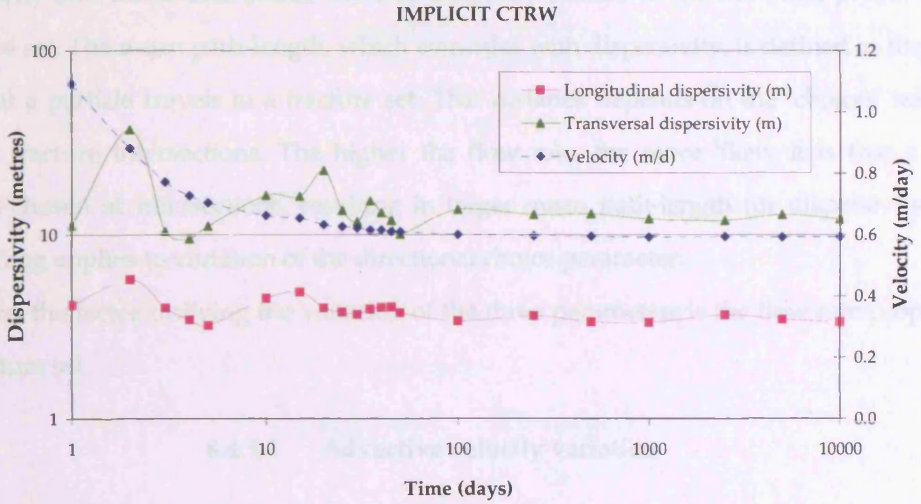

Figure 6.31 – Velocity and dispersivity variation with time, for particles tracked by the Implicit CTRW with power-law distributed path-lengths. Notice that these values of velocity and dispersivity are computed assuming a Fickian transport model.

hydraulic gradient orientation.

Section 6.2.1.4 defined the hydrogeologic meaning of the CTRW parameters when the path-lengths are exponentially distributed. However, the same analysis was not possible for CTRW with power-law distributed path-lengths (section 6.2.2.3), rendering it unfeasible to characterize parameter variation for this later case. Consequently, the analysis conducted in this section is applicable only to the 2-D CTRW with exponentially distributed path-lengths.

6.4.1 Parameter variation with hydraulic gradient orientation

The 2-D CTRW with exponentially distributed path-lengths depends on the following parameters (see equations 6.28 and 6.48):

- v_j, advective velocity in each movement direction, which can also be defined as $\frac{\gamma_j}{\lambda_j}$, the product of step rate and mean path-length;
- α_j, dispersivity in each movement direction, also defined as $\frac{1}{\lambda_j}$, the mean path-length;
- ρ_j, directional choice[1].

Advective velocity is expected to vary with hydraulic gradient orientation, since it is a function of flow rate in each fracture set, which is itself a function of the angle between fracture set and hydraulic gradient.

Dispersivity and directional choice are also indirectly related to the flow rate proportion in each fracture set. The mean path-length, which coincides with dispersivity, is defined as the mean distance that a particle travels in a fracture set. That distance depends on the 'choices' taken by particles at fracture intersections. The higher the flow rate, the more likely it is that a given direction is chosen at intersections, resulting in larger mean path-length (or dispersivity). The same reasoning applies to variation of the directional choice parameter.

Therefore, the factor unifying the variation of the three parameters is the flow rate proportion in each fracture set.

6.4.1.1 Advective velocity variation

For the case of a model comprising n sets of fractures where each set comprises an infinite number of infinitely long parallel fractures, which are all of the same aperture and separation (fig. 6.32), hydraulic conductivity (K) in the hydraulic gradient direction can be adapted from Barker (2002) as:

$$K_\Theta = 8C_1 \sum_{j=1}^{n} b_j^3 \cos^2(\theta_j - \Theta) \tag{6.54}$$

where $2b$ is fracture aperture, θ is fracture orientation and Θ is the hydraulic gradient orientation. C_1 is a constant of proportionality and the subscript j refers to the different fracture sets.

The bulk flow rate in the hydraulic gradient direction (Q_Θ) will then be:

$$Q_\Theta = K_\Theta J = 8JC_1 \sum_{j=1}^{n} b_j^3 \cos^2(\theta_j - \Theta) \tag{6.55}$$

where J is the hydraulic gradient value.

The flow rate in each fracture set, q_j, is equivalent to:

[1] In fact, ρ_j, directional choice is only required in the Implicit CTRW procedure.

$$|q_j| = \frac{K_j|\cos(\theta_j - \Theta)|J_j}{\sum_{i=1}^{2n} K_i|\cos(\theta_i - \Theta)|J_i} \frac{Q_\Theta}{|\cos(\theta_j - \Theta)|} = \frac{K_j J_j}{\sum_{i=1}^{2n} K_i|\cos(\theta_i - \Theta)|J_i} Q_\Theta \tag{6.56}$$

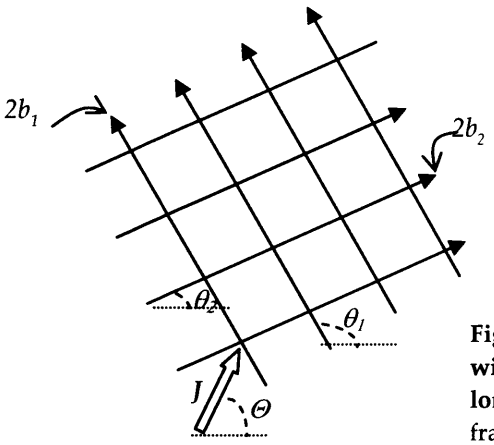

Figure 6.32 – Two-dimensional fracture network model, with two sets composed of an infinite number of infinitely long fractures. Arrows indicate direction of flow along fractures. *b* is half-fracture aperture.

where J_j is the regional hydraulic gradient projection on the direction of fracture set *j*.

In a model such as the one depicted in figure 6.32, in which fractures are infinitely long, flow will always be in the down-gradient direction. In this situation the projection of the hydraulic gradient in the direction of each fracture set would be:

$$\begin{cases} J_j = J\cos(\theta_j - \Theta) & |\theta_j - \Theta| < 90^\circ \\ 0 & |\theta_j - \Theta| \geq 90^\circ \end{cases} \tag{6.57}$$

with positive values only for $-90^\circ < \theta_j - \Theta < 90^\circ$ and no flow occurring in the up-gradient directions.

However, if fractures are not infinitely long, there will be flow against the regional hydraulic gradient to ensure continuity. In such situation, the projection of the hydraulic gradient can no longer be represented by the equation above, because flow will occur for directions at more than 90° with the hydraulic gradient. The problem is then so complex that it cannot be solved analytically. Nevertheless, it is possible to introduce a simplification and assume that the projection of the hydraulic gradient into non-infinite fractures is given by:

$$J_j = J\left[C_{2,j} + C_3\cos(\theta_j - \Theta)\right] \tag{6.58}$$

which states that the hydraulic gradient component in each fracture set is comprised of two parts:

- a constant part, represented by $C_{2,j}$, that represents the residual gradient necessary for the j^{th} fracture set to ensure connectivity between the other sets. Notice that the constant of proportionality $C_{2,j}$ varies between fracture sets, since the amount of flow that will cross

each set just to ensure connectivity will depend on the fracture geometry (aperture and density);

- a varying part represented by the second term, and that represents the influence of the hydraulic gradient projection into fracture set j. C_3 is a constant of proportionality equal for all fracture sets.

Equation (6.58) permits positive values for J_j in the range $-180^\circ < \theta_j - \Theta < 180^\circ$.

Replacing equation (6.58) into equation (6.56):

$$|q_j| = \frac{K_j\left[C_{2,j} + C_3\cos(\theta_j - \Theta)\right]}{\sum_{i=1}^{2n} K_i\left|\cos(\theta_i - \Theta)\right|\left[C_{2,i} + C_3\cos(\theta_i - \Theta)\right]} Q_\Theta \tag{6.59}$$

Assuming that fractures have constant aperture $2b_j$, advective velocity v_j will be:

$$|v_j| = \frac{b_j^2\left[C_{2,j} + C_3\cos(\theta_n - \Theta)\right]}{2\sum_{i=1}^{2n} b_i^3\left|\cos(\theta_i - \Theta)\right|\left[C_{2,i} + C_3\cos(\theta_i - \Theta)\right]} Q_\Theta \tag{6.60}$$

or using equation (6.55) into (6.60):

$$|v_j| = \frac{b_j^2\left[C_{4,j} + \cos(\theta_j - \Theta)\right]}{2\sum_{i=1}^{2n} b_i^3\left|\cos(\theta_i - \Theta)\right|\left[C_{4,i} + \cos(\theta_i - \Theta)\right]} JC_1\sum_{i=1}^{n} 8b_i^3\cos^2(\theta_i - \Theta) \tag{6.61}$$

where $C_{4,i} = \frac{C_{2,i}}{C_3}$.

Consequently, the variation of velocity with hydraulic gradient orientation is dependent on three parameters: b_j, $C_{4,j}$ and C_1. Because movement can occur in the up-gradient and the down-gradient direction of each fracture set and since $\cos(\theta_j + 180^\circ) = -\cos(\theta_j)$, equation (6.61) can be simplified to:

$$|v_j| = 4JC_1\frac{b_j^2\left[C_{4,j} + \cos(\theta_j - \Theta)\right]}{\sum_{i=1}^{2n} b_i^3\left|\cos(\theta_i - \Theta)\right|C_{4,i}}\sum_{i=1}^{n} b_i^3\cos^2(\theta_i - \Theta) \tag{6.62}$$

Equation (6.62) is thus proposed to approximate advective velocity variation with respect to hydraulic gradient orientation, for a fracture network with finite length fractures. However, this equation is not directly useful to the 2-D CTRW implementation. It is necessary to retrieve values of advective velocity for any hydraulic gradient orientation, knowing v_j for a single hydraulic gradient orientation, Θ. That is, the goal is to depart from a situation such as depicted in table 6.1 above (page 206), to obtain the velocities for any hydraulic gradient orientation.

If a change in the initial hydraulic gradient orientation occurs and the new orientation is denoted by Θ', then advective velocity in each movement direction will vary and is now represented by v_j', the ratio of which with the initial velocity v_j is given by:

$$\frac{|v_j'|}{|v_j|} = \frac{\left[C_{4,j} + \cos(\theta_j - \Theta')\right]\sum_{i=1}^{2n} b_i^3 \left|\cos(\theta_i - \Theta)\right| C_{4,i} \sum_{i=1}^{n} b_i^3 \cos^2(\theta_i - \Theta')}{\left[C_{4,j} + \cos(\theta_j - \Theta)\right]\sum_{i=1}^{2n} b_i^3 \left|\cos(\theta_i - \Theta')\right| C_{4,i} \sum_{i=1}^{n} b_i^3 \cos^2(\theta_i - \Theta)} \tag{6.63}$$

depending only on two parameters, $C_{4,j}$ and b_j.

The ratio of initial velocities in opposite directions of a same fracture set leads to the values of $C_{4,j}$, according to:

$$\frac{|v_j|}{|v_{j+n}|} = \frac{C_{4,j} + \cos(\theta_j - \Theta)}{C_{4,j} - \cos(\theta_j - \Theta)} \tag{6.64}$$

since the fracture aperture, b_j, is the same. In addition, the ratio between velocities in each movement direction with respect to velocity in the $j = 1$ direction (chosen arbitrarily), is given by:

$$\frac{|v_j|}{|v_1|} = \frac{b_j^2 \left|\cos(\theta_j - \Theta)\right|\left[C_{4,j} + \cos(\theta_j - \Theta)\right]}{b_1^2 \left|\cos(\theta_1 - \Theta)\right|\left[C_{4,1} + \cos(\theta_1 - \Theta)\right]} \tag{6.65}$$

the absolute cosine terms resulting from the need to reduce the velocity vectors to comparable values along the gradient orientation.

Consequently, because $C_{4,j}$ is given by equation (6.63), the ratio b_j/b_1 can always be computed.

Since equations (6.64) and (6.65) provide the values for $C_{4,j}$ and indirectly the values for the aperture (by setting for instance $b_1 = 1$), equation (6.63) can be used to compute the value of advective velocity for any hydraulic gradient orientation, starting from a known initial value.

This methodology was applied to the velocity values indicated in table 6.1, which correspond to a hydraulic gradient orientation $\Theta = 180°$.

Figure 6.33 shows the values of velocity obtained by the methodology above for several orientations of the hydraulic gradient and the values computed using the STATMOV module and SDF discrete model. Although some noticeable errors occur, which are a result of the simplifications inherent to the method, it is striking that the main tendencies are followed. Therefore, although equation (6.63) is far from perfect, it characterises the variation of velocity with hydraulic gradient orientation.

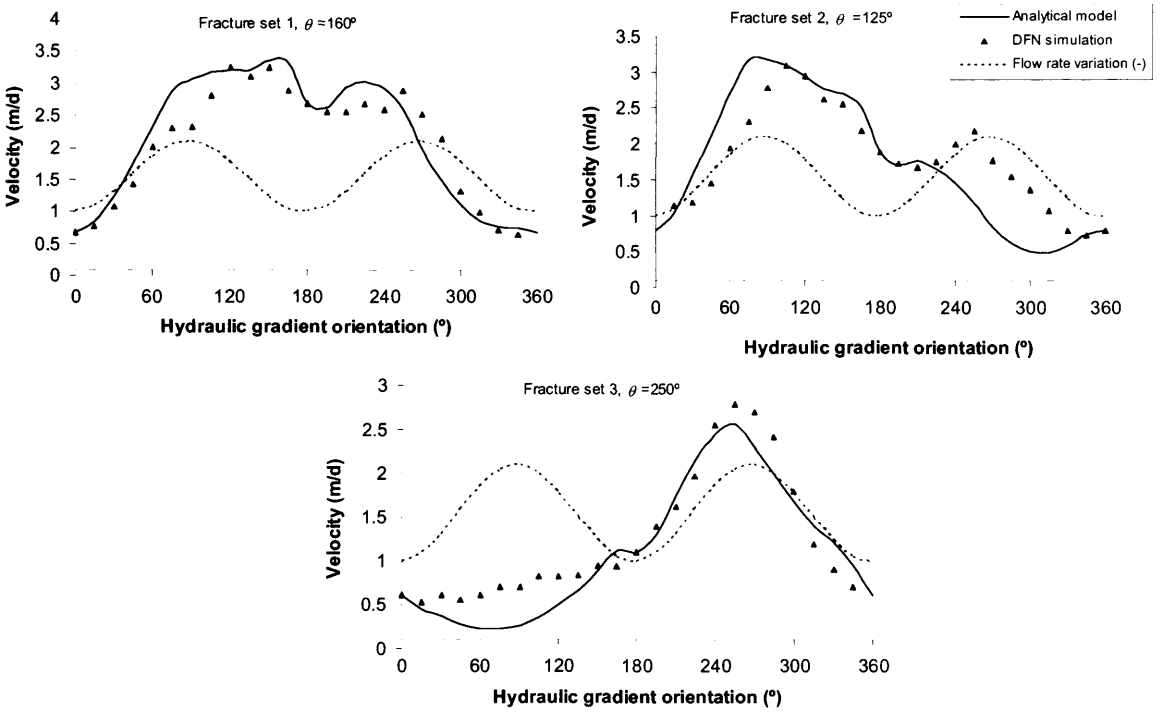

Figure 6.33 – Variation of velocity with hydraulic gradient orientation, for 3 directions of movement. The analytical model solution is obtained from equation (6.63), while the discrete model solution was obtained from a single realisation of the fracture network. Also shown is the change in flow rate with hydraulic gradient orientation. Refer to table 5.1 and fig. 5.13 for characteristics of the fracture network.

6.4.1.2 Dispersivity variation

For implementation of the 2-D CTRW it is also necessary to define the variation of dispersivity with hydraulic gradient orientation.

The discrete fracture model, SDF, which generates the fracture networks used as the base case (section 5.2), conducts particle tracking at fracture intersections by setting the probability of particles taking any direction as the proportion of flow rate in the intersecting fracture segments. This is usually referred as the **complete mixing** model. Other models exist, such as the **stream tube-routing** model (Hull et al. 1987, Berkowitz and Braester 1991), in which mass travels through a fracture intersection without crossing streamlines.

It is usually accepted that the complete mixing model is appropriate for situations in which mass resides in the intersection a sufficiently long time that it may diffuse across streamlines, while the stream tube-routing is more appropriate for higher velocities. This is currently an issue of research, with Reynolds and Peclet Numbers being used to characterize the scope of acceptability of both models (Mourzenko et al. 2001). However, in two-dimensional discrete networks it has been suggested that the differences between the two methods are negligible (Parney 1999).

A thorough discussion of the distinction between the two models is not within the scope of this thesis, and the Complete Mixing model will be assumed henceforth, since it is the one on which comparisons can be made using SDF.

According to the complete mixing model, the probability of a particle following any direction at a fracture intersection is proportional to the flow rate in each fracture segment. Dispersivity corresponds to the mean path-length, which depends on the 'choices' taken by particles at fracture intersections. The higher the flow rate, the more likely it is that a given direction is chosen at intersections, resulting in larger path-length (or dispersivity). That is:

$$\alpha_j = C_{5,j}\left(\frac{2b_j|v_j|}{\sum_{i=1}^{2n}2b_i|v_i|}\right)+C_{6,j} = C_{5,j}\left(\frac{|q_j|}{\sum_{i=1}^{2n}|q_i|}\right)+C_{6,j} \tag{6.66}$$

The proportionality constant $C_{5,j}$ is related to the geometric features of the fracture set and imply that once a particle enters a fracture, the mean distance that travels along it increases at a rate equivalent to $C_{5,j}$. The constant $C_{6,j}$ indicates that there is a minimum path-length for each fracture set, since particles must always move along the fracture set to ensure connectivity of the fracture set.

Because the values of q_j can be computed from equation (6.56), the difference between dispersivities in opposite directions of the same fracture set allows us to compute $C_{5,j}$.

$$\alpha_j - \alpha_{j+n} = C_{5,j}\left(\frac{|q_j|-|q_{j+n/2}|}{\sum_{i=1}^{2n}|q_i|}\right) \tag{6.67}$$

Knowing the values for $C_{5,j}$ it is then possible to compute dispersivity for any hydraulic gradient orientation, according to:

$$\alpha_j' = \alpha_{j+n} - C_{5,j}\left(\frac{|q_j|}{\sum_{i=1}^{2n}|q_i|}-\frac{|q_j'|}{\sum_{i=1}^{2n}|q_i'|}\right) \tag{6.68}$$

This methodology was implemented with the data from table 6.1 as the initial values. Figure 6.34 compares the values obtained by the methodology above for several orientations of the hydraulic gradient and the values computed using the STATMOV module and SDF discrete model. The fit is far from perfect, which probably is due to the inaccuracies already visible in velocity variation (fig. 6.33). Nevertheless, the main tendencies are once again preserved.

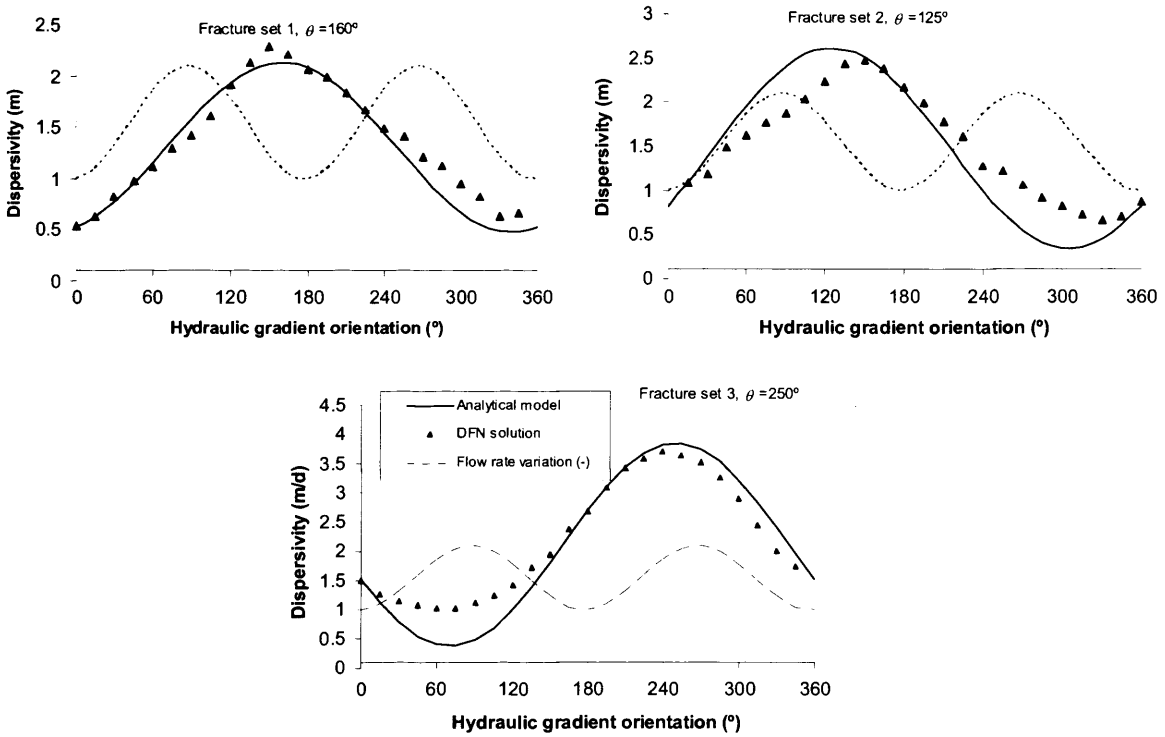

Figure 6.34 – Variation of dispersivity with hydraulic gradient orientation, for three directions of movement. The analytical model solution is obtained from equation (6.68), while the discrete model solution was obtained from a single realisation of the fracture network. Also shown is the change in flow rate with hydraulic gradient orientation. Refer to table 5.1 and fig. 5.13 for characteristics of the fracture network.

6.4.1.3 Directional choice variation

The directional choice parameter, ρ_j, being an indication of the probability of any direction being chosen, is also addressed using the Complete Mixing Model.

The probability of a particle taking a given j direction will depend not only on the proportion of flow rate in each direction, but also on the number of intersections. It is thus possible to assume a correlation such as:

$$\rho_j = C_{7,j}\left(\frac{|q_j|}{\sum_{i=1}^{2n}|q_i|}\right) \tag{6.69}$$

where the constant $C_{7,j}$ is related to the density of fracture intersections of the j^{th} movement direction, which should not be confused with fracture density.

If knowledge about the value of ρ_j in opposite directions of the same fracture exist, such as in table 6.1, then it is possible to determine $C_{7,j}$, which is the same for the two directions of the fracture. Consequently, and since the values of q_j can be determined from equation (6.56), it is possible to establish the value of ρ_j for any hydraulic gradient orientation.

Figure 6.35 compares the ρ_j values for several orientations of hydraulic gradient using the relation provided by equation (6.69) and the values computed with module STATMOV. The data in table 6.1 was used as the initial values, for an orientation of hydraulic gradient Θ =180°. The comparison is favourable, except for (θ-Θ) close to 180°. Because these are the situations where ρ_j tends to zero, it was decided to accept equation (6.69) as valid, although it is recognised that improvements should be made.

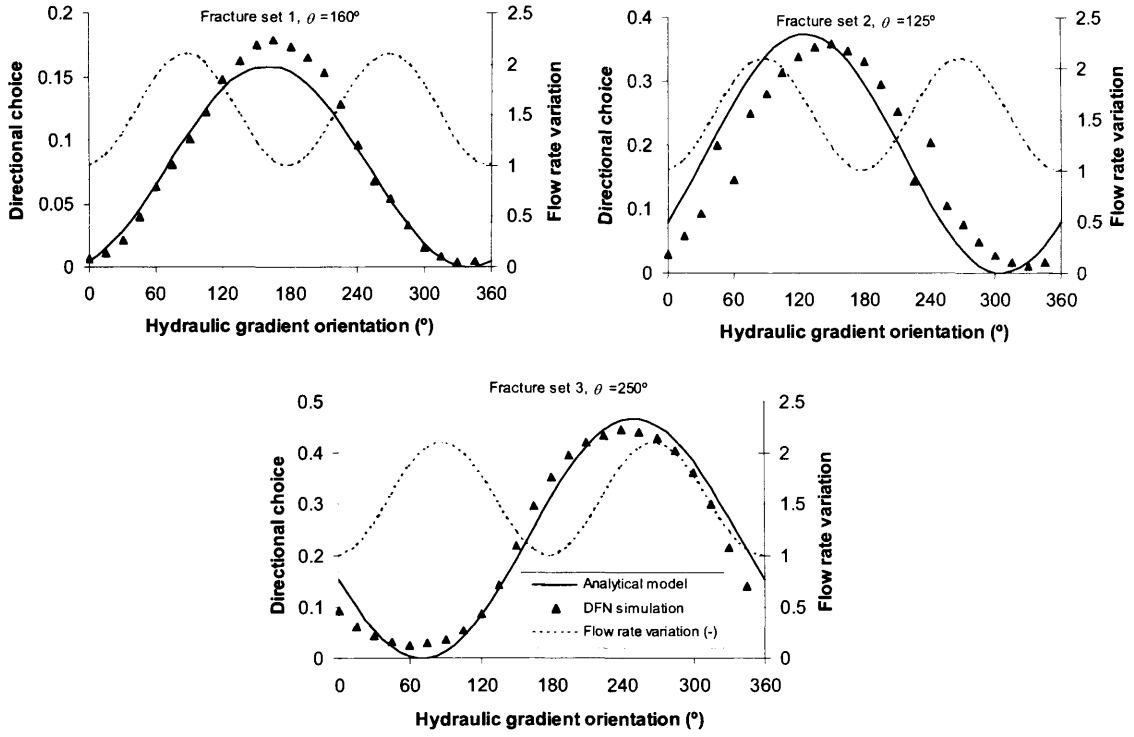

Figure 6.35 – Variation of directional choice with hydraulic gradient orientation, for 3 directions of movement. The analytical model solution is obtained from equation (6.69), while the discrete model solution was obtained from a single realisation of the fracture network. Also shown is the change in flow rate with hydraulic gradient orientation. Refer to table 5.1 and fig. 5.13 for characteristics of the fracture network.

6.4.2 Implementation of the 2-D CTRW under varying hydraulic gradient conditions

The CTRW parameter variation as defined in the previous section was implemented in a sub-routine of the module SCPATH described in section 5.2. The 2-D CTRW can then be conducted in a non-uniform flow field, both in its Explicit and Implicit procedures. With respect to the procedures described in section 6.3, where uniform flow conditions exist, further steps anticipate

the CTRW procedures. The code must now identify the orientation of the hydraulic gradient and, using the initial input parameters, compute advective velocity, dispersivity and, in the Implicit CTRW procedure, directional choice, for each movement direction.

The flow chart for those new steps is shown in figure 6.36 and should be added to the flow charts for the Explicit and Implicit CTRW procedures (fig. 6.22 and 6.25, respectively) where the asterisk is shown. An interface with a numerical model flow solution (for instance MODFLOW) is necessary to make possible the evaluation of the hydraulic gradient at every particle locations.

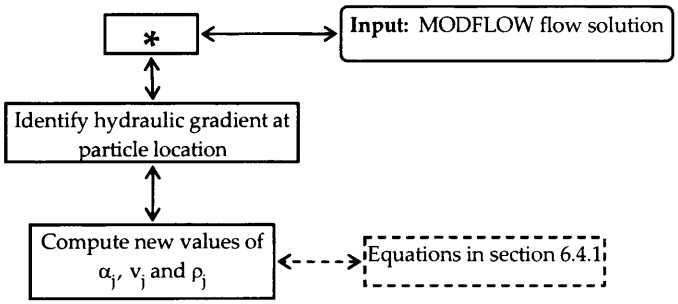

Figure 6.36 – Flow chart of the steps implied by application of the two-dimensional CTRW procedures to a situation with a varying hydraulic gradient. This flow chart interfaces with the flow charts for the Explicit CTRW (fig. 6.22) and the Implicit CTRW (fig. 6.23) where the asterisk is shown in these figures.

Figure 6.37 shows plumes of particles tracked in a flow field similar to the one depicted in figure 6.23, except that the hydraulic gradient orientation varies from figure 6.37a to figure 6.37d. That is, uniform flow conditions exist, but the initial parameters (table 6.1) apply only to figure 6.37a. SCPATH identifies the hydraulic gradient orientation and computes the relevant parameters. Particle tracking was conducted with the Implicit CTRW procedure for 1-day travel time.

Notice that the shape of the plumes varies considerably with hydraulic gradient orientation, showing that overall dispersion and advection characteristics could not be adequately simulated using an Equivalent Porous Medium approach.

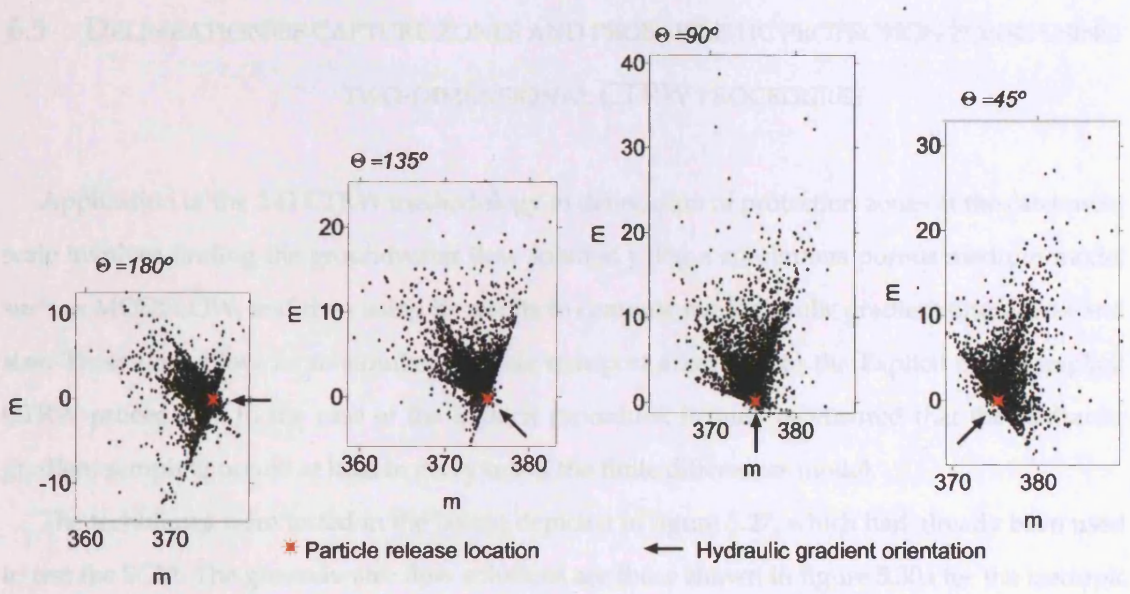

Figure 6.37 – Plumes of particles tracked by the Implicit CTRW during 1 day, for several hydraulic gradient orientations. 5000 particles were released at location $X_0 = 375$ m, $Y_0 = 0$ m.

The two procedures defined for the 2-D CTRW, Explicit and Implicit procedures, can be equally applied to the non-uniform flow case. However, in the case of the Explicit procedure it is no longer possible to define the location of the particles in a single step, using equation (6.52) and the total travel time. It is necessary to sample the hydraulic gradient a sufficient number of times to ensure that non-uniformity of flow is accurately represented. This implies the need to use steps of time duration lower than the total travel time and apply the 2-D CTRW Explicit procedure to each time-step. The Explicit procedure then becomes in nature very similar to the way in which particle tracking is usually conducted in codes such as, for instance, MODPATH, except that Fickian transport is not assumed.

This need to consider multiple time-steps denotes a weakness of the Explicit CTRW procedure since it imposes selection of a travel time for which the scale effect (see fig. 6.28a) has already attenuated. Therefore, a REV is indirectly selected, in which Fickian behaviour is not necessarily an assumption, but where the scale effects are no longer taking place.

As for the Implicit CTRW procedure, no modifications are necessary, since it already considers multiple time steps, equivalent to the time necessary to complete each path-length. The scale effects are preserved because, at each step, particles move in a single direction and the time taken to complete it varies according to a continuous distribution.

6.5 DELINEATION OF CAPTURE ZONES AND PROBABILISTIC PROTECTION ZONES USING TWO-DIMENSIONAL CTRW PROCEDURES

Application of the 2-D CTRW methodology to delineation of protection zones at the catchment scale involves finding the groundwater flow solution using a continuous porous medium model such as MODFLOW, and then using its results to compute the hydraulic gradient orientation and size. These data allow us to simulate particle transport according to the Explicit or the Implicit CTRW procedures. In the case of the Explicit procedure, it must be ensured that the hydraulic gradient sampling occurs at least in every cell of the finite differences model.

The techniques were tested in the layout depicted in figure 5.27, which had already been used to test the SCM. The groundwater flow solutions are those shown in figure 5.30a for the isotropic K case and in figure 5.30b for the anisotropic K case. The CTRW parameters used as input were those of table 6.1.

Figure 6.38 shows the capture zones delineated by both CTRW procedures for the isotropic K solution. Differences between the two procedures are not apparent, while comparison with figure 5.31a shows that differences to SCM results are also negligible. In addition, the differences with the EPM solution, found using PMPATH, are those expected from the characteristics of the fracture network that was assumed to compose the fractured aquifer[1].

The time step used in the Explicit CTRW procedure was $t = 10$ days, which according to figure 6.28a ensures that 'apparent' advective velocity and dispersivity have stabilised.

The capture zones for the case where the groundwater flow solution was found with anisotropy in K, is depicted in figure 6.39. Again, the differences between the two procedures are negligible, indicating that they are equally valid, while the difference with the SCM results (see fig. 5.31b) still remain acceptable and in accordance with the fracture network characteristics.

[1] See fig. 5.13 and table 5.1 for the characteristics of the fracture network on which the CTRW parameters of table 6.1 were collected

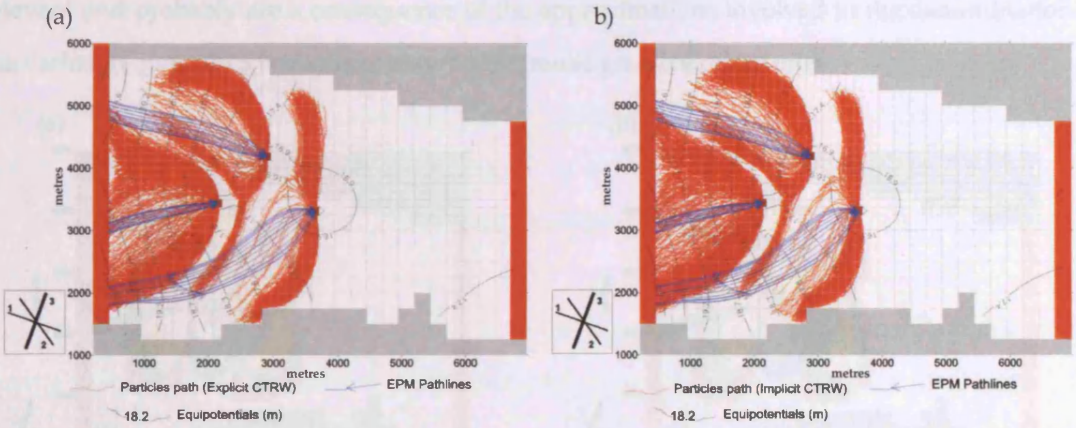

Figure 6.38 – Capture zones delineated by particle tracking conducted by: a) Explicit CTRW; b) Implicit CTRW. ***Flow solution computed with*** $K_x = K_y$ Also shown capture zone delineated using an EPM approach. 1000 particles were backtracked from each well. In the CTRW procedures particles were tracked for 10000 days, which explains that some of the paths do not reach the limit of the capture zone.

The probability contours of the protection zone were computed using the location of particles at time *t*, using the same process as in section 5.2.5. Essentially, the module PROBCONT, described in section 5.2.5, is used on the CTRW output, assigning probabilities to each cell that particles departing from it will take longer than time *t* to reach the well.

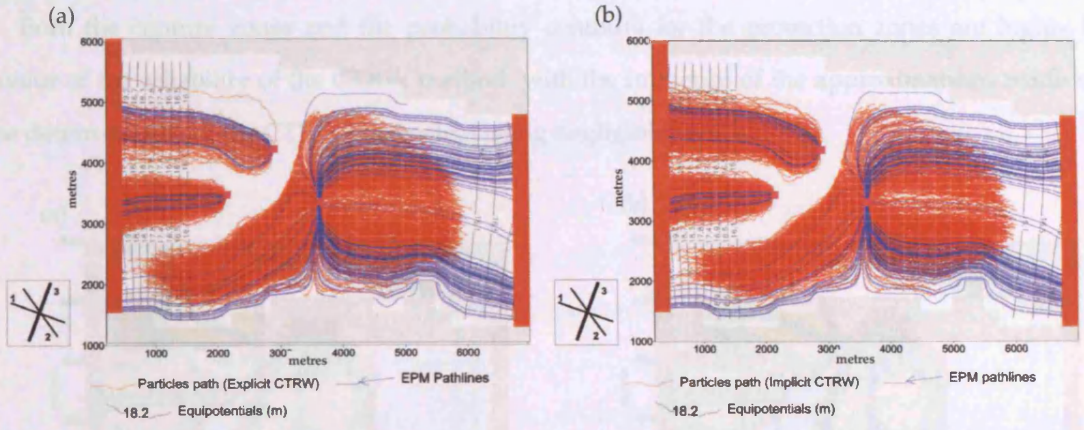

Figure 6.39 – Capture zones delineated by particle tracking conducted by: a) Explicit CTRW; b) Implicit CTRW. ***Flow solution computed with*** $K_y/K_x = 5.8$. Also shown capture zone delineated using an EPM approach. 1000 particles were backtracked from each well. In the CTRW procedures particles were tracked for 10000 days, which explains that some of the paths do not reach the limit of the capture zone.

Figure 6.40 shows the 10-year isochrone probability contours for the isotropic K solution, for both CTRW procedures. As expected, the differences between the two are not apparent, while comparison with figure 5.32 indicates that differences with respect to the SCM results are not

relevant and probably are a consequence of the approximations involved in the determination of the variation of the CTRW parameters with hydraulic gradient orientation.

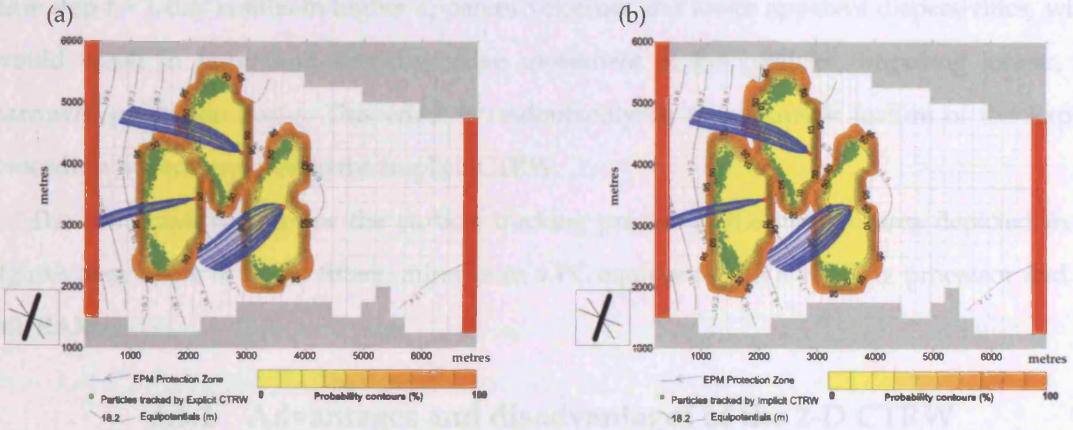

Figure 6.40 – Ten-year protection zone delineated by: a) Explicit CTRW; b) Implicit CTRW. ***Flow solution computed with $K_x = K_y$.*** Contours represent the probabilistic capture zone computed with the output from the CTRW. Blue lines depict the protection zone as computed with a continuous porous media model (PMPATH).

The same conclusions can be drawn from the probability contours found for the anisotropic K solution (fig. 6.41), which should be compared with figure 5.33 for the SCM and the EPM protection zones results.

Both the capture zones and the probability contours for the protection zones are highly in favour of the reliability of the CTRW method, with the influence of the approximations made on the determination of the CTRW parameters being negligible.

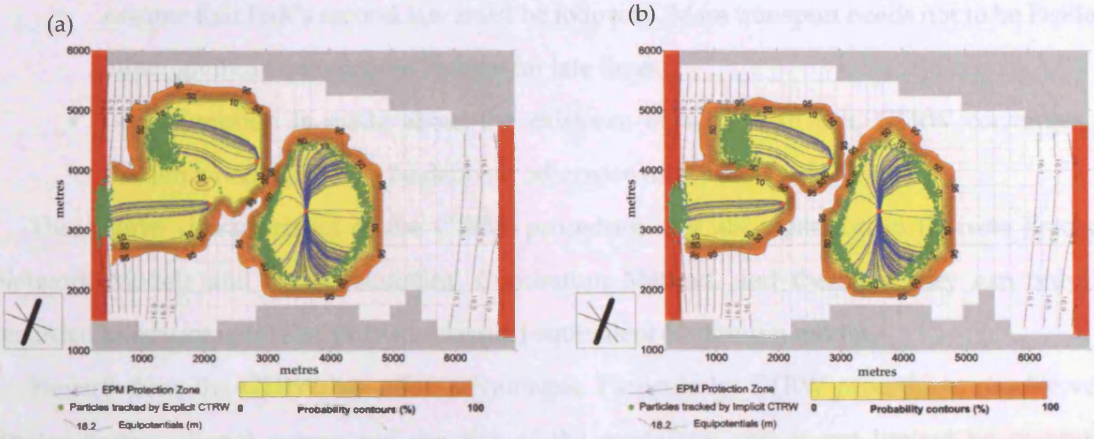

Figure 6.41 – Ten-year protection zone delineated by: a) Explicit CTRW; b) Implicit CTRW. ***Flow solution computed with $K_y/K_x = 5.8$.*** Contours represent the probabilistic capture zone computed with the output from the CTRW. Blue lines depict the protection zone as computed with a continuous porous media model (PMPATH).

If in the Explicit CTRW procedure, a different time step was chosen, the probability contours could result in a longer protection zone, if the scale effects were still apparent. For instance using a time step t = 1 day results in higher apparent velocities and lower apparent dispersivities, which would result in faster and less dispersive movement of the particles, imposing longer, but narrower protection zones. This effect is undoubtedly an unfavourable feature of the Explicit procedure when compared to the Implicit CTRW.

The computation time for the particle tracking process in the domain area depicted in the figures above was of about fifteen minutes in a PC equipped with a 1.3 GHz processor and 256 Mb RAM.

6.5.1 Advantages and disadvantages of the 2-D CTRW

The results presented in this section indicate that the use of Continuous Time Random Walks to simulate solute transport in fractured rocks may have several advantages over other methods, such as Discrete Fracture Network models, hybrid models or the Equivalent Porous Medium model.

The CTRW procedures overcome some of the problems identified in the introduction to chapter 6, namely:

- movement is along the fracture sets and no assumption is made about the direction of movement based on the orientation of the hydraulic gradient;
- solute transport is not based on Brownian motion and therefore there is no need to assume that Fick's second law must be followed. Mass transport needs not to be Fickian, although it can converge to Fickian for late times;
- no assumption is made about the existence of a REV. In fact, CTRW converges to Fickian when a REV can be defined; otherwise transport is non-Fickian;

These three characteristics of the CTRW procedures are also common to Discrete Fracture Network Models and to the Statistical Continuum Method, and therefore they can only be regarded as advantages relative to the classical equivalent continuum model.

Nevertheless, the CTRW has other advantages. Particularly, CTRW procedures require very limited computational power and the size of the modelling area is not limited by computer resources. The computational power required is very similar to the one required for particle tracking procedures in continuous porous medium models such as MODPATH.

In addition, because the structure of the CTRW is the same as the random walks usually conducted in solute transport modelling, they can easily be made to work with the flow solution of numerical models such as MODFLOW.

As for the advantages relative to methods such as the Statistical Continuum or DFN models, they are mostly related to the input data required, which is far less in the CTRW than in those methods. The same can be said relative to other hybrid methods such as **hierarchical models** (Clemo and Smith 1997) or models that use discrete fracture networks to generate effective parameters or distributions of parameters (Robinson and Barker 1999).

The major disadvantage of the CTRW methodology is the likely difficulty of determining the values of the hydraulic parameters that compose it. This is particularly the case for directional choice, ρ_f, which may prove more illusive to determine than dispersivities or advective velocities.

6.6 SUMMARY OF CHAPTERS 5 AND 6 – PROTECTION ZONES FOR FRACTURE NETWORKS

Due to the complexity of the work carried out in relation to the definition of groundwater protection zones in fracture networks, which spreads through two chapters and several sections, it is appropriate to include a summary of the main research activities and results.

Section 5.2 was devoted to the generalization of a hybrid modelling technique, the Statistical Continuum method, so that it can be applied to the delineation of protection zones at the catchment scale. The SCM was implemented so that it uses a small scale DFN domain in which particle tracking is conducted to gain knowledge about the transport features of that particular fracture network. A computer code, STATMOV, gathers statistics about the velocity, path-length and direction taken by particles in the DFN domain. Those statistics are then used by a second code, SCPATH, to conduct particle tracking in a catchment scale domain. SCPATH uses a continuous porous media flow solution (e.g. MODFLOW) from which it reads the hydraulic gradient orientation and then conducts particle tracking, essentially replicating the movement in the smaller scale domain.

Sections 6.2 to 6.4 developed a different technique, the Continuous Time Random Walk (CTRW), which attempts to simplify the process of solute transport in fracture networks by discarding DFN models, while still maintaining the most important features imposed by the fracture network.

In section 6.2 two analytical solutions for solute transport according to one-dimensional CTRWs were established. The two solutions differ in the distribution assumed for the path-lengths (the length of each individual movement); a first solution assumes exponentially distributed path-lengths (section 6.2.1) and a second solution assumes power-law distributed path-lengths (section 6.2.2). The main difference implied by the two analytical solutions is that the exponentially distributed path-lengths cause solute transport to be non-Fickian at early times, but eventually will tend to Fickian transport, while the power-law distributed path-lengths may give rise to anomalous transport regardless of the observation time.

Section 6.3 was concerned with the use of those 1-D CTRW solutions to build procedures that enable two-dimensional solute transport to be modelled according to CTRW. The use of the 1-D CTRW solutions is necessary due to the difficulty in evaluating the general CTRW equation when multiple directions of movement are involved. The 2-D CTRW solute transport procedures are based on the generation of vectors from the 1-D CTRW, which are then added to find the new location of a particle. Two different procedures were defined, designated as Explicit and Implicit CTRW procedures.

Section 6.4 studied the variation of the CTRW parameters with hydraulic gradient orientation and implemented the 2-D CTRW procedures. Implementation was once again in code SCPATH, thus requiring the use of a MODFLOW flow solution at the catchment scale.

Both the SCM and the CTRW methodologies were applied to delineation of protection zones, using the SCPATH particle location output to conduct a statistical analysis with code PROBCONT, which assigns probabilities to each cell of the catchment scale finite difference domain to be included in a given protection zone. The commercial software SURFER can then be used to build contours of probability for the protection zone.

Figure 6.42 attempts to depict the work developed with respect to delineation of protection zones in fracture networks, as well as illustrating the connection between the several distinct parts of the research conducted.

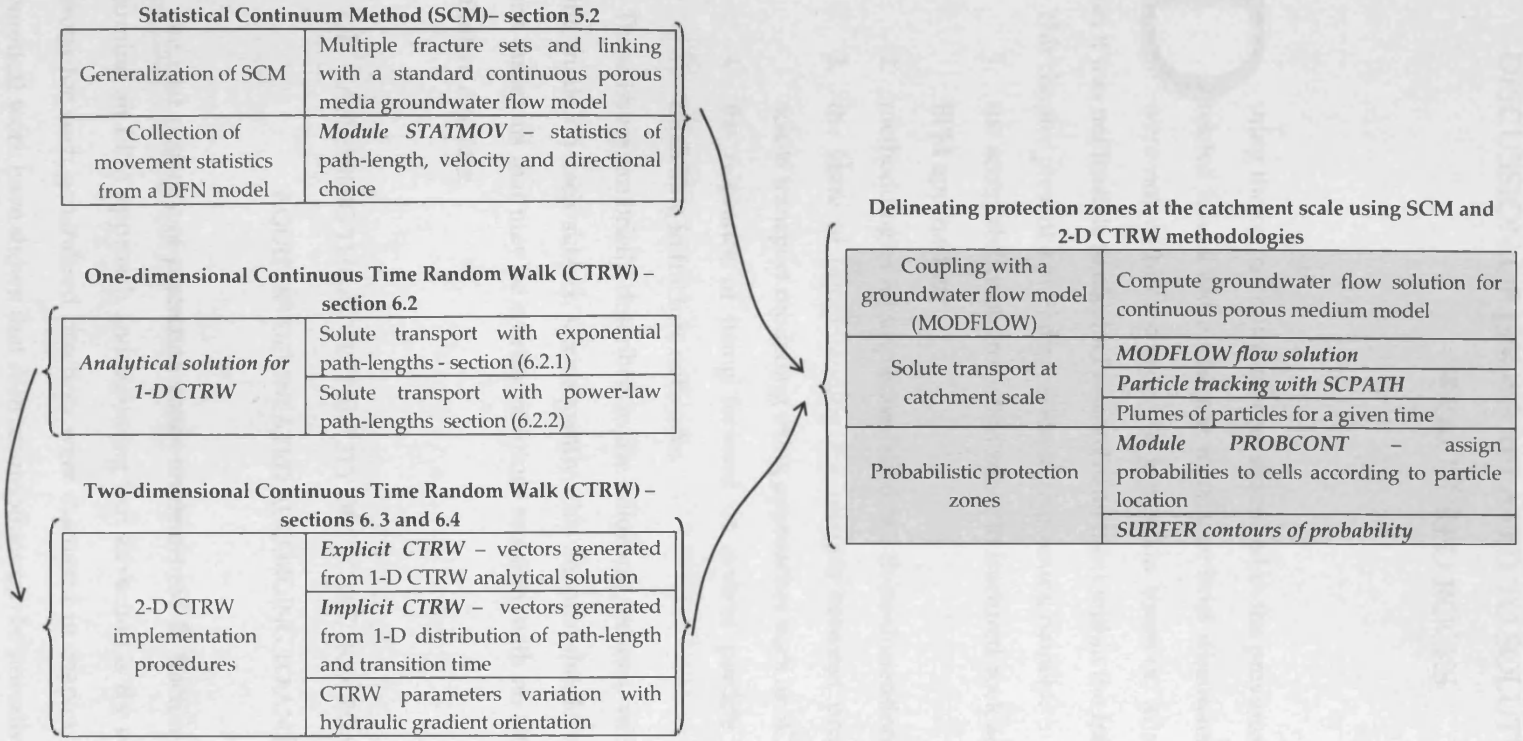

Figure 6.42 – Summary of research conducted with respect to delineation of protection zones in fracture networks (Chapters 5 and 6)

Chapter 7

DISCUSSION OF ISSUES RELATED TO SOLUTE TRANSPORT IN FRACTURED ROCKS

During the course of the studies described in the previous chapters some additional and related issues arose that are worthy of brief discussion. Either because those issues were not within the scope of protection zones or, in some cases, due to the lack of time, it was not feasible to conduct research into them within the framework of this thesis.

This chapter present a brief discussion of four issues, namely:

1. the acceptability of protection zones in fractured-rock aquifers delineated according to EPM approaches;
2. methodologies for implementation of a three-dimensional CTRW;
3. the issue of understanding the relation between probability and concentration in solute transport modelling using approaches such as SCM, CTRW or DFN models;
4. the relevance of using forward or reverse particle tracking on solute transport modelling in fracture networks.

These issues are briefly described in the following sections, with some general considerations being made on each subject. Consequently, this chapter should be seen as an attempt to raise some questions that may be worthy of future research, with no attempt being made here to find definitive answers.

7.1 ASSESSING THE ACCEPTABILITY OF PROTECTION ZONES IN FRACTURED-ROCK AQUIFERS DELINEATED ACCORDING TO AN EPM APPROACH

The vast majority of protection zones implemented in fractured-rock aquifers are delineated assuming an EPM approach and assuming that advection is the only transport mechanism. The reasons for such generalised practices were discussed in chapter two. However, both field and theoretical work have shown that such assumptions can be unrealistic.

The methods presented in chapter five, namely the SCM and the CTRW methods, allow the delineation of protection zones without the need to make general assumptions about the transport behaviour. Section 6.4 also shows that transport may be non-Fickian at early times, but that it may tend to Fickian behaviour for late times, with a REV being definable. This is particularly the case for 2-D CTRW with exponentially distributed path-lengths.

The time (or distance) necessary for Fickian behaviour to be achieved is a measure of the acceptability of the EPM approach. If convergence to Fickian behaviour occurs rapidly, then it should be reasonable to delineate protection zones using the relatively simple and well-studied EPM based methodologies.

7.1.1 Differences between Fickian transport and CTRW transport

Assuming that a 2-D CTRW with exponentially distributed path-lengths can provide an acceptable description of transport in a fracture network, the differences in solute transport modelling between the CTRW methodology and the advective-dispersive (Fickian) models are:

a) dispersion will always occur in a fracture network, even if non-dispersive advection is the only transport mechanism within each individual fracture;
b) the main flow direction may not coincide with the hydraulic gradient orientation;
c) the CTRW parameters that describe the transport mechanism will vary according to hydraulic gradient orientation;
d) in each fracture direction, dispersion will not be normally distributed in space and skewness may be very important but, for late times, solute distribution will tend to a normal distribution.

Quantifying items a) through d) above should provide a measure of the acceptability of the EPM approach.

7.1.2 The importance of dispersive effects

Because the EPM-based methodologies for delineating protection zones usually regard advection as the single transport mechanism, it is interesting to consider the relative importance of advection and dispersion in transport in fracture networks.

The relevance of the dispersive effects can be assessed using the **Peclet number**, a dimensionless number that relates the effectiveness of transport by advection to the effectiveness of transport by dispersion (Fetter 1999). The Peclet number is defined as:

$$P_e = \frac{vl}{D} \tag{7.1}$$

where v is advective velocity, D is the dispersion coefficient and l is some characteristic length. The larger the Peclet number the more dominant is advection over dispersion.

Using the mean travelled distance as the characteristic length, the Peclet number can be expressed as:

$$P_e = \frac{v^2 t}{D} \tag{7.2}$$

where t is travel time.

For the 1-D CTRW described by equation (6.28), and using the definitions of velocity and dispersion given by equations (6.25) and (6.26), respectively, the Peclet number is evaluated as:

$$P_e = \gamma t \tag{7.3}$$

where γ is the step rate. That is, the Peclet number of a 1-D CTRW is the number of steps occurring in time t. As expected, for large times, advection gains importance over dispersion, implying that the EPM approach becomes increasingly acceptable with increasing travel time.

For 2-D flow, it is necessary to define advective velocity as the resultant of movements in multiple directions. The overall advective speed will then derive from the sum of n differently orientated vectors:

$$v^2 = \left[\sum_{j=1}^{2n} v_j \cos(\theta_j)\right]^2 + \left[\sum_{j=1}^{2n} v_j \sin(\theta_j)\right]^2 \tag{7.4}$$

or using equations (6.27) and (6.48):

$$v^2 = \left[\sum_{j=1}^{2n} \frac{\gamma_j^T}{\lambda_j} \cos(\theta_j)\right]^2 + \left[\sum_{j=1}^{2n} \frac{\gamma_j^T}{\lambda_j} \sin(\theta_j)\right]^2 \tag{7.5}$$

where θ_j denotes the movement orientation and γ_j^T is the overall step rate (equation 6.48)[1]. The subscript j refers to the j^{th} movement direction.

Because longitudinal or transverse dispersion coefficients cannot be defined since, at least for early times, movement cannot be described according to a dispersion tensor, it is necessary to define an overall dispersion coefficient. Using equation (6.26), the following was adopted:

$$D = \sum_{j=1}^{2n} D_j = \sum_{j=1}^{2n} \frac{\gamma_j^T}{\lambda_j^2} \tag{7.6}$$

Applying equations (7.5) and (7.6) in equation (7.2), returns a 2-D Peclet number:

[1] Notice that there is no need to volume weight the overall velocity vector in equation (7.5) because the parameter γ_j^T (the overall step rate) already encompasses the influence of differences in fracture length and fracture spacing for the several fracture sets.

$$P_e = \frac{\left[\sum_{j=1}^{n} \frac{\gamma_j^T}{\lambda_j} \cos(\theta_j)\right]^2 + \left[\sum_{j=1}^{n} \frac{\gamma_j^T}{\lambda_j} \sin(\theta_j)\right]^2}{\sum_{j=1}^{n} \frac{\gamma_j^T}{\lambda_j^2}} t \tag{7.7}$$

This Peclet number should vary with hydraulic gradient orientation since the values of the parameters γ and λ are also dependent on that same variable. However, and as seen in section 6.2, the equations that describe the variation of those parameters are very complex and it is unfeasible to describe the Peclet number as a function of hydraulic gradient orientation.

7.1.3 Deviation from Fickian dispersion

The differences in the dispersive properties of the CTRW and the Fickian models can be assessed by studying the deviation between the CTRW distribution (equation 6.28) and the normal distribution. Such deviation can be quantified using the skewness (Ω) of the CTRW distribution, which is given by equation (6.29), rewritten here as:

$$\Omega_j = \frac{3}{\sqrt{2t\gamma_j}} \tag{7.8}$$

Due to the inverse proportionality with respect to t, the larger the observation time, the smaller is skewness.

If it is taken into account that in every fracture set, movement can occur in two opposite directions, we can choose to define the 1-D skewness imposed by every fracture set as the difference of skewness in the opposite movement directions of each fracture set:

$$\Omega = \frac{3}{\sqrt{2t}}\left(\frac{1}{\sqrt{\gamma_i}} - \frac{1}{\sqrt{\gamma_{i+n}}}\right) \tag{7.9}$$

where $2n$ refers to the total number of possible movement directions (twice the number of fracture sets, n).

To get an overall value of 2-D skewness it is assumed that the skewness of every fracture set can be added to the skewness imposed by the other sets, so that:

$$\Omega = \frac{3}{\sqrt{2t}} \sum_{i=1}^{n}\left(\frac{1}{\sqrt{\gamma_i}} - \frac{1}{\sqrt{\gamma_{i+n}}}\right) \tag{7.10}$$

This overall value of skewness is zero when transport is Fickian, while in the 2-D CTRW model varies in the range $[-\infty, \infty]$, with deviation from Fickian behaviour increasing with increasing absolute value of skewness.

7.1.4 Deviation in flow orientation

The main flow direction in the CTRW model is a function not only of hydraulic gradient orientation, but also of fracture orientation. The main flow direction (η) can be computed simply by finding the orientation of the sum of vectors that represent movement in all possible directions[1]:

$$\eta = \tan^{-1}\left[\frac{\sum_{j=1}^{2n} v_j \sin(\theta_j)}{\sum_{j=1}^{2n} v_j \cos(\theta_j)}\right] = \tan^{-1}\left[\frac{\sum_{j=1}^{2n} \frac{\gamma_j^T}{\lambda_j} sin(\theta_j)}{\sum_{j=1}^{2n} \frac{\gamma_j^T}{\lambda_j} \cos(\theta_j)}\right] \tag{7.11}$$

As seen in section 5.2, fracture networks are very likely to show anisotropy both in terms of hydraulic conductivity and in terms of effective porosity – a 'complete' anisotropy. Since under isotropic and homogenous conditions the flow direction and the hydraulic gradient orientation (Θ) coincide, the difference between Θ and η is a measure of the anisotropy imposed by the fracture network geometry.

That deviation (ω) can be computed as:

$$\omega = \frac{2(\Theta - \eta)}{\pi} \tag{7.12}$$

where $\pi/2$ is introduced only to normalize the error, so that it varies in the domain [0, 1], with $(\Theta - \eta)$ being expressed in radians.

The standard procedure for delineating protection zones usually considers isotropic systems, or, in more comprehensive studies, anisotropy in hydraulic conductivity. Anisotropy in the effective porosity is never considered. Therefore, the measure of 'complete' anisotropy given by ω can be envisaged as a measure of how adequate are isotropic and anisotropic K models for delineating protection zones in fracture network aquifers.

7.1.5 Validity of the EPM approach

The three indices defined in the previous sections give some insight into the validity of using the EPM approach to model transport in a fracture network:

- P_e, the Peclet number, returns information on the relative importance of advection and dispersion in the fracture network. The higher the result of equation (7.7) the less important are the dispersive effects and the more acceptable is the EPM approach;

[1] The same remark previously made about volume weighting applies to equation (7.11)

- ω, is the relative error between mean flow direction and hydraulic gradient orientation, and the closer it is to zero the more acceptable is the use of isotropic and anisotropic K continuum models;
- $|\Omega|$, the absolute deviation of skewness from the normal distribution is also a measure of the importance of non-Fickian transport in the fracture network. The validity of the EPM assumption increases when this parameter approaches zero.

The joint use of these three parameters should give a preliminary indication of the acceptability of protection zones delineated according to methodologies based on the EPM approach.

To test the effectiveness of the parameter mentioned above, the fracture network thus far designated as the **base case** was once again used (see fig. 5.13 and table 5.1), with the corresponding CTRW parameters according to table 6.1. The indices computed are displayed in figure 7.1.

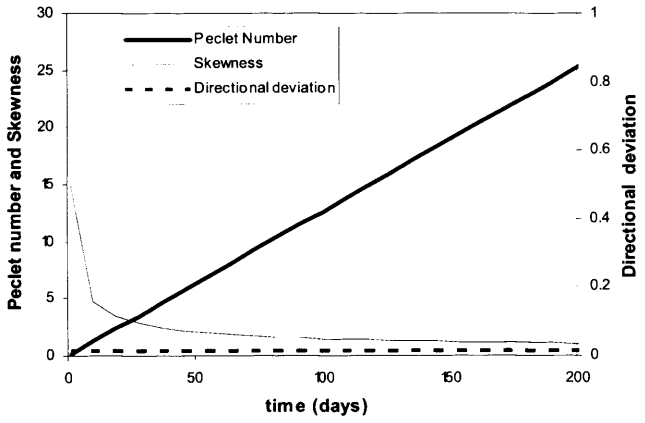

Figure 7.1 – Peclet number, skewness and deviation in flow orientation for the base case. CTRW parameters according to Table 6.1.

For early times, up to around 10 days, the Peclet number indicates that dispersion dominates over advective transport. For t = 100 days, P_e = 12.6 and advection is predominant, but it is likely that dispersive effects cannot be ignored. As for skewness, $|\Omega|$, its value decreases rapidly from 15 at 1 day, to 1.5 at 100 days. Finally, the error in movement direction, ω, is constant with time and is small, 0.014.

It can be concluded that:

- the error in the main movement direction is negligible, indicating that the use of isotropic continuum models would be acceptable to represent advective movement;

- dispersive effects cannot be ignored for times up to 10 days, certainly, and maybe even for later times, around 100 days. This is highly unfavourable for adoption of the EPM model;
- distortion of the plumes is considerable, although decreasing rapidly with time. Comparison with figure 6.26, depicting plumes tracked by the Implicit CTRW and by the SCM, show consistency with the skewness factors computed, with the plumes highly skewed for 1 day ($|\Omega| = 15$) and approaching a bivariate normal distribution for 100 days ($|\Omega| = 1.5$). Therefore, this parameter shows that for early times, say up to 100 days, it would not be adequate to assume an EPM approach.

Of the three parameters defined in this section two indicate that the EPM assumption is not adequate for early times, say until t = 100 days. Therefore, isochrone delineation for those times would require the use of methods that represent accurately the transport features of a fracture network.

However, the question arises if it would be adequate to delineate protection zones for large time isochrones, say 10000 days, using an EPM approach. Obviously, for such large times the skewness and dispersive effects are not relevant, since transport by advection would largely dominate and any plumes would be described by bivariate normal distributions.

Although further and more systematic research should be carried, it is argued that the main constraints on the shape of the protection zones, isochrones or plume of contaminants are imposed by the transport features at early times. If particles were to be tracked by the CTRW, the SCM or by any DFN model, the transport features at early times would result in a set of paths that could not be replicated either by the purely advective model or by any Fickian transport model that required the definition of a REV. Although for later times such differences would attenuate, the fact would be that the paths initially taken by the particles would influence their full paths, rendering it impossible to be approached by an EPM assumption.

Of course, this effect of propagation of the non-Fickian and non-advective behaviour is directly proportional to the time length necessary to admit an EPM assumption. For instance, in the base case under consideration, that time is around 100 days, which allows the particles to travel for 100 days without their paths being replicated by the EPM model. After 100 days the EPM approach becomes acceptable and the Fickian model could then be used to simulate solute transport for the remaining travel time. However, the resulting final paths would depend upon the locations at t = 100 days, thus making them impossible to be reproduced by any Fickian model that had been

used from the onset of transport, since the paths delineated at t = 100 days would be different in the two situations.

Were the time necessary to accept the EPM assumption much smaller, for instance 0.1 days, particles would not be able to spread a large distance and the EPM results would be more adequate at late times. The larger the time t_0 necessary to admit the EPM assumption, the less viable is the use of the EPM approach for times above t_0. This effect is likely to become particularly important under non-uniform flow conditions, such as around wells or close to hydraulic boundaries.

Notice, for instance, figure 6.38 and figure 6.39, depicting the 10000-day capture zone for three wells. The capture zones were delineated using the CTRW model with the same parameters used to compute the parameters above and the purely advective model. Although the travel time is very large, much above the 100 days necessary to validate the EPM assumption, there are considerable differences between the results of the CTRW model and of the EPM model. Such dissimilarities are due to the transport features at very short times, which cause the particles to take paths that cannot be reproduced by the EPM model. This effect is enhanced by the use of reverse particle tracking, because particles are travelling larger distances at early times, in the immediate vicinity of the pumping wells where hydraulic gradients are steep.

7.2 CONSIDERATIONS ON THE IMPLEMENTATION OF A THREE-DIMENSIONAL CTRW

Realistic use of Discrete Fracture Network models to simulate solute transport should preferably be done in a 3-D environment. Even under hydraulic conditions involving fully confined aquifers, where flow may be regarded as two-dimensional, the use of DFN models would usually require consideration of three dimensions.

The need to consider 3-D environments is not directly related to the hydraulic features to be modelled, but rather to the geometric characteristics of the fracture network. If field data were used to define a fracture pattern that is going to be transposed into a 2-D DFN model, most likely the 2-D network would not be connected. The third dimension is necessary to ensure connectivity of the fracture system.

Because the SCM is based on the previous use of a DFN model, the same requirement of 3-D modelling must be imposed, even though the use of the SCM in the continuum environment can actually be conducted solely in two dimensions (provided the flow field is regarded as horizontal).

As for the Continuous Time Random Walk method, there is no obvious necessity to use three-dimensional modelling, as long as the flow field can be envisaged as predominantly horizontal. Because the CTRW is based uniquely on hydraulic parameters of the fracture network, and fracture orientation is the only geometric feature used, then there are no issues of connectivity involved.

Nevertheless, normally flow conditions cannot be regarded as purely horizontal and vertical flow and transport occurs, either because the aquifers are not confined, or due to the hydraulic boundaries of the aquifers. Under such conditions, any modelling tool must consider that transport will occur also in the vertical dimension. Therefore, it would be interesting to try to implement the CTRW method in three dimensions.

This can be achieved in two different manners, firstly considering that all movement occurs along the plane of fractures and can be modelled adding 1-D CTRW vectors and secondly assuming that transport in the vertical direction can be assimilated to Fickian transport.

7.2.1 Movement along fractures planes modelled according to 1-D CTRWs

Solute transport in a 3-D fracture network is still restrained to the planes of the fractures. Instead of solutes (or particles) moving only in the direction (strike) of the fracture, such as in 2-D networks, the particles can now move in the plane of the fracture.

Although a path, from the point a particle enters the fracture to the point it leaves it, may be very complex depending on the distribution of hydraulic potential in the plane of the fracture, it is always possible to define a simplified path. This coincides with the vector that joins the point of entrance and the point where it leaves the fracture. Therefore, each fracture plane defines a 2-D domain where a set of vectors will determine the movement of the particles.

Parney (1999) studied the path of particles in a 3-D fracture domain, using the FRACMAN / MAFIC suite. He concluded that the paths inside each fracture can be described in terms of two angles (fig. 7.2), the angle with the horizontal (θ) and the angle with the vertical (ϕ). Each direction taken by the particles could be described by a simple function relating these two angles, with the fit between that function and the actual path being quite good (fig. 7.3).

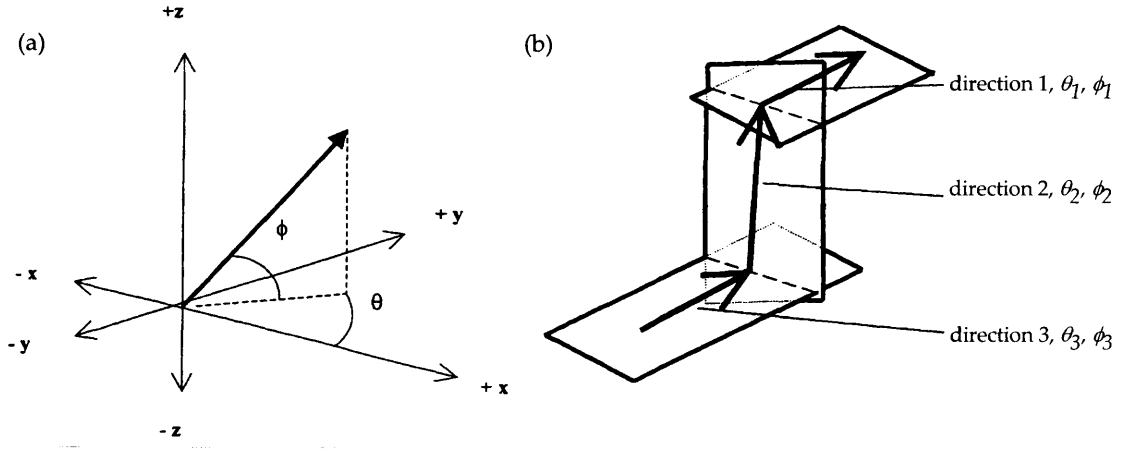

Figure 7.2 – a) definition of θ and ϕ (note the axis is rotated for display purposes). **b) Diagram illustrating particle movement according to vectors defined by θ and ϕ.** After Parney (1999).

Each of those directions is related to a certain probability of occurrence and with distributions of path-length and velocity. That is, the structure of movement in each 2-D fracture plane is essentially the same as defined for a 2-D fracture network, with CTRW dependent on path-length, transition times and directional choice parameters.

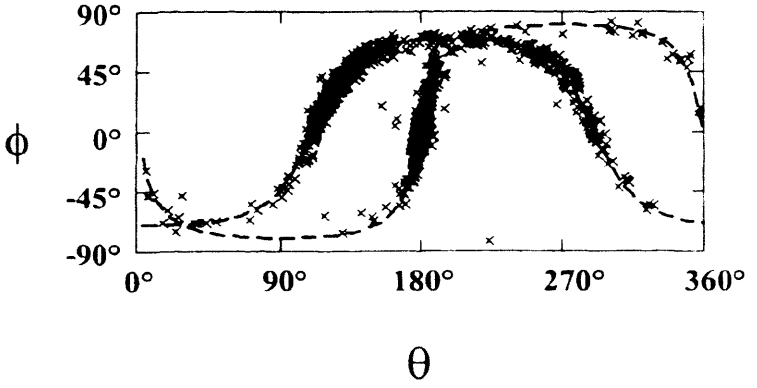

Figure 7.3 – Scatterplot of θ and ϕ with a theoretical relationship overlaid. Symbol × are vectors in the planes of two distinct fracture sets; dashed lines are theoretical relationships. From Parney (1999).

The important difference to the 2-D fracture network is that a continuous ensemble of possible movement directions spans the whole fracture plane (fig. 7.4). The difficulty of implementing a 3-D CTRW is related to the way on which this ensemble of paths could be dealt with.

The most viable way is to consider the ensemble of paths as a set of independent vectors, thus defining a group of discrete movement directions. That is, the continuous distributions of orientations would be discretized into a finite number of vectors (fig. 7.4), each of which could be modelled according to 1-D CTRW.

Therefore, the 3-D CTRW could be conducted in essentially the same way as the Implicit 2-D CTRW. At each step, a fracture plane would be selected and the CTRW would be conducted in the 2-D fracture plane, with a vector direction being selected and the CTRW general equation allowing to find the probability of particles travelling some distance along that vector.

Although the procedure should not be too difficult to implement, a different issue is how to define the variation of the CTRW parameters (step rate and path-length) with hydraulic gradient orientation. It is not clear if the methodology followed in section 6.4.1 would be adaptable.

The general ideas stated here need verification by conducting systematic research. Nevertheless, it is considered that the procedure could be implemented, although issues such as how to determine the relevant parameters could be very difficult to solve.

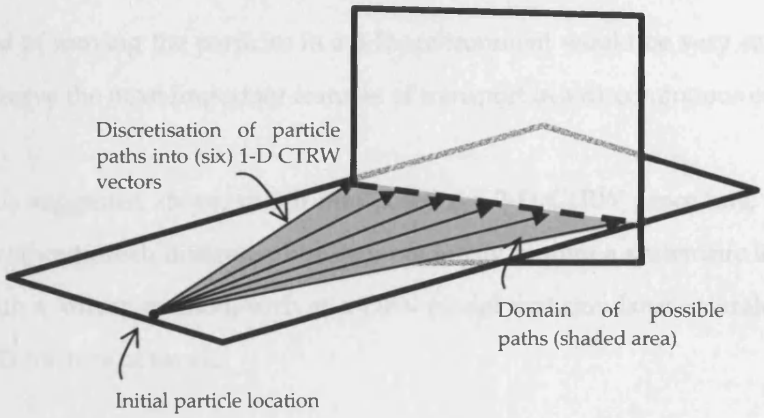

Figure 7.4 – Discretisation of paths on a fracture plane into a set of vectors, each described by θ_j and ϕ_j and treated as a one-dimensional CTRW.

7.2.2 Fickian transport assumption in the vertical direction

The need to use CTRW in fracture networks arose from the fact that the transition times (the time that a particle takes to complete a path-length), can be quite large when compared to the observation time, invalidating the similarity with the Brownian motion, on which the Fickian laws are based. However, the need to use the CTRW approach to describe vertical solute transport movement can be disputed.

In natural groundwater systems horizontal movement of water will prevail over vertical movement, except at recharge and discharge areas. Therefore, the frequency of particles travelling in the vertical direction (directional choice) is small and such movement will coincide with smaller path-lengths and shorter transition times.

This is particularly the case in fractured-rock environments, where vertical movements will be induced mostly by the need to ensure connectivity and will tend to occur with equal probabilities in the 'upward' and 'downward' directions. Given that path-lengths and transition times are shorter and with equal probabilities of occurring in opposite directions, the CTRW should soon tend to a normal distribution, and the Fickian assumption should be acceptable.

This reasoning needs confirmation but, if valid, the 3-D CTRW would simply be conducted in two steps: the first step being any of the 2-D CTRW procedures described in section 6.2 (simulation of solute transport by generating vectors from the 1–D CTRW for each direction of movement and add those vectors to find the particle location); the second step would simulate dispersion in the vertical direction by using a dispersion coefficient, as is usually done in Fickian transport.

This method of moving the particles in a 3-D environment would be very easy to implement and would preserve the most important features of transport in a discontinuous environment.

The methods suggested above, to put into practice a 3-D CTRW procedure, can probably be implemented without much difficulty, but they obviously require a systematic investigation and comparison with a 'direct' method, such as a DFN model that simulates accurately the transport features of a 3-D fracture network.

7.3 PROBABILITY AND RELATIVE CONCENTRATION IN FRACTURE NETWORK MODELLING

The equations that describe Fickian transport, such as the advection-dispersion equation (6.4), are expressed in terms of solute concentration and attempt to define its variation in time or space. This occurs despite the Fickian model being the statistical representation of a random phenomenon, Brownian motion.

In fact, application of the Fickian model simply gives the concentration of a substance, knowing that its travel distance is distributed according to a normal probability density function. Therefore, probability and relative concentration are used interchangeably in the Fickian model. This was clear in section 4.2, where delineation of protection zones in dual-porosity aquifers was conducted according to the standard equations for relative concentration variation and its result was interpreted in terms of probability.

The issue is to understand if probability and relative concentration can still be regarded as equivalent under non-Fickian conditions, such as those modelled by the SCM, the CTRW or DFN models.

The plumes of particles tracked by the SCM, the CTRW or by multiple realisations of DFN models, do in fact represent the probability of a single particle being at a given location at a certain time. This, of course, requires that the density of particles at a given area is divided by the total number of particles tracked (fig. 7.5). However, it is argued that this probability cannot be interpreted as relative concentration.

The reasoning is probably easier to understand by referring to Discrete Fracture Networks, although the conclusions are equally valid for the SCM or the CTRW models.

Assuming that a DFN model is an acceptable representation of a fractured-rock aquifer, then, of the infinite number of possible fracture network realisations, only one realisation represents exactly the geometry and hydraulic characteristics of the aquifer to be modelled. If a solute (or an ensemble of particles) were to be released at any location of that specific fracture network, the spread at fracture intersections would represent the actual solute dispersion (fig. 7.6a). Probability and relative concentration would coincide.

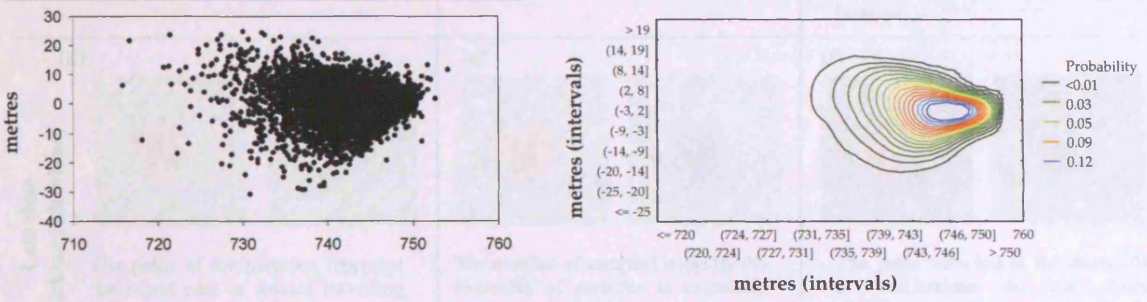

Figure 7.5 – Relation between particle location and probability. a) plume of particles developed after t = 10 days; b) corresponding probabilities of a single particle being located at some point of the domain. 5000 particles were released at x =750 m, y =0 m, and were tracked for t = 10 days. Uniform flow from right to left.

However, such concentration is only correct for the specific realisation that represents accurately field conditions. An infinite number of other realisations would return spreads of particles that would not represent the dispersion of the solute as it would actually occur (fig. 7.6b). Since it is not possible to distinguish the 'correct' realisation, and since in principle every realisation has the same chance of occurring, then it is not possible to say that any of the particle plumes give solute concentration.

In fact, each realisation would represent an equally valid 'relative concentration'. The ensemble of possible 'relative concentrations' would merely represent the probability of a certain

concentration occurring in any location and not the average (or any other measure) concentration that would occur at that site.

If multiple realisations of the DFN are combined, which is essentially the same that is done in the SCM and CTRW methodologies, it is possible to build a single plume (fig. 7.6c). This single plume represents the probability of a particle reaching some location and the density of particles in one place is related to the probability of some concentration occurring at such place.

Therefore, under the conditions modelled by DFN models and by the SCM and CTRW methods, probability and relative concentration are not necessarily interchangeable concepts.

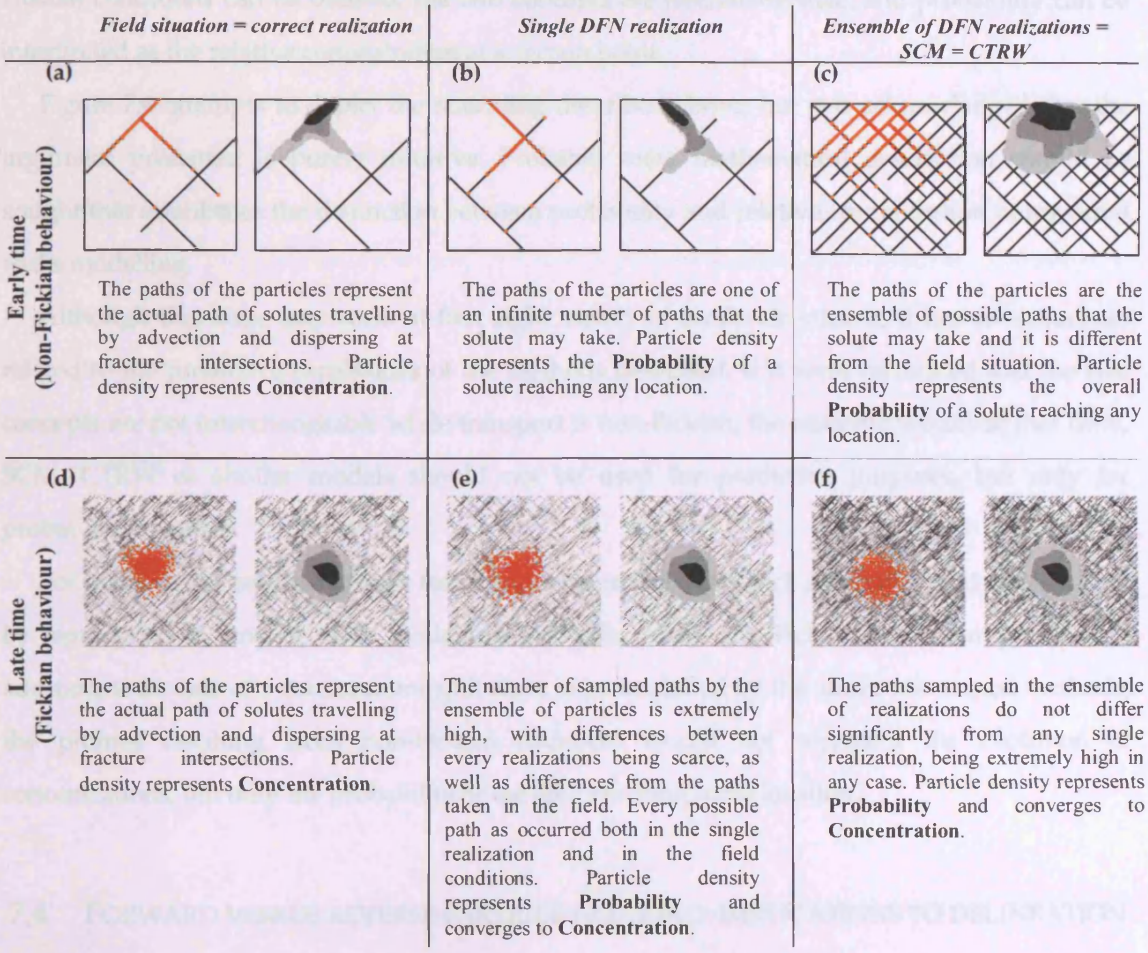

Figure 7.6 – Diagram illustrating the differences in the probability and concentration concepts in solute transport simulation in fractured rocks domains, under non-Fickian and under Fickian conditions. Red dots represent particles and shaded contours refer to probability or relative concentration as indicated.

However, as was already stated in previous chapters, depending on the fracture characteristics, solute transport in fracture networks might tend to Fickian behaviour for large times or travel distances (fig. 7.6d). Solute transport can then be accurately represented by

dispersion coefficients. Under such circumstances, it is not relevant which of the fracture networks is correct or not. The particles would have sampled so many path-lengths that any realisation would return the full range of paths represented by dispersion coefficients (fig. 7.6e and 7.6f). The plumes thus delineated would allow retrieving probability and this would coincide with relative concentration.

Summarising, the methods for modelling solute transport in fractured rocks, such as DFN models, SCM or CTRW, return probabilities of particles reaching some location, but while non-Fickian behaviour prevails, do not return relative concentration at that location. As soon as Fickian conditions can be defined, the two concepts are interchangeable, and probability can be interpreted as the relative concentration at a certain point.

Figure 7.6 attempts to depict the reasoning described above, but it is acknowledged that the argument presented is purely intuitive. Probably some mathematical description should be sought that establishes the distinction between probability and relative concentration in fractured rocks modelling.

Although this issue may seem at first sight merely of academic interest, it has consequences related to the predictive capabilities of the methods described. If it were confirmed that the two concepts are not interchangeable while transport is non-Fickian, the outcome would be that DFN, SCM, CTRW or similar models should not be used for predictive purposes, but only for probabilistic studies.

For instance, the results of tracer tests conducted in fractured-rock aquifers would certainly not be reproduced by any of those modelling methods, where non-Fickian behaviour prevails. In addition, if the fate of a contaminant spill were to be modelled by the above-mentioned methods, the plumes resulting from non-Fickian transport would not represent the evolution of concentrations, but only the probability of the spill reaching some location.

7.4 FORWARD VERSUS REVERSE PARTICLE TRACKING: IMPLICATIONS TO DELINEATION OF PROBABILISTIC PROTECTION ZONES

It is usually accepted that reverse and forward particle tracking procedures will lead to similar results in terms of the particles paths. In the specific case of delineation of protection zones the two methods are widely used, although with clear prevalence of reverse particle tracking. This predominance has to do with the fact, as explained in section 3.3, that reverse particle tracking is computationally more efficient.

It is also of common knowledge that protection zone delineation is slightly more precise if forward particle tracking is conducted, because all possible flow paths can be defined, not only those that end up at the pumping well. However, this increase in precision is negligible and certainly does not compensate for the loss of efficiency.

Throughout this thesis, particle tracking procedures always took the 'reverse' form, although the codes developed permit forward particle tracking. Yet again due to computational efficiency, reverse particle tracking was chosen.

However, in fractured-rock aquifer modelling, the issue of using reverse or forward particle tracking may not be negligible and the two procedures may not lead, in general, to the same results, particularly if a probabilistic approach is to be used.

Consider, for instance, figure 7.7 illustrating two fractures, one of which connects two points, A (upstream) and B (downstream). If reverse particle tracking were to be conducted, with particles being release at location B, it would be obvious that 100% of the particles would have travelled through location A. However, if forward particle tracking was initiated at location A, and since the two diverging similar fractures segments are orientated at 45°, only 50% of the particles would reach location B.

Thus, in the case of the reverse procedure, A would be located in the 0% probabilistic capture zone of B (0% particles travelling through A would not attain location B), while in the forward procedure it would be located in the 50% contour (50% of the particles travelling through A would not arrive at location B)[1].

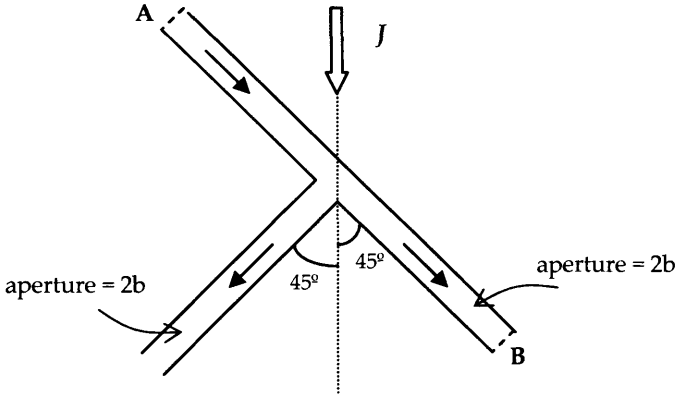

Figure 7.7 – Diagram for purposes of illustrating differences in forward and reverse particle tracking. The two fractures are hydraulically similar and after intersecting, carry the same amount of flux. Arrows indicate flow direction.

[1] Recall that the probabilistic contours of protection zones were defined in section 5.2 as "the percentage of particles that would take longer than time t to reach the well".

Although the example above is very simple, it allows us to draw the basic conclusion that, if particles are tracked backwards from a pumping well, all the possible paths conducting to that well will be sampled. However, and because of dispersion occurring at fracture intersections, if forward tracking were initiated at the end points of the reverse paths, a certain number of paths would not reach the well. Because of the probabilistic analysis that is usually associated with fractured-rock modelling, different probability calculations would result.

Figure 7.8 is a Venn diagram representing the differences in the number of particles that, starting from location A would reach a well, in both particle tracking procedures.

Forward procedure:

a) X is the number of particles released at location A; due to 'dispersive' effects at fracture intersections only Y_1 ($\leq X$) particles will reach the well, regardless of travelling time; of these a proportion P will reach the well after isochrone time *t*. Thus, the probability of particles arriving at the well after time *t* is $P_{forward} = Z_1/X$, where $Z_1 = PY_1$.

Reverse procedure

b) if the same number X of particles is released at the well, only Y_2 ($\leq X$) particles will eventually travel through location A; of these a proportion P will cross A after isochrone time *t*. Thus, the probability of particles travelling through A after time *t* is $P_{reverse} = Z_2/X$, where $Z_2 = PY_2$.

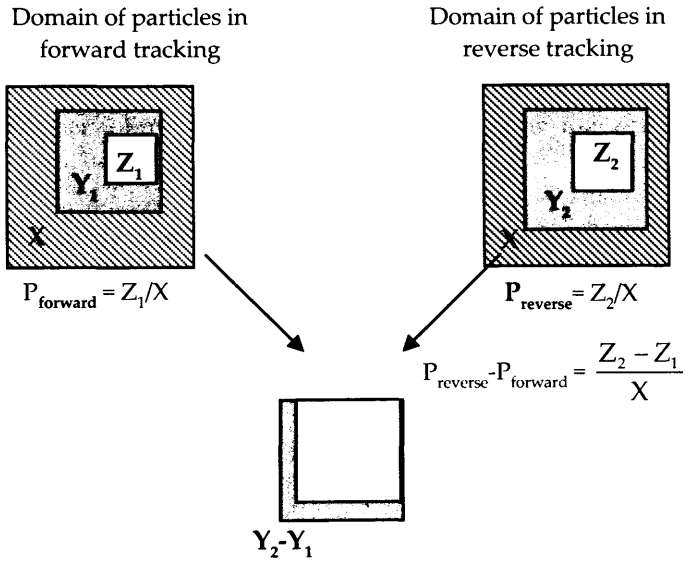

Figure 7.8 – Venn diagram illustrating the differences in probabilistic calculations between forward and reverse particle tracking procedures. X is the number of tracked particles; Y_1 is the number of particles reaching the well (forward direction), Y_2 is the number of particles passing through A (reverse direction); Z_1 and Z_2 are the proportion of Y_1 and Y_2 that reach the well or A after time *t*. The reverse procedure will return probabilities, $P_{reverse}$, higher than or equal to the forward procedure, $P_{forward}$.

Due to the effect depicted in fig. 7.7, and discussed above, $Y_2 \geq Y_1$ and therefore, $P_{reverse} \geq P_{forward}$. When conducting reverse particle tracking A would be classified in the $P_{reverse}$ probability contour. In the forward procedure it would be classified in the $P_{forward}$ probability contour. Thus, probabilistic protection zones delineated by the reverse procedure will be larger and wider than protection zones delineated by the forward particle tracking procedure

This fact has some connection with the success rate of tracer tests conducted in fractured-rock environments. It is well known that often those tests fail, with no recover occurring, or with recover much smaller than expected. If reverse particle tracking were to be conducted from the point of tracer collection, then a large area would be indicated as being within the capture zone of the well, leading to expectation of high success rates in tracer testing, which is in obvious disagreement with the above stated. On the other hand, forward tracking would indicate that the tracer could follow, at every intersection, other paths that would not reach the well, resulting in a smaller success rate for tracer tests, much in agreement to field situations.

A further example can be used to illustrate the differences between the two procedures. Figure 7.9 illustrates a fracture network domain, on which uniform flow was imposed from left to right, with impermeable boundaries on the top and bottom limits of the domain. The implicit CTRW procedure was used to simulate solute transport. Reverse particle tracking was done by releasing particles at location x_0 = 750 m, y_0 = [-10m, 10m]. All the particles left the domain at x = 400m, y= [-156m, 175m]. Particles were then released at this interval and forward tracking conducted. If the results of forward and reverse particle tracking were equivalent, particles should leave the domain at the right boundary in the interval x =705 m, y = [-10m, 10m]. However, particles left the domain in a much wider *y* limit, y = [-266m, 285m], indicating that the two procedures are not equivalent.

The reason why particle tracking in a continuous porous medium returns the same results whether the procedure is conducted in its forward or reverse forms, is that no dispersion is involved, since particle movement is modelled using strictly advection. In fractured-rock media, and although advection is the only transport mechanism at every fracture, dispersion occurs at fracture intersections, causing reverse and forward particle tracking to return different results.

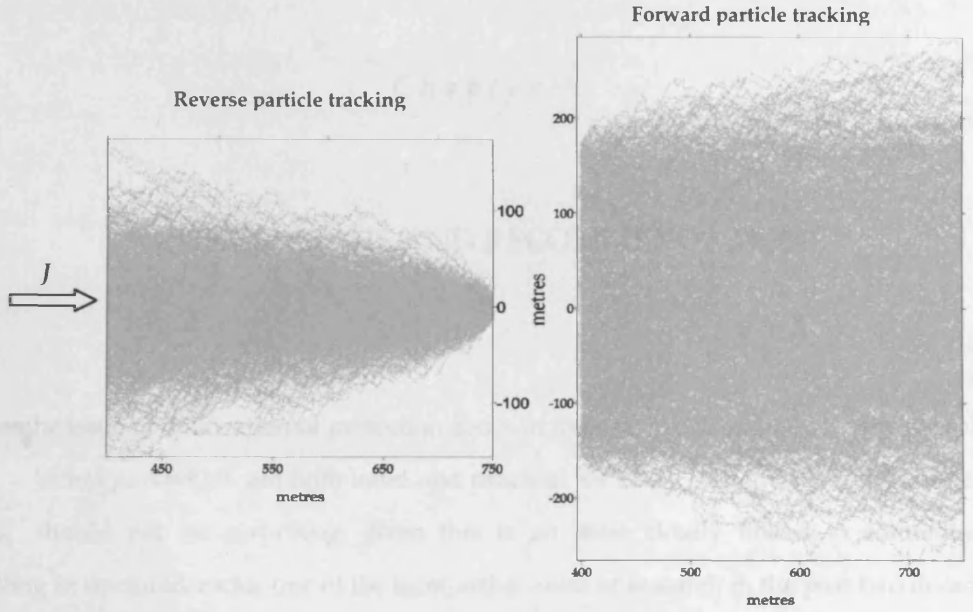

Figure 7.9 – Particles path in reverse and forward particle tracking procedures in a fracture network, under uniform hydraulic gradient conditions (from left to right). In the reverse procedure particles were released at x=750 m, y=[-10m, 10m] and left the domain at x=400m, y =[-156m, 175m]. These locations were used for forward tracking but the particles left at x= 750m, y =[-266m, 285m].

That being the case, should the probabilistic protection zones be delineated using forward or backward particle tracking? Because reverse tracking results in wider and longer protection zones a more conservative approach would recommend the use of that procedure. However, it is not clear what approach would be most convenient, particularly since the results of the forward procedure seem to be more in agreement to what is experienced in field studies involving tracer tests.

The fact is that the two procedures provide different information:.

- the reverse particle tracking procedure, gives '***x****% of the particles that have reached the well, coming from location z, took longer than time t to reach the well*';
- the forward particle tracking procedure, gives '***y****% of the particles released at location z will take longer than time t to reach the well* '.

Although the difference may seem merely linguistic, ***x*** will always be less than or equal to ***y***. It may be that the difference between the two is irrelevant and that any of the procedures will return similar probabilistic protection zones. Nevertheless, the importance of the difference between the two methods should be appreciated and should be investigated further.

Chapter 8

CONCLUSIONS AND RECOMMENDATIONS

The issue of delineation of protection zones in fractured-rock aquifers is very complex and techniques which are both valid and practical for every case are yet to be defined. This should not be surprising, given this is an issue closely linked to solute transport modelling in fractured-rocks, one of the most active areas of research in the past two decades, but that still has to produce definitive answers and tools to address the problem.

To overcome these difficulties with the hydrodynamic behaviour of fractured-rocks it has been usual practice to consider those environments as hydraulically equivalent to continuous single porosity media, thus allowing the use of well-established analytical and numerical solutions for delineation of protection zones. However, theoretical, laboratory and field studies have proved that, very often, the assumption of equivalence to a porous medium is not acceptable and results in protection zones that are hard to defend.

The aim of this thesis was to contribute to the development of methodologies for delineation of protection zones in fractured-rock aquifers that, while acknowledging that the hydrogeologic information available is often scarce, also preserves the flow and transport characteristics that are specific to fractured environments.

8.1 CONCLUSIONS

This thesis addressed delineation of groundwater protection zones in three different types of fractured-rock aquifers, each with distinct hydraulic properties. A first group is made up by **composite aquifer systems**, that is, aquifers comprised of a single long linear structure embedded in a homogeneous country-rock. **Dual and multiple-porosity aquifers** compose a second group, while the third group is composed of **fracture network aquifers**, more specifically; aquifers in which the fracture pattern is marked by some degree of randomness and fractures are regarded as finite in length.

In each case, motivation was to delineate protection zones taking into account the flow and transport features that are specific to each group of fractured-rocks, while overcoming the need to make *a priori* assumptions about equivalence to a continuous single porosity medium.

8.1.1 Composite aquifer systems

It is not uncommon for long linear structures, such as faults, dykes or veins, to be the target of groundwater exploration strategies, which aim to take advantage of the sometimes increased permeability of those structures. In the present study, consideration was given that the well to protect can be located either in the linear structure or in the country-rock. The linear structure is regarded as infinite and the country-rock is treated as an Equivalent Porous Medium (although it can be a fractured-rock, as long as the length of the fractures is negligible when compared to the length of the linear structure, and the fractures are sufficiently dense to ensure good connectivity).

The approach to delineate protection zones in this environment was analytical, with equations for the drawdown imposed by a pumping well being derived for transient and for steady-state conditions. The superposition of drawdown and a uniform hydraulic gradient allowed computation of flow velocities and led to a derivation of the stream function equation. The *Mathematica* software was used to contour the value of the stream function, thus making it possible to visualise the capture zone of a well.

Delineation of the isochrones in composite aquifer systems was achieved through a semi-analytical procedure, which computes the velocity at any location and conducts reverse particle tracking to delineate the isochrone, i.e. the protection zone. This procedure was realized as a FORTRAN code designated GPZFAULT.

Consideration of the hydraulic properties of both the linear structure and the country-rock is essential in delineating the protection zone. As expected, the orientation of the regional hydraulic gradient with respect to the linear structure is very important, affecting significantly the size, shape and symmetry of the capture zone and isochrones.

8.1.2 Dual and multiple-porosity aquifers

Delineation of protection zones in dual-porosity aquifers was also dealt with analytically. The problem was undertaken by finding the transport solution for a well injecting a contaminant, under steady-state flow conditions, into an aquifer where a uniform hydraulic gradient pre-exists.

Because the mathematical description of injecting a solute or of pumping a solute is symmetrical, the breakthrough curves also represent the time for a solute to reach a pumping

well. That is, the breakthrough curves are related to the protection zone isochrones. Since matrix diffusion causes retardation in transport, first arrivals tend to occur much later than predicted by a single porosity model and the solute concentration varies in time. This variation in concentration can be interpreted in terms of the cumulative probability of a single particle reaching a well within the isochrone t.

The solution found assigns probabilities of a particle reaching the well and, as such, defines the size of a probability related protection zone. Comparison with isochrones computed using single-porosity models shows that the protection zones in dual-porosity aquifers can be dramatically smaller, even if first arrivals (and not probabilities) are regarded as the criteria to define isochrones. The solution was implemented in a FORTRAN code, designated GPZDUALP.

However, the analytical solution presented is only valid for diffusing contaminants, not allowing for large particulate contaminants, and does not consider the possibility of occurrence of channelling. Further, the solution depends on the matrix diffusion coefficient, which varies between substances. Therefore, the solution presented should be regarded as a tool to assess the influence of the dual-porosity behaviour on the size and shape of protection zones, rather than as a tool for direct delineation of protection zones.

Besides addressing the problem of dual-porosity in the context of groundwater protection zones, the thesis also presents a new analytical multiple-porosity model. The model is intended to simulate the behaviour of hierarchical fracture systems, that is, fractured-rocks in which the main flow system is composed by 1st-order fractures, which are fed by a 2nd-order fracture system, which itself is fed by a 3rd-order fracture system, and so on. The 2-D flow and the 1-D transport solutions are presented in terms of block geometry functions to be used with the generalised well function. Both solutions allow for n hierarchical fracture sets and are implemented in MULTIPOROSITY, a FORTRAN code with an EXCEL interface.

MULTIPOROSITY allows computation of drawdown curves and concentration build-up curves (for slug or continuous sources). The results of MULTIPOROSITY compared favourably with aquifer tests simulated using a numerical 3-D fracture network code. The 3-D fracture networks were generated with FRACMAN code and included up to three fracture sets organised in a hierarchical pattern. The aquifer tests in those networks were simulated using MAFIC and the drawdown results were in general agreement with the ones predicted using the MULTIPOROSITY code, thus verifying the multiple-porosity solution.

8.1.3 Fracture network aquifers

Protection zone delineation for fracture networks is a more complex subject than the above and is not amenable to be dealt with the analytical and semi-analytical approaches adequate for the other fractured-rock groups.

The approaches used were based on trying to replicate the specific solute transport features that are observed in this type of fractured-rock aquifer. It was considered that neither the Discrete Fracture Network (DFN) models, nor the Continuum models (be it deterministic or stochastic) are practical for purposes of delineation of protection zones. A hybrid approach, combining the use of a DFN with a deterministic continuum model, was one of the methods used in this thesis.

The Statistical Continuum Method (SCM), a hybrid model developed during the 1980's and 1990's, was adapted to delineation of protection zones. Particle tracking was conducted in a small-scale DFN domain (75 m × 75m) and statistics of movement of the particles were collected. MODFLOW was then used to compute the hydraulic heads in a catchment-scale domain. Particle tracking was conducted in this larger domain by mimicking the statistics of movement found in the smaller DFN domain. The locations of the particles at time t were then analysed statistically to establish probabilistic protection zones.

A series of FORTRAN codes were written to implement this methodology, which is considered to have several advantages. Namely, it simulates solute transport in a large-scale domain whilst preserving the most relevant features imposed by the geometric and hydraulic characteristic of the fracture network. The procedure is computationally very efficient, allowing for multiple simulations in a straightforward manner. The main disadvantage of the method is the need to use a DFN domain to gather the statistics of movement, thus requiring a great deal of geometric and hydraulic information about the fracture sets.

A second approach to delineation of protection zones in fracture networks is based on an analytical solute transport model that, however, does not need to assume Fickian dispersion. This is accomplished by acknowledging that the Brownian motion theory, which can be used to explain dispersion coefficients in Fick's 2nd law, is not an adequate description of solute transport in fractured-rocks, where the time to complete each step may not be negligible compared to the observation period or protection zone time (thus opposing a fundamental assumption of Brownian motion). Instead of a random walk based on Brownian motion, it was argued that solute transport in fractured-rocks can be modelled according to a **Continuous Time Random Walk (CTRW)**.

Using the general formulation for a CTRW, the equations that describe solute transport were found. This was accomplished for 1-D transport considering both exponentially distributed and power-law distributed path-lengths. In every case, the probability of occurrence of a step was assumed to follow a Poisson distribution.

The 1-D CTRW with exponentially distributed path-lengths, which simulates fracture networks with a single scale length, shows non-Fickian behaviour for short times (or distances), while converging to a normal distribution (Fickian behaviour) for late times (or distances). Interestingly, although non-Fickian behaviour is observed, no scale effect occurs since dispersivity is constant throughout the whole process.

The 1-D CTRW with power-law distributed path-lengths, which simulates fracture networks with multiple scale lengths and/or with fractal properties, shows persistent non-Fickian behaviour, never converging to a normal distribution, for certain values of the β, the power-law exponent. In addition, a scale effect may also be observed.

The statistical parameters of the 1-D CTRW can be translated into hydrogeological significant parameters (advective velocity and dispersivity), allowing the purely statistical CTRW equations to be written in a form more appropriate to solute transport in fractured-rocks.

Formulations for the 2–D CTRW were also found, even though it was not possible to find purely analytical solutions for the multivariate probability density functions that describe the spread of solutes in a network. The solutions found are semi-analytical in that they add vectors generated from the 1-D CTRW equations taking into account the fracture set orientation. Based on those semi-analytical formulations, two procedures were defined for conducting solute transport according to a 2-D CTRW: an **'Explicit' CTRW** and an **'Implicit' CTRW** procedure.

The 'Explicit' procedure uses directly the 1-D CTRW equations, while the 'Implicit' procedure utilises distributions for both path-length and transition time (time to complete a step) in order to generate the vectors that need to be added to find the particle locations. These procedures were implemented both for the uniform flow case and for a varying hydraulic gradient case. Because the parameters of the CTRW (advective velocity and dispersivity) vary with hydraulic gradient orientation, relations between those parameters and the hydraulic gradient orientation had to be defined. In that manner, the 2-D CTRW could be implemented jointly with a continuous porous medium model (MODFLOW was used) to conduct particle tracking in catchment-scale domains, while maintaining the major features of solute transport imposed by the fracture network.

The CTRW methodology for modelling solute transport in fracture networks has several advantages over other methods, since it is computationally very efficient and preserves the

features of solute transport without the need to consider each fracture individually. It maintains the transport features imposed by fracture orientation and permits modelling of both Fickian and non-Fickian behaviour, since no assumptions are made *a priori*. Further, the CTRW methodology does not require much input information and, with the exception of fracture orientation, is based solely on hydraulic information, so that no issues of connectivity arise.

The main disadvantage identified so far is related with the need to find hydraulic parameters in the direction of the fracture orientations. Further work is necessary in this area.

8.1.4 Other issues

Besides addressing the problem of delineation of protection zones in the fractured-rock types aforementioned, some related issues were discussed in this thesis. Specifically, a methodology was suggested for assessing the acceptability of groundwater protection zones in fractured-rock aquifers delineated according to equivalent porous medium approaches. The methodology is based on the 2-D CTRW and on the evaluation of three indices: *Peclet number*, which quantifies the relevance of the dispersion imposed by the fracture network; *Skewness factor*, which evaluates the deviation of the CTRW from a normal distribution; *Directional deviation*, the angle between the hydraulic gradient orientation and the main advective movement direction. It is hoped that, together, these three indices provide a simple measure of the reliability of a protection zone delineated according to an equivalent porous medium approach.

Consideration was also given to methods for implementing a 3-D CTRW, with two approaches being suggested. A first one considering that addition of 1-D CTRW distributed vectors could be used in a 3-D environment, while a second method considers that vertical transport might be modelled as Fickian, while horizontally a 2-D CTRW would apply.

The issues of probability versus concentration and of forward versus reverse particle tracking were also briefly addressed. It was shown that, in fractured-rock aquifers, it is not necessarily true that the equations describing solute transport can be interpreted interchangeably in terms of relative concentration or probability. It was argued that while the solute transport behaviour remains non-Fickian, the models based on random walks or on Monte Carlo procedures return probabilities, and that these probabilities can only be interpreted as relative concentrations when Fickian behaviour is reached.

As for forward and reverse particle tracking, it was shown how the two procedures can return different results when conducted in fracture networks for obtaining probabilistic plumes of particles. This occurs due to the dispersive effects inherent to intersections in fracture networks,

which are fully represented in forward particle tracking, while being only partially characterised in reverse particle tracking.

The methods presented in this thesis are far from being definitive, widely applicable tools. However, the methodologies developed for composite aquifer systems and dual-porosity aquifers can be applied in a straightforward manner, as they require a limited amount of information about geologic conditions and hydraulic properties of the aquifers. The CTRW methodologies are at a less-developed stage, requiring further research efforts.

8.2 RECOMMENDATIONS FOR FURTHER RESEARCH

Several of the issues addressed in this thesis are thought to be worth of follow-up research. Obviously, one of the most interesting extensions of this thesis would be to try to implement the suggested methods under real field situations. However, the more theoretical research topics listed below would also be interesting ways forward:

8.2.1 Composite aquifer systems

1) An important assumption of the model developed in chapter three was that the linear structure did not impose a significant distortion to the regional uniform hydraulic gradient. This assumption is acceptable because the linear structure is considered as infinite, not acting either as a recharge or discharge conduit and that the width of the structure is negligible compared to the area of interest. It would be interesting to develop an equivalent model allowing for distortion of the regional flow field, so that the linear structure would act, at some distance, as a discharge boundary (probably a common situation under field conditions). Although the problem may be difficult to solve analytically, it should be possible to study the problem numerically;
2) It may also be interesting to study the velocity field imposed by a finite linear structure of known extent. This problem possibly can be dealt with semi-analytically, using models similar to the Gringarten and Witherspoon (1972) model for drawdown imposed by a well located in a finite fracture;
3) The model presented in chapter three also considered that the country-rock had the same hydraulic properties on both sides of the linear structure. Faults often create

situations of contact between different geological formations, with very distinct hydraulic properties. It would be useful to try to generalise the model so that it includes heterogeneity between each side of the linear structure;

4) The code GPZFAULT needs to be modified so that it can conduct particle tracking when the well is not located in the linear structure. This was not possible due to difficulties with the code structure (developed initially for a well located in the linear structure) and with a conceptual problem related to the width of the linear structure, which must be assumed when conducting particle tracking.

8.2.2 Dual and multiple-porosity aquifers

5) The MULTIPOROSITY code allows for block geometry shapes of slabs, cylinders and spheres. Each hierarchical level may have different geometries. The code could be generalized to allow for other geometries, with particular relevance for the *n*-dimensional sphere (which can be made to represent other shapes, such as slabs, cylinders, spheres) and for the mixture of shapes;

6) The multiple-porosity model, as well as the dual-porosity solutions, assume that water, heat or solute exchanges between 1st-order fractures and higher orders (or with matrix) occurs only through diffusion. However, in hierarchical fracture systems it is possible that, under some circumstances, higher order (shorter but more dense fractures) are more permeable than the 1st-order fractures, and therefore, multiple-permeability models should be used. This situation was discussed and analysed in section 4.4.3, but more systematic research should be conducted into the development of suitable analytical and numerical tools.

8.2.3 One-dimensional Continuous Time Random Walks

7) Further mathematical analysis of the one-dimensional CTRW with power-law path-lengths solution presented in section 6.2 is necessary. Such analysis should aim at defining the behaviour of the probability density function at late times, to establish if there is convergence to stable distributions, implying that Fickian behaviour is never attained;

8) Mathematical analysis of the 1-D CTRW with power-law distributed path-lengths should also aim at establishing unequivocally the hydrogeological meaning of the statistical parameters in that CTRW solution;

9) For the 1-D CTRW with power-law distributed path-lengths it was assumed that the steps of the random walk would follow a Poisson counting process, which is a common situation for many physical phenomena. Nevertheless, a DFN model could be used to generate fracture networks with power-law distributed fracture lengths, and eventually with fractal properties, to study the transition time distributions. If the Poisson process proves inadequate, the corrected distributions should be used to re-evaluate the 1-D CTRW;
10) A further improvement of the 1-D CTRW would be to incorporate matrix diffusion. It is not clear how this could be done, but certainly it would relate to the definition of step rates, the distribution of which would vary along the path of the particles.

8.2.4 Two-dimensional Continuous Time Random Walks

11) The 2-D CTRW solution defined in section 6.3 relies on the addition of vectors generated from the 1-D CTRW equation. Mathematical studies should be conducted in order to attempt to find a multivariate CTRW probability density function;
12) The CTRW parameter variation with hydraulic gradient orientation was characterised in section 6.4. The relations presented in that section are just approximations and should be improved through a more systematic mathematical analysis of the problem;
13) Research should be conducted in order to find methods for determining, using field test data, the hydraulic parameters that characterise the CTRW. These are directional parameters (direction coinciding with the orientation of the fracture sets) and methods should be sought to identify those parameters from field tests, such as tracer tests;
14) Application of Continuous Time Random Walks to model solute transport in fractured-rocks has been performed by other authors in manners completely different, and possibly more sophisticated, than the method presented in this thesis. It would be interesting to investigate thoroughly the differences between methodologies and try to find the common ground.

8.2.5 Related issues

Chapter 7 presented some issues that were regarded as interesting for further investigation. Those issues were discussed in some detail in that chapter so they are only briefly summarized here:

15) Establishing the acceptability of groundwater protection in fractured-rock aquifers delineated with equivalent porous medium approaches is an important subject. Not only are most of the protection zones implemented nowadays based on those methods but it is also likely that such practices will continue. It would be interesting to study whether the indices suggested in section 7.1 are really suitable to be used for that purpose and, if so, try to establish a clear methodology of application;
16) Try to implement the two methods suggested in section 7.2 for conducting a 3-D CTRW and compare those methods with the results of a 3-D DFN model (such as FRACMAN or NAPSAC);
17) Investigate in a systematic way the possibilities suggested in section 7.3 that probability and relative concentration might only be interchangeable concepts in fractured-rocks when Fickian behaviour is established. This may have interesting consequences on interpretation of modelling results and on the predictive capacities of stochastic modelling tools;
18) Compare the results of forward and reverse particle tracking in DFN models and in the SCM and CTRW methodologies. The FORTRAN codes developed for implementation of the SCM and the CTRW can be easily adapted to conduct forward particle tracking. A further way to address this issue may be using Graph theory, specifically Digraphs.

These research topics arise directly from the work described in this thesis and are not intended to establish a list of priority research interests for the general problem of delineation of protection zones or solute transport in fractured-rocks. While the topics stated seem the most interesting extensions of this work, it is emphasized that the most important complementary research would be implementation, under actual field conditions, of the methodologies developed.

Although much research is required, it is hoped that this thesis has produced some contributions to the quantitative analysis of the problem of delineation of protection zones in fractured-rock aquifers. Moreover, the attack on this problem has led to some theoretical investigations that may be of broad interest in the study of flow and transport in fractured rocks.

REFERENCES

Abdassah, D., and I. Ershaghi. 1986. Triple-porosity systems for representing naturally fractured reservoirs. Society of Petroleum Engineers Journal **281**:113-127.

Adamic, L. A. 2000. Zipf, Power-laws, and Pareto - a ranking tutorial. Xerox Palo Alto Research Center, Palo Alto.

Adams, R., and G. Parkin. 2002. Development of a coupled surface-groundwater-pipe network model for the sustainable management of karstic groundwater. Environmental Geology **42**:513-517.

Almendinger, J. E. 1994. The travel-time ellipse - an approximate zone of transport. Journal of Hydrology **161**:365-373.

Andersson, P., J. Byegard, and A. Winberg. 2002. Final report of the TRUE block scale project. TR-02-14, SKB, Stockholm.

Ando, K., A. Kostner, and S. P. Neuman. 2003. Stochastic continuum modeling of flow and solute transport in a crystalline rock mass: Fanay-Augéres, France, revisited. Hydrogeology Journal **11**:521-535.

Bai, M., D. Elsworth, and J. C. Roegiers. 1993. Multiporosity multipermeability approach to the simulation of naturally fractured reservoirs. Water Resources Research **29**:1621-1633.

Bair, E. S., and T. D. Lahm. 1996. Variations in capture-zone geometry of a partially penetrating pumping well in an unconfined aquifer. Ground Water **34**:842-852.

Bair, E. S., C. M. Safreed, and E. A. Stasny. 1991. A Monte-Carlo based approach for determining travel time related capture zones of wells using convex hulls as confidence regions. Ground Water **29**:849 - 855.

Bakker, M., and O. Strack. 1996. Capture zone delineation in two-dimensional groundwater flow models. Water Resources Research **32**:1309-1315.

Barenblatt, G. E., I. P. Zheltov, and I. N. Kochina. 1960. Basic concepts in the theory of seepage of homogeneous liquids in fissured rocks. J. Applied Mathematics and Mechanics **24**:1286 - 1303.

Barkai, E., R. Metzler, and J. Klafter. 2000. From continuous time random walks to the fractional Fokker-Planck equation. Physical Review E **61**:132-138.

Barker, J. A. 1982. Laplace transform solutions for solute transport in fissured aquifers. Advances in water resources **5**:98 - 104.

Barker, J. A. 1985a. Block-geometry functions characterizing transport in densely fissured media. Journal of Hydrology **77**:263-279.

Barker, J. A. 1985b. Generalised well-function evaluation for homogeneous and fissured aquifers. Journal of Hydrology **76**:143 - 154.

Barker, J. A. 1991. Transport in fractured rock. Pages 199 - 216 *in* R. A. Downing and W. B. Wilkinson, editors. Applied groundwater hydrogeology. Oxford Science Publications, Clarendon Press, Oxford.

Barker, J. A. 2002. Directional porosity. Appendix I. *in* J. N. Robinson unpublished PhD thesis - A fractured/fissured rock approach to groundwater protection zones. University College London, London.

Barker, J. A., W. Burgess, L. Fellman, T. Licha, J. McArthur, and N. Robinson. 1999. The impact of highway drainage on groundwater control. Research report 3, Jackson Environment Institute, London.

Barker, J. A., and D. M. J. MacDonald. 1990. A study of some simple models for the identification of protection zones around single wells. BGS Hydrogeology Series, Technical Report WD/90/58R.

Barker, J. A., and D. M. J. MacDonald. 2000. A manual for BGSPT: programs to simulate and analyse pumping tests in large-diameter wells. BGS Technical Report WC/00/17, British Geological Survey, Wallingford.

Barker, J. A., T. E. J. Wright, and B. A. Fretwell. 2000. A pulsed-velocity method of double-porosity solute transport modelling. *in* A. Dassargues, editor. Tracers and modelling in hydrogelogy. IAHS pub. 262, Liege, Belgium.

Barton, J. B., D. W. Risser, D. G. Galeone, and R. W. Conger. 1999. Case study for delineating a contributing area to a water-supply well in a fractured crystalline-bedrock aquifer, Stewartstown, Pennsylvania. Report 99-4047, USGS.

Bazant, L. 2001. Topics in applied mathematics: Random walks and diffusion. *in*. MIT lectures in applied mathematics.

Bear, J., and M. Jacobs. 1965. On the movement of water bodies injected into aquifers. Journal of Hydrology **3**:37 - 57.

Bear, J., C.-F. Tsang, and G. de Marsily. 1993. Flow and contaminant transport in fractured rock. Academic Press, San Diego.

Bear, J., and A. Verruijt. 1987. Modeling groundwater flow and pollution : with computer programs for sample cases. D. Reidel Pub. Co., Boston.

Benson, A. B. 1998. The fractional advection-dispersion equation: development and application. Unpublished PhD thesis. University of Nevada, Reno.

Berkowitz, B. 2001. Continuous Time Random Walk (CTRW) Theory. *in*. Brian Berkowitz website (http://www.weizmann.ac.il/ESER/People/Brian/CTRW/main.html).

Berkowitz, B., and C. Braester. 1991. Solute transport in fracture channel and parallel plate models. Geophysical Research Letters **18**:227 - 230.

Berkowitz, B., and H. Scher. 1995. On characterization of anomalous dispersion in porous and fractured media. Water Resources Research **31**:1461 - 1466.

Berkowitz, B., and H. Scher. 1997. Anomalous transport in random fracture networks. Physical Review Letters **79**:4038-4041.

Berkowitz, B., and H. Scher. 1998. Theory of anomalous chemical transport in random fracture networks. Physical Review E **57**:5858-5869.

Berkowitz, B., H. Scher, and S. E. Silliman. 2000. Anomalous transport in laboratory-scale, heterogeneous porous media. Water Resources Research **36**:149-158.

Bhatt, K. 1993. Uncertainty in wellhead protection area delineation due to uncertainty in aquifer parameter values. Journal of Hydrology **149**:1 - 8.

Bibby, R. 1981. Mass transport of solutes in dual porosity media. Water Resources Research **17**:1075 - 1081.

Blum, M. 1970. On the sums of independently distributed Pareto variables. SIAM Journal of Applied Mathematics **19**:191-198.

Boehmer, W. K., and J. Boonstra. 1987. Analysis of drawdown in the country-rock of composite dike aquifers. Journal of Hydrology **94**:199-214.

Bonnet, E., O. Bour, N. E. Odling, P. Davy, I. Main, P. Cowie, and B. Berkowitz. 2001. Scaling of fracture systems in geological media. Reviews of Geophysics **39**:347-383.

Boonstra, J., and W. K. Boehmer. 1986. Analysis of data from aquifer and well tests in intrusive dikes. Journal of Hydrology **88**:301-317.

Bourdet, D., T. M. Whittle, A. A. Douglas, and Y.-M. Pirard. 1983. A New set of type curves simplifies well test analysis. World Oil:95-106.

Bradbury, K. R., and M. A. Muldoon. 1993. Preliminary comparison of a discrete fracture model with a continuum model for groundwater movement in fractured dolomite. Open file report 93-6, Wisconsin Department of Natural Resources.

Bradbury, K. R., and M. A. Muldoon. 1994. Effects of fracture density and anisotropy on wellhead protection area delineation in fractured aquifers. Applied hydrogeology **3**:17-23.

Brown, S. R. 1987. Fluid flow through rock joints: The effect of surface roughness. Journal of Geophysical Research **92**:1337 - 1347.

Cacas, M. C., E. Ledoux, G. de Marsily, A. Barbreau, P. Calmels, B. Gaillard, and R. Margritta. 1990a. Modeling fracture flow with a stochastic discrete fracture network - calibration and validation .2. The transport model. Water Resources Research **26**:491-500.

Cacas, M. C., E. Ledoux, G. de Marsily, B. Tillie, A. Barbreau, E. Durand, B. Feuga, and P. Peaudecerf. 1990b. Modeling fracture flow with a stochastic discrete fracture network - calibration and validation .1. The flow model. Water Resources Research **26**:479-489.

Chen, C., and W. D. Stone. 1993. Asymptotic calculation of Laplace inverse in analytical solutions of groundwater problems. Water Resources Research **29**:207-209.

Chen, Z. X. 1989. Transient flow of slightly compressible fluids through double-porosity, double-permeability systems - a state of the art review. Transport in Porous Media **4**:147-186.

Chevalier, S., M. A. Bues, J. Tournebize, and O. Banton. 2001. Stochastic delineation of wellhead protection area in fractured aquifers and parametric sensitivity study. Stochastic Environmental Research and Risk Assessment **15**:205-227.

Chiang, W.-H., and W. Kinzelbach. 2001. 3D-groundwater modeling with PMWIN: a simulation system for modeling groundwater flow and pollution. Springer, Berlin ; New York.

Chung, K. L. 1979. Elementary probability theory with stochastic processes. Springer-Verlag, New York.

Clemo, T., and L. Smith. 1997. A hierarchical model for solute transport in fractured media. Water Resources Research **33**:1763-1783.

Clemo, T. M. 1989. Representative elements: a step to large scale fracture system simulation. Pages 212-227 *in* Geostatistical methods for groundwater flow, and radionuclide transport modelling.

Closmann, P. J. 1975. An aquifer model for fissured reservoirs. Society of Petroleum Engineers Journal **259**:385-389.

Daly, D. 1995. A proposed groundwater protection scheme for Ireland: Draft for consultation. Geological Survey of Ireland, Dublin.

Dassargues, A., S. Brouyere, and J. Derouane. 1996. From calibration on tracer test data to computation of protection zones: upscalling difficulties in a deterministic modelling framewok. Pages 253-263 *in* Calibration and reliability in Grounwater modelling. ModelCARE96, Golden, Colorado.

de Marsily, G. 1986. Quantitative hydrogeology : groundwater hydrology for engineers. Academic Press, Orlando, FL.

Delay, F., and J. Bodin. 2001. Time domain random walk method to simulate transport by advection-dispersion and matrix diffusion in fracture networks. Geophysical Research Letters **28**:4051-4054.

Dershowitz, B., and T. Eiben. 1999. SR-97 Alternative models project. Discrete fracture network modelling for perfomance assessment of Aberg. SKB Technical report 99/43:110.

Dershowitz, B., G. Lee, J. Geier, T. Foxford, P. R. La Pointe, and A. Thomas. 1995. FRACMAN - interactive discrete feature data analysis, geometric modeling and exploration simulation. User documentation. Report 923-1089, Golder Associates, Seattle.

Dershowitz, W., and C. Fidelibus. 1998. Steady state flow prediction for a 3D discrete fracture network by means of an equivalent pipe system. Report WR98-242, Golder associates.

Dershowitz, W., and C. Fidelibus. 1999. Derivation of equivalent pipe network analogues for 3 dimensional discrete fracture networks by the boundary element method. Water Resources Research **35**:2685-2692.

Doe, T. 2002. Fracture network modelling. IGWMC Newsletter **XX**:3.

Doerfliger, N., and F. Zwahlen. 1998. Cartographie de la vulnerabilité en régions karstiques (EPIK). Guide pratique. L'environnement pratique. OFEFP - Office fédéral de l'environnement, des forêts et du paysage (Suisse), Berne.

Endo, H. K., J. Long, C. K. Wilson, and P. Witherspoon. 1984. A model for investigating mechanical transport in fractured media. Water Resources Research **20**:1390-1400.

Environment Agency. 2001. Protecting Groundwater. An international Conference on: Applying policies and decision making tools to land-use planning. Pages 343 *in*. Environment Agency, Birmingham, UK.

Evers, S., and D. N. Lerner. 1995. Zones of certainty and uncertainty in estimating borehole catchments. In "Groundwater quality, remediation and protection" IAHS Publ. 225, Prague,:483 - 491.

Faybishenko, B. A., I. Javandel, and P. A. Witherspoon. 1995. Hydrodynamics of the capture zone of a partially penetrating well in a confined aquifer. Water Resources Research **31**:859-866.

Fetter, C. W. 1999. Contaminant hydrogeology. Prentice Hall, Upper Saddle River, NJ.

Feyen, L., K. J. Beven, F. De Smedt, and J. Freer. 2001. Stochastic capture zone delineation within the generalized likelihood uncertainty estimation methodology: conditioning on head observations. Water Resources Research **37**:625-638.

Feyen, L., P. J. Ribeiro, F. De Smedt, and P. J. Diggle. 2002. Bayesian methodology to stochastic capture zone determination: conditioning on transmissivity measurements. Water Resources Research **38**:art. no.-1164.

Feyen, L., P. J. Ribeiro, J. J. Gomez-Hernandez, K. J. Beven, and F. De Smedt. 2003. Bayesian methodology for stochastic capture zone delineation incorporating transmissivity measurements and hydraulic head observations. Journal of Hydrology **271**:156-170.

Forchheimer, P. 1935. Tratado de hidraulica. Editorial Labor, Barcelona,.

Foster, S. S. D., T. Hirata, D. Gomes, D. E. M., and M. Paris. 2002. Groundwater quality protection : a guide for water utilities, municipal authorities and environment agencies. World Bank, Washington, D.C.

Fouché, O., A. Savajol, N. Monin, D. Fabre, and A. Pouya. 2003. Assessment of free groundwater hazard in tunnelling: use of stochastic fracture network simulation and homogeneisation. Pages 335-336 *in* J. Krasny, Z. Hrkal, and J. Bruthans, editors. Groundwater in fractured rocks. IAH, Prague.

Franke, O. L., T. E. Reilly, D. W. Pollock, and J. W. LaBaugh. 1998. Estimating areas contributing recharge to wells. Lessons from previous studies. USGS Survey Circular 1174, Denver.

Franz, T., and N. Guiguer. 1992. FLOWPATH (Version 4): Steady state 2D aquifer simulation model. Waterloo Hydrogeologic software. Waterloo, Ontario.

Franzetti, S., and A. Guadagnini. 1996. Probabilistic estimation of well catchments in heterogenous aquifer. Journal of Hydrology **174**:149 - 171.

Freeze, R. A., and J. A. Cherry. 1979. Groundwater. Prentice-Hall, Englewood Cliffs, N.J.

Gorenflo, R., and F. Mainardi. 2003. Fractional diffusion processes: Probability distributions and continuous time random walk. Pages 148-166 *in* Processes with Long-Range Correlations: Theory and Applications. Springer-Verlag Berlin, Berlin.

Gringarten, A. C., and H. J. Ramey. 1974. Unsteady state pressure distributions created by a well with a single horizontal fracture, partial penetration or restricted entry. Society of Petroleum Engineers Journal:413-426.

Gringarten, A. C., and P. Witherspoon. 1972. A method of analyzing pump test data from fractured aquifers. Pages 1-9 *in* Symposium of Rock Mechanics, Stuttgart.

Grisak, G. E., and P. F. Pickens. 1980. Solute transport through fractured media 1. The effect of matrix diffusion. Water Resources Research **16**:719 - 730.

Grubb, S. 1993. Analytical model for estimation of steady-state capture zone of pumping wells in confined and unconfined aquifers. Ground Water **31**:27-32.

Grubert, D. 2001. Effective dispersivities for a two-dimensional periodic fracture network by a continuous time random walk analysis of single-intersection simulations. Water Resources Research **37**:41-49.

Guadagnini, A., and S. Franzetti. 1999. Time-related capture zones for contaminants in randomly heterogeneous formations. Ground Water **37**:253-260.

Guérin, F., and D. M. Billaux. 1994. On the relationship between connectivity and the continuum approximation in fracture flow and transport modelling. Applied hydrogeology **2**:24-31.

Guiguer, N., and T. Franz. 1991. Development and application of a wellhead protection area delineation computer program. Water science and technology **24**:51 - 62.

Gylling, G., and L. Eriksson. 2001. Assessment model validity document - HYDRASTAR: a stochastic continuum program for groundwater flow. R-01-61, SKB, Stockholm.

Haitjema, H. H., J. Wittman, V. Kelson, and N. Bauch. 1994. WHAEM: program documentation documentation for the wellhead analytic element model. EPA/600/R-94/210, US Environment Protection Agency, Washington D.C.

Haitjema, H. M., O. Strack, and S. R. Kraemer. 1995. Demonstration of the analytic element method for wellhead protection. Project summary. EPA/600/SR-94/210, US Environment Protection Agency, Washington D.C.

Haneberg, W. C. 1995. Steady-state groundwater-flow across idealized faults. Water Resources Research **31**:1815-1820.

Hendricks-Franssen, H. 2000. Inverse stochastic modelling of groundwater flow and mass transport. Unpublished PhD thesis. Universidad Politecnica de Valencia, Valencia.

Herbert, A. W. 1993. Application of the NAPSAC fracture network program in the preliminary assessment of Sellafield. NSS/B010, AEA technology, Harwell.

Herbert, A. W., and G. W. Lanyon. 1995. Fracture networks and the use of the REV concept. NSS/R358, AEA Technology, Harwell.

Hestir, K., and J. C. S. Long. 1990. Analytical expressions for the permeability of random two-dimensional poisson fracture networks based on regular lattice percolation and equivalent media theories. Journal of Geophysical Research **95 - B13**:21565 - 21581.

Hicks, S., D. Bruel, P. Connolly, Y. Podlachikov, and N. Rodrigues. 2000. Modelling the influence of fault zone heterogeneity and the hydrodynamics of fault movement in hydrogeological systems. EUR 19134EN, Office for official publications of the European Communities, Luxembourg.

Horne, R. N. 1997. Modern well test analysis : a computer-aided approach. *in*. Petroway, Palo Alto, CA.

Hsieh, P. A. 2002. Some thoughts on modelling flow in fractured rocks. IGWMC Newsletter **XX**:2.

Hsu, H. 1996. Probability, random variables and random processes. McGraw-Hill, New York.

Hull, L. C., J. D. Miller, and T. M. Clemo. 1987. Laboratory and simulation studies of solute transport in fracture networks. Water Resources Research **23**:1505 - 1513.

Javandel, I., and C. F. Tsang. 1986. Capture-Zone Type Curves - a Tool for Aquifer Cleanup. Ground Water **24**:616-625.

Johnson, N. L., S. Kotz, and N. Balakrishnan. 1994. Continuous univariate distributions, 2nd edition. Wiley & Sons, New York.

Kazemi, H. 1969. Pressure transient analysis of naturally fractured reservoirs with uniform fracture distribution. Trans. Society of Petroleum Engineers AIME **24**:451-462.

Kazemi, H., and J. R. Gilman. 1993. Multiphase flow in fractured petroleum reservoirs. Pages 267-323 *in* J. Bear, C. F. Tsang, and G. de Marsily, editors. Flow and contaminant transport in fractured rock. Academic Press, inc., San Diego.

Keating, T., and M. J. Packman. 1996. Groundwater protection zones: manual of standard zone delineation methodologies. Environment Agency, Bristol.

Kinzelbach, W., M. Marburger, and W.-H. Chiang. 1992. Determination of catchment areas in two and three spatial dimensions. Journal of Hydrology **134**:221 - 246.

Kinzelbach, W., and S. Vassolo. 1996. Determination of capture zones of wells by Monte Carlo simulation. IAHS publication 237.

Klafter, J., and R. Silbey. 1980. Derivation of the Continuous-Time Random-Walk Equation. Physical Review Letters **44**:55-58.

Kosakowski, G., B. Berkowitz, and H. Scher. 2001. Analysis of field observations of tracer transport in a fractured till. Journal of contaminant hydrology **47**:29-51.

Kruseman, G. P., and N. A. de Ridder. 1994. Analysis and evaluation of pumping test data, 2nd edition. International Institute for Land Reclamation and Improvement, Wageningen, The Netherlands.

Kunstmann, H., and W. Kinzelbach. 2000. Computation of stochastic wellhead protection zones by combining the first-order second-moment method and Kolmogorov backward equation analysis. Journal of Hydrology **237**:127-146.

Lawrence, A., M. Fahy, R. Bianchi, M. McKeown, and J. Chatoian. 2003. Efects of tunnelling on the groundwater resources of the southwestern San Bernardino Mountains, California, USA. Pages 315-316 *in* J. Krasny, Z. Hrkal, and J. Bruthans, editors. Groundwater in fractured rocks. IAH, Prague.

Lee, C. H., B. S. Lin, and J. L. Yu. 1994. Dispersion and connectivity in flow-through fractured networks. J. of the Chinese Institute of Engineers **17**:521 - 535.

Lerner, D. N. 1992. A semi-analytical model for borehole catchments and time of travel zones which incorporates recharge and aquifer boundaries. Quarterly Journal of Engineering geology **25**:137 - 144.

Levy, M., and B. Berkowitz. 2003. Measurement and analysis of non-Fickian dispersion in heterogeneous porous media. Journal of contaminant hydrology **64**:203-226.

Long, J. C. S., and D. M. Billaux. 1987. From field data to fracture network modelling. Water Resources Research **23**:1201 - 1216.

Long, J. C. S., J. S. Remer, C. R. Wilson, and P. A. Witherspoon. 1982. Porous media equivalents for networks of discontinuous fractures. Water Resources Research **18**:645 - 658.

Long, J. C. S., and P. A. Witherspoon. 1985. The relationship of the degree of interconnection to permeability in fracture networks. Journal of Geophysical Research **90**:3087 - 3098.

Louis, C. 1974. Rock Hydraulics. Bureau de recherche géologique et minière, Paris.

Lu, Z. M., and D. X. Zhang. 2003. On stochastic study of well capture zones in bounded, randomly heterogeneous media. Water Resources Research **39**:art. no.-1100.

Mallet, A. 2000. NumericalInversion. *in*. Wolfram Research Inc. website (www.wolfram.com).

Maloszewski, P., A. Herrmann, and A. Zuber. 1999. Interpretation of tracer tests performed in fractured rock of the Lange Bramke basin, Germany. Hydrogeology Journal **7**:209-218.

Margolin, G., and B. Berkowitz. 2000. Application of continuous time random walks to transport in porous media. Journal of Physical Chemistry B **104**:3942-3947.

Marschall, P., and M. Elert. 2003. Overall evaluation of the modelling of the TRUE-1 tracer tests - task 4. The Aspo task force on modelling of groundwater and transport of solutes. TR-03-12, SKB, Stockholm.

Mathias, S. A., and R. W. Zimmerman. 2003. Laplace transform inversion for late-time behavior of groundwater flow problems. Water Resources Research **39**:1283, doi:1210.1029/2003WRR002246.

Mauldon, A. D., K. Karasaki, S. J. Martel, J. C. S. Long, M. Landsfeld, A. Mensch, and S. Vomvoris. 1993. An inverse technique for developing models for fluid-flow in fracture systems using Simulated Annealing. Water Resources Research **29**:3775-3789.

McDonald, M. G., and A. W. Harbaugh. 1988. A modular three dimensional finite difference groundwater flow model. USGS Techniques of water resource investigations TWRI Book 6- chapter A1, USGS, Washington D. C.

McElwee, C. D. 1991. Capture zones for simple aquifers. Ground Water **29**:587 - 590.

Meerschaert, M. M., and H. P. Scheffler. 2000. Portfolio modeling with heavy tailed random vectors. Pre-print from Mark Meerschaert's website (http://unr.edu/homepage/mcubed/):43.

Miller, I., G. Lee, and B. Dershowitz. 1999. MAFIC - matrix/fracture interaction code with heat and solute transport user documentation. Report 923-1089, Golder Associates, Washington.

Moench, A. F. 1984. Double-porosity models for a fissured groundwater reservoir with fracture skin. Water Resources Research **20**:831-846.

Montroll, E. W., and H. Scher. 1973. Random walks on lattices. IV. Continuous-time walks and influence of absorbing boundaries. Journal of Statistical Physics **9**:101-135.

Montroll, E. W., and G. H. Weiss. 1965. Random walks on lattices. Journal of Mathematical Physics **6**:167-181.

Mourzenko, V. V., B. Kolbah, J. Thovert, F. Yousefian, and P. M. Adler. 2001. Solute transport at fracture intersections. Extended abstract. Pages 31 *in* Fractured rock 2001, Toronto.

Muskat, M. 1937. The flow of homogeneous fluids through porous media, first edition. McGraw-Hill Book Company inc., New York.

Nakao, S., J. Najita, and K. Karasaki. 2000. Hydraulic well testing inversion for modeling fluid flow in fractured rocks using simulated annealing: a case study at Raymond field site, California. Journal of Applied Geophysics **45**:203-223.

National Research Council, editor. 1996. Rock fractures and fluid flow: contemporary understanding and applications. National Academy Press, Washington, D.C.

Neuman, S. P. 1990. Universal scaling of hydraulic conductivities and dispersivities in geologic media. Water Resources Research **26**:1749 - 1754.

Neuman, S. P. 1993. Comment on "A critical review of data on field-scale dispersion in aquifers". Water Resources Research **29**:1863-1865.

Neuman, S. P. 1995. On advective transport in fractal permeability and velocity fields. Water Resources Research **31**:1455 - 1460.

Niemi, A. 1994. Modeling flow in fractured medium. Uncertainty analysis with the stochastic continuum approach. PhD thesis. Technical research centre of Finland, Espoo.

Nolan, J. P. 1999. Fitting data and assessing goodness-of-fit with stable distributions. Pre-print from John Nolan's website (http://academic2.american.edu/~jpnolan/).

Nolan, J. P. 2002. Multivariate Stable distributions: approximation, estimation, simulation and identification. Pre-print from John Nolan's website (http://academic2.american.edu/~jpnolan/).

Ohman, J., and A. Niemi. 2003. Upscaling of fracture hydraulics by means of an oriented correlated stochastic continuum model. Water Resources Research **39**:art. no.-1277.

Outters, N., and D. Shuttle. 2000. Sensitivity analysis of a discrete fracture network model performance assessment of Aberg. R-00-48, SKB, Stockholm.

Painter, S. 1999. Long-range spatial dependence in fractured rock - empirical evidence and implications for tracer transport. SKB report **R-99-03**:34.

Parney, R., and L. Smith. 1995. Fluid velocity and path length in fractured media. Geophysical Research Letters **22**:1437-1440.

Parney, R. W. 1999. Statistical continuum modelling of mass transport through fractured media, in two and three dimensions. Unpublished PhD thesis. Univ. of British Columbia.

Pinder, G. F., P. S. Huyacorn, and E. Sudicky. 1993. Simulation of flow and transport in fractured porous media. Pages 395-435 *in* J. Bear, C. F. Tsang, and G. de Marsily, editors. Flow and contaminant transport in fractured rock. Academic Press, Inc., San Diego.

Pochon, A. 2002. Guide Practique - délimitation des zones de protection des eaux souterraines en milieu fissuré. OFEFP - Office fédéral de l'environnement, des forêts et du paysage (Suisse), Berne.

Podgorney, R. K., and R. W. Ritzi. 1997. Capture zone geometry in a fractured carbonate aquifer. Ground Water **35**:1040 - 1049.

Pollock, D. W. 1989. Documentation of computer programs to compute and display pathlines using results from the USGS modular 3D finite difference groundwater model. USGS open file report 89-381.

Priest, S. D., and J. A. Hudson. 1976. Discontinuity spacings and rock mass geometry. Intl. J. Rock Mech. Min. Sci. and Geomech. Abs. **13**:135 - 148.

Ramey, H. J., and A. C. Gringarten. 1976. Effect of high-volume vertical fractures on geothermal steam well behavior. Pages 1759-1762 *in* Second U. N. development and use of geothermal resources. U.S. Govenment printing office, San Francisco.

Rasmuson, A. 1985. Analysis of hydrodynamic dispersion in discrete fracture networks using the method of moments. Water Resources Research **21**:1677 - 1683.

Rasmussen, H., and A. Rouleau. 2003. Guide de détermination d'aires d'alimentation et de protection de captages d'eau souterraine. CERM, Université du Québec à Chicoutimi, Québec.

Rayne, T., K. R. Bradbury, and M. A. Muldoon. 2001. Delineation of capture zones for municipal wells in fractured dolomite, Sturgeon bay, Wisconsin, EUA. Hydrogeology Journal **9**:432-450.

Risser, D. W., and G. J. Barton. 1995. A strategy for delineating the area of ground-water contribution to wells completed in fractured bedrock aquifers in Pennsylvania. Report 95-4033, USGS.

Robins, N. S. 1999. Groundwater occurrence in the lower palaeozoic and precambrian rocks of the UK: Implications for source protection. Journal of the Chartered Institution of Water and Environmental Management **13**:447-453.

Robinson, J. N. 2003. A fractured/fissured rock approach to groundwater protection zones. Unpublished PhD thesis. University of London, London.

Robinson, J. N., and J. A. Barker. 1999. A fractured/fissured approach to groundwater protection zones. Draft Project Record. W6D(96)2, Jackson Environmental Institute. University College London, London.

Robinson, P. C. 1984. Connectivity, flow and transport in network models of fractured media. Unpublished PhD thesis. Oxford University, Oxford.

Rock, G., and H. Kupfersberger. 2002. Numerical delineation of transient capture zones. Journal of Hydrology **269**:134-149.

Ross, B. 1986. Dispersion in fractal fracture networks. Water Resources Research **22**:823-827.

Rouleau, A., and J. E. Gale. 1987. Stochastic discrete fracture simulation of groundwater flow into an underground excavation in granite. Intl. J. Rock Mech. Min. Sci. & Geomech. Abstr. **24**:99-112.

Sahimi, M. 1993. Flow phenomena in rocks - From continuum models to fractals, percolation, cellular-automata, and simulated annealing. Reviews of Modern Physics **65**:1393-1534.

Sahimi, M. 1995. Flow and transport in porous media and fractured rock - from classical methods to modern approaches. VCH, Weinheim.

Schafer-Perini, A. L., Wilson, J.L. 1991. Efficient and accurate front tracking for two dimensional groundwater flow models. Water Resources Research **27**:1471 - 1485.

Scher, H., and M. Lax. 1973. Stochastic transport in a disordered solid. I. Theory. Physical Review B **7**:4491-4502.

Schumer, R., D. A. Benson, M. M. Meerschaert, and B. Baeumer. 2003. Multiscaling fractional advection-dispersion equations and their solutions. Water Resources Research **39**:art. no.-1022.

Schumer, R., D. A. Benson, M. M. Meerschaert, and S. W. Wheatcraft. 2001. Eulerian derivation of the fractional advection-dispersion equation. Journal of contaminant hydrology **48**:69-88.

Schwartz, F. W., and L. Smith. 1988. A continuum approach for modelling mass transport in fractured media. Water Resources Research **24**:1360 - 1372.

Shan, C., I. Javandel, and P. A. Witherspoon. 1995. Characterization of leaky faults: Study of water flow in aquifer-fault-aquifer systems. Water Resources Research **31**:2897-2904.

Smith, L., T. Clemo, and M. Robertson. 1990. New approaches to the simulation of the field-scale solute transport in fractured rocks. Pages 329-342 *in* S. Bachu, editor. Proc. 5th Canadian/American Conference on Hidrogeology. National Waterwell Association, Dublin (Ohio).

Smith, L., and F. W. Schwartz. 1993. Solute transport through fracture networks. Pages 129-165 *in* J. Bear, C. F. Tsang, and G. de Marsily, editors. Flow and contaminant transport in fractured rock. Academic Press, San Diego.

Snow, D. T. 1968. Rock fracture spacings, openings and porosities. J. Soil Mech. and Civ. Eng. **94**:73 - 91.

Snow, D. T. 1969. Anisotropic permeability of fractured media. Water Resources Research **5**:1273 - 1289.

Spiegel, M. R., and J. Liu. 1999. Mathematical handbook of formulas and tables, 2nd edition. McGraw-Hill, New York.

Steward, D. R., and W. Jin. 2003. Drawdown and capture zone topology for nonvertical wells. Water Resources Research **39**:art. no.-1219.

Sudicky, E., and E. Frind. 1982. Contaminant transport in fractured porous media: analytical solutions for a system of parallel fractures. Water Resources Research **18**:1634-1642.

Svensson, U. 1999. Representation of fracture networks as grid cell conductivities. TR 99/25, SKB, Stockholm.

Tang, D. H., E. Frind, and E. Sudicky. 1981. Contaminant transport in fractured porous media: Analytical solution for a single fracture. Water Resources Research **17**:555-564.

Todd, D. K. 1959. Ground water hydrology. Wiley, New York,.
Uchaikin, V. V., and V. M. Zolotarev. 1999. Chance and stability. Stable distributions and their applications. VSP, Utrecht.
USEPA. 1987a. DRASTIC - a standardized system for evaluating groundwater pollution potential using hydrologic settings. EPA 600/2-87/035, US Environment Protection Agency.
USEPA. 1987b. Guidelines for delineation of wellhead protection areas. US Environment Protection Agency, Washington D.C., EPA 440/5-93-001.
USEPA. 1991a. Delineation of wellhead protection areas in fractured rocks. EPA 570/9-91-009, US Environment Protection Agency, Washington.
USEPA. 1991b. Fracture trace analysis for wellhead protection area delineation. US Environment Protection Agency, Las Vegas.
USEPA. 1993a. Wellhead protection: A guide for small comunities. EPA/625/R-93/002, US Environment Protection Agency, Washington.
USEPA. 1993b. WHPA well head protection area delineation code. US Environment Protection Agency, Washington D.C.
USEPA. 1994. Handbook. Ground water and wellhead protection. EPA 625/R-94/001, US Environment Protection Agency, Washington.
van Leeuwen, M. 2000. Stochastic determination of well capture zones conditioned on transmissivity data. PhD Thesis. Imperial College London.
van Leeuwen, M., C. B. M. te Stroet, A. P. Butler, and J. A. Tompkins. 1998. Stochastic determination of well capture zones. Water Resources Research **34**:2215-2223.
Varljen, M. D., and J. M. Shafer. 1991. Assessment of uncertainty in time related capture zones using conditional simulation of hydraulic conductivity. Ground Water **29**:737 - 748.
Vassolo, S., W. Kinzelbach, and W. Schafer. 1998. Determination of well head protection zone by stochastic inverse modelling. Journal of Hydrology **206**:268 - 280.
Warren, J. E., and P. J. Root. 1963. The behavior of naturally fractured reservoirs. Society of Petroleum Engineers Journal **3**:245-255.
Weisstein, E. W. 1999. CRC concise encyclopedia of mathematics. CRC Press, Boca Raton, Fla.
Witherspoon, P. A., J. Y. S. Wang, K. Iwai, and J. E. Gale. 1980. Validity of cubic law for fluid flow in a deformable rock fracture. Water Resources Research **16**:1016 - 1024.
Wolfram, S. 1999. The mathematica book, 4th edition. Wolfram Media. Cambridge University Press, Champaign, IL. New York.
Yaxley, L. M. 1987. Effect of a partially communicating fault on transient pressure behavior. SPE Formation Evaluation **2**:590-598.
Yeo, I. W., and K. K. Lee. 2003. Analytical solution for arbitrarily located multiwells in an anisotropic homogeneous confined aquifer. Water Resources Research **39**:art. no.-1133.
Zawadzki, W., D. W. Chorley, and G. Patrick. 2002. Capture-zone design in an aquifer influenced by cyclic fluctuations in hydraulic gradients. Hydrogeology Journal **10**:601-609.
Zhan, H. B. 1999. Analytical study of capture time to a horizontal well. Journal of Hydrology **217**:46-54.
Zhang, D. X., and Z. M. Lu. 2004. Stochastic delineation of well capture zones. Stochastic Environmental Research and Risk Assessment **18**:39-46.
Zheng, C. 1994. Analysis of particle tracking errors associated with spatial discretisation. Ground Water **32**:821 - 828.
Zimmerman, R. W., and G. S. Bodvarsson. 1996a. Effective transmissivity of two-dimensional fracture networks. Int. J. Rock Mech. and Min. Sci. and Geomech. Abs. **33**:433-438.
Zimmerman, R. W., and G. S. Bodvarsson. 1996b. Hydraulic conductivity of rock fractures. Transport in Porous Media **23(1)**:1 - 30.
Zimmerman, R. W., D. Chen, and N. G. W. Cook. 1992. The effect of contact area on the permeability of fractures. Journal of Hydrology **139**:79-96.
Zlotnik, V. A. 1997. Effects of anisotropy on the capture zone of a partially penetrating well. Ground Water **35**:842-847.

Appendix A

THE MULTIPLE-POROSITY MODEL

Full derivation of the analytical solution (based on a note provided by J. A. Barker)

Let $s_1(r,t)$ be the average drawdown in the 1st-order fracture system at distance r from the well, at time t after the start of pumping. The flow equation in the 1st-order fracture set, the ones directly pumped by the well, is given by:

$$S_1 \frac{\partial s_1}{\partial t} = \frac{T_1}{r}\frac{\partial}{\partial r}\left(r\frac{\partial s_1}{\partial r}\right) - q_2(r,t) \tag{A.1}$$

where $q_2(r,t)$ represents discharge from the 2nd-order fractures into the 1st-order fractures per unit area of the aquifer.

Drawdown $s_2(r,\vec{z}_2,t)$, in the 2nd-order fracture set, at distance r from the well and at distance $\vec{z}_2$ from the lower order fractures is given by:

$$S_2 \frac{\partial s_2}{\partial t} = T_2 \frac{\partial^2 s_2}{\partial z_2^2} - q_3(r,\vec{z}_3,t) \tag{A.2}$$

or generalizing for ith-order fractures:

$$S_i \frac{\partial s_i}{\partial t} = T_i \frac{\partial^2 s_i}{\partial z_i^2} - q_{i+1}(r,\vec{z}_{i+1},t) \tag{A.3}$$

where $\vec{z}_i = \{\vec{z}_2,\vec{z}_3,...,\vec{z}_n\}$ and $q_i(r,\vec{z}_i,t)$ is obtained by applying Darcy's law at the block surfaces, with A_i being the fracture area per unit area of the aquifer:

$$q_i(r,t) = -A_i K_i \frac{\partial s_i(r,a_i,t)}{\partial z_i} \tag{A.4}$$

As a result of symmetry of the model there will be no-flow across the centre of any fractures of order higher than 1:

$$\left.\frac{\partial s_i}{\partial z_i}\right|_{z_i=0} = 0 \qquad i>1 \tag{A.5}$$

Drawdown at the interface between fractures of successive orders will be equal:

$$s_i(r,a_i,t) = s_{i-1}(r,a_{i+1},t) \tag{A.6}$$

Initially drawdown at every location is zero:

$$s_i(r,\vec{z}_i,0)=0 \tag{A.7}$$

The solution of the problem is found using Laplace transforms with respect to time (t), with p as the Laplace transform variable and with the transformed variable being represented with an over-bar, such as in $\overline{s_1}$.

The Laplace transform of equation (A.2) returns:

$$S_i p\overline{s_i} - s_i(r,\vec{z}_i,0) = T_i \frac{d^2\overline{s_i}}{dz_i^2} - \overline{q}_{i+1}(r,\vec{z}_{i+1},t) \tag{A.8}$$

which applying the initial condition given by equation (A.7) becomes:

$$S_i p\overline{s_i} = T_i \frac{d^2\overline{s_i}}{dz_i^2} - \overline{q}_{i+1}(r,\vec{z}_{i+1},t) \tag{A.9}$$

The Laplace transform of the equation (A.4) for flow rate from the i+1 fracture set into the i fracture set is:

$$\overline{q}_{i+1} = -K_{i+1}A_{i+1}\left.\frac{d\overline{s}_{i+1}}{dz_{i+1}}\right|_{z_{i+1}=a_{i-1}} \tag{A.10}$$

Replacing equation (A.10) into equation (A.8) gives:

$$S_i p\overline{s_i} = T_i \frac{d^2\overline{s_i}}{dz_i^2} - -K_{i+1}A_{i+1}\left.\frac{d\overline{s}_{i+1}}{dz_{i+1}}\right|_{z_{i+1}=a_{i-1}} \tag{A.11}$$

which for the highest order (n) becomes:

$$\frac{d^2\overline{s}_n}{dz_n^2} = \frac{pS_n\overline{s}_n}{T_n} \tag{A.12}$$

The solution of this ordinary differential equation:

$$\overline{s}_n = C_1\cosh\left(z_n\sqrt{\frac{pS_n}{T_n}}\right) + C_2\sinh\left(z_n\sqrt{\frac{pS_n}{T_n}}\right) \tag{A.13}$$

where C_1 and C_2 are constants. The 1st derivative of equation (A.13) with respect to z, returns:

$$\frac{d\overline{s}_n}{dz_n} = -C_1\sqrt{\frac{pS_n}{T_n}}\sinh\left(z_n\sqrt{\frac{pS_n}{T_n}}\right) + C_2\sqrt{\frac{pS_n}{T_n}}\cosh\left(z_n\sqrt{\frac{pS_n}{T_n}}\right) \tag{A.14}$$

Applying boundary conditions provided by equation (A.5) which states that the first derivative (A.14) equals zero when z equals zero, allows to retrieve C_2=0 and equation (A.13) becomes:

$$\overline{s}_n = C_1\cosh\left(z_n\sqrt{\frac{pS_n}{T_n}}\right) \tag{A.15}$$

The remaining constant C_1 can be evaluated using boundary condition (A.6) in equation (A.5), resulting:

$$C_1 = \bar{s}_{n-1} \Big/ \cosh\left(a_n \sqrt{\frac{pS_n}{T_n}}\right) \tag{A.16}$$

Thus, the solution of the ordinary differential equation that describes flow in the highest hierarchical level (n^{th} level) is:

$$\bar{s}_n = \bar{s}_{n-1} \cosh\left(z_n \sqrt{\frac{pS_n}{T_n}}\right) \Big/ \cosh\left(a_{n-1} \sqrt{\frac{pS_n}{T_n}}\right) \tag{A.17}$$

of which the first derivative at $z_n=a_{n-1}$, is:

$$\frac{d\bar{s}_n}{dz_n} = -\sqrt{\frac{pS_n}{T_n}} \tanh\left(a_{n-1} \sqrt{\frac{pS_n}{T_n}}\right) \tag{A.18}$$

Applying equation (A.18) in the equation of flow in the (*n-1*) order (equation A.11) allows retrieving:

$$S_{n-1} p\bar{s}_{n-1} = T_{n-1} \frac{d^2\bar{s}_{n-1}}{dz_{n-1}^2} - K_n A_n \bar{s}_{n-1} \sqrt{\frac{pS_n}{T_n}} \tanh\left(a_{n-1} \sqrt{\frac{pS_n}{T_n}}\right) \tag{A.19}$$

or:

$$\frac{d^2\bar{s}_{n-1}}{dz_{n-1}^2} = \frac{p\bar{s}_{n-1}}{T_{n-1}} \left[1 + K_n A_n \frac{S_n}{T_n S_{n-1}} \tanh\left(a_{n-1} \sqrt{\frac{pS_n}{T_n}}\right) \Big/ \sqrt{\frac{pS_n}{T_n}}\right] \tag{A.20}$$

Since A_n (the fracture area per unit area of the aquifer) for slab shaped matrix blocks equals H/a_n, where H is the aquifer thickness, equation (A.20) becomes:

$$\frac{d^2\bar{s}_{n-1}}{dz_{n-1}^2} = \frac{p\bar{s}_{n-1}}{T_{n-1}} \left[1 + \frac{S_n}{S_{n-1}} \frac{\tanh(u_n)}{u_n}\right] \tag{A.21}$$

where $u_n = a_{n-1} \sqrt{\frac{pS_n}{T_n}}$ for large values of n. Using the Block Geometry Function for slabs shaped matrix blocks, $B(u_n) = \tanh(u_n)/u_n$, leads to:

$$\frac{d^2\bar{s}_{n-1}}{dz_{n-1}^2} = \bar{s}_{n-1} \frac{pS_{n-1}}{T_{n-1}} \beta_{n-1} \tag{A.22}$$

and

$$\beta_{n-1} = 1 + \frac{S_n}{S_{n-1}} B(u_n) \tag{A.23}$$

The solution of the ordinary differential equation (A.22), by analogy with the solution (A.17) for n^{th} level is:

$$\bar{s}_{n-1} = \bar{s}_{n-2} \cosh\left(z_{n-1} \sqrt{\frac{pS_{n-1}\beta_{n-1}}{T_{n-1}}}\right) \Big/ \cosh\left(a_{n-1} \sqrt{\frac{pS_{n-1}\beta_{n-1}}{T_{n-1}}}\right) \tag{A.24}$$

Now, notice that if the first derivative of equation (A.24) were to be used in the equation of flow for the *n-2* level, according to a procedure similar to the one used from equations (A.18) to (A21) it would be possible to rewrite the differential equations describing flow in the *n* (equation A.12), *n-1* (equation A.22) and *n-2* level as:

$$\begin{cases} \dfrac{d^2\overline{s}_n}{dz_n^2} = \dfrac{pS_n\overline{s}_n}{T_n} \\ \dfrac{d^2\overline{s}_{n-1}}{dz_{n-1}^2} = \overline{s}_{n-1}\dfrac{pS_{n-1}}{T_{n-1}}\beta_{n-1} \\ \dfrac{d^2\overline{s}_{n-2}}{dz_{n-2}^2} = \overline{s}_{n-2}\dfrac{pS_{n-2}}{T_{n-2}}\left[1+\dfrac{S_{n-1}}{S_{n-2}}\beta_{n-1}\mathrm{B}(u_{n-1})\right] \end{cases} \tag{A.25}$$

The three equations in (A.25), representing flow in three consecutive levels, can be written in a similar form as:

$$\frac{d^2\overline{s}_i}{dz_i^2} = \overline{s}_i\xi_i^2 \tag{A.26}$$

provided the following terms are redefined:

$$\xi_i^2 = p\frac{S_i}{T_i}\left[1+\frac{S_{i+1}}{S_i}\beta_{i+1}\mathrm{B}(u_{i+1})\right] \tag{A.27}$$

and

$$\beta_i = 1+\frac{S_{i+1}}{S_i}\beta_{i+1}\mathrm{B}(u_{i+1}) \tag{A.28}$$

taken into account that $\beta_n = 1$, and that $\frac{S_{n+1}}{S_n} = 0$, which implies $\xi_n^2 = \overline{s}_n\frac{pS_n}{T_n}$.

Since equations (A.26) and (A.27) are recursive equations, if they are combined and expanded for $i \geq 1$ it is possible to get:

$$\xi_1^2 = p\frac{S_1}{T_1}\left\{1+\frac{S_2}{S_1}\mathrm{B}(u_2)+\frac{S_3}{S_1}\mathrm{B}(u_2)\mathrm{B}(u_3)+\frac{S_4}{S_2}\mathrm{B}(u_2)\mathrm{B}(u_3)\mathrm{B}(u_4)+\ldots\right\} \tag{A.29}$$

which can be written in concise format as:

$$\xi_i^2 = p\frac{S_i}{T_i}\left\{1+\frac{1}{S_i}\sum_{j=i+1}^{n}S_j\left[\prod_{l=i+1}^{j}\mathrm{B}(u_l)\right]\right\} \tag{A.30}$$

where

$$\mathrm{B}(u_i) = \frac{\tanh(u_i)}{u_i}, \text{ for slabs at every hierarchical level} \tag{A.31}$$

Notice that the term u_i must now be redefined (see for instance equation A. 24) as:

$$u_i = a_{i-1}\sqrt{\frac{pS_i\beta_i}{T_i}} \tag{A.32}$$

which, taking account the recursive nature of β (equation A.28) becomes:

$$u_i = \xi_i a_{i-1} \tag{A.33}$$

As expected for a multiple-porosity system, the effect of each order of fractures is included in the effect of the immediately preceding order (equation A.30). Therefore, of the flow equation in the 1st- order fractures (the ones conducting flow to the well) solution is still the generalized well function:

$$\bar{s}_1(r,p) = Q\frac{K_0(\xi_1 r)}{p\pi T_1} \tag{A.34}$$

where ξ_1 is defined according to equation (A.30) for $i \geq 1$. If it is chosen to write ξ_1 as is usually done in the generalised well function solution:

$$\xi_1^2 = p\frac{S_1}{T_1}\left\{1+\frac{S_2}{S_1}B_{eff}(u)\right\} \tag{A.35}$$

with and effective block geometry function being defined from equation (A.30) as:

$$B_{eff}(u) = \frac{1}{S_2}\sum_{j=1}^{n} S_{j+1}\left[\prod_{l=2}^{j} B_l(u_l)\right] \tag{A.36}$$

where the subscript l on B_l indicates that the block shape at each hierarchical level may not be the same.

Properties of the effective BGF for the multiple-porosity model

The effective BGF, $B_{eff}(u)$, for the multiple-porosity model can be expressed in terms of u_2 only (defined in section 4.3), by:

$$B_{eff}(u) = \frac{u_2^2}{p}B_2(u_2) \tag{A.37}$$

where p is the Laplace transform variable, B_2 is the BGF for the 2nd hierarchical level and u_2 is given by equation (4.50) in section 4.3.1.3.

Figure A.1 shows an example of variation of the effective BGF, $B_{eff}(u)$, with u, as well as the asymptotes for early time ($u \to \infty$) and for very late time ($u \to 0$). Since at very early time only the 2nd-order fractures are contributing flow to the primary fractures, then for early time ($u \to \infty$) $B_{eff}(u) = B_2(u_2)$ and the asymptotic is the same as would be for any dual-porosity BGF, i.e.:

$$B_{eff}(u) \sim \frac{1}{u_2} \text{ as } u_2 \to \infty \tag{A.38}$$

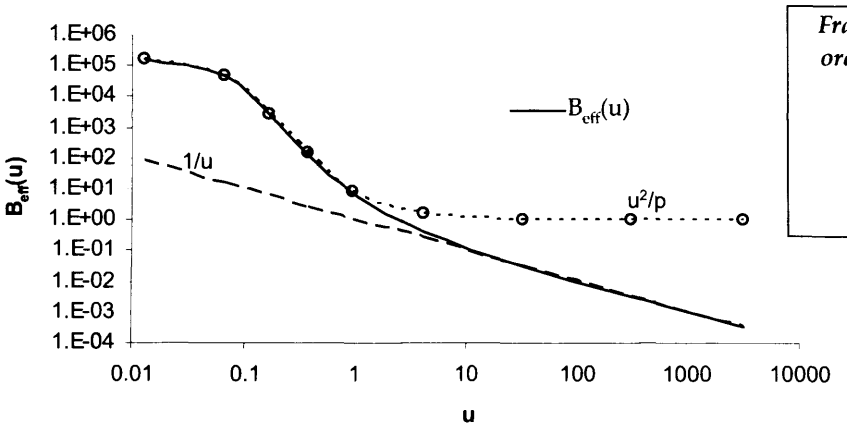

Fracture order (i)	S_i	T_i (m^2/s)
1	10^{-5}	2.56
2	10^{-4}	6.4×10^{-2}
3	10^{-3}	1.6×10^{-3}
4	10^{-2}	4×10^{-5}
5	10^{-1}	10^{-6}

Figure A.1 – Plot of the effective BGF, $B_{eff}(u)$, and asymptotes, for the multiple-porosity model. Five orders of fractures are included with storativity (S_i) and transmissivity (T_i) as indicated.

For the dual-porosity, the late time behaviour ($u \to 0$) is represented by $B_{eff}(u) \sim 1 - c_1 u^2$ as $u \to 0$, where c_1 is a constant. Applying this to B_2 in equation (A.37) it is possible to retrieve the asymptotic for late time as:

$$B_{eff}(u) \sim \frac{u_2^2}{p} \text{ as } u_2 \to 0 \tag{A.39}$$

since the 4th power of u vanishes rapidly.

Contrary to what happens in dual-porosity models, the limit of the effective BGF as $u \to 0$ is not 1. Using the definition of u_2 provided by equations (4.49) and (4.50) into equation (A.37), and knowing that at each level j the BGF converges to 1, it is possible to compute that:

$$\lim_{u\to 0} B_{eff}(u) = 1 + \frac{1}{S_2}\sum_{j=2}^{n-1} S_{j+1} \tag{A.40}$$

which will be a very large number, since S_2 is usually very small (10^{-4} to 10^{-6}).

As for the limit as $u \to \infty$, equation (A.38), the asymptotic for that case shows that:

$$\lim_{u\to\infty} B_{eff}(u) = 0 \tag{A.41}$$

which is similar to the limit of the dual-porosity model.

Since the limit of the effective BGF given by equation (A.40) is essentially related to the total storage of the fracture system, which is a constant value, it is possibly to normalise the effective BGF, by dividing it by the right side of equation (A.40), so that the limit of the effective BGF as $u \to 0$ is 1. Combining equations (A.37) and (A.40) the revised effective BGF (B'_{eff}) is:

$$B'_{eff}(u) = \frac{S_2 u_2^2 B_2(u_2)}{S_T p} \tag{A.42}$$

where $S_T = \sum_{j=2}^{n} S_j$ is now used to indicate the **total storage** of the fracture system ($j > 1$) contributing water to the first order fractures.

This revised equation for the effective BGF is as valid as the one provided in equation (A.37). However, equation (A.42) enables greater similarity with the dual-porosity models, since its limits and asymptotes are now the same as for any dual-porosity media BGF.

Appendix B

MOMENT GENERATING FUNCTIONS[1]

The moment generating function of a continuous random variable X is defined by:

$$M_X(z) = E\left(e^{zX}\right) = \int_{-\infty}^{\infty} e^{zx} f_X(x)dx \tag{B.1}$$

where z is a real variable. Note that $M_X(z)$ may not exist for all random variables X. In general, $M_X(z)$ will exist only for those values of z for which the integral of equation (B.1) converges absolutely. Suppose that $M_X(z)$ exists then the i^{th} moment of X is given by:

$$m_i = \frac{d^i}{dz^i} M_X(z)\bigg|_{z=0} \tag{B.2}$$

It is also possible to rewrite the equation for the moment generating function in terms of the i^{th} moment of X as:

$$M_X(z) = 1 + m_1 z + m_2 \frac{z^2}{2!} + m_3 \frac{z^3}{3!} + \ldots \tag{B.3}$$

or:

$$M_X(z) = \sum_{i=0}^{\infty} m_i \frac{z^i}{i!} \tag{B.4}$$

The joint moment generating function $M_{XY}(z_1, z_2)$ of two random variables X and Y is defined by:

$$M_{XY}(z_1, z_2) = E\left(e^{z_1 X + z_2 Y}\right) \tag{B.5}$$

In a similar fashion, we can define the joint moment generating function of n random variables $X_1, \ldots, X_n$ by:

$$M_{X_1 \ldots X_n}(z_1, \ldots, z_n) = E\left(e^{z_1 X_1 + \ldots + z_n X_n}\right) \tag{B.6}$$

If $X_1, \ldots, X_n$ are independent random variables, then:

$$M_{X_1 \ldots X_n}(z_1, \ldots, z_n) = E\left(e^{z_1 X_1}\right) \ldots E\left(e^{z_n X_n}\right) = M_{X_1}(z_1) \ldots M_{X_n}(z_n) \tag{B.7}$$

[1] From Hsu (1996) – Probability, random variables and random processes. Schaum's outlines. McGraw-Hill. New York.

Two important lemmas concerning moment generating functions are stated as following:

- if two random variables have the same moment generating functions, then they must have the same distribution;
- given cumulative distribution functions $F(x)$, $F_1(x)$, $F_2(x)$, ..., with corresponding moment generating functions $M(t)$, $M_1(t)$, $M_2(t)$, ..., then $F_n(x) \rightarrow F(x)$ if $M_n(z) \rightarrow M(z)$.

Appendix C

CONVERGENCE OF THE 1-D CTRW WITH EXPONENTIALLY DISTRIBUTED PATH-LENGTHS TO FICKIAN TRANSPORT

In order to demonstrate that the transport solution of the 1-D CTRW with exponentially distributed path-lengths converges, at late time, to Fickian transport it is necessary to demonstrate that the CTRW distribution provided by equation (6.28):

$$P(x,t)=\frac{1}{\alpha}\sqrt{\frac{vt}{x}}e^{-\frac{(vt+x)}{\alpha}}I_1\left(\frac{2\sqrt{vtx}}{\alpha}\right)+\delta(x)e^{-\frac{vt}{\alpha}} \qquad x\geq 0,\ t\geq 0 \tag{C.1}$$

converges to the normal probability distribution:

$$P(z)=\frac{1}{\sqrt{2\pi}\sigma_z}e^{-\frac{(z-\bar{\mu}_z)^2}{2\sigma_z^2}} \tag{C.2}$$

where, z is a real variable, $\bar{\mu}_z$ and σ_z are, respectively, the mean and the standard deviation of the distribution.

For late time behaviour, the modified Bessel function I_1 can be replaced by its asymptotic:

$$I_1(y)\sim\frac{e^y}{\sqrt{2\pi y}} \tag{C.3}$$

Given that the term multiplied by the Dirac delta function will converge to zero, the 1-D CTRW can then be written for very large t, as:

$$P(x,t)=\frac{1}{\alpha}\sqrt{\frac{vt}{x}}e^{-\frac{(vt+x)}{\alpha}}\frac{e^{\frac{2\sqrt{vtx}}{\alpha}}}{\sqrt{2\pi\frac{2\sqrt{vtx}}{\alpha}}} \tag{C.4}$$

which, after some manipulation, gives:

$$P(x,t)=\frac{1}{\sqrt{2\pi}}\frac{(vt)^{1/4}}{\sqrt{2\alpha}x^{3/4}}e^{-\frac{1}{\alpha}\left(-\sqrt{vt}+\sqrt{x}\right)^2} \tag{C.5}$$

This asymptotic equation for the 1-C CTRW with exponentially distributed path-lengths is essentially identical to the normal distribution, given by equation (C.2), provided the following transformations are made:

$$\begin{cases} \sigma_z = \dfrac{\sqrt{2\alpha}}{(vt)^{1/4}} x^{3/4} \\ \bar{\mu}_z = \dfrac{2}{(vt)^{1/4}} x^{5/4} \\ z = 2(vt)^{1/4} x^{3/4} \end{cases} \tag{C.6}$$

Appendix D

SUM OF *n* INDEPENDENT PARETO RANDOM VARIABLES

The Pareto distribution is represented by the following equation:

$$P_1(x) = \frac{\beta}{x^{1+\beta}}\mu(x-1), \qquad \beta > 0,\ x > 1 \tag{D.1}$$

where μ is the unit step function, included to guarantee that x>1.

Because x is always positive, it is possible to apply the Laplace transform with respect to x, using p as the transform variable and depicting the transformed variable by a super-script as in $\overline{P}_1(p)$.

The Laplace transform of equation (D.1) is:

$$\overline{P}_1(p) = \beta p^{\beta}\Gamma(-\beta, p) \tag{D.2}$$

where $\Gamma(-\beta, p)$ is the incomplete gamma function, defined as $\Gamma(-\beta, p) = \int_p^{\infty} z^{-\beta-1}e^{-z}dz$.

Given any two independent random variables (X_1 and X_2) with known distributions $P(x_1)$ and $P(x_2)$, the probability distribution of its sum ($Y=X_1+X_2$) is (Hsu 1996):

$$P(y) = \iint P(x_1, x_2)dx_1dx_2 = \int_{-\infty}^{\infty} P(x_1)P(y-x_1)dx_1 \tag{D.3}$$

The right-hand term is known as the ***convolution*** of $P(x_1)$ and $P(x_2)$ as is usually denoted by $P(x_1)*P(x_2)$. In the same manner, the sum of n independent random variables is given by the convolution of n successive terms. Therefore, the sum of n random variables distributed according to a Pareto distribution, $P_n(x)$, would be:

$$P_n(x) = \int\!\!\cdots\!\int P_{1\ldots n}(x_1 \ldots x_n)dx_1 \ldots dx_n \tag{D.4}$$

The convolution property of the Laplace transform states that (Spiegel 1965):

$$\int_0^x f(u)g(x-u)du = f(x) * g(x) = \mathcal{L}^{-1}\left[\overline{f}(p)\overline{g}(p)\right] \tag{D.5}$$

where $f(x)$ and $g(x)$ are two known functions and $\mathcal{L}^{-1}$ stands for the inverse Laplace transform operator. That is, in Laplace space the convolution is equivalent to the product of the Laplace transformed functions. Equation (D.4) becomes in Laplace space:

$$\overline{P}_n(p) = \overline{P}_1(p)\overline{P}_1(p)....\overline{P}_1(p) = \left[\overline{P}_1(p)\right]^n \tag{D.6}$$

or using equation (D.2):

$$\overline{P}_n(p) = \left[\beta p^{\beta}\Gamma(-\beta, p)\right]^n \tag{D.7}$$

Appendix E

CUMULATIVE PROBABILITY FUNCTION OF THE ONE-DIMENSIONAL CTRW

1-D CTRW with exponentially distributed path-lengths

The probability density functions for the 1-D CTRW with exponentially distributed path-lengths is given by equation (6.28) as:

$$P(x,t)=\frac{1}{\alpha}\sqrt{\frac{vt}{x}}e^{-\frac{(vt+x)}{\alpha}}I_1\left(\frac{2\sqrt{vtx}}{\alpha}\right)+\delta(x)e^{-\frac{vt}{\alpha}} \qquad x\geq 0,\ t\geq 0 \tag{E.1}$$

The cumulative distribution function, F(x), of any given probability density function, P(x), can be found from:

$$F(x,t)=\int_0^x P(z,t)dz \qquad x\geq 0,\ t\geq 0 \tag{E.2}$$

Evaluation of the integral in equation (E.2) when P(z, t) is replaced by equation (E.1) is very complex to be achieved in a straightforward manner. However, taking into account the following operational property of the Laplace transform:

$$\mathcal{L}\left[\int_0^x f(z)dz\right]=\frac{\bar{f}(p)}{p} \tag{E.3}$$

where p is the Laplace transform variable and $\mathcal{L}$ stands for the Laplace transform operator, the problem of finding the cumulative probability function becomes just a problem of finding the Laplace transform with respect to x of the probability density function, since equation (E.2) becomes:

$$\bar{F}(p,t)=\frac{\bar{P}(p,t)}{p} \tag{E.4}$$

The Laplace transform of the 1-D CTRW (equation E.1) can be found simply by resorting to analogy between the Fourier transform and Laplace transform. Recall that the moment generating function of equation (E.1) was already given as equation (6.21) and was computed using the Fourier transform for x>0. Since for x>0 this transform differs from the Laplace transform only in

the sign of the transform variables, it is possible to rewrite equation (6.21) so that it now represents the Laplace transform of the 1-D CTRW with exponentially distributed path-lengths:

$$\overline{f}(p) = e^{-\frac{t\gamma p}{\lambda + p}} \tag{E.5}$$

while the cumulative probability function is:

$$\overline{F}(p) = \frac{e^{-\frac{t\gamma p}{\lambda + p}}}{p} \tag{E.6}$$

Using the definitions for advective velocity and dispersivity provided by equations (6.25) and (6.27) respectively, equation (E.6) becomes:

$$\overline{F}(p) = \frac{e^{-\frac{pvt}{1+p\alpha}}}{p} \tag{E.7}$$

Figure E.1 shows a plot of the 'standard' cumulative probability function, i.e. with parameters v and α set to one.

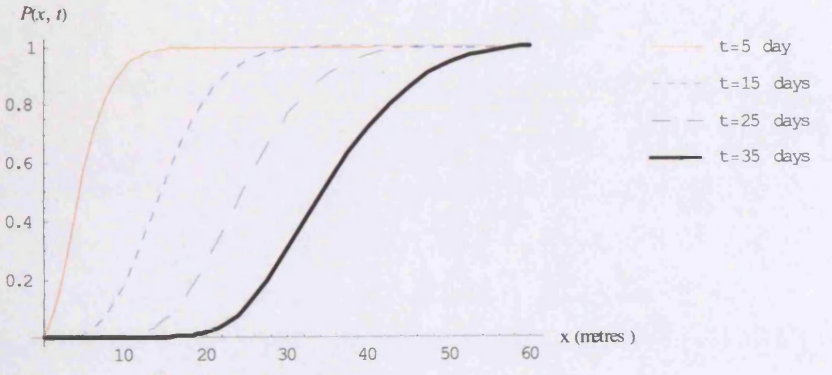

Figure E.1 – Cumulative probability function of the 1-D CTRW with exponentially distributed path-length (v=1, α=1), for several times.

1-D CTRW with power-law distributed path-lengths

The probability density functions for the 1-D CTRW with power-law distributed path-lengths is given by equation (6.39) as:

$$\overline{P}(p,t) = e^{-\gamma t\left[1-\beta p^{\beta}\Gamma(-\beta,p)\right]} \tag{E.8}$$

Since this result was already obtained in terms of the Laplace transform, equation (E.4) can be directly applied to obtain the cumulative probability function as:

$$\overline{F}(p,t) = \frac{1}{p} e^{-\gamma t\left[1-\beta p^{\beta}\Gamma(-\beta,p)\right]} \tag{E.9}$$

Figure E.2 shows a plot of the cumulative probability function with parameters β and γ set to one.

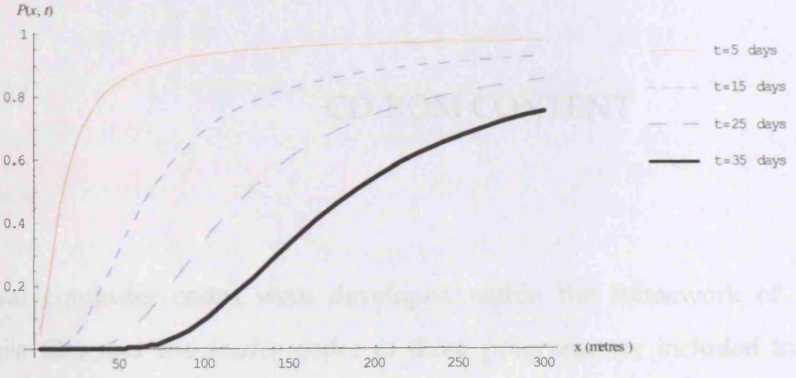

Figure E.2 – Cumulative probability function of the 1-D CTRW with power-law distributed path-length ($\beta = 1, \gamma = 1$), for several times.

Appendix F

CD-ROM CONTENT

Several computer codes were developed within the framework of this PhD thesis. The executable files and the source codes of those programs are included in the CR-ROM that is supplied with the thesis.

Development of the computer codes was not in itself an objective set up initially and rather they were written as research went along with the purpose of illustrating or implementing the techniques described in the thesis. Thus, the codes are not a central part of the thesis, which can be fully understood without resorting to their use. Nevertheless, it is thought interesting to provide them as supplementary tools that may allow for a better understanding of the general problem of solute transport in fractured-rocks and, more specifically, of delineation of protection zones in those geologic environments. In fact, it is hoped that some of those codes can be of assistance to anyone that may be involved in the process of protection zone definition.

Eighteen computer programs were developed using the FORTRAN and the *Mathematica* programming languages. VISUAL BASIC was used in one of the programs to create an interface with a FORTRAN written Dynamic Link Library (DLL).

This appendix describes the codes following the same structure adopted for the thesis, by grouping them according to their intended use for delineating protection zones in linear structures, in dual and multiple-porosity aquifers or in fracture network aquifers.

Protection zones involving faults, dykes and other linear structures

Within the scope of delineation of protection zones for wells located in composite aquifer systems, two *Mathematica* notebooks and one FORTRAN code were written:

1. *GPZ FOR WELL IN LINEAR STRUCTURE*

A *Mathematica* notebook (*gpz for well in linear structure.nb*) that defines the capture zone of a well pumping a composite aquifer system for the case of well located in the linear structure (d=0).

The notebook was described in section 3.3.1 and it computes the equipotentials and the stream function induced by the well. The equipotentials and the stream function are plotted in a user specified domain by evaluating the corresponding equations (described in section 3.2.2) in multiple x, y locations and subsequently by contouring the results. The user specifies all the necessary hydraulic parameters of the country-rock and linear structure, as well as the size of the domain to plot. Although the capture zone of the well is not directly plotted, it is clearly defined by the stream function.

This notebook, as all others included in the CD-ROM, can be edited with the *Mathematica* front-end, or visualised with the MATHREADER program, which is also supplied in the CD-ROM.

2. *GPZ FOR WELL OUTSIDE THE LINEAR STRUCTURE*

A *Mathematica* notebook (*gpz for well outside the linear structure.nb*) that defines the capture zone of a well pumping a composite aquifer system for the case of well located in the country-rock (d>0).

A notebook similar to the preceding one, but implementing the equipotentials and stream function solutions described in section 3.2.3. This notebook was used to create the figures that illustrate section 3.3.2. The structure of the notebook is analogous to the *GPZ for well in linear structure.nb* notebook.

3. *GPZFAULT*

A FORTRAN code intended to delineate the isochrones of a well pumping a composite aquifer system, for the case of well located in the linear structure (d=0).

This code was described in some detail in section 3.3.1. It is based on reverse particle tracking, taking advantage of the possibility of computing the advective velocity at any location using the equations provided in section 3.3.1.

The code runs in a DOS environment and input is via a file designated *input.txt*, which includes the hydraulic parameters of country-rock and linear structure, as well as aquifer thickness and pumping rate. Input for the number of particles to track and isochrone time is requested interactively. Output is to a mapping file named *isochrone.bln* that can be plotted using the program SURFER. An additional file, *partlocal.txt*, is written, which stores the particles final locations for isochrone t, so that it can be used as the particles initial locations of the following GPZFAULT simulation for isochrone $t+\Delta t$, thus decreasing the run time for definition of several isochrones.

The executable file, GPZFAULT.EXE, and the input file, *input.txt*, must be located in the same directory.

Dual and multiple-porosity behaviour: relevance to protection zone delineation

A Mathematica notebook and a FORTRAN code were developed to implement the procedure for delineation of protection zones in dual-porosity environments, while a third code implements the multiple-porosity flow and transport solutions.

4. *GPZ IN DUAL-POROSITY AQUIFERS*

A *Mathematica* notebook (*gpz in dual-porosity aquifers.nb*) that defines the size of probabilistic protection zones along the *x-axis* (parallel to the regional hydraulic gradient direction) and the *y-axis* of a horizontal domain in a dual-porosity aquifer.

The notebook implements the equations developed in section 4.2.3 and, for each axis, a curve of probability versus distance to the pumping well is plotted for two values of matrix diffusion coefficient. The user specifies all the necessary hydraulic parameters of dual-porosity aquifer.

5. *GPZDUALP*

A FORTRAN code that delineates probabilistic protection zones for a well pumping dual-porosity aquifer system.

This code was used and described in section 4.2.3. It implements equation (4.29) which allows to compute the probability of each x, y location being included in a given t isochrone. The code was structured to first compute the t isochrone using the single-porosity solution (Bear and Jacobs 1965), and then to compute the probability at 200 points inside an area bounded by the single-porosity isochrone. The probability values must then be contoured to find the probability lines.

The code runs in a DOS environment and input is made through a file designated *input.txt*, which includes the hydraulic parameters of dual-porosity aquifer, as well aquifer thickness, pumping rate and matrix-diffusion coefficient. Input for the isochrone time is requested interactively. Output is to two files: a mapping file named *isochrone.bln*, which contains the coordinates of the single-porosity isochrone and that can be plotted using SURFER; a file designated *probability.txt*, which contains the 200 probability values, as well as the corresponding x, y locations, and that must be used in SURFER to find the probability contours.

The executable file, GPZDUALP.EXE, and the input file, *input.txt*, must be located in the same directory.

6. *MULTIPOROSITY*

A code that implements the solutions for radial flow and for one-dimensional transport in a multiple-porosity environment, as described in section 4.3.

This program is made up of two files. File *Multiporosity.dll* is the actual FORTRAN code that implements the equations described in section 4.3.1 for the radial flow solution, and in section 4.3.3 for the one-dimensional transport solution. File *Multiporosity.xls* is the front-end of the program, where input is made and output is visualised. VISUAL BASIC macros written in EXCEL provide the link between the two files.

The program allows for a maximum of 10 hierarchical levels and for three block geometries: cylinders, spheres and slabs, which can vary in different levels of the hierarchical system.

The two files do not have to be in the same directory, but the VISUAL BASIC macros were written to search for the file *multiporosity.dll* in a directory C:\Multiporosity. However, the location of the *.dll* file can be easily changed by editing, in EXCEL, the first line of the *Main* and *Transport* macros and typing the desired file location

Protection zones for fracture networks I: Overview and Statistical Continuum Method

The implementation of the Statistical Continuum Method (SCM) and the definition of probabilistic protection zones in fracture network aquifers required the development of four FORTRAN codes.

7. *STATMOV*

A code that collects the particle movement statistics necessary to implement the SCM, as described in section 5.2. The executable file is *STATMOV.EXE.*

This code runs in a DOS environment and takes control of SDF (a Discrete Fracture Network model not developed within the scope of this thesis) to produce multiple realisations of a fracture network and collects the relevant statistics of movement of particles tracked in the fracture network domain. STATMOV rotates the fracture network by 15° degrees increments so that a matrix of statistics of movement versus hydraulic gradient orientation is produced.

Input to the code is interactive, in that the program prompts for information on the number of realisations and the number of times the network should rotate by 15° degrees increments. However, the information related to the fracture network geometry and hydraulic parameters must be supplied in the format required by SDF. Such input file is designated by *Sample.ini.* A second input file, designated as *Partrack.ini,* with the particles initial locations must also be supplied in the format required by SDF.

The files that are necessary to run SDF are also supplied in the CD-ROM and are files *Netwrkvm.exe, Nodes.exe, Partrack.exe, Files.txt, Maxmin.pas* and *Fracs.pas*. The batch file *SCM standard.bat* is necessary to run the SDF files. Due to the unfeasibility of changing the SDF code, all the files mentioned so far must be included in the same directory as the executable *STATMOV.EXE*.

Output is made to three files: *StandardSCM output.txt* includes all the statistics of movement; *Correlation.txt* relates to the data characterising the correlation between path-length and velocity in each fracture element; *Elements.txt* includes all the information about the fracture segments along which the particles were tracked and, thus, it can be a very large file.

This code produces a large amount of output to the screen, which can not be prevented due to the difficulty in changing SDF.

8. SCPATH

A code which aims to simulate solute transport in fracture network aquifers, preserving the main characteristic features of particle movement in that environment, while using the flow solution provided by MODFLOW. The executable file is *SCPATH.EXE*.

This code conducts particle tracking in three different manners:

- mode 1, uses the statistics of movement collected by STATMOV to conduct particle tracking in a catchment scale domain. The movement of particles is forced to replicate the behaviour of particles at the much smaller discrete fracture network domain. This process was described in section 5.2.4;
- mode 2, conducts particle tracking as if the aquifer was a continuous porous medium environment with advection as the single driving force. The main difference with respect to MODPATH and similar codes is that anisotropy in effective porosity is allowed;
- mode 3, conducts particle tracking according to a two-dimensional CTRW with exponentially distributed path-lengths, both in its Explicit and Implicit procedure forms, as described in section 6.4.

The code requires several input files that vary according to the running mode selected. The following table lists the necessary files.

Table F.1 – Input to code SCPATH

File name	*Data*	*Running mode*
StandardSCM output.txt	Matrix of statistics of movement collected by STATMOV.	Mode 1
Correlation.txt	Correlation between path-length and velocity in the Statistical Continuum Method	Mode 1
Effectivepor.txt	Effective porosity along the x-axis in each MODFLOW cell. The code prompts for anisotropy factor. To be built using the PMWIN MODFLOW interface.	Mode 2
CTRW.txt	Parameters of the CTRW method (fracture orientation, directional choice parameter and directional dispersivities and advective velocities).	Mode 3
Partlocal.txt	Initial particle location, in terms of I and J MODFLOW cells indices and x,y location in each cell.	Mode 1, 2 and 3
Boundaries.txt	Code for the boundary type of the MODFLOW model domain. To be built using the PMWIN MODFLOW interface.	Mode 1, 2 and 3
Flowfront.txt	Flow along the front face of each MODFLOW cell. To be built using the PMWIN MODFLOW interface.	Mode 1, 2 and 3
Flowrigth.txt	Flow along the right face of each MODFLOW cell. To be built using the PMWIN MODFLOW interface.	Mode 1, 2 and 3
Hydcond.txt	Hydraulic conductivity along the x-axis in each MODFLOW cell. The code prompts for anisotropy factor. To be built using the PMWIN MODFLOW interface.	Mode 1, 2 and 3
Spacing.grd	MODFLOW cells spacing along the I and J directions. To be built using the PMWIN MODFLOW interface.	Mode 1, 2 and 3

Notice that the input files must all be located in a common folder, INPUT, placed in the same directory as the executable *SCPATH.EXE.*

Several input files, related to the MODFLOW modelling domain and flow solution, must be built using the Processing MODFLOW for Windows (PMWIN) interface. A link is provided in the CD-ROM to an internet site from where a fully functional version of PMWIN can be downloaded.

Output also varies with the running mode. Table F.2 lists the output files. The first three files of table F.2 can be very large (several Mbytes) for large modelling domains.

Table F.2 – Output from code SCPATH

File name	*Data*	*Running mode*
SCpart location.bln	SURFER mapping file with the path of each particle.	Mode 1, 2 and 3
SCpart output1.txt	Particle location with time	Mode 1 and 3
SCpart output2.txt	Additional information on particle location with time	Mode 1 and 3
CTRW constants.txt	Constants characterising the variation of the CTRW parameters with hydraulic gradient orientation, according to equations in section 6.4.1.	Mode 3
CTRW measure.txt	Matrix of CTRW parameters versus hydraulic gradient orientation.	Mode 3

9. *PARTLOCAL*

A code that generates the files with the particles initial locations for programs SCPATH and SDF (which is run via STATMOV).

The code prompts for keyboard input and files *Partrack.ini* or *Partlocal.txt* are generated for SDF or SCPATH, respectively. The main difference between input requested to build the two files is that SDF requires only the x, y location in the discrete domain, while SCPATH requires the I and J MODFLOW cell indices and the x, y locations in each cell. In both cases, particles can be placed in a circle or along a line.

10. *PROBCONT*

A code written with the main purpose of establishing the probability of each finite difference cell modelled by SCPATH being part of a probabilistic protection zone.

The code runs in two modes. A first mode finds the particles location at a specified time from the SDF output file *Partrack.ou2* or the SCPATH output file *SCpart output1.txt*. This mode allows to define particle plumes that can be plotted using EXCEL or SURFER. Output is to file *location.txt*.

A second mode computes the probability of a particle tracked using SCPATH reaching any given cell of the continuum domain before a specified time t. Such probability is assimilated to the probability of the cell being included in a probabilistic protection. This mode is an implementation of the procedure described in section 5.2.5. The output file is designated *probability.txt* and SURFER can be used to establish the probability contours.

Notice that the executable file PROBCONT.EXE must be placed in the same directory as SCPATH since it requires not only its output file, but also needs to access the finite difference grid information provided by file *Spacing.grd* which is located in the folder INPUT of code SCPATH. Thus, PROBCONT must access both input and output files of SCPATH.

Protection zones for fracture networks II: Continuous Time Random Walks

Overall, eight codes were written related to the use of Continuous Time Random Walks (CTRW) to simulate solute transport in fractured rocks. The codes described in this section are primarily intended to simulate one-dimensional transport or two-dimensional transport under constant uniform flow conditions.

11. *SUM OF PARETO*

A *Mathematica* notebook (*sum of pareto.nb*) that finds the probability density function resulting from the sum of n independent identically distributed Pareto variables.

The notebook plots the density function by evaluating equation (6.36) in section 6.2.2. The number of Pareto variables to sum is user specified, as well as the shape parameter (β) of the Pareto distribution. The minimum value of the Pareto distribution is set to one.

12. SUMPAR

A FORTRAN code that generates variates distributed according to the sum of n independent identically distributed Pareto variables.

The code runs in a DOS environment and generates n random numbers from a Pareto distribution with scale parameter β and minimum value set to one. The n random numbers are added to find the variates following the probability density function provided by equation (6.36) in section 6.2.2. This program, together with the notebook *Sum of Pareto.nb* was used to produce figure 6.18 in section 6.2.2.

13. CTRW EXPONENTIAL

A *Mathematica* notebook (*ctrw exponential.nb*) that plots the probability density function and the cumulative probability function of a CTRW with exponentially distributed path-lengths.

The notebook plots the density function by evaluating equation (6.28) in section 6.2.1 and the corresponding cumulative probability function as provided by equation (E.7) in appendix E. The user specifies the dispersivity parameter (α) and the advective velocity parameter (v) of the CTRW equation.

Both functions are plotted as 1-D graphs, for fixed distances with varying time and for fixed time with varying distance. Additionally, 2-D graphs of the probability density function are produced, with time and distance varying simultaneously.

14. CTRWEXP

A FORTRAN code that generates random variates distributed according to a CTRW with exponentially distributed path-lengths, for a fixed time. The variates can be interpreted as representing 1-D particle movement according to the mentioned CTRW, as explained in section 6.2.1.

This code generates random variates from the numerical inversion of the cumulative probability function provided by equation (E.7) in appendix E. A root-finding algorithm is used to invert the relevant equation.

The code prompts for keyboard input of dispersivity (α) and advective velocity (v) of the CTRW equation, as well as for time and the number of random variates to generate. Output is to file *output.txt*.

15. CTRW2DEXP

A FORTRAN code that simulates two-dimensional solute transport in a fracture network according to an Explicit CTRW procedure with exponentially distributed path-lengths, under uniform flow conditions. The executable file is CTRW2D.EXE.

This code relies on the generation of random variates, essentially using the same algorithm as CTRWEXP, for several possible directions (the fracture orientations) of particle movement. The final location of the particles is found by adding the vectors that represent movement in each direction, as explained in section 6.3.1. Essentially, this code is an implementation of equation (6.53) in section 6.3.1.

Input is made through file *CTRW.txt*, which includes data about the number of movement directions, its orientation with respect to the x-axis, and the CTRW parameters in each direction, that is, directional dispersivity, advective velocity and directional choice. The code prompts for keyboard input of hydraulic gradient value (parallel to the x-axis), time and number of particles to move. Output is to file *CTRWoutput.txt*, which can be used to build plumes of particles using EXCEL or SURFER.

Notice that simulation of solute transport according to a two-dimensional CTRW with exponentially distributed path-lengths under conditions of varying hydraulic gradient is conducted using the SCPATH code.

16. CTRW POWERLAW

A *Mathematica* notebook (*ctrw powerlaw.nb*) that plots the probability density function and the cumulative probability function of a CTRW with power-law distributed path-lengths.

The notebook plots the density function by evaluating equation (6.39) in section 6.2.2 and the corresponding cumulative probability function as provided by equation (E.9) in appendix E. The user specifies the shape parameter (β) and the step rate parameter (γ) of the CTRW equation.

Both functions are plotted as 1-D graphs, for fixed distances with varying time and for fixed time with varying distance. Additionally, 2-D graphs of the probability density function are produced, with time and distance varying simultaneously.

17. CTRWPOWER

A FORTRAN code that generates random variates distributed according to a CTRW with power-law distributed path-lengths, for a fixed time. The variates can be interpreted as representing 1-D particle movement according to the mentioned CTRW, as explained in section 6.2.2.

This code generates random variates from the numerical inversion of the cumulative probability function provided by equation (E.9) in appendix E. A root-finding algorithm is used to invert the relevant equation.

The code prompts for keyboard input of shape parameter (β) and step rate parameter (γ) of the CTRW equation, as well as for time and the number of random variates to generate. Output is to file *output.txt*.

18. CTRW2DPOWER

A FORTRAN code that simulates two-dimensional solute transport in a fracture network according to a CTRW with power-law distributed path-lengths, under uniform flow conditions. Both the Explicit and the Implicit CTRW procedures are used. The executable file is 2DCTRWPOWER.EXE.

This code relies on the generation of random variates, essentially using the same algorithm as CTRWPOWER, for several possible directions (the fracture orientations) of particle movement. The final location of the particles is found by adding the vectors that represent movement in each direction, as explained in section 6.3.1. Essentially, this code is an implementation of equation (6.53) in section 6.3.1.

Input is made through file *CTRWpower.txt*, which includes data about the number of movement directions, its orientation with respect to the x-axis, and the CTRW parameters in each direction, that is, shape, step rate and directional choice. The code prompts for keyboard input of hydraulic gradient value (parallel to the x-axis), time and number of particle to move. Output is to file *CTRWoutput.txt*, which can be used to build plumes of particles using EXCEL or SURFER.

Utilities

The CD-ROM includes several other files, grouped in the directory UTILITIES, which were not developed by the author of the thesis but that are regarded as important, either because they might be necessary to run or visualise the result of some of the codes, or because they must be used if recompilation of the FORTRAN codes is to be done.

Folder *FORTRAN routines* – includes routine CINGAM, which evaluates the incomplete gamma function with complex arguments, and that is necessary to recompile codes CTRWPOWER, CTRW2DPOWER and GPZFAULT. It also includes routine PARRAN which generates random numbers distributed according to a Pareto distribution, and that is necessary to recompile code CTRW2DPOWER. The authors of these routines are identified in the files.

Folder *Mathematica add-on* – includes the file *numericalinversion.m*, a *Mathematica* add-on that conducts numerical inversion of Laplace transforms according to several different algorithms. This file is not included with the standard *Mathematica* add-ons and must be placed in the folder *\AddOns\StandardPackages\NumericalMath* of the *Mathematica* directory structure. The developer of the code is Mallet (2000) and information about the available tools can be obtained by invoking 'CommandsNumericalInversion' in the *Mathematica* front-end. This add-on is necessary to run the notebooks *Ctrwexponential, Ctrwpowerlaw, Gpz in dual-porosity aquifers* and *Sum of pareto.*

Folder *MATHREADER* - contains the program MATHREADER that is distributed freely by Wolfram Research. MATHREADER is a viewer for notebook documents created with *Mathematica.* To create, edit, and print notebooks, you need the *Mathematica* front end. In its absence, MATHREADER enables the display and print of *Mathematica* notebooks, animate graphics, play sounds, and copy information from notebooks to other documents. MathReader can be used to visualise all the notebooks supplied with the CD-ROM.

Folder *SDF* – contains the discrete fracture network model SDF. The files necessary to run code STATMOV are supplied, as well as the complete SDF code, which is provided as the auto-executable file *SDF.exe.* Alain Rouleau originally developed the SDF code, but the version included in the CD-ROM has some improvements introduced by researchers of the Wisconsin Geological and Natural History Survey (WGNHS). Ken Bradbury, from WGNHS, supplied this version.

Folder *PMWIN_PMPATH* link – contains an internet link to the official website of the PMWIN (Processing MODFLOW for Windows) software. A free, full working version of this software can be downloaded from this website. PMWIN is necessary to find the continuous porous medium flow solution that must be provided as input to code SCPATH.